THEORY OF QUANTUM DEGENERATE GASES

BY

ERICH JON MUELLER

B.S., University of British Columbia, 1996

THESIS

Submitted in partial fulfillment of the requirements
for the degree of Doctor of Philosophy in Physics
in the Graduate College of the
University of Illinois at Urbana-Champaign, 2001

Urbana, Illinois

THEORY OF QUANTUM DEGENERATE GASES

Erich Jon Mueller, Ph.D.
Department of Physics
University of Illinois at Urbana-Champaign, 2001
Gordon Baym, Advisor

Motivated by experiments on cold alkali atoms, I present a theoretical study of weakly interacting quantum degenerate particles. These experiments observe a wide range of phenomena and consequently this thesis has a broad scope, involving issues of coherence, stability, superfluidity, and kinetics. I explore six topics which exemplify the rich and exciting physics of cold alkali atoms: first, the effect of interactions on the transition temperature of a dilute Bose gas; second, the connection between broken non-gauge symmetries and the appearance of multiple condensates in a Bose gas; third, the role of thermally activated "phase slip" events in destroying superfluidity near the critical temperature of a Bose gas; fourth, mechanical instabilities in clouds of attractive bosons; fifth, the kinetics of a gas of partially condensed atoms; and sixth, the nonlinear optical properties of an atomic gases.

Acknowledgments

This Ph.D. thesis was a five year project, and it is rather daunting to enumerate all of the people who played important roles in its production. I should begin by thanking my wife Sue, with whom I am looking forward to a wonderful life, and her family who have been very welcoming. I also want to thank my parents for their continued support.

I have had several important mentors here at UIUC. Gordon Baym, my advisor, who has infinite patience, and who has tried his best to show me how physics is done; Paul Goldbart, who walked me through my first research project, provided much encouragement, and who runs a truly unique and wonderful seminar series, the "meso meetings"; Tony Leggett, a keen mind, who has always given me kindly and well thought out advice.

I have also benefited from the expert guidance of many physicists from all areas of the world. Most of these people I met at one of three institutions. First, the Institute for Theoretical Physics in Santa Barbara, directed by David Gross, where in 1998 there was a program devoted to the study of Bose-Einstein Condensation. I truly thank the organizers, Keith Burnett, Ataç Imamoglu, and Tony Leggett, who generously allowed me to spend over a month in Santa Barbara, and who contributed some financial support. Second, the Laboratoire Kastler Brossel at the Ecole Normale Supérieure in Paris, where I spent six months in 1999. The trip, and the research performed there, was facilitated by a cooperative agreement between the University of Illinois at Urbana-Champaign and the Centre National de la Recherche Scientifique. The third institution is the idyllic Aspen Center for Physics which has hosted two workshops on Bose condensation; one in 1999, and the other in 2001. I would like to thank Jane Kelly and the other staff members at Aspen, as well as the organizers of the workshops, Gordon Baym, Sandy Fetter, Jason Ho, Murray Holland, Randy Hulet, Chris Pethick, Mark Kasevich, and Andre Ruckenstein

Of these researchers that I met while abroad, I would like to make a list of a few who made a particular impression on me: James Anglin, Bernard Bernu, Eric Braaten, Iacoppo Carusotto, Yvan Castin, Jean Dalibard, David Guery-Odelin, Allan

I apologize to the many people who I forgot to mention. Please blame my negligence on the stress of writing a thesis, and not on any malice.

Contents

List of Tables

List of Figures

Guide to Notation

$A(k,\omega)$	The spectral density for single-particle excitations.
a_s	An s-wave scattering length.
$\mathbf{B}$	A magnetic field.
β	The inverse temperature, $\beta = 1/k_B T$.
$C_d(s)$	Lattice sums tabulated in table B.1.
$\tilde{C}_d(s)$	Lattice sums tabulated in table B.2.
δ	A scattering phase shift.
δ_{ij}	A Kronecker delta function.
$\delta(x)$	A Dirac delta function.
E	An energy.
E_c	An energy cut-off.
ε_i	A single particle energy level.
F	A free energy in the canonical ensemble.
F_{ex}	The free energy of the non-condensed particles within the canonical ensemble.
$\mathcal{F}$	A free energy in the grand canonical ensemble.
$\mathcal{F}_{\text{ex}}$	The free energy of the non-condensed particles within the grand canonical ensemble.
f_k	Coefficients of the expansion of $\mathcal{F}_{\text{ex}}$ in powers of $\beta\mu$ (cf. B.3).
$f(k,R,t)$	A phase space distribution function.

G	A single particle Green's function.
g	A coupling constant, also g_F and g_J.
$g_\nu(z)$	The polylogarithm function $g_\nu(z) = \sum_j z^j/j^\nu$.
Γ	A decay rate.
$\Gamma(k,\omega)$	Spectral density for the self-energy, $\Sigma(k,\omega) = \int \frac{dz}{\omega-z}\Gamma(z)$.
H	A many-body Hamiltonian.
δH	A perturbation of the Hamiltonian.
$\hbar$	Planck's Constant; $\hbar = 1.054 \cdot 10^{-34}$ Js.
$I[f]$	A collision integral.
$\mathbf{k}$	A momentum.
k_B	Boltzmann's Constant; $k_B = 1.38 \cdot 10^{-23}$ J/K.
L	The characteristic size of a system.
λ	The thermal wavelength; $\lambda = \sqrt{2\pi\hbar^2/mk_BT}$.
m	A mass. Typically the mass of an atom.
N	The number of particles in a system.
n	The number density of particles.
n_i	The occupation of the i'th energy level.
$\mathcal{O}$	The order of. The statement $f(x) = \mathcal{O}(x^n)$ as $x \to \infty$ $(x \to 0)$ means that $f(x)/x^n$ is bounded as $x \to \infty$ $(x \to 0)$.
Ω	The frequency of a harmonic trap.
p	A momentum.
$Q_d(s)$	Lattice sums tabulated in table B.4.
$Q'_d(0)$	Lattice sums tabulated in table B.5.
q	A momentum.

$\rho(E)$	A density of states.
$\Sigma(k, \omega)$	A self-energy evaluated at momentum k and energy ω.
σ	A scattering cross-section.
T	The temperature, or the kinetic energy.
T_c	The Bose-Einstein condensation phase transition temperature.
T_*	A cross-over temperature discussed in Sec. 2.3.3.
ΔT	The interaction induced shift in the phase transition temperature.
U	Potential energy.
M	A scaled measure of the number of condensed particles defined in Eq. (2.34).
μ	A chemical potential.
V	Potential energy.
v	A velocity.
ξ	The coherence length governing the fall-off of G.
ξ_{MF}	The healing length of the condensate.
Z	A partition function in the canonical ensemble. Also Z_N, where N denotes the number of particles.
$\mathcal{Z}$	A partition function in the grand canonical ensemble.
$\zeta(\nu)$	The Riemann zeta function, defined as the analytic continuation of $\zeta(\nu) = \sum_j j^{-\nu}$.
$\{\ldots, \ldots\}$	Poisson brackets (see equation (6.10))

Chapter 1

General Introduction

1.1 Overview

In 1995 three groups of atomic physicists announced that they had observed Bose-Einstein condensation in clouds of trapped alkali atoms [1, 2, 3]. These initial experiments spawned a new field of study which combines atomic, laser and condensed matter physics to explore the quantum mechanical behavior of matter. In this thesis I present a series of theoretical studies motivated by these experiments. This introductory Chapter briefly describes each of these studies and provide an introduction to the relevant experiments.

1.1.1 Phase transition

At sufficiently low temperatures, a Bose gas undergoes a phase transition to a state in which a single mode (in free space the $k = 0$ mode) is macroscopically occupied. Although this phase transition is well understood in a uniform non-interacting cloud [4], it is much more difficult to understand the transition in atomic clouds where inhomogeneities and interactions complicate the picture. In Chapter 2, I systematically address these complications; first exploring the phase transition in a non-interacting, but finite system, and then use perturbation theory to extend these results to an interacting system.

As with all second order phase transitions, the Bose-Einstein condensation transition is associated with a diverging coherence length ξ, implying that long wavelength modes determine the behavior of a system near the transition. Consequently, in the thermodynamic limit perturbation theory is infrared divergent and breaks down, making it *prima facia* impossible to use perturbation theory to understand the role of interactions in the phase transition. I use finite size scaling to overcome this difficulty,

1

and calculate the interaction shift of T_c.

1.1.2 Fragmentation

Quite surprisingly, several models of Bose gases have produced ground states with more than one condensate [5, 6, 7]. In Chapter 3, I explain the origin of this "fragmentation" of the condensate, demonstrating that it is related to degeneracies in the single particle spectrum and that it only occurs in mesoscopic, not macroscopic, systems; the necessary degeneracies arise from the presence of a strictly conserved symmetry which is spontaneously broken in the thermodynamic limit. This Chapter describes the experimental signatures of fragmentation, showing that with enough control of initial conditions one can distinguish fragmented and singly-condensed states.

1.1.3 Persistent currents

Like ^{4}He below the λ temperature, the condensed phase of a Bose gas is superfluid. A consequence of superfluidity is that current set in motion in an annular trap would have an extremely long lifetime. This lifetime is limited by rare "phase slip" events triggered by quantum or thermal fluctuations. In Chapter 4, I calculate the rate of dissipation due to thermal phase slips, showing that near the critical temperature they can destroy superfluidity.

1.1.4 Attractive interactions

Attractive interactions in a gas of particles drive an instability towards "clumping up." Such instabilities are well studied in astrophysical contexts where they lead to the formation of stars and galaxies [8]. In Chapter 5, I study the competition between such attractive interactions and the stabilizing effects of quantum and thermal pressure within a cloud of bosons. The central result of this Chapter is a finite temperature phase diagram of an attractive gas, containing three phases; a normal phase, a Bose-condensed phase, and an unstable region in which the cloud physically collapses to a small volume. Using the techniques developed for this study of mechanical instabilities I also examine the possibility of BCS-type "pairing" in the attractive Bose gas, finding that the mechanical instability prevents any pairing.

The mechanical instability in a cloud with attractive interactions is very similar to the instability towards phase separation in a mixture of two immiscible gases. Using this analogy, I discuss the formation of domains in spinor condensate experiments at MIT [9].

1.1.5   Kinetic theory

In Chapter 6, I derive a kinetic theory for describing trapped alkali atoms at finite temperature. Such a kinetic theory is needed to model non-equilibrium finite temperature experiments where both quantum coherence and classical thermal fluctuations are important. For example, one would like to understand experiments [10] where a vortex is found to have a finite lifetime. Current theories suggest that the vortex decays by transferring its angular momentum to the cloud of non-condensed atoms which surround the condensate. Modeling this scenario requires a non-equilibrium theory which simultaneously describes the coherent motion of the condensate and the incoherent motion of non-condensed particles.

The kinetic theory derived here is quite complicated. I elucidate the essential structure by applying this formalism to investigate a toy problem in which a uniform gas experiences a sudden change of interaction strength. Looking at the excitations formed during this process helps clarify the distinction between quasiparticles and collective excitations. This distinction is unusual in a condensed gas since the condensate nominally hybridizes the two types of excitations.

1.1.6   Electromagnetically induced transparency

In Chapter 7, I give a detailed analysis of experiments that use a cold atomic gas as a tunable non-linear media to control the behavior of light [11, 12]. By coupling photons to a dark-state polarization wave, these experimentalists are able to slow light, and even stop it. I analyze these experiments with two approaches, mean field theory and equilibrium Green's functions.

1.2   Experiments

Having outlined the main topics, I now give a brief review of the experiments which have motivated this thesis. For further details I highly recommend several recent reviews [13, 14, 15, 16], as well as an excellent elementary introduction by Carl Wieman [17]. I limit my descriptions to the experiments referred to in the rest of this thesis.

1.2.1 Cooling and trapping

Quantum mechanics limits the precision with which one can know both the position and momentum of a particle. This restriction is encapsulated in the Heisenberg uncertainty principle, $\delta x \cdot \delta p \geq \hbar$, which states that the product of the uncertainties in position and momentum are bounded below by the constant $\hbar \approx 1.054 \cdot 10^{-34}$Js. At finite temperature, random thermal motion leads to a large uncertainty in momentum, and consequently there is very little uncertainty in the positions of the atoms. For example, a room temperature a sodium atom has a root mean square velocity of $500\,$m/s, about 1.5 times the speed of sound in air, leading to a spread, $\delta x \approx 6 \cdot 10^{-12}$m, much smaller than the size of a sodium atom. Thus room temperature atoms behave as classical particles. As they are cooled to lower temperatures, T, the atoms slow down, and the thermal wavelength $\lambda = \sqrt{2\pi\hbar^2/mk_BT}$, which measures the uncertainty in the position of an atom of mass m, decreases. For Bose Einstein condensation to occur, the particles must be cooled until λ is of order the interparticle spacing (precisely, $n\lambda^3 = \zeta(3/2) = 2.61\ldots$). At this point the particles lose their individual identity, and behave collectively.

The great experimental challenge of achieving Bose condensation with an atomic vapor lies in the difficulty of cooling and compressing the vapor to the point where $n\lambda^3$ is of order unity. Liquid helium, with a number density comparable to water $n \sim 2 \cdot 10^{22}$cm^{-3} and a very low mass, Bose condenses at $2.17\,$K. Alkali gases have densities comparable to a good vacuum $n \sim 10^{12}$cm^{-3}, and need to be cooled to temperatures of order 100nK. The 1997 Nobel prize was awarded to Steven Chu, Claude Cohen-Tannoudji, and Bill Phillips for developing laser cooling techniques, which are necessary to cool to such unbelievably low temperatures.

Cooling is performed in several stages. The atoms, initially loaded into the apparatus by boiling them off of a metallic filament, are first cooled by a series of optical means, the most ingenious of which is the "optical molasses" consisting of six laser beams focussed on a small point. This geometry is illustrated in Fig. 1.1. These lasers are red detuned relative to an atomic transition. If an atom is moving towards one of the six lasers, the light is blue-shifted into resonance and the atom absorbs a photon. The recoil from absorbing the photon slows the atom down. This mechanism can cool a gas to the recoil temperature, found by equating the thermal energy of an atom with its recoil energy. For typical parameters, the recoil temperature is of order 10μK.

Further cooling relies on trapping the particles in a magnetic trap. The basic principle is that alkali atoms, with one valence electron, have a magnetic moment
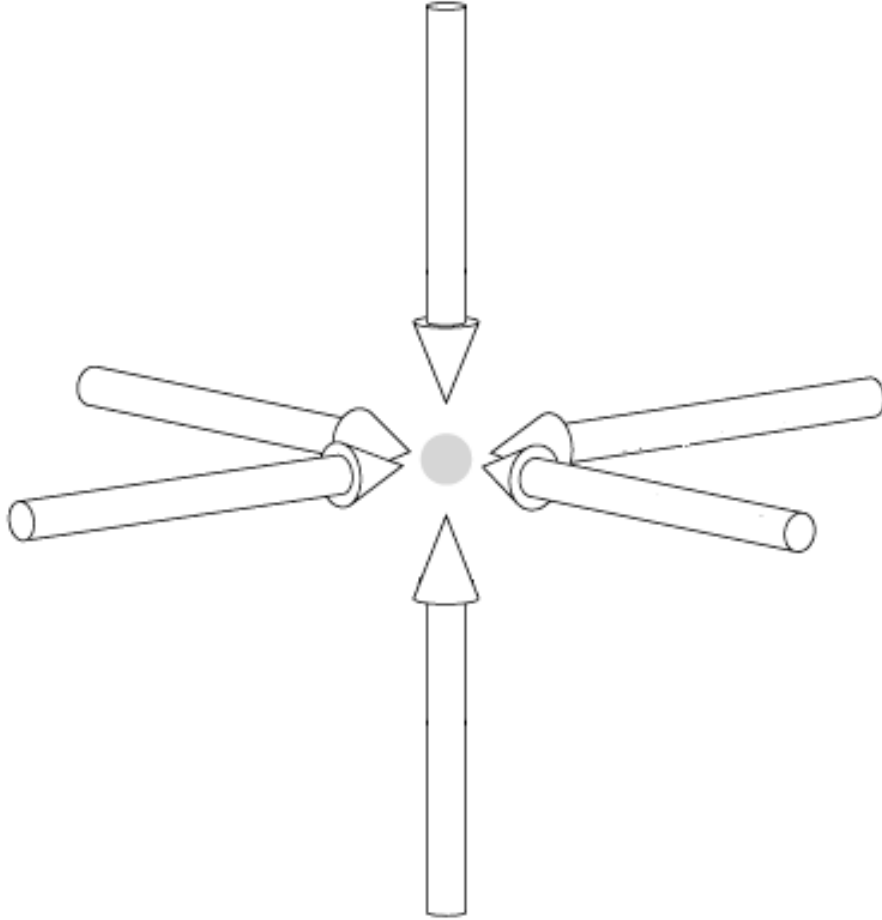
Figure 1.1: Schematic drawing of the laser beam configuration for an optical molasses. Lasers are incident from all directions. These lasers are red-detuned relative to an atomic transition so that light will only be absorbed from a beam which is doppler shifted into residence. Consequently the atoms experience a drag which tends to slow them down.

and will therefore feel a force when placed in a magnetic field gradient. A magnetic trap consists of a set of magnets which produce a field with a local minimum at some point in space. Atoms are trapped near this minimum. Magnetic trapping is demonstrated by the quadrupole trap illustrated in Fig. 1.2, which simply consists of two magnets with their north poles facing each other. The resulting magnetic field configuration has $B = 0$ at the center, and $|B|$ increasing linearly as one departs from that point. Simple quadrupole traps are rarely used in current experiments, as these traps are "leaky." Atomic spins can flip where $B = 0$, resulting in lost atoms. Adding an extra "Ioffe" magnet to the quadrupole configuration produces a trap where the field does not vanish at the minimum, thus eliminating these losses. A typical Ioffe trap is illustrated in Fig. 1.3. In such traps $|B|$ varies quadratically as one moves from the center, and the particles feel a harmonic potential $V_{\mathrm{trap}}(r) \approx m\Omega^2 r^2/2$, where m is the atomic mass, and Ω is the frequency of oscillation in the trap. Typically Ω is of order $100Hz$.

The trap serves two important purposes. First, it compresses the atomic cloud, increasing the density. Second, it allows for efficient evaporative cooling. Evaporative cooling works by removing the most energetic atoms from the cloud. Upon rethermalizing, the gas is at a lower temperature. In the magnetic trap, the most energetic atoms are farthest away from the center of the trap. One selectively removes these atoms to cool the cloud. To exclusively remove these atoms, one relies upon the fact that they experience a larger magnetic field than the other atoms, and therefore the Zeeman splitting between different hyperfine spin states is greatest in these atoms. By tuning a radio-frequency field to the splitting of these energetic atoms, one can selectively excite them, flipping their magnetic moment and causing them to be ejected from the trap.

When the phase space density is sufficiently large ($n\lambda^3 \geq 2.61$), quantum statistical mechanics predicts that the lowest energy state in the harmonic trap will be macroscopically occupied. In typical experiments, there are 10^6 atoms in this condensate. In the absence of interactions, the characteristic size of the condensate, L, is set by a competition between the kinetic zero-point energy for confining the atoms $T \approx \hbar^2/mL^2$ and the trapping energy $V \approx m\Omega L^2$. For typical traps, this length is $L \approx d = \sqrt{\hbar/m\Omega} \approx 1\mu\mathrm{m}$. If 10^6 atoms were placed in such a small space, the number density would be $10^{18}\mathrm{cm}^{-3}$ (just one order of magnitude less than the density of air at standard temperature and pressure). In practice, the repulsive interactions between atoms restrict this density to a much lower value, and one finds L by comparing three energies; T, V and the interaction energy $U \sim \hbar^2 N a_s/mL^3$. The scattering
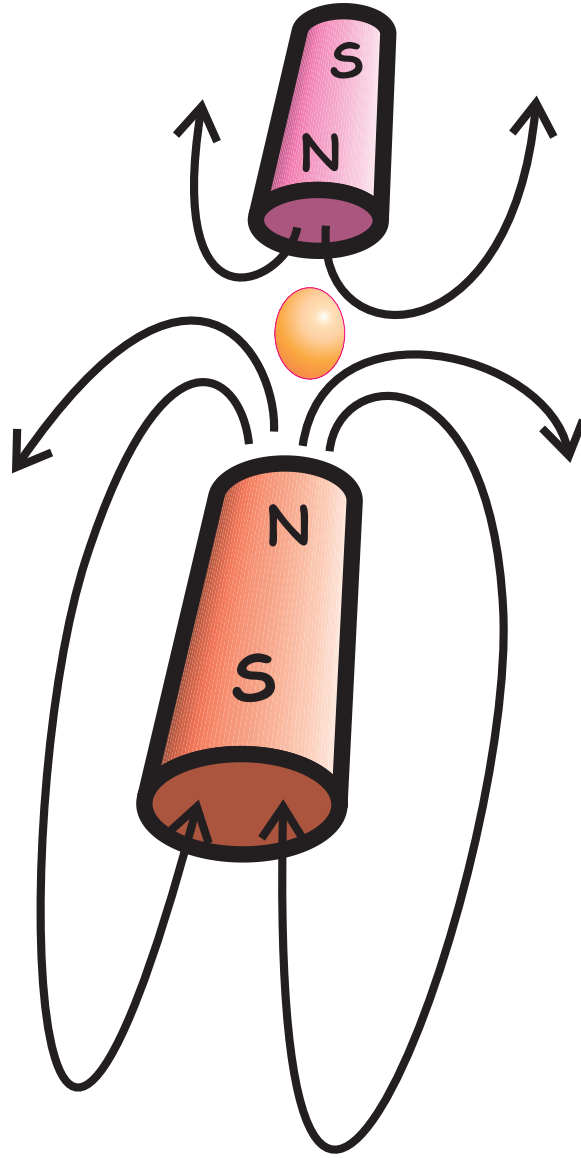
Figure 1.2: Schematic drawing of a quadrupole trap. Two magnets with their poles facing each other create a quadrupolar field in the region between them. The small ovoid represents an atomic cloud trapped at the minimum of the magnetic field.
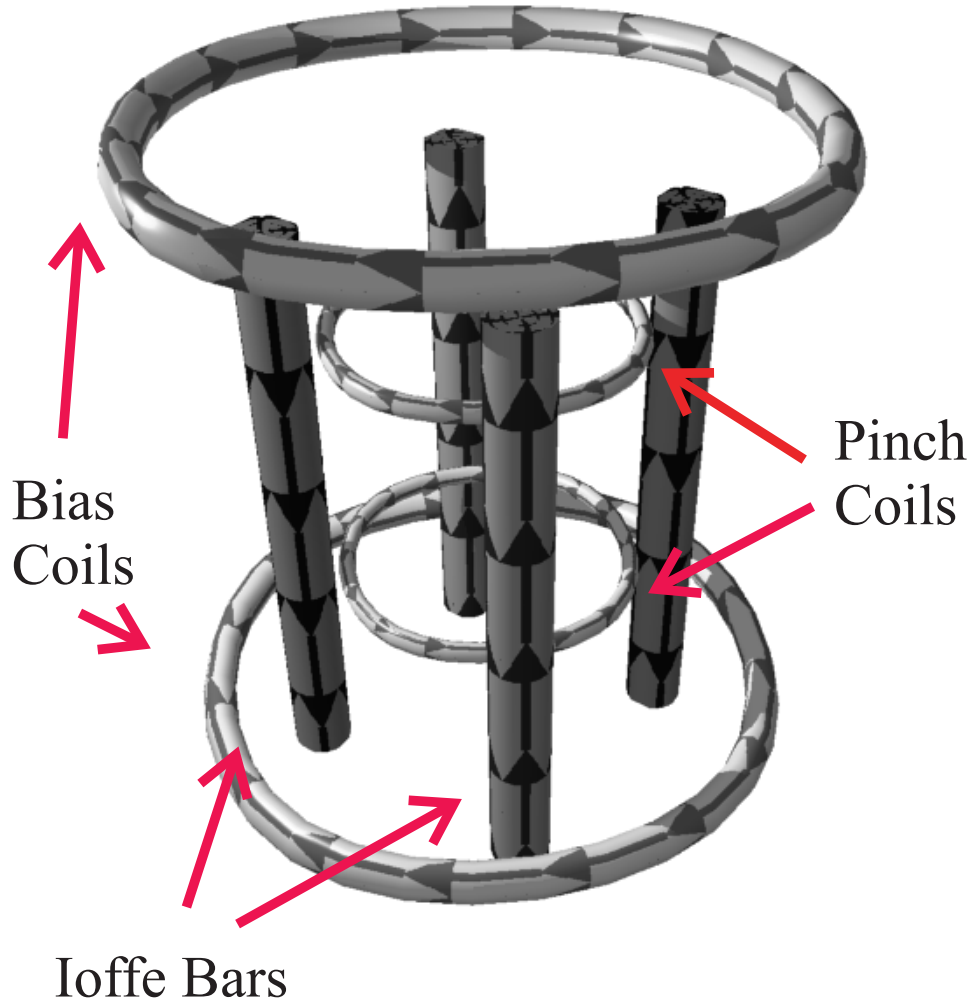
Figure 1.3: Ioffe-Pritchard trap, as used in current BEC experiments. All lines represent wires carrying electric currents in the directions indicated by the arrows. The Ioffe bars create an in-plane quadrupole field. The pinch coils turn this into a 3D quadrupole field, and the bias coils (or compensation coils) generate a non-zero magnetic field at the center of the trap.

length a_s parameterizes the interactions[1] and, with a few notable exceptions, a_s is positive and of order $5\,$nm, implying that $U \gg T$, and that the size of the condensate is determined by a competition between U and V. Comparing these energies gives $L \approx (Na_s/m^2\Omega^2)^{1/5}$ which is of order 10μm, resulting in a density $n \sim 10^{13}\mathrm{cm}^{-3}$ [18]. This density is much greater than the density of atoms above the condensation temperature $n = 10^{11}\mathrm{cm}^{-3}$, and the phase transition therefore coincides with the appearance of a large spike in the density of atoms at the center of the trap. An example of the experimental density profile is shown in Fig. 1.4. The density spike is clearly visible at temperatures below T_c.
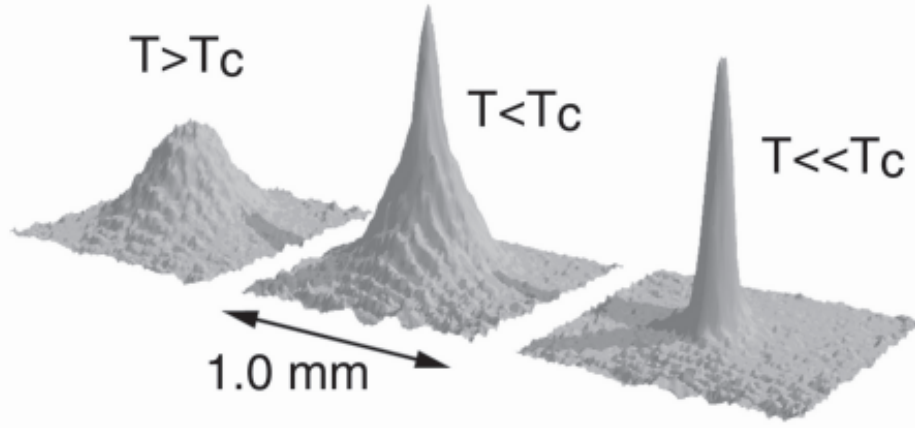
Figure 1.4: Density profile of trapped atoms above and below T_c, reproduced with permission from the MIT group's web site `http://cua.mit.edu/ketterle_group/Projects_1995/Three_peaks/3peaks%20gray1.jpg`. These pictures are absorption images of the cloud after ~ 100ms of free expansion, the height representing the optical depth (see Section 1.2.2).

1.2.2 Measurement procedures

In order to interpret the experimental data, one needs to understand the principle techniques used to probe atomic clouds. These techniques have enabled experimentalists to produce pictures which beautifully illustrate the quantum mechanical nature of atoms. All of the methods that I discuss can be used in two ways; either as *in situ* measurements, in which the trapped atoms are directly probed, or as expansion measurements, in which the trap is turned off and the cloud expands before the measurement is made. The main advantage of *in situ* measurements is that one directly measures the properties of the trapped gas. However, due to the small size of the

---

[1]For a detailed discussion of atomic scattering, see appendix F
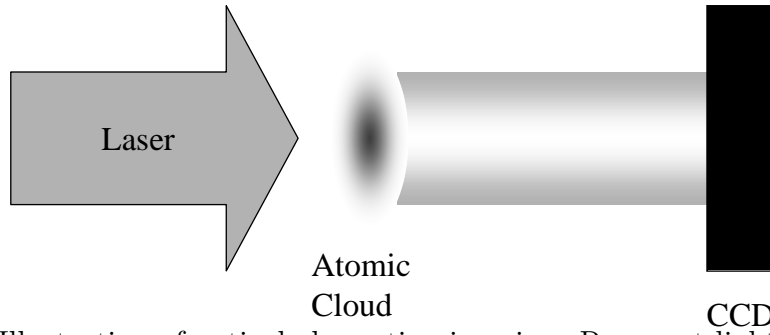
Figure 1.5: Illustration of optical absorption imaging. Resonant light is incident on a cloud of atoms. The light is absorbed in proportion to the column density of the cloud. The light that gets through is imaged on a CCD camera.

condensate, $L \sim 1\mu$m, it is impossible to observe the internal structure using this sort of measurement. In expansion experiments, such fine details are magnified and can be investigated. Most data that I discuss is from expansion measurements.

Optical absorption imaging

Optical absorption imaging provides one of the simplest probes of an atomic gas. The basic idea is that the attenuation of light resonant with an atomic transition is proportional to the integrated atomic density along the path of the light. Therefore if one positions a laser on one side of the cloud, and a piece of film on the other side of the cloud, one will record a shadow which measures the column density of the gas (see Fig. 1.5). In practice a CCD (video camera) is used rather than conventional film.

The signal from optical absorption is proportional to the column density of the cloud. The resolution of the image is primarily limited by the wavelength of light $\lambda \sim 0.5\mu$m. Since many photons are absorbed by the cloud, the measurement heats the cloud and destroys the condensate. Absorption imaging is therefore a destructive technique.

Phase contrast imaging

Phase contrast imaging is similar to absorption imaging, except that the light is detuned from an atomic transition so that no absorption occurs. To this off-resonant light the atomic cloud has an index of refraction which varies linearly with the atomic density. By placing a wave plate in the Fourier plane of the imaging optics, the density profile of the atomic cloud can be imaged. Since photons are not absorbed there is very little heating from this form of imaging, making this a non-destructive method

10

suitable for making "movies" of a single cloud.

RF spectroscopy

As an alternative to imaging the cloud, one can use spectroscopic probes to study an atomic gas. One spectroscopic approach, currently restricted to hydrogen experiments [19], takes advantage of the pressure shift of an atomic transition. The 1s-2s two-photon transition in hydrogen is red shifted under increased pressure. The microscopic basis for this shift is that atoms in the 2s state interact less strongly with 1s atoms than 1s atoms interact with themselves. Thus the energy of the 2s state relative to the 1s state is reduced as the atomic density in increased. By measuring the frequency of the 1s-2s transition one can determine the density of a uniform atomic cloud. More importantly, in an inhomogeneous cloud, the 1s-2s line will be broadened, the line shape giving a histogram of the density of the cloud.

Atom detection

Experiments on gases of excited He atoms have made use of yet another measurement scheme. Ground state He atoms cannot be magnetically trapped as they do not have a magnetic moment. Using a long lived excited state, two groups of experimentalists have successfully trapped a gas He atoms, and cooled them below the BEC transition temperature [20, 21]. In the latter experiment [21], the system is probed by releasing the atoms from the atomic trap and letting them fall onto a microchannel plate. At the plate, the excited atoms drop into their ground state, each releasing an easily measurable 20 eV of energy. A plot of the signal voltage versus time gives the density profile of the cloud.

1.2.3 Fermions

Alkali gas experiments are performed with both bosonic and fermionic isotopes. Most of this thesis is concerned with bosonic atoms, but experiments on fermions are quite exciting [22] and much of the material in Chapters 5 and 6 is readily extended to include fermions. Quantum degeneracy does not correspond to a phase transition in a Fermi gas, just a cross-over from classical behavior to quantum behavior as the Fermi surface becomes sharper. Fermionic atoms are cooled and imaged in the same manner as bosons, with the caveat that evaporative cooling works poorly. The problem is that in evaporative cooling, after the most energetic atoms are removed, the remaining atoms must thermalize. As a Fermi surface develops the phase space

available for collisions becomes small, and the thermalization time becomes very long. This difficulty is compounded by the absence of s-wave collisions between identical fermions in the same spin state. These collisions are forbidden because the Fermi wavefunction is antisymmetric.

To help circumvent these problems, some fermion experiments rely upon sympathetic cooling, where a mixture of Fermi and Bose atoms are loaded into the magnetic trap. The Bose atoms are easier to cool, and can be used as a buffer gas which absorbs the heat from the fermions. In this manner temperatures as low as one third of the Fermi temperature have been achieved. A major goal of these fermion experiments is to achieve BCS pairing in a gas of alkali atoms.

1.2.4 Coherence experiments

A Bose condensate is to a normal gas as a laser is to a thermal light source. A condensate has a high degree of *coherence*. This coherence can be seen in various sorts of interference experiments. The simplest of these is an analogy of a double-slit experiment [23], in which investigators create an atomic trap with two distinct minima and an insurmountable barrier between them. They cool a cloud in this double-well trap, forming two condensates. When the trap is turned off, the clouds expand and overlap, as sketched in Fig. 1.6. Absorption images, reproduced in Fig. 1.7, revealed a distinct interference pattern, reminiscent of the pattern seen in a classic two-slit diffraction experiment. This interference pattern shows a form of coherence, and would not occur in a non-condensed gas.

This experiment raises some very subtle issues. Suppose the two clouds were formed completely independently. Bose condensation implies that there should be coherence between any two points in the same cloud, such that if you split one of the clouds it would interfere with itself. It is not clear, however, that the two independent clouds would interfere with each other. A detailed analysis of why interference is seen will be given in Section 3.2.2 (page 46).

1.2.5 Collapse of an attractive gas

Although most alkali atoms interact with repulsive interactions, there exist several atoms with attractive interactions, most notably ^{7}Li and ^{85}Rb [24, 25]. A Bose gas with attractive interactions is unstable towards a mechanical collapse. At zero temperature stability can be understood through a simple dimensional argument where one explores how the energy of a cloud varies as one changes the size of the system L.
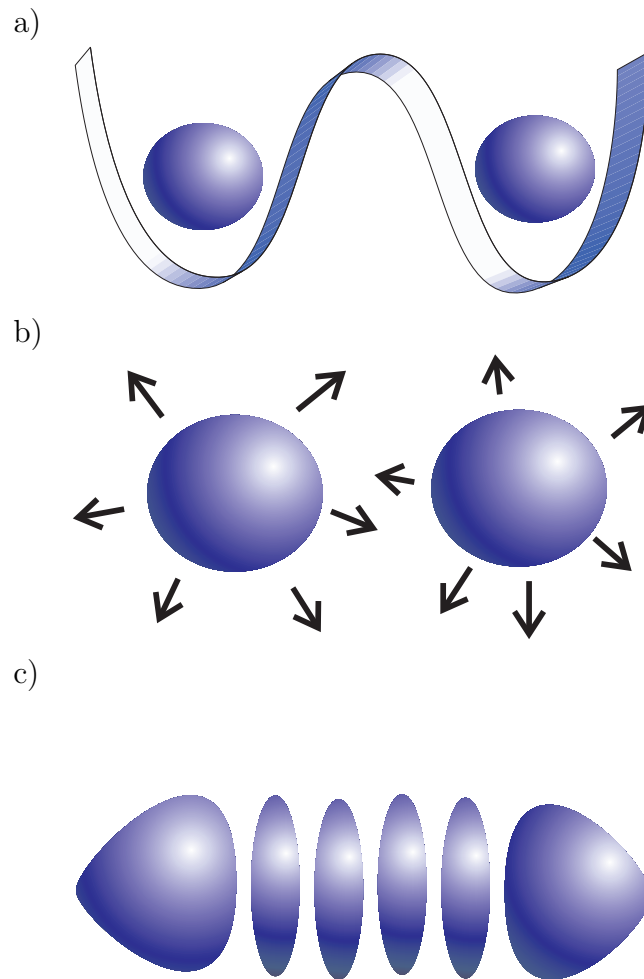
Figure 1.6: Diagram to illustrate an atom wave interference experiment. a) Two condensates are created in a double-well trap. b) The trap is turned off and the clouds expand. c) The overlapping clouds interfere with one another to form a modulated density pattern.
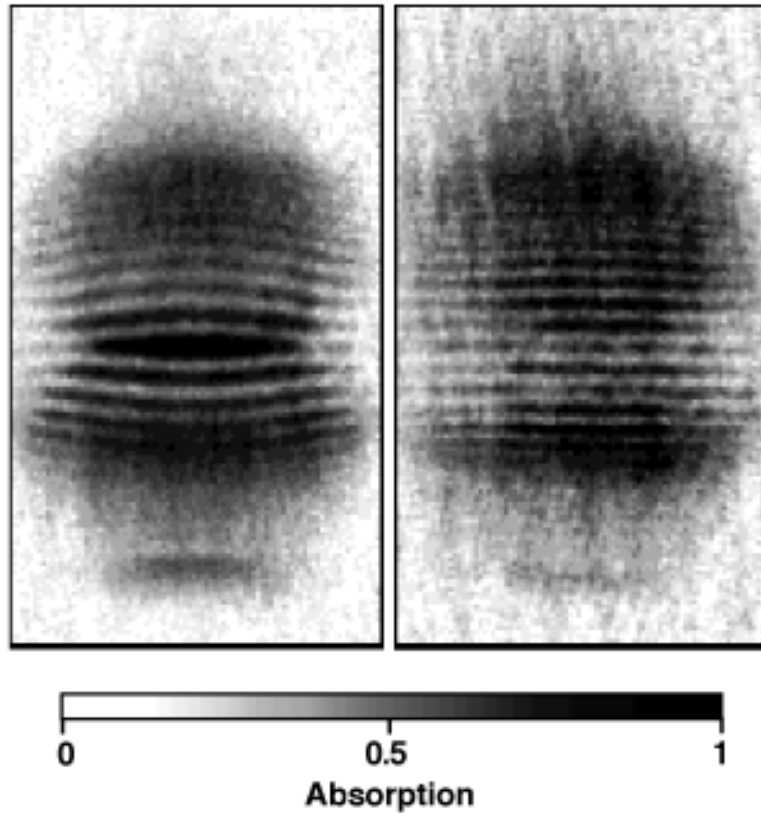
Figure 1.7: Absorption image from an experiment where two atomic condensates are allowed to overlap and interfere. Darker colors correspond to larger column densities. Data reproduced from [23].

As previously discussed, these three contributions to the energy are: kinetic energy $T \sim \hbar^2/mL^2$, trapping energy $V \sim m\Omega^2 L^2$, and interaction energy $U \sim \hbar^2 a_s n/m$. Typical scattering lengths are $a_s = -1.45\,\text{nm}$ for ^{7}Li and $a_s = -20\,\text{nm}$ for ^{85}Rb. In Fig. 1.8, I plot the total energy $E \equiv K + U + V$ as a function of L for different values of $N_0|a_s|$. In the absence of interactions, E has an absolute minimum at $L = d$, where $d = (\hbar/m\omega)^{1/2}$ is the characteristic length scale of the harmonic trap. Adding weak interactions causes the global minimum of E to move to $L = 0$ but a local minimum remains near $L = d$. This local minimum signifies that a metastable condensate can exist. The barrier separating the two minima has a maximum near $L = |a_s N_0|$. When $|a_s N_0|$ is of order d the local minimum disappears and the cloud becomes strictly unstable. Thus for a given a_s and d there is a maximum number of particles which can be in the condensate. More sophisticated calculations [26, 27] show that the point of instability is given by

$$N_0 = N_{\text{max}} = 0.575 d/|a_s|. \tag{1.1}$$

In Li experiments [24], where $d \approx 1\mu$m this maximum is of order $N_{\text{max}} \approx 1000$.
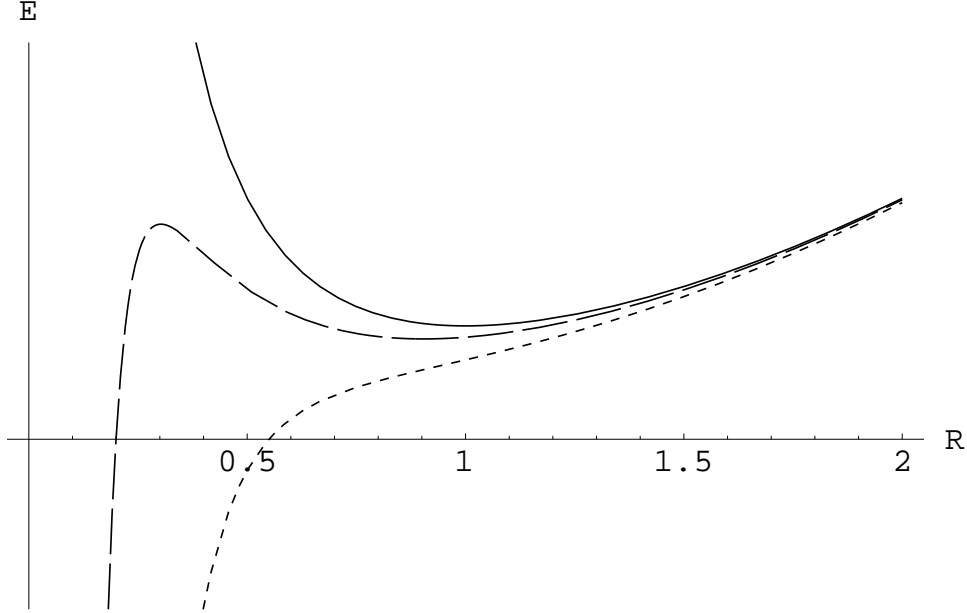
Figure 1.8: Energy E of a condensate of size L (measured in units of the trap size $d = (\hbar/m\omega)^{1/2}$) with attractive interactions $a_s < 0$. Solid – noninteracting ($N|a_s|/d = 0$), long dashes – $N|a_s| \approx d/5$, short dashes – $N|a_s| \gg d$. These curves are based upon the simple dimensional estimates described in section 1.2.5.

Experimentally, this instability is observed in one of two ways. First, images of clouds of Li atoms never show more than $N_{\text{max}} \approx 1000$ particles in the condensate

[24]. Second, by using Feshbach resonances,[2] the scattering length a_s of ^{85}Rb atoms can be tuned from positive to negative. With $a_s > 0$, a stable condensate is formed. The scattering length is then gradually reduced until collapse occurs [25], and one finds, as expected, that $N_{\max} \propto 1/|a_s|$.

1.2.6 Spin relaxation

A very rich class of phenomena involve the hyperfine spin of a gas of alkali atoms. The spin degree of freedom is frozen in magnetic traps, but can be accessed in optical traps. In Section 5.6 I give a theoretical explanation of one experiment on spinor condensates [9]. In this experiment a spinor cloud with ferromagnetic interactions is placed in a state in which the magnetization is everywhere zero. This is an excited state of the system and it relaxes to a state which is locally magnetized. Since magnetization is conserved during the dynamics, a domain structure is formed where each region is polarized in a different direction. In Section 5.6 I only discuss the stability of the initial state. The formalism of Chapter 6 can be used to describe the actual dynamics of the domain formation.

1.2.7 Electromagnetically induced transparency

In experiments at Rowland Institute [11] and at Harvard [12], experimentalists have used a cold atomic gas as a nonlinear media to manipulate light. Their most striking achievements have involved actually freezing a beam of light for several milliseconds. I discuss the theory in Chapter 7. The basic idea is that light couples polarization waves in an atomic gas. The small velocities of these polarization waves are inherited by the hybridized excitations, and the light therefore propagates very slowly through the media. Stopping the light involves adiabatically transforming the photons into polarons, then reversing the process several milliseconds later.

1.2.8 Feshbach resonance

In recent experiments, experimentalists demonstrated the ability to tune the interaction strength of a dilute gas [28]. This technique is used to explore the collapse of attractive gases (see section 1.2.5). The interactions are controlled by using magnetic fields to adjust the energy of a scattering resonance, bringing it near threshold. Scat-

---

[2]Feshbach resonances are magnetically induced scattering resonances, and are discussed in appendix F on page 183

tering resonances are discussed in detail in appendix F, where the general theory of atomic scattering is reviewed.

It would be extremely exciting to use this technique to study the highly correlated state of matter that would be formed when the interactions are made very strong. In particular one could study a regime where there is a distinct separation of length scales, with the scattering length a_s much larger than the interparticle spacing $n^{-1/3}$, which in turn is much larger than the physical size of the atom. In such a limit one expects both the scattering length and the size of the atom to drop out of the problem, and a gas of such atoms should behave in some universal manor. Experiments in this regime have been hampered by large inelastic losses which are not fully understood.

Chapter 2

Theory of the BEC Phase Transition

The dominant feature in the thermodynamics of cold Bose gases is the presence of a phase transition to a Bose condensed state where a single-particle level is macroscopically occupied. Although Bose-Einstein condensation was predicted in 1925 [29], some aspects of the phase transition have only recently been understood. In particular, it was not until the path integral Monte-Carlo calculations of Grüter, Ceperley and Laloë [30] that the influence of interactions on the phase transition of a uniform Bose gas was systematically explored.[1] Their results, plotted in Fig. 2.1, show that for small interaction strength the critical temperature increases with interactions, while for larger interactions the opposite behavior occurs. The drop in T_c can be qualitatively understood as an effective mass effect. An atom moving through the fluid must drag other atoms with it, giving it a larger effective mass. Since $T_c \propto m^{-1}$, the critical temperature is reduced.

The weakly interacting case has only recently been understood analytically [32, 33]. An intuitive argument is that repulsive interactions reduce density fluctuations and therefore increase the occupation of the $k = 0$ mode, raising T_c. Quantifying this argument is difficult, and the calculations of T_c [32, 33] rely upon very mathematical arguments whose physical interpretations are not directly evident.

Here I use a novel approach to calculating the change in T_c, based upon perturbation theory in powers of the interaction. One cannot directly use perturbation theory to calculate T_c since the perturbation series suffers from infrared divergences

---

[1]As the phase transition temperature is of fundamental importance, many earlier works discussed this topic [31], but the first systematic and authoritative review of the subject was due to Grüter, Ceperley, and Laloë.
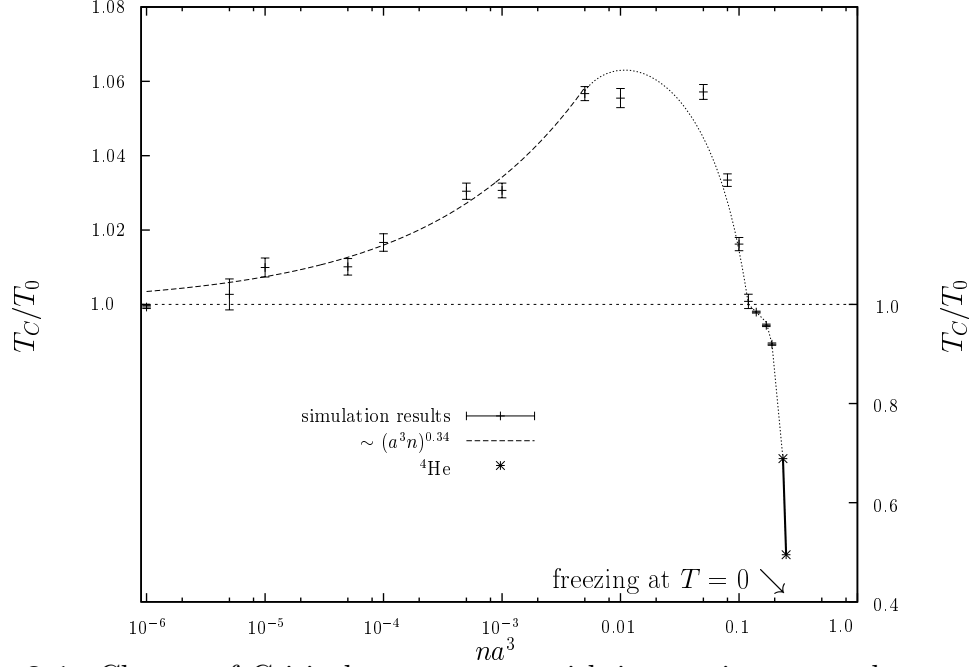
Figure 2.1: Change of Critical temperature with interaction strength, reproduced with permission from [30]. For $na^3 < 0.01$ the transition temperature increases with interaction strength, while for larger na^3 the opposite occurs. The apparent discontinuity of the slope at $na^3 \approx 0.1$ is an artifact of using a different scale for $\Delta T > 0$ and $\Delta T < 0$. The dashed line is a power-law fit to the small na^3 data, and the dotted line is a guide to the eye. In this chapter I discuss the regime where $na^3 \ll 1$.

at the critical point. These divergences are a common feature of second order phase transitions where long wavelength properties dominate the behavior of the system. I avoid these singularities by working in small systems where the finite system size provides a low energy cutoff. Studying the scaling properties of these small systems reveals the phase transition temperature.

Although this discussion of the phase transition of a uniform system is of extreme fundamental importance, it is not particularly relevant to experiments on trapped atoms. In a harmonic trap the dominant shift in the transition temperature is due to the way in which interactions change the shape of the cloud. This shift is describable within mean field theory, and has been experimentally verified [34].

This Chapter is organized as follows. First I review the elementary text-book level description of Bose-Einstein condensation. Next I look at finite size effects, and investigate scaling in small systems. I then combine these results with perturbation theory to calculate the first order shift in the critical temperature ΔT. Finally I give a brief calculation of the shift in a harmonically trapped cloud. The work presented in this Chapter was performed in collaboration with Gordon Baym and Markus Holzmann, and has been accepted for publication [35].

2.1 Elementary description

To preface my discussion of the phase transition, I give an elementary review of Bose condensation in an ideal gas [4] in the grand canonical ensemble. I begin by considering a cloud of non-interacting Bosons in an external potential. Special consideration is given to the case where the particles are in a box of volume V with periodic boundary conditions, and the case of a harmonic trap.

All thermodynamic quantities are determined by the grand free energy $\mathcal{F}$, defined in terms of the grand partition function,

$$\mathcal{Z} = e^{-\beta \mathcal{F}} = \text{Tr}\, e^{-\beta(H-\mu N)}, \tag{2.1}$$

where $\beta = 1/k_B T$, H is the Hamiltonian operator, μ is the chemical potential, N is the number operator, and the trace is taken over all possible states of the system with any possible number of particles. I will use units where Boltzmann's constant k_B, is equal to unity. As we are dealing with non-interacting particles, the states are defined by occupation numbers n_i, corresponding to the single particle energy levels

ε_i. The trace is explicitly written as

$$\mathcal{Z} \;=\; \sum_{\{n_i\}} e^{-\beta \sum_i (\epsilon_i - \mu) n_i}, \tag{2.2a}$$

$$=\; \prod_i \frac{1}{1 - e^{-\beta(\epsilon_i - \mu)}}, \tag{2.2b}$$

which implies that the free energy has the form

$$\mathcal{F} \;=\; -T \sum_i \log\left(1 - e^{-\beta(\varepsilon_i - \mu)}\right). \tag{2.3}$$

To extract the structure of this free energy, I introduce the density of states

$$\rho(E) = \sum_i \delta(E - \varepsilon_i). \tag{2.4}$$

Near the phase transition, infrared modes dominate the sum (2.3). Looking at this low energy sector of Eq. (2.3), one can approximate $\log(1 - e^{-\beta(E-\mu)}) \approx \log(\beta E - \beta\mu)$, yielding a free energy

$$\mathcal{F} \;\approx\; T \int_0^{E_c} dE\, \rho(E)\, \left[\log(\beta E) + \log(1 - \mu/E)\right]. \tag{2.5}$$

The cutoff, E_c, eliminates the high energy modes which are not correctly accounted for by this approximation. In the exact expression (2.3), the temperature plays the role of this cutoff;, thus E_c should be of order $k_B T$. The phase transition occurs at $\mu = 0$, where either $\mathcal{F}$, or one of its derivatives is singular. Assuming a power law density states, $\rho(E) \sim E^\alpha$ as $E \to 0$, the k'th derivative $\partial^k \mathcal{F}/\partial \mu^k$ is singular for all $k \geq \alpha$. Since $N = \partial \mathcal{F}/\partial\mu$, there exists a phase transition at finite density if and only if $\alpha > 1$.

For example, particles in d-dimensional free space have a power-law density of states satisfying $\alpha = d/2 - 1$, and Bose condensation occurs in all dimensions greater than 2. For harmonically trapped particles, $\alpha = d - 1$, and Bose condensation occurs in all dimensions greater than 1. In the following two subsections I explicitly calculate the transition temperature in each of these examples.

2.1.1 Uniform gas

Most elementary textbooks, e.g. [4], describe the Bose condensation transition of particles in a box of size L with periodic boundary conditions, where the single-particles energies are $\varepsilon = (2\pi^2\hbar^2/mL^2)(n_x^2 + n_y^2 + n_z^2)$, with $n_\nu = 0, \pm 1, \pm 2, \ldots$, and

m is the particle mass. To calculate the free energy it is convenient to expand the logarithm in (2.3) and write the free energy as

$$\mathcal{F} = T \sum_{j=1}^{\infty} \frac{1}{j} \sum_i e^{-\beta j (\varepsilon_i - \mu)}. \tag{2.6}$$

Ignoring the discrete nature of the spectrum at hand, one finds

$$\mathcal{F} \;=\; -T \sum_j \frac{z^j}{j} \left(\int dn \, e^{-\beta j \left(\frac{2\pi^2 \hbar^2}{mL^2} \right) n^2} \right)^3, \tag{2.7a}$$

$$\;=\; -T \frac{V}{\lambda^3} \sum_j \frac{z^j}{j^{5/2}}. \tag{2.7b}$$

Here I have introduced the fugacity $z = e^{\beta \mu}$ and the thermal wavelength $\lambda = (2\pi \hbar^2 \beta / m)^{1/2}$. The series $g_\nu(z) = \sum_j z^j / j^\nu$ is known as either a "Bose" function, or a polylogarithm. The latter name reflects the fact that $g_1(z) = -\log(1 - z)$. These functions are discussed at length in Appendix A.1. Replacing the sum over n with an integral is equivalent to replacing the discrete density of states with a smooth function $\rho(E) \propto E^{1/2}$.

To calculate the number of particles one differentiates (2.7b) to find

$$N = -\frac{\partial \mathcal{F}}{\partial \mu} = \frac{V}{\lambda^3} g_{3/2}(z), \tag{2.8}$$

which is bounded above by $N_c = V/\lambda^3 \zeta(3/2)$, where $\zeta(3/2) = g_{3/2}(1) \approx 2.61 \ldots$ is the Riemann zeta function. Thus this semiclassical approximation is incapable of describing a Bose gas at a temperature below

$$T_c = \frac{2\pi}{mk_B} \left(\frac{n}{\zeta(3/2)} \right)^{2/3}. \tag{2.9}$$

This approximation breaks down because the lowest energy state becomes macroscopically occupied below T_c. By removing this one state from the integral one avoids this problem, finding

$$\mathcal{F} \;=\; T \log(1 - z) - T \frac{V}{\lambda^3} \sum_j \frac{z^j}{j^{5/2}}. \tag{2.10}$$

Unless $|\beta \mu| < \lambda^3 / V$, the first term in negligible compared to the latter. Within this extended theory,

$$N \;=\; \frac{z}{1 - z} + \frac{V}{\lambda^3} g_{3/2}(z). \tag{2.11}$$

22

We now take the thermodynamic limit $N \to \infty$, and $V \to \infty$, with $n = N/V$ fixed. If $n < \zeta(3/2)/\lambda^3$ the thermodynamic limit is reached at fixed z, and the density is given by Eq. (2.8). If $n > \zeta(3/2)/\lambda^3$, one must scale z with the system volume such that $\beta\mu \sim V^{-1}$ as $V \to \infty$, giving for $T < T_c$,

$$\bar{n} = \bar{n}_0 + \zeta(3/2)/\lambda^3, \tag{2.12}$$

where $\bar{n}_0 = \bar{N}_0/V = (-\beta\mu V)^{-1}$ is the density of condensed particles.

2.1.2 Harmonically trapped gas

As discussed in Section 1.2, in recent experiments the particles are trapped in harmonic potentials $V(r) = m\Omega^2 r^2/2$. The energy levels in a harmonic trap are of the form $\varepsilon_i = \hbar\Omega(n_x + n_y + n_z + 3/2)$, where $n_\nu = 0, 1, 2, \ldots$. The zero point energy $(3/2)\hbar\Omega$ plays no role in the following arguments and I will neglect it. The free energy of the harmonically trapped gas has the same structure as the gas in free space, and I jump to the equivalent of Eq. (2.10),

$$\mathcal{F} = T\log(1-z) - T\sum_j \frac{z^j}{j}\left(\int_0^\infty dn\, e^{-\beta\hbar\Omega nj}\right)^3, \tag{2.13a}$$

$$= T\log(1-z) - \frac{T}{(\beta\hbar\Omega)^3}\sum_j \frac{z^j}{j^4}, \tag{2.13b}$$

giving a mean number of particles,

$$\bar{N} = \frac{z}{1-z} + \frac{1}{(\beta\hbar\Omega)^3}g_3(z). \tag{2.14}$$

In the trap, the thermodynamic limit is approached by letting $N \to \infty$ and $\Omega \to 0$ such that $\Omega^3 N$ is constant, which keeps constant the density at the center of the trap. As in the analysis of Eq. (2.11), at fixed z the number of particles is bounded by $\bar{N} \leq \zeta(3)/(\beta\hbar\Omega)^3$, equality representing the Bose-Einstein condensation phase transition. If one treats the $\mu \to 0$ limit in a similar fashion to Section 2.1.1 one finds for $T < T_c$,

$$\bar{N} = \bar{N}_0 + \frac{\zeta(3)}{(\beta\hbar\Omega)^3}. \tag{2.15}$$

2.2 Finite size effects

Although statistical mechanics tells us that there are no phase transitions in finite systems, we apparently see phase transitions all around us. Conventionally, this contradiction is resolved by stating that the finite system possesses a crossover between

two distinct behaviors. As the system size increases, the crossover becomes sharper and mimics a phase transition.

A rather sophisticated understanding of finite size effects comes from studying the renormalization group [36]. In these studies, one imagines an abstract space parameterized by all the possible couplings which could exist in the model being studied – for instance temperature, interaction strength, and system size. The renormalization group (RG) is a mapping of this space onto itself where each model is coarse grained and reduced in scale. Under this mapping, systems will flow to various fixed points. Each stable fixed point represents a different phase of matter. Critical points are associated with unstable fixed points – the system flows in different directions depending upon which side of the critical point it starts on. A schematic depiction of the RG flow for a Bose gas is portrayed in Fig. 2.2, where two of the couplings, the temperature and the system size, are shown. Two fixed points are depicted, the critical fixed point and a low temperature fixed point corresponding the the Bose condensed phase. A few sample flow lines are drawn as well as two regions, a critical region and a finite size scaling region, both of which are discussed below.

In this thesis I do not calculate any RG flows, however I will use one of the generic results; namely that if a system is in the critical region near a fixed point, its behavior is dominated by that fixed point, and physical quantities obey a set of scaling relationships. In particular, the finite size scaling hypothesis holds. This hypothesis states that all physical quantities scale as functions of the ratio of the correlation length ξ to the system size L. The correlation length ξ is a measure of the fall off of the two-point function $\langle \psi^\dagger(r)\psi(0)\rangle$, and diverges at the critical point. An example of this scaling is the prediction that the number of condensed particles should scale as

$$\frac{\langle N_0\rangle}{V} \sim L^{-y}\Phi(L/\xi), \tag{2.16}$$

where $y = \beta/\nu = 1$ is the ratio of the critical exponents for N_0/V and the correlation length, and Φ is a scaling function. As $L/\xi \to \infty$, this function must diverge as $\Phi(L/\xi) \sim (L/\xi)^y$, while as $L/\xi \to 0$, Φ approaches a constant. The region where $L << \xi$ is the finite size scaling regime, and the scaling law (2.16) can be used to systematically find the critical point ($\xi \to \infty$) by looking solely at the properties of a finite system.

As an example of using Eq. (2.16) to find the critical point, consider the numerical calculations of Grüter et al. [30] discussed in the introduction of this Chapter. In that calculation, the authors used a Monte-Carlo technique to find the superfluid density ρ_s (which on dimensional grounds scales as N_0/V) as a function of temperature and
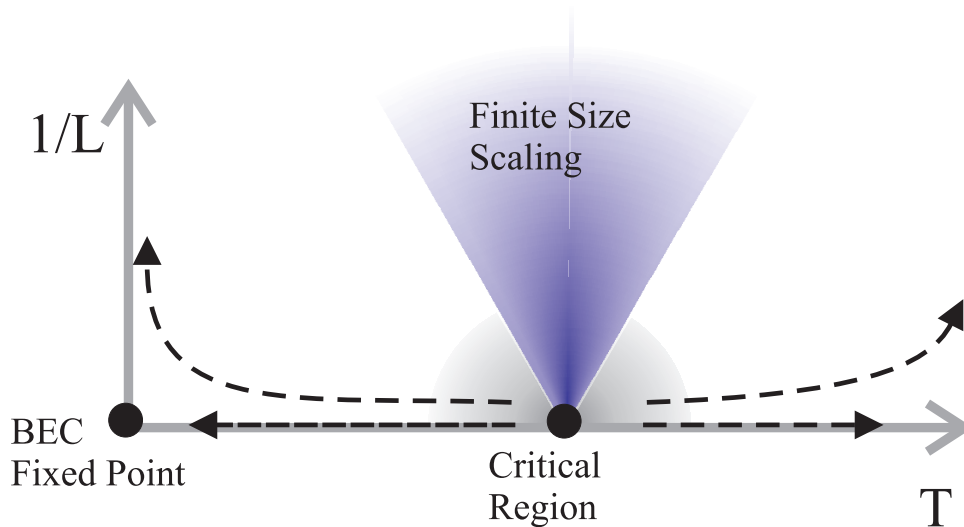
Figure 2.2: Schematic renormalization group flow diagram for a Bose gas. Points on this graph represent Bose gases of a given temperature T and system size L. The dashed arrows show how a system changes under the renormalization group – a coarse graining and rescaling procedure. Two fixed points of this operation are shown as large dots; the critical point and the BEC fixed point. A critical regime, where physical quantities obey power law scaling relationships is shown. Also depicted is the finite-size scaling regime where the coherence length is large compared to the system size, $\xi \gg L$. In this regime the finite size scaling laws apply.

system size for various small systems. Curves of $L^y \rho_s$ as a function of temperature for different L all crossed at a temperature T_*. According to Eq. (2.16) this is the temperature at which the coherence length diverges, which is by definition the critical temperature.

In the following sections I use elementary means to explicitly verify the scaling relation (2.16) for the non-interacting gas. I then use this relationship to calculate the phase transition temperature of an interacting gas.

2.2.1 Scaling in the ideal gas

Here I identify the BEC phase transition in a non-interacting gas from the scaling of the number of condensed particles. This simple example illustrates the technique which I use to calculate T_c for the interacting system. I first perform this calculation in the grand canonical ensemble, and then in the canonical ensemble. In the presence of a condensate the thermodynamics of an ideal gas are sensitive to the ensemble used. This sensitivity is demonstrated by looking at the distribution function $P(N_0)$ for the number of condensed particles. Within the grand canonical ensemble, $P(N_0) \propto$

$e^{-\beta(\varepsilon_0-\mu)N_0}$, is exponentially decaying at all temperatures. On the other hand, at zero temperature in the canonical ensemble, $P(N_0) = \delta_{N,N_0}$ is a delta function, as all of the particles are in the condensate. Thus $P(N_0)$, a macroscopic observable, behaves qualitatively differently depending on the ensemble. Any observable which depends on fluctuations in the number of condensed particles (like the compressibility) will likewise be sensitive to the ensemble.

Despite these differences, the phase transition temperature is expected to be independent of the ensemble. It turns out that it is easier to perturbatively calculate ΔT within the canonical ensemble than within the grand canonical ensemble.

Grand canonical results

Here I calculate the phase transition temperature of the ideal gas within the grand canonical ensemble. My general strategy is to fix the average density $n = N/V$ and the temperature T, and look at how the number of condensed particles N_0 varies with the system size L. To carry out this approach one needs an expression for the chemical potential μ as a function of n, T, and L; requiring that one inverts Eq. (2.11). The inversion is performed by expanding (2.11) in powers of $\beta\mu$. Using the expansion of the polylogarithm given in Appendix A.1, one finds

$$n = \frac{1}{\lambda^3}\left[\zeta(3/2) + \frac{\lambda}{L}\left(-\frac{1}{\beta\mu L^2/\lambda^2} - 2\sqrt{-\pi\beta\mu L^2/\lambda^2}\right) + \cdots\right]; \qquad (2.17)$$

the neglected terms are of higher order in $\beta\mu$, and are negligible near the transition temperature as long as $N \gg 1$. The terms proportional to $1/\beta\mu$ and $\sqrt{-\beta\mu}$ are respectively the contributions from the condensed and non-condensed particles. Finding $\beta\mu$ as a function of n, T, and L, requires solving a cubic equation. I define the function $F(x)$, plotted in Fig. 2.3, as the solution to

$$\frac{1}{F(x)} - 2\sqrt{\pi F(x)} - x = 0, \qquad (2.18)$$

so that the chemical potential can be expressed as,

$$\beta\mu = -\frac{\lambda^2}{L^2}F\left(\frac{L}{\lambda}\left(\lambda^3 n - \zeta(3/2)\right)\right). \qquad (2.19)$$

The positive, monotonic $F(x)$ has the properties

$$F(0) = (4\pi)^{-1/3} \qquad (2.20)$$

$$F(x) \xrightarrow[x\to-\infty]{} x^2/4\pi \qquad (2.21)$$

$$F(x) \xrightarrow[x\to+\infty]{} 1/x. \qquad (2.22)$$

26

Thus, as $L \to \infty$, the order parameter $N_0 \approx -1/\beta\mu$, has three distinct behaviors, corresponding to non-condensed, critical, and condensed regimes, depending on whether n is less than, equal to, or greater than $\zeta(3/2)/\lambda^3$. In the non-condensed regime, N_0 is microscopic, in the condensed regime, N_0 is extensive, and at the critical temperature, N_0 scales as L^2, i.e.,

$$n < \zeta(3/2)/\lambda^3, \qquad N_0 \sim L^0 \tag{2.23}$$

$$n = \zeta(3/2)/\lambda^3, \qquad N_0 \sim L^2 \tag{2.24}$$

$$n > \zeta(3/2)/\lambda^3, \qquad N_0 \sim L^3. \tag{2.25}$$
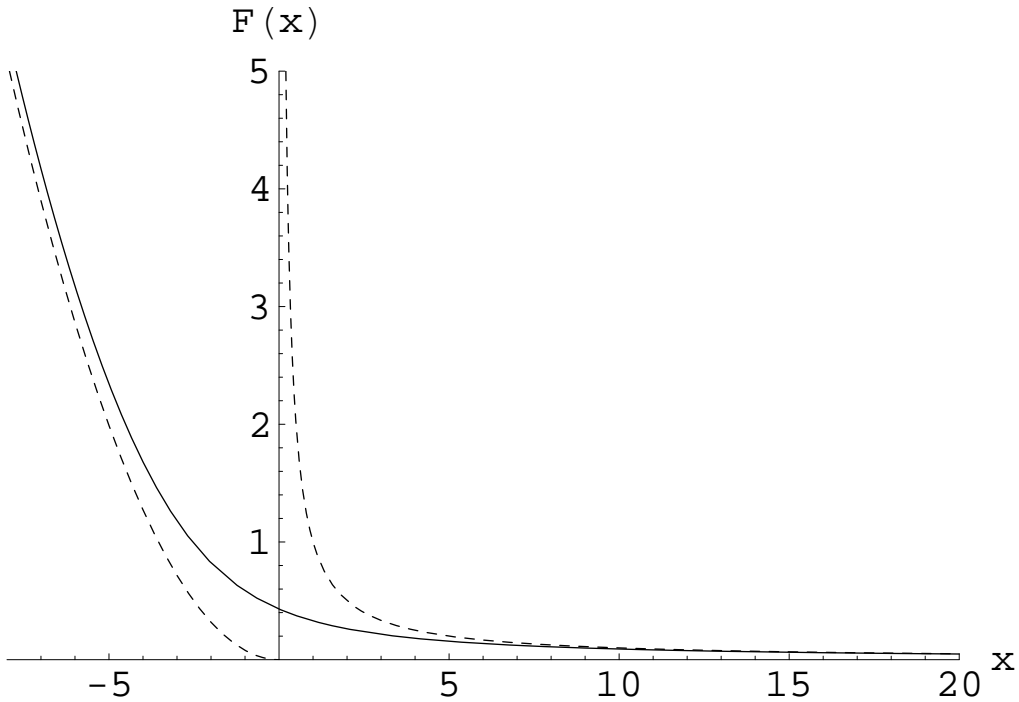
Figure 2.3: The function $F(x)$, defined as the solution to Eq. (2.18), which relates the chemical potential and density of a non-interacting Bose gas via Eq. (2.19). The asymptotic expressions (2.21) and (2.22) are plotted as dashed lines.

This scaling behavior is illustrated by Fig. 2.4, which shows the condensate fraction N_0/N as a function of N for different values of the reduced temperature $t = T/T_c$. The various power laws can be read directly from the graph. Note that for small N, the critical regime where $N_0 \sim N^{2/3}$ has a finite width. This width is estimated by linearizing the chemical potential (2.19) about the point $n = \zeta(3/2)/\lambda^3$ to find

$$N_0 = \frac{L^2}{\lambda^2}(4\pi)^{1/3} + \frac{L^3}{\lambda^3}\frac{2}{3}\left(\lambda^3 n - \zeta(3/2)\right) + \frac{L^2}{\lambda^2}\mathcal{O}\left(\frac{L}{\lambda}(\lambda^3 n - \zeta(3/2))\right)^2. \tag{2.26}$$

27

The number of condensed particles scales as L^2 over a temperature range $\delta T/T_c \approx \lambda/L$, and then crosses over to the asymptotic behavior described in Eqs. (2.23) and (2.25).
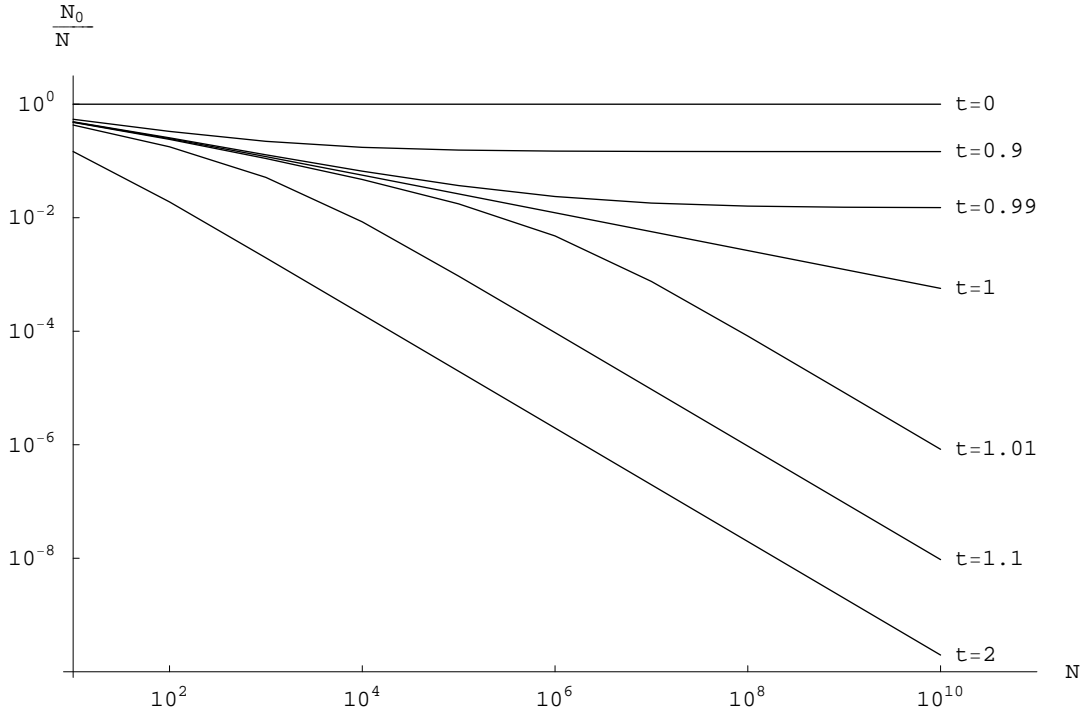
Figure 2.4: Condensate fraction N_0/N versus N for various values of the reduced temperature $t = T/T_c$. The three scaling regimes for $t < 1$, $t = 1$, and $t > 1$, correspond to the condensed, critical, and non-condensed regimes, in which $N_0 \sim N$, $N_0 \sim N^{2/3}$, and $N_0 \sim N^0$.

2.2.2   Scaling in the canonical ensemble

I now repeat the calculation of Section (2.2.1) in the canonical ensemble. As previously mentioned, in the presence of the condensate, thermodynamic properties of an ideal Bose gas are sensitive to the ensemble used.

In this section I look at scaling in $P(N_0)$ rather than just at N_0, as was done in Section (2.2.1). Generalizing Eq. (2.16), one expects that at T_c the probability distribution function can be written as

$$P(N_0) = \frac{\lambda^2}{L^2}\psi(N_0\lambda^2/L^2),\tag{2.27}$$

with some scaling function ψ. As I demonstrate here, this relationship holds for the non-interacting gas.

The canonical distribution function can be expressed as

$$P(N_0) = \frac{1}{Z_N} \underset{N,N_0 \text{ fixed}}{\text{Tr}} e^{-\beta H} = \frac{1}{Z_N} e^{-\beta F(N,N_0)}, \tag{2.28}$$

where the trace is taken at fixed N and N_0, and β is the inverse temperature. This equation defines the free energy $F(N, N_0)$, and uses the partition function, $Z_N = \sum_{N_0} e^{-\beta F(N,N_0)}$, to normalize the probability distribution. In the non-interacting gas, $F(N, N_0)$ is only a function of $N_{\text{ex}} = N - N_0$ and is identifiable as the free energy of the non-condensed particles,

$$F(N, N_0) = F_{\text{ex}}(N_{\text{ex}}). \tag{2.29}$$

Although the condensate's behavior depends crucially on the ensemble, one expects that the properties of the non-condensed particles will be insensitive to the ensemble, and one should be able to calculate F_{ex} via a Legendre transformation of the grand free energy,

$$F_{\text{ex}}(N_{\text{ex}}) = \mathcal{F}_{\text{ex}}(\mu(N_{\text{ex}})) + \mu(N_{\text{ex}})N_{\text{ex}}, \tag{2.30}$$

where $\mu(N_{\text{ex}}) = \partial F_{\text{ex}}/\partial N_{\text{ex}}$ is a chemical potential which represents the free-energy cost of exchanging particles between the condensate and the non-condensed particles. Intuitively, the condensate acts as a particle bath for the non-condensed system. The chemical potential varies with N_{ex} since as one depletes the condensate the cost of removing particles from the condensate changes.

As in Section 2.2.1, I need to relate N_{ex} and μ. The approximation of Eq. (2.17) is not sufficient, since I will need to take the limit $\mu \to 0$. The relevant asymptotics are evaluated in Appendix B, where according to Eq. (B.13), μ and N_{ex} are related by

$$N_{\text{ex}} = f_1 = \left(\frac{L}{\lambda}\right)^3 \zeta(3/2) + \left(\frac{L}{\lambda}\right)^2 h\left(\frac{\beta\mu L^2}{\lambda^2}\right) + \mathcal{O}(L/\lambda), \tag{2.31}$$

$$h(x) = \sum_{k=0}^{\infty} \frac{x^k}{k!} C_3(k+1). \tag{2.32}$$

The coefficients $C_3(k+1)$ are tabulated in Table. B.1. Inverting the series, and replacing N_{ex} with $N - N_0$ gives

$$\beta\mu = \frac{\lambda^2}{L^2}\left(-\frac{1}{C_3(2)}M - \frac{C_3(3)}{2(C_3(2))^2}M^2 + \cdots\right), \tag{2.33}$$

$$M = N_0\frac{\lambda^2}{L^2} + C_3(1) - \frac{\lambda^2}{L^2}\left(N - \frac{L^3}{\lambda^3}\zeta(3/2)\right), \tag{2.34}$$

29

from which the free energy is

$$\beta F(N, N_0) = -\int dN_0 \,(\beta\mu) \tag{2.35}$$

$$= \beta\bar{F}(N) + \frac{1}{2C_3(2)}M^2 + \frac{C_3(3)}{6(C_3(2))^2}M^3 + \cdots \tag{2.36}$$

$$\equiv \beta\bar{F}(N) + g(M), \tag{2.37}$$

where $\bar{F}(N)$ is an extensive function which is independent of N_0, and $g(M)$ is defined by Eqs. (2.36,2.37). If $n = N/V = \zeta(3/2)/\lambda^3$, then M depends on L only through the variable $N_0\lambda^2/L^2$, implying that $P(N_0)$ is of the form

$$P(N_0) = \frac{\lambda^2}{L^2}\psi(N_0\lambda^2/L^2), \tag{2.38}$$

where the scaling function ψ is found by exponentiating (2.35). For any other value of the density, M has additional L dependence, and $P(N_0)$ does not scale like (2.38), implying that the scaling holds only at T_c. In Fig. 2.5 I plot $P(N_0)$ at the critical point. The Gaussian approximation, where only the term proportional to M^2 is kept, is also plotted, and agrees quite well with the full result.
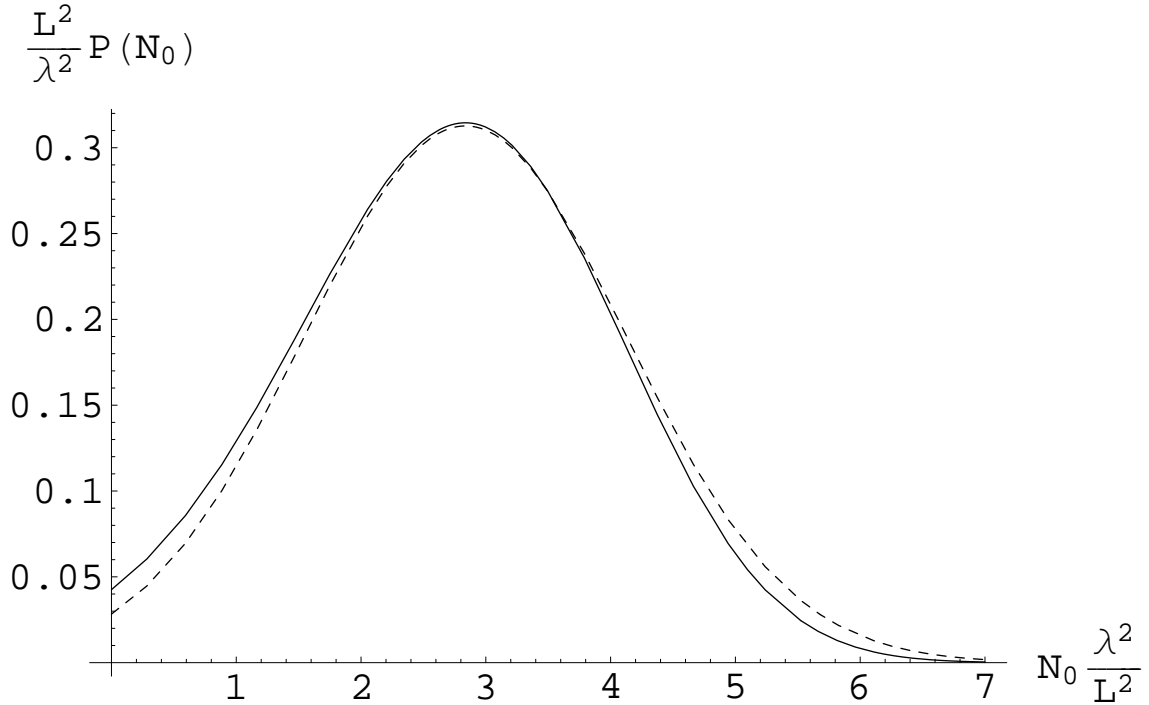
Figure 2.5: Probability distribution $P(N_0)$ for the number of condensed particles at the critical temperature in a non-interacting Bose gas within the canonical ensemble. Dashed line is a Gaussian approximation. At the critical point, P has the scaling form (2.38).

2.3   Perturbative calculation of ΔT.

In this section I use first order perturbation theory to calculate the critical temperature of a weakly interacting Bose gas. In Section 2.3.1 I present the structure of perturbation theory, demonstrating that due to infrared divergences it breaks down in the thermodynamic limit. In Section 2.3.2 I use the techniques of Section 2.2.2 to circumvent these difficulties and calculate the transition temperature.

Here I work in the canonical ensemble. Within the grand canonical ensemble, first order perturbation theory changes the energy of each momentum state by the same amount. This shift can therefore be absorbed into the chemical potential, leaving the transition temperature unchanged. The first effects start at higher order; exploring how higher order perturbation theory in conjunction with finite size scaling can be used to calculate the shift of T_c in the grand canonical ensemble is beyond the scope of this thesis.

2.3.1   Perturbation theory

A cloud of bosons that interact through a short range potential is described by a Hamiltonian

$$H = \sum_q \frac{\hbar^2 q^2}{2m} b_q^\dagger b_q + H_{\text{int}}, \tag{2.39}$$

where

$$H_{\text{int}} = \frac{2\pi\hbar^2 a_s}{mV} \sum_{\mathbf{pkq}} b_p^\dagger b_q^\dagger b_{q-k} b_{p+k}, \tag{2.40}$$

and a_s is the scattering length, b_q is the annihilation operator for particles with momentum q, m is the particle mass, and $V \equiv L^3$ is the volume of the system.

As in Section 2.2.2, the function of interest is the probability distribution for the number of condensed atoms. $P(N_0) \propto e^{-\beta F(N,N_0)}$. Expanding $F(N, N_0)$ to first order in the interaction,

$$F(N, N_0) = F_0(N, N_0) + \langle H_{\text{int}} \rangle_{N,N_0}, \tag{2.41}$$

where the expectation value is in the *free* ensemble, and $F_0 \equiv F(a = 0)$ is the free energy of the non-interacting system.

It is straightforward to calculate $\langle H_{\text{int}} \rangle$ using the approximation of Section 2.2.2. The expectation value involves the sum

$$\sum_{pqk} \langle b_p^\dagger b_q^\dagger b_{q-k} b_{p+k} \rangle = 2N^2 - \sum_p \langle N_p(N_p + 1) \rangle, \tag{2.42}$$

31

where $N_p = b_p^\dagger b_p$. Using the assumption that for a fixed N_0 the non-condensed particles are grand-canonically distributed,

$$\sum_p \langle N_p(N_p + 1)\rangle = N_0(N_0 + 1) + \frac{\partial N_{\text{ex}}}{\partial \mu_{\text{ex}}}. \tag{2.43}$$

At T_c, each of these terms scale as $(L/\lambda)^4$. The first order correction to $F(N, N_0)$ therefore scales as

$$\Delta F(N, N_0) \sim k_B T\, a_s L/\lambda^2 \equiv k_B T\, \eta, \tag{2.44}$$

which defines η. Higher order terms in the expansion of the free energy involve additional powers of βH_{int}. Successive terms are of relative size $\langle (\beta H_{int})^m \rangle / \langle (\beta H_{int})^{m-1} \rangle \sim \eta$. Thus the perturbation expansion is valid only for sufficiently small η. Since η involves the product $a_s \times L$, the limits $a_s \to 0$ and $L \to \infty$ are not interchangeable.

2.3.2 Calculation of ΔT

Here I calculate ΔT, the interaction induced change in T_c. My strategy is to find the temperature at which the first order expression (2.41) has the scaling form (2.27). This temperature should be close to the transition temperature of the ideal gas $T_c^{(0)}$, so I write, $T = T_c^{(0)} + \Delta T$, and expand to first order in ΔT. The resulting expression is

$$\beta F(N, N_0, T) = \beta F_0(T_c^{(0)}) + \Delta T \frac{\partial F_0}{\partial T} + \Delta F(T_c^0), \tag{2.45}$$

where for clarity I have omitted the arguments N and N_0 on the right hand side. The first order correction ΔF is given in Eq. (2.41). If one substitutes Eq. (2.36) for F_0, this free energy can be expressed as

$$\beta F(N, N_0, T) = \beta \bar{F}_0 + g(M_0) - \frac{\Delta T}{T}\frac{\lambda^2}{L^2}N_0 g'(M_0) \tag{2.46}$$

$$+ \frac{3}{2}\frac{\Delta T}{T}\frac{L}{\lambda}\zeta(3/2)g'(M_0) - \frac{2\pi\hbar^2 a_s}{mVT}\left(N_0^2 + 2\sum_{k\neq 0} N_k(N_k + 1)\right),$$

where the argument $M_0 = N_0(\lambda^2/L^2) + C_3(1)$ is the scaled condensate number measured from the peak of the distribution. The first two terms are the free energy of the non-interacting gas at $T_c^{(0)}$, while the remaining terms give the first order corrections in ΔT and a_s. These corrections are only small if $\eta = a_s L/\lambda^2 \ll 1$. The sum $\sum_{k\neq 0} N_k(N_k + 1)$ can be identified with $\partial N_{\text{ex}}/\partial(\beta\mu_0)$, and expressed as a series in

$\beta\mu_0 L^2/\lambda^2$ via Eq. (2.31). Equation (2.33) can be used to eliminate μ, yielding,

$$
\begin{aligned}
F(T) \;=\; & F_0(T_c^{(0)}) - \frac{\Delta T}{T}\frac{\lambda^2}{L^2}N_0 g'(M_0) \\
& + \frac{L}{\lambda}\left[\frac{3\zeta(3/2)}{2}\frac{\Delta T}{T}\left(\frac{1}{C_3(2)}M_0 + \frac{C_3(3)}{2C_3(2)^2}M_0^2 + \cdots \right)\right. \\
& - \frac{2\pi\hbar^2 a_s}{m\lambda^3 T}\left(C_3(1)^2 + 2C_3(2) - 2\left(C_3(1) + \frac{C_3(3)}{C_3(2)} \right)M_0 \right. \\
& \left.\left. + \left(1 + \frac{C_3(2)C_3(4) - C_3(3)^2}{C_3(2)^3} \right)M_0^2 + \cdots \right)\right].
\end{aligned}
\tag{2.47}
$$

Scaling of the form in Eq. (2.27) holds if and only if the factor multiplied by L/λ is independent of M_0. Eliminating the coefficient of the first power of M_0 enforces scaling near the peak of $P(N_0)$, in which case

$$
\frac{\Delta T}{T} \;=\; -\frac{8\pi\hbar^2 a_s}{3m\lambda^3 T\zeta(3/2)}\left(C_3(1)C_3(2) + C_3(3) \right)
\tag{2.48}
$$

$$
\approx\; 1.6a_s n^{1/3}.
\tag{2.49}
$$

The coefficient 1.6 should be compared with the numerical value 2.3 calculated by Holzmann and Krauth [37]. The discrepancy lies within the accuracy expected of my approximations. The important point to note is that the coefficient is positive and of order unity.

The neglect of terms of higher order in a_s during the calculation is based on the assumption that they do not change the structure of the scaling function. (Note that recent calculations of ϕ^4 theory on a lattice [39, 40] may indicate that this assumption is not valid.) A more involved study, where these higher order terms are explicitly calculated would help verify whether perturbation theory is valid within finite size scaling.

2.3.3 Connection with other approaches

The calculation of the phase transition temperature in Section 2.3.2 was motivated by a perturbative calculation performed by Wilkens, Illuminati, and Krämer [38]. Unlike my calculation, these authors did not use finite size scaling to extrapolate to the thermodynamic limit, and derived an incorrect result; namely that the transition temperature decreases with interaction strength. This result contradicts not only Eq. (2.49), but also the results of [32, 33]. It is instructive to reproduce their calculation and see where their method breaks down.

Wilkens et al. found T_c by looking for the temperature, T_*, at which the distribution function $P(N_0)$ becomes flat at $N_0 = 0$. As seen by Fig. 2.5 in an ideal gas at

33

T_c, $P(N_0)$ has a positive slope at $N_0 = 0$, and consequently $T_* > T_c$. These authors neglect the difference $T_* - T_c$, noting that it vanishes in the thermodynamic limit. For the rest of this section, I will likewise ignore this difference.

In terms of $F(N, N_0)$, Wilkens et al.'s criterion for T_c gives an implicit equation for the critical temperature of the interacting system $T_c^{(a)}$,

$$\left. \frac{\partial F(N, N_0)}{\partial N_0} \right|_{N_0=0, T=T_c^{(a)}} = 0. \tag{2.50}$$

As in Fermi liquid theory, $\partial F / \partial N_0$ is the energy of a $k = 0$ quasiparticle measured from the chemical potential [41], and can therefore be expressed as

$$\frac{\partial F}{\partial N_0} = \Sigma(k = 0, \omega = 0) - \mu, \tag{2.51}$$

where $\Sigma(k, \omega)$ is the self-energy at momentum k and energy ω (cf. Appendix C). Thus this criterion for the critical temperature is essentially that used by Baym et al. [33] in the grand canonical ensemble. An important difference between the two approaches is that in the present calculation only quantities at $N_0 = 0$ are involved. As seen in Section 2.2.2, the fluctuations in N_0 are very large at the critical temperature, $\langle N_0^2 \rangle - \langle N_0 \rangle^2 \sim N^{4/3}$ [42]. The criterion (2.50) yields a qualitatively different shift in the transition temperature if the derivative is evaluated at the expectation value of N_0 rather than at $N_0 = 0$.

I now expand the criterion (2.50) for T_c in powers of a, to calculate perturbatively the transition temperature, $T_c^{(a)}$, of the interacting system. Since $\partial F / \partial N_0$ is evaluated at $T = T_c^{(a)}$, we must consider not only the explicit variation of F with a, but also the implicit contribution due to the dependence of T on a. It is convenient to decompose the free energy as $F(a) = F_0 + \Delta F(a)$, where F_0 is the free energy of the non-interacting gas and $\Delta F(a)$ is the correction due to interactions. In the free system, the condensate only contributes to the free energy by reducing the occupation of other modes, i.e.,

$$\frac{\partial F_0(N, N_0)}{\partial N_0} = -\frac{\partial F_0(N, N_0)}{\partial N} \equiv -\mu_0, \tag{2.52}$$

which defines the free chemical potential μ_0, a function of N, N_0 and T. By construction, when $N_0 = 0$ this chemical potential vanishes at the transition temperature of the non-interacting gas, $T_c^{(0)}$, and to first order in the interaction,

$$\left. \frac{\partial F_0}{\partial N_0} \right|_{N_0=0, T=T_c^{(a)}} = -\mu_0(N_0 = 0, T = T_c^{(a)}) \tag{2.53}$$

$$= -\Delta T_c \left. \frac{\partial \mu_0}{\partial T} \right|_{N_0=0, T=T_c^{(0)}} + \mathcal{O}(a^2). \tag{2.54}$$

34

The derivative is taken at fixed N and N_0, and $\Delta T_c = T_c^{(a)} - T_c^{(0)}$ is the shift in the transition temperature for scattering length a. Thus, to first order in a, the left hand side of Eq. (2.50) becomes $\partial(\Delta F)/\partial N_0 - \Delta T_c \, \partial \mu_0/\partial T$, evaluated at $T = T_c^{(0)}$ and $N_0 = 0$. Solving for ΔT_c, we have

$$\Delta T_c = \left. \frac{(\partial(\Delta F)/\partial N_0)}{(\partial \mu_0/\partial T)} \right|_{N_0 = 0, T = T_c^{(0)}}. \tag{2.55}$$

Aside from the use of continuous derivatives in place of Wilkens et al.'s discrete derivatives, this is the result of [38]. Correctly evaluating these functions for a finite sized system is challenging. I estimate their magnitude by using the approximations of Section 2.2.2; *i.e.* replacing the canonical expectation values in Eq. (2.42) by the grand canonical result $\langle N_k(N_k + 1) \rangle = 2\langle N_k \rangle (\langle N_k \rangle + 1)$, and approximately write $\langle N_k \rangle \approx (e^{\beta(\epsilon_k - \mu_0)} - 1)^{-1}$. This assumption provides a simple relationship between $N = N_0 + \sum_k \langle N_k \rangle$ and μ_0, and yields an expression,

$$\frac{\partial(\Delta F)}{\partial N_0} = -\frac{\partial(\Delta F)}{\partial N_{\text{ex}}} = -\left(\frac{\partial(\Delta F)}{\partial \mu_0} \right) \left(\frac{\partial \mu_0}{\partial N_{\text{ex}}} \right) \tag{2.56}$$

$$= \left(\frac{\partial(\Delta F)}{\partial \mu_0} \right) \left(\frac{\partial \mu_0}{\partial T} \right)_{N_{\text{ex}}} \left(\frac{\partial T}{\partial N_{\text{ex}}} \right)_{\mu_0}. \tag{2.57}$$

Since all quantities are evaluated in the free ensemble, the derivatives are straightforwardly evaluated, leading to

$$\frac{\Delta T_c}{T_c} \approx -\frac{8\pi\hbar^2 a}{3mNVk_BT} \sum_{k \neq 0} \langle N_k \rangle^3, \tag{2.58}$$

where $\langle N_k \rangle$ is evaluated at $\mu_0 = 0$. The sum is infrared divergent, scaling as V^2, and yielding a finite temperature shift proportional to $-an^{1/3}$, where $n = N/V$. The constant of proportionality is of the same order of magnitude as the one calculated in [38] using a sophisticated series of asymptotic expansions; its exact numerical value is unimportant here. The key observation is that contrary to the expected behavior, the temperature shift predicted by this argument is negative.

This negative temperature shift depends crucially upon the constraint $N_0 = 0$. At finite N_0, the numerator of Eq. (2.55) has an additional contribution due to the derivative of the first term of Eq. (2.43). This contribution has the opposite sign, and dominates when $N_0 \sim N^{2/3}$, yielding a positive temperature shift. As already emphasized, at the critical temperature, the expectation value of N_0 is of order $N^{2/3}$.

2.4 ΔT in a harmonic trap

In free space, interactions change T_c by reducing density fluctuations, encouraging occupation of the low k modes. In a harmonic trap, interactions not only reduce dynamical density fluctuations, but also change the shape of the cloud, making it flatter and more homogeneous. This flatter density profile implies that at a given temperature more particles must be added to reach the same central density. Condensation occurs when the central density $n(0)$ equals $\zeta(3/2)/\lambda^3$. Thus at fixed particle number the transition temperature of a harmonically trapped gas is reduced by repulsive interactions.

Following Giorgini et al. [43], one can estimate this temperature shift via a Hartree-Fock approximation to the density,

$$n(r) = \int \frac{d^3p}{(2\pi)^3} \left(\frac{1}{e^{\beta(\epsilon_p + V(r) + 2gn(r) - \mu)} - 1} \right), \tag{2.59}$$

where $g = 4\pi\hbar^2 a_s/m$ parameterizes the interactions, $\epsilon_p = p^2/2m$ is the free particle dispersion, and $V(r) = m\Omega^2 r^2/2$ is the trapping potential. At T_c the chemical potential equals $2gn(0)$, so that modes at the center of the trap start becoming macroscopically occupied. In the absence of interactions, the density is

$$n(r) = \frac{1}{\lambda^3} g_{3/2}(e^{-\beta V(r)}). \tag{2.60}$$

The first order shift is

$$\Delta n(r) = \frac{2\beta g}{\lambda^6} (\zeta(3/2) - g_{3/2}(e^{-\beta V(r)})). \tag{2.61}$$

Integrating over all space gives the shift in the number of particles at T_c,

$$\Delta N = \int d^3r\, \Delta n(r) = \frac{2\beta g \zeta(3/2)\zeta(2)}{\lambda^3 (\beta\hbar\Omega)^3} (1 - S), \tag{2.62}$$

where

$$S = \frac{1}{\zeta(3/2)\zeta(2)} \sum_{jk} \frac{1}{j^{1/2}k^{3/2}(j+k)^{3/2}} \approx 0.281. \tag{2.63}$$

Since $N \propto T^3$, the shift in the transition temperature at fixed N is

$$\frac{\Delta T}{T} = -\frac{1}{3}\frac{\Delta N}{N} = -\frac{N^{1/6}a_s}{d}\left(\frac{4\zeta(3/2)\zeta(2)}{3\sqrt{2\pi}\zeta(3)^{7/6}}\right)(1 - S) \tag{2.64}$$

$$= -1.33\frac{a_s N^{1/6}}{d}, \tag{2.65}$$

where $d = \sqrt{\hbar/m\Omega}$ is the characteristic size of the trap. The slow N dependence is a consequence of the slow dependence of the shape of the interacting cloud on the

number of particles. In 1996, the experimental group at JILA attempted to measure this shift [34]. Using 40000 rubidium atoms ($a_s = 5$nm) in a trap with $\Omega = 1200$s^{-1}, their trap had a characteristic trap size of $d = 560$nm, for which equation (2.65) predicts a 5% shift.

With such a small number of particles one finds a comparable shift from corrections to the semiclassical approximation used in Eq. (2.13a). These corrections are easily calculated by writing

$$\mathcal{F} = T \sum_j \frac{z^j}{j} \left(\mathcal{F}_j\right)^3, \tag{2.66}$$

where

$$\mathcal{F}_j = \sum_{n=0}^{\infty} e^{-j\beta\hbar\Omega n} \tag{2.67}$$

$$= \frac{e^{\beta\hbar\Omega j}}{e^{\beta\hbar\Omega j} - 1} \tag{2.68}$$

$$\approx \frac{e^{\beta\hbar\Omega j}}{\beta\hbar\Omega} \left(1 + \beta\hbar\Omega/2 + \cdots\right). \tag{2.69}$$

Keeping the first term gives Eq. (2.13a), while keeping the first two terms gives,

$$\mathcal{F} = T \left(\frac{1}{(\beta\hbar\Omega)^3} g_4(z) + \frac{3}{2} \frac{1}{(\beta\hbar\Omega)^2} g_3(z) + \cdots\right). \tag{2.70}$$

Calculating the number of particles shows that the critical temperature is shifted by

$$\frac{\Delta T}{T} = -\frac{\zeta(2)}{2N^{1/3}\zeta(3)^{2/3}}. \tag{2.71}$$

For the Ensher experiment [34] this is a 2% shift. The experimental data is shown in Fig. 2.6. The solid and dashed lines are the ideal gas predictions with and without the finite size correction (2.71). The difference between the non-interacting theory (2.71) and experiment is consistent with interactions (2.65). Recently, Arnold and Tomasik [44] calculated the shift in the transition temperature to second order in a_s.
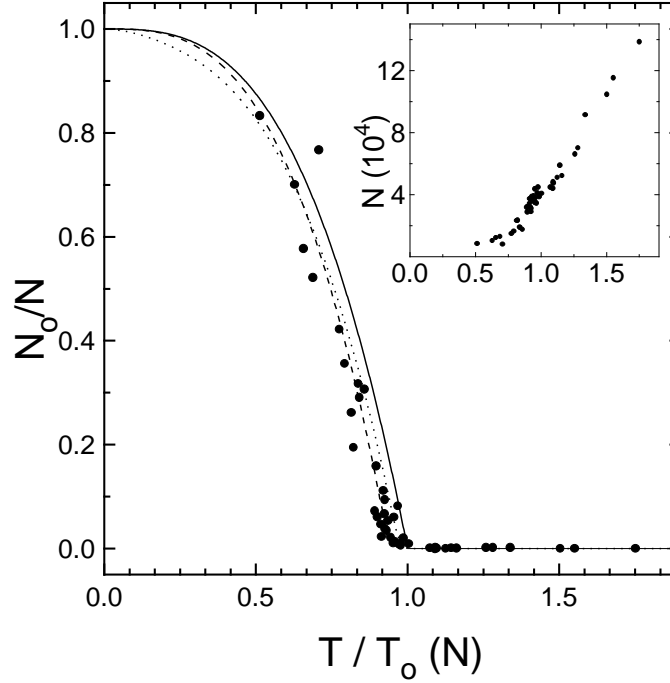
Figure 2.6: Total number N (inset) and ground-state fraction N_0/N as a function of scaled temperature T/T_0. The presence of fewer particles at lower temperatures is a consequence of evaporative cooling. The scale temperature $T_0(N) = \hbar\Omega/k_B(N/\zeta(3))^{1/3}$ is the predicted critical temperature, in the thermodynamic limit, for an ideal gas in a harmonic potential [cf. Eq. (2.15)]. The solid (dotted) line shows the infinite (finite) N theory curves. At the transition, the cloud consists of 40 000 Rb atoms at 280 nK. The dashed line is a least squares fit to the form $N_0/N = 1 - (T/T_c)^3$ which gives $T_c = 0.94(5)T_0$. Each point represents the average of three separate images. *Figure reprinted with permission from [34]. Copyright 1997 American Association for the Advancement of Science.*

Chapter 3

Fragmentation

3.1 Introduction

In the standard paradigm of Bose-Einstein condensation a single particle mode is macroscopically occupied [45, 46]. Here I address Boson systems where more than one such mode is macroscopically occupied. These multiply condensed, or fragmented, systems are rather novel and there is great interest in experimentally producing one of these states. In this Chapter I explain the origin and consequences of fragmentation.

By definition, fragmentation occurs when two or more single-particle modes are macroscopically occupied with no coherence between the separate condensates. Here I am interested in fragmentation in an equilibrium setting. Distinct issues are raised by non-equilibrium fragmented systems where the bosons are carefully manipulated to produce the desired state. These issues go beyond the scope of this thesis and will be discussed in future work. As a simple example of creating a non-equilibrium condensate, one could condense atomic clouds in two separate traps, trivially producing two condensates with no phase coherence between them.

In a weakly interacting setting, equilibrium fragmentation requires that the important modes are nearly degenerate, for otherwise a condensate would simply form in the lowest energy modes. Interactions soften this degeneracy requirement, as interaction energy may be saved by occupying the higher energy state. (Furthermore, for sufficiently strong interactions this single particle picture breaks down.) This reliance on degeneracies makes fragmentation extremely delicate, as an arbitrarily small perturbation will lift the degeneracy.

Degeneracies are often related to symmetries of the Hamiltonian. For example, in a spherically symmetric potential the eigenfunctions, labeled by quantum numbers

n, ℓ, m, are degenerate if they share the same n and ℓ. An arbitrarily small symmetry breaking perturbation will lift these degeneracies and destroy the possibility of equilibrium fragmentation. It is important to note that if one destroys a fragmented state by adding a symmetry breaking perturbation, then the singly-condensed state which is formed will break the symmetry. These observations can be summed up by saying that *fragmentation occurs in the symmetry unbroken state of a system with a spontaneously broken symmetry.*

Although I focus on atomic gases, fragmentation can occur in more general mesoscopic superfluids and superconductors. Fragmentation is unlikely to be observed in macroscopic systems where stray couplings inevitably lead to a singly condensed state. For example, early studies of fragmentation [47, 48, 49] focussed on bulk ^{4}He and found that fragmentation never occurs. Alkali gases, with their small number of particles (10^3 to 10^7), and highly controllable environments make the ideal setting for experimental studies fragmentation.

In this Chapter I develop a coherent framework for understanding fragmented systems, and in the context of alkali gases discuss the detection and creation of such states. To extract the generic features of fragmentation I give a detailed discussion of the properties of a simple two level model. I then apply these concepts to present unified descriptions of a series of other physically relevant models. Much of the work presented in this Chapter was performed in collaboration with Gordon Baym, Jason Ho, and Masahito Ueda, and will be submitted for publication [50].

3.1.1   Bose-Einstein condensation and fragmentation

Bose-Einstein condensation is characterized in terms of the single particle density matrix $\rho_I(r, r') = \langle \psi^\dagger(r')\psi(r) \rangle = \sum_\nu n_\nu \phi_\nu^*(r')\phi_\nu(r)$, where n_ν and $\phi_\nu(r)$ are respectively the eigenvalues and eigenfunctions of this matrix, and $\psi(r)$ is the annihilation operator for a particle at position r. The eigenfunctions are normalized by $\int d^3r \, |\phi(r)|^2 = 1$, and the eigenvalues sum to the number of particles $\sum_\nu n_\nu = N$. Physically, each eigenfunction $\phi_\nu(r)$ is a single-particle mode occupied by n_ν particles. In terms of the many-body wave function $\psi(r_1, \ldots, r_n)$, where r_i represents the position of the i'th particle, the single particle density matrix is found by tracing over all but one of the particles,

$$\rho_I(r, r') = \int dr_2 \cdots dr_n \, \psi^*(r', r_2, \ldots, r_n)\psi(r, r_2, \ldots, r_n). \qquad (3.1)$$

In a non-condensed state, each of the eigenvalues n_ν are of order unity. In a singly condensed state, one eigenvalue n_0 is of order N, while in a fragmented state, several

eigenvalues are of order N. Since these characterizations involve large N asymptotics, they are only precisely defined in the limit $N \to \infty$. Furthermore, some systems do not fit neatly into this framework, for example, a one dimensional gas of hard core bosons has a density matrix which is diagonal in momentum space, and has a power law distribution of occupation numbers: $n_k \sim (n/k)^{1/2}$ as $k \to 0$, where $n = N/L$ is the linear density [51]. In a finite size system the lowest accessible k modes have $k \sim 1/L$, implying that these modes have occupation of order $N^{1/2}$, which lies between the values found in condensed and non-condensed systems.

Although throughout this Chapter I only consider the above definition of Bose-Einstein condensation, it is useful to connect this description to the idea of spontaneously broken gauge symmetry, as often used in condensed matter physics [52]. In this latter formalism the field operator is coupled to a fictitious field, $\eta(r)$, via a Hamiltonian $H_\eta = \int d^3r [\eta(r)\psi^*(r) + \eta^*(r)\psi(r)]$. If $\langle \psi \rangle \equiv \lim_{\eta \to 0} \langle \psi \rangle_\eta \neq 0$, the system is said to be condensed, with order parameter $\langle \psi \rangle$. If in the absence of η the single particle density matrix has a single large eigenvalue n_0 with eigenfunction ϕ_0, this procedure yields $\langle \psi \rangle = \sqrt{n_0}\phi_0$. If, instead, the single particle density matrix has m large eigenvalues, $\lambda_1, \ldots, \lambda_m$, eigenfunctions $\phi_1, \ldots, \phi_m$, then the result is slightly different. The coupling field can be written in terms of the modes $\eta = (\sum_i^m |\eta_i| e^{i\theta_i} \phi_i)$, with phases θ_i. In the limit where each of the $\eta_i \to 0$, one should find $\langle \psi \rangle = \sum_i^m \sqrt{n_i} e^{i\theta_i} \phi_i$, which is a linear combination of all the modes in which the relative phases between the various condensates are set by the phases in η. When the modes $\phi_1, \ldots, \phi_m$ have disparate symmetries, choosing the phases ϕ_i breaks those symmetries. For example, if one of these states is an s wave state and another a p wave state, the combination breaks rotational symmetry.

The η construction produces a single condensate because the phases between all of the states are specified. If these phases were averaged over, the resulting state would be fragmented. This will be illustrated later.

A concept closely related to fragmentation is the notion of a *quasicondensate*, where the correlation function $\langle \psi^\dagger(r)\psi(r') \rangle$ falls off as a power law as $|r - r'|$ becomes large. Such quasicondensation occurs in lower dimensions [53, 54] or when a Bose gas is rapidly cooled below the BEC temperature [55]. In Section 3.5 I give an example of a finite temperature vortex lattice which also has this quasicondensate structure, where thermal fluctuation of vortex lines destroy long range ordering of the phase. In a quasicondensate one generally has a power law distribution of occupation numbers n_k.

3.1.2 An illustrative example

To illustrate the nature of fragmentation I review a simple model, proposed by Nozières [6], consisting of N bosons which can be in one of two single particle modes. Depending upon the couplings between the modes, the ground state can be fragmented or singly condensed. This model generically describes systems that can fragment into two condensates. Nozieres model is readily generalized to systems with more condensed modes.

This model is most easily described in second quantization where the operators a and b annihilate bosons in the two modes. As a concrete example to motivate the model, suppose, as in Fig. 3.1a, that the two modes are momentum eigenstates $e^{ik \cdot r}$ and $e^{-ik \cdot r}$, and that the particles interact via a short range interaction. In the two mode approximation, the field operator is $\psi(r) = (ae^{ik \cdot r} + be^{-ik \cdot r})/\sqrt{V}$. Assuming local interactions of strength g, this system is described by a Hamiltonian

$$
\begin{aligned}
H &= (gV/2) \int d^3 r \, \psi^\dagger \psi^\dagger \psi \psi \qquad\qquad (3.2) \\
&= (g/2)N(N-1) + g a^\dagger b^\dagger b a.
\end{aligned}
$$

As defined, g has dimensions of energy and scales as the inverse of the system volume. Translational invariance implies that momentum is conserved, and therefore the occupation numbers $n_a = \langle a^\dagger a \rangle$ and $n_b = \langle b^\dagger b \rangle$ are constants of motion. Attractive interactions encourage particles to clump, giving the gas a tendency to break translational invariance. As I demonstrate below, this clumping implies that the symmetry unbroken state is fragmented. Adding a local impurity that breaks translational invariance adds a term $-t(a^\dagger b + b^\dagger a)$ to the Hamiltonian, and will result in a singly condensed ground state.

A second concrete example of the two state model is a "Josephson junction" formed by a gas of bosons in a double well potential (see Fig. 3.1). If only a single mode in each of the two wells is occupied, the Hamiltonian is

$$
\begin{aligned}
H &= -t(a^\dagger b + b^\dagger a) + (g_J/2)(a^\dagger a^\dagger a a + b^\dagger b^\dagger b b) \qquad\qquad (3.3) \\
&= (g_J/2)N(N-1) - t(a^\dagger b + b^\dagger a) - g_J a^\dagger b^\dagger b a,
\end{aligned}
$$

where a and b annihilate bosons in the individual wells, and where t parameterize the tunneling and g_J the interactions. For a very large barrier t vanishes, and by identifying g_J with $-g$ from (3.2), one sees that aside from an inconsequential constant, Eq. (3.3) with $t = 0$ is the same as Eq. (3.2). For $t = 0$ and repulsive interactions I will show that it is energetically favorable to incoherently occupy each of these two
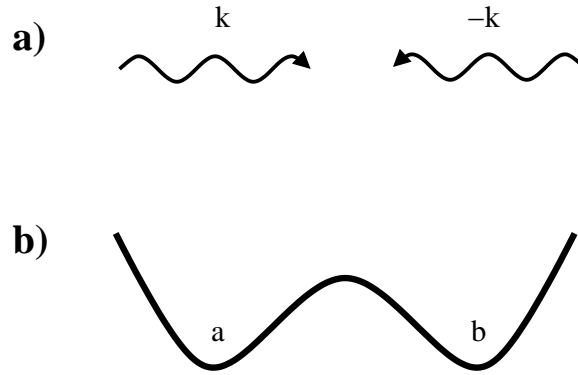
Figure 3.1: Schematic picture of systems which can be truncated to a two state model with a fragmented ground state. In a) I model an attractive gas in free space by considering two momentum states $e^{ik \cdot r}$ and $e^{-ik \cdot r}$. In b) I model particles in a double-well potential by considering the lowest energy modes in the left and right wells.

modes. The tunneling is analogous to a local impurity in the last model, and for $t \neq 0$ a singly-condensed state is favored. The immediate discussion focuses on $t = 0$.

The two level model has qualitatively different behavior depending on whether $g > 0$ or $g < 0$ (equivalently, $g_J < 0$ or $g_J > 0$). When $g > 0$ the ground state of N particles is singly condensed, with all of the particles in the a state or in the b state. For $g < 0$ the ground state is

$$|n_a = N/2, n_b = N/2\rangle \; = \; (a^\dagger)^{N/2}(b^\dagger)^{N/2}|\text{vac}\rangle, \tag{3.4}$$

where $|\text{vac}\rangle$ is the vacuum containing no particles, leading to a single particle density matrix,

$$\begin{pmatrix} \langle a^\dagger a\rangle & \langle a^\dagger b\rangle \\ \langle b^\dagger a\rangle & \langle b^\dagger b\rangle \end{pmatrix} = \begin{pmatrix} N/2 & 0 \\ 0 & N/2 \end{pmatrix} \tag{3.5}$$

which clearly has two large eigenvalues, and is by definition fragmented.

The state (3.4) is a condensate of pairs, $(a^\dagger b^\dagger)^{N/2}|\text{vac}\rangle$, and has off-diagonal order in the 2-particle density matrix, but not in the 1-particle density matrix. As discussed by Yang [56], and later by Kohn and Sherrington [57], order in the n-particle density matrix implies order in the $(n+1)$-particle density matrix, but the converse is false. When the two states involved are momentum eigenstates, the implications of this result are particularly transparent. The pair created by the operator $a^\dagger b^\dagger$ has a wave-function $\psi(r_1, r_2) \propto \cos k(r_1 - r_2)$, in which the two particles are bunched up, but their center of mass is spread uniformly throughout space.

Further insight into this fragmented ground state is gained by studying Eq. (3.2) within mean field theory. For a Bose gas, mean field theory is conveniently imple-

mented as a variational method using singly condensed wavefunctions; here the most general singly-condensed wavefunction takes the form $|\alpha, \beta\rangle = (\alpha a^\dagger + \beta b^\dagger)^N |\text{vac}\rangle$. For $g < 0$ the energy is minimized by setting $|\alpha|^2 = |\beta|^2 = 1/2$, with the phases $\phi_\alpha = \text{Arg}(\alpha)$ and $\phi_\beta = \text{Arg}(\alpha)$ completely arbitrary, resulting in a huge degeneracy.

Again considering the case where a and b correspond to momentum eigenstates, each of the states with $|\alpha|^2 = |\beta|^2 = 1/2$ has a density $\langle \psi^\dagger(r)\psi(r)\rangle = (N/2V)\cos^2(k \cdot r + (\phi_\alpha - \phi_\beta)/2)$ which is inhomogeneous. Averaging over the position of the density peak restores the ground state,

$$\int d\phi (a^\dagger e^{-i\phi/2} + b^\dagger e^{i\phi/2})^N |\text{vac}\rangle \propto (a^\dagger b^\dagger)^{N/2} |\text{vac}\rangle. \tag{3.6}$$

Generically one finds that fragmented ground states are expressible through averaging over a family of degenerate singly-condensed states.

As already emphasized, adding a symmetry breaking term to the Hamiltonian will favor single condensation over fragmentation. In fact, only an infinitesimal perturbation is needed to break the symmetry, making this an example of a spontaneously broken symmetry. One understands the strong susceptibility to the perturbation as due to the continuous degeneracy of the states with different ϕ.

In this simple two level model one can explicitly calculate the crossover between singly condensed and fragmented ground states when a symmetry breaking perturbation is added. The mathematical details are discussed in Section 3.7.1, here I just review the major results and sketch the crossover. This crossover is typically discussed in the context of a Josephson junction, Eq. (3.3), where three regimes are identified [16]. For $t \ll g_J/N$ one is in the Fock regime, where tunneling rarely occurs, and the ground state is fragmented. For $g_J/N \ll t \ll Ng_J$ one is in the Josephson regime, where tunneling occurs at a rate governed by the Josephson plasma frequency $\omega_J^2 = 2tg_J N$, and the ground state is singly condensed with sub-Poissonian fluctuations in the number of particles in each well. For $Ng_J \ll t$ one is in the Rabi regime, where the system behaves as a collection of non-interacting particles undergoing Rabi oscillations between the two wells, and the ground state is singly condensed with Poissonian fluctuations in the number of particles in each well.

The key observation is that a tunneling of strength $t \sim g_J/N$ is large enough to break the relative phase symmetry between wells. Note that a crude energetics argument of comparing the mean-field states $|\alpha, \beta\rangle$ with the fragmented state $(a^\dagger b^\dagger)^{N/2} |\text{vac}\rangle$, incorrectly predicts a crossover at much stronger tunneling, $t \sim g_J$.

I conclude this Section with a few remarks about experimental realizations of this model. First, as presented in Eq. (3.2), Nozières' model can be applied to a uniform

Bose gas. Although it is a crude model and cannot be used to make quantitative predictions, it provides a qualitative picture which does stand up to more sophisticated analysis. Namely, the ground state of an attractive gas is localized, and averaging over all possible positions for the localized gas results in a fragmented state [59].

When applied to spatially separated modes, as in Eq. (3.3), this model can make quantitative predictions. By theoretically studying clouds of atoms in double-well traps, Zapata, Sols and Leggett [58] found that the parameters g and t should scale as

$$g \quad \propto \quad N^{-3/5}(a_s/d)^{2/5}\hbar\omega \tag{3.7a}$$

$$t \quad \propto \quad N^{-2/3}(a_s/d)^{-2/3}\hbar\omega\frac{\exp(-S_0)}{\tanh(S_0/2)}, \tag{3.7b}$$

where a_s is the scattering length, ω is the frequency of each of the traps, $d = \sqrt{\hbar/m\omega}$, and S_0 is the classical action for the path joining the two wells. Within a WKB approximation, and assuming a quartic barrier $V(r) = V_0(1 - (r/r_0)^2)^2$ of height V_0 and width $r_0 = m\omega^2/8V_0$, the action is $S_0 \propto (V_0 - \mu)/\hbar\omega$, where μ is the chemical potential. Thus t is exponentially sensitive to the barrier height, and experimentalists should be able to tune from the singly condensed regime $t \gg g/N$ to the fragmented regime $t \ll g/N$.

3.2 Discussion and generalization

In this Section I extract the general features of the two level model previously introduced. These features are generic, as all systems with fragmented ground states can be mapped onto models similar to (3.2). In Section 3.3 I present a large number of systems with fragmented ground states and explicitly demonstrate the wide applicability of this analysis.

3.2.1 Spontaneous symmetry breaking

As already emphasized, in addition to the spontaneously broken global gauge symmetry which singly condensed systems possess, the Hamiltonians (3.2) and (3.3), have an additional broken symmetry corresponding to the relative phase of the two states. This is a generic feature of fragmentation, and this broken symmetry can take on many forms. In Section 3.3, I present models where fragmentation is associated with translational, rotational, and parity symmetries. These models also share the feature

that the fragmented ground state can be recovered from symmetry broken states by averaging over all values of the broken symmetry [cf. Eq. (3.6)].

3.2.2   Measurement

Here I ask the question "Can fragmented states be distinguished from singly condensed ones?". The answer is "yes", but in many cases, such an investigation is difficult. Our discussion focuses on the two level system, but our conclusions are more general.

Measuring the Broken Symmetry

In the two level system, the definitive difference between a condensed and a fragmented state is that in the fragmented state the expectation value $\langle a^\dagger b \rangle$ vanishes, while in the singly condensed state $\langle a^\dagger b \rangle = (N/2)e^{i\phi}$, for some phase angle ϕ (for the choice of tunneling given in equation (3.3) this phase is $\phi = 0$). That is, the relative phase symmetry is broken in the singly condensed state. Clearly one can distinguish the fragmented and singly condensed states by measuring $\langle a^\dagger b \rangle$.

An impediment to detecting this broken symmetry is that $\langle a^\dagger b \rangle$ can not be measured by making successive single particle measurements on a given state. As shown by Javanainen and Yoo [60] and by Castin and Dalibard [61], sequential single particle measurements project the system into a singly condensed state (this result is analogous to how measuring the momentum of a particle projects it into a momentum eigenstate). Consequently, in order to measure $\langle a^\dagger b \rangle$, multiple copies of the quantum state must be created and a single particle measurement must be made on each of them.

For concreteness, consider the MIT interference experiment [23] described on page 12 of the Introduction. In this experiment two spatially separated clouds (modes a and b), are allowed to expand towards each other, overlapping in some region. In the overlap region, the two modes are momentum eigenstates, e^{ikx} and e^{-ikx}, and the density $\langle \psi^\dagger(r)\psi(r) \rangle$ is proportional to $\langle a^\dagger a \rangle + \langle b^\dagger b \rangle + \langle a^\dagger b \rangle e^{-ikx} + \langle b^\dagger a \rangle e^{ikx}$. By measuring the Fourier transform of the density one can therefore measure $\langle a^\dagger b \rangle$. In these experiments photographs were taken of the overlapping clouds, and beautiful interference fringes were seen (Fig. 1.7). Counter-intuitively, these pictures do not imply that $\langle a^\dagger b \rangle$ is non-zero since the photography process involves a sequence of single particle measurements on a single realization of the state. To measure $\langle a^\dagger b \rangle$ one would need to repeat the experiment on multiple copies of the state, averaging

over the density pattern seen. If the initial state was fragmented, each run of the experiment would feature a different position for the density fringes. Averaging over multiple runs would result in a featureless density pattern. This phenomenon is schematically depicted in Fig. 3.2.
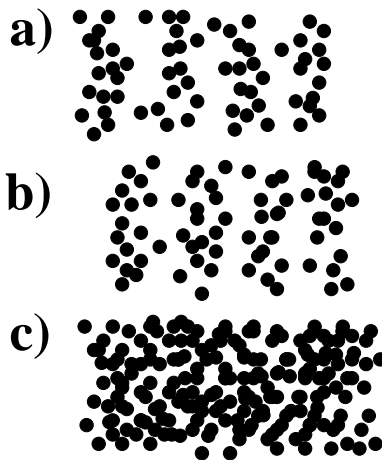
Figure 3.2: Schematic picture of interference pattern formed when the fragmented state (3.4) is imaged. Figures a and b, represent individual runs of the experiment, each dot represents the position of a single atom. Interference fringes are clearly visible, though the phase of the interference pattern shifts between runs. Figure c illustrates the pattern formed when several individual runs of the experiment are superimposed, and a uniform distribution of particles is observed.

The presence of fringes in a single run of the experiment can be understood without relying on measurement theory. The central observation is that although the expectation value of the density is uniform in the fragmented state, the density-density correlation function $\langle \rho(r)\rho(r') \rangle$ is modulated at wave-vector k. This modulation of the density-density correlation function means that if a particle is detected at position r, one is more likely to find another particle at a position $r + 2\pi n/k$, for any integer n. Consequently, when particles are sequentially detected (i.e. the cloud is photographed) fringes are seen. The position of the fringes will be random from run to run.

The requirement of averaging over several runs of an experiment brings up a second caveat. Suppose one is in the regime where stray fields break the symmetry and the ground state is condensed. If these fields are systemic, and do not change from run to run, then one will find that the ensemble average $\langle a^\dagger b \rangle$ is non-zero and correctly reflects the singly condensed nature of the state. Conversely, if the fields fluctuate, then the ensemble average $\langle a^\dagger b \rangle$ will vanish, as if the system had a fragmented condensate. Generalizing this observation, one expects that a fragmented

state is indistinguishable from an appropriate ensemble of singly condensed states. This statement can be made mathematically precise: in Section 3.7.2 I prove that up to terms of order $n/(N-n)$, the n-particle reduced density matrix of an N particle system, is identical for an ensemble of singly condensed states and for a fragmented state. The only property that this proof requires is that the fragmented state can be expressed as a sum over the symmetry-broken condensed states which make up the ensemble.

Other Measurement strategies

Given the experimental difficulty of using the broken symmetry to distinguish fragmented and singly condensed states, it is useful to ask if there are any other possible ways to distinguish these states. One very useful, though indirect, approach is to infer the state of the system by its dynamics. In the Fock regime, where the ground state is fragmented, it takes an energy g to excite the system. In the Josephson regime, where the ground state is singly condensed, an analogous excitation has energy $\omega_J = \sqrt{2tNg}$. Measuring the excitation energy tells you which regime you are in.

A third possibility for detecting fragmentation is to look at the number fluctuation in each of the states a and b. In the fragmented state, these fluctuations vanish. Unfortunately, in the Josephson regime there exist condensed states with arbitrarily small number fluctuations $\delta N^2 \sim \mathcal{O}(N^0)$, making it impossible to distinguish fragmented and singly condensed states on this basis. These "squeezed" states are explicitly constructed in Section 3.7.1.

3.2.3 Commensurability

The arguments of Section 3.1.2 require an even number of particles. For an odd number of particles $N = 2m + 1$, the ground state of Eq. (3.2) is degenerate, of the form $(\alpha a^\dagger + \beta b^\dagger)(a^\dagger b^\dagger)^m |\text{vac}\rangle$, for arbitrary α and β. Adding an infinitesimal tunneling of the form $H_t = -t(a^\dagger b + b^\dagger a)$, breaks this degeneracy, leading to a ground state with $\alpha = \beta = 1/\sqrt{2}$. This state has two eigenvalues of size $3N/4 + 1/4$ and $N/4 - 1/4$. It is remarkable that a single particle tunneling between the two wells can increase the coherence to such a great extent.

Many other models have the property that the degree of fragmentation is dependent on the value of N. This result is intuitive, and is best illustrated by a model of bosons restricted to a lattice. This model is discussed at length in Section 3.3.4.

Suppose one has N particles on M lattice sites with very strong repulsion between particles on the same site. If N/M is integral, the particles will be localized in the wells, the energy cost of a density fluctuation outweighing the kinetic energy cost of localizing the particles. With an incommensurate number of particles, there is no energy cost for moving the excess particles around and therefore some particles will be delocalized, reducing the extent of the fragmentation.

Similar behavior is seen in an asymmetric Josephson junction discussed in Appendix 3.7.1, where instead of changing the number of particles one changes the asymmetry between the two wells. Consider an even number of particles. When the wells are degenerate and the tunneling is weak the ground state is $(a^\dagger)^{N/2}(b^\dagger)^{N/2}|\text{vac}\rangle$. Gradually lowering the energy of state a relative to state b the ground state will eventually become $(a^\dagger)^{N/2+1}(b^\dagger)^{N/2-1}|\text{vac}\rangle$, where one particle has jumped from the b well into the a well. At some intermediate value of the asymmetry these two states will become degenerate. An infinitesimal tunneling will at that point allow a single particle to tunnel back and forth, greatly increasing the size of the largest eigenvalue of the single particle density matrix.

Such sensitivity to the parameters of the Hamiltonian and to the exact number of particles in the system further demonstrates the fragility of fragmented states.

3.3 Other models

To demonstrate that the physics of the two level model occurs in more general circumstances I give a list of various systems which have fragmented ground states. I verify that all of these models have the generic characteristics discussed in Section 3.2.

3.3.1 Spin 1

After the Josephson Junction, the simplest Bose-gas model with a fragmented ground state is a gas of spin-1 atoms. Such a gas is realized in experiments at MIT [62], and has received a great deal of theoretical attention. Notably, theoretical studies of the spin 1 system have demonstrated that the ground state of the system with antiferromagnetic interactions is fragmented [7, 63, 64]. As demonstrated here, this fragmentation is a associated with a spontaneously broken rotational symmetry.

Looking only at the spin degree of freedom, the Hamiltonian for a gas of atoms, each with spin $\mathbf{s_i}$ is

$$H = J\mathbf{S} \cdot \mathbf{S}, \tag{3.8}$$

where $\mathbf{S} = \sum_i \mathbf{s_i}$ is the total spin of the system. For $J < 0$ the interaction is ferromagnetic and the ground state is singly condensed. I will concentrate on antiferromagnetic interactions, $J > 0$. The exact ground state of this Hamiltonian is a singlet ($S = 0$). For systems with an even number of particles, the simplest way to create a singlet is to form a condensate of singlet pairs. To this end, I introduce operators $\{a_i, i = -1, 0, 1\}$, which annihilate particles with spin projection i along the z axis. From these operators one produces Cartesian creation operators $\{A_\nu, \nu = x, y, z\}$ defined by $a_{\pm 1} \equiv (A_x \mp iA_y)/\sqrt{2}$ and $a_o \equiv A_z$. I use the symbol $\mathbf{A}$ for the vector with components A_ν. The operator which annihilates a singlet pair is $\mathbf{A} \cdot \mathbf{A} = a_0^2 - 2a_1a_{-1}$. One constructs a singlet state by placing pairs of particles into singlet states,

$$|S = 0\rangle = \frac{1}{\sqrt{(N+1)!}} \left(\mathbf{A}^\dagger \cdot \mathbf{A}^\dagger \right)^{N/2} |\mathrm{vac}\rangle. \qquad (3.9)$$

For spin 1 particles, this state is the unique $S = 0$ state (uniqueness is demonstrated in [64] via a state counting argument). On symmetry grounds, the single particle density matrix $\{\langle A_i^\dagger A_j \rangle; i, j = x, y, z\}$ is $N/3$ times the identity matrix, and has 3 large eigenvalues. This ground state is fragmented. As the particles are all paired, this state has order in the two particle density matrix.

For comparison, consider the lowest energy mean field state of the form [65]

$$|\nu\rangle = \left(\sum_{j=-1}^{1} \zeta_j a_j^\dagger \right)^N |\mathrm{vac}\rangle, \qquad (3.10)$$

which has a single condensate for all choices of the coefficients ζ_j. The expectation value of the Hamiltonian in this state is $\langle H \rangle = JN(N-1)\langle \mathbf{s} \rangle^2 + 2NJ$, where $\langle \mathbf{s} \rangle = \langle \nu | \mathbf{S} | \nu \rangle / N$ is the magnetization per particle. The states with lowest energy are therefore those with $\langle \mathbf{s} \rangle = 0$. The states with this property are rotations of $|\nu\rangle = a_0^{\dagger N}|\mathrm{vac}\rangle/\sqrt{N!}$. These rotated states are conveniently parameterized by a unit vector $\hat{\mathbf{n}}$ which represents the axis along which the spin and all its moments vanish,

$$|\hat{\mathbf{n}}\rangle = \frac{(\hat{\mathbf{n}} \cdot \mathbf{A}^\dagger)^N}{\sqrt{N!}} |\mathrm{vac}\rangle. \qquad (3.11)$$

The mean field states $|\hat{\mathbf{n}}\rangle$ principally differ from the singlet state $|S = 0\rangle$ in that a particular direction in space is selected; i.e. they break rotational symmetry. In analogy to Eq. (3.6), one constructs the exact ground state from these mean-field states by averaging over the broken symmetry. Representing an element of solid

angle by $d\Omega$ and integrating, one finds that the symmetry restored state, $|SR\rangle$, is

$$|SR\rangle \quad \propto \quad \int \frac{d\Omega}{4\pi} |\hat{\mathbf{n}}\rangle, \tag{3.12a}$$

$$= \quad \int_{-1}^{1} \frac{d\cos\theta}{2} \frac{(\sqrt{\mathbf{A}^\dagger \cdot \mathbf{A}^\dagger} \cos\theta)^N}{\sqrt{N!}} |\text{vac}\rangle, \tag{3.12b}$$

$$= \quad (\mathbf{A}^\dagger \cdot \mathbf{A}^\dagger)^{N/2} |\text{vac}\rangle / (N+1)\sqrt{N!}, \tag{3.12c}$$

which is the singlet state. In the intermediate step I formally treated $\mathbf{A}$ as a c-number vector, and θ is the angle between this vector and $\hat{\mathbf{n}}$.

By choosing an appropriate weight factor in Eq. (3.12a) one constructs states with finite magnetization,

$$|m\rangle \quad \propto \quad \int d\theta \, d\cos\phi \, Y^*_{mm}(\theta, \phi) |\hat{\mathbf{n}}\rangle \tag{3.13a}$$

$$\propto \quad (a_1^\dagger)^m \cdot \left(A^\dagger \cdot A^\dagger\right)^{(N-m)/2} |\text{vac}\rangle. \tag{3.13b}$$

The spherical harmonic $Y_{mm} = (\sin\phi \, e^{i\phi})^m$ projects out a state with total angular momentum $\sqrt{m(m+1)}$, and projection m.

Like the phase symmetry in the two well example, the rotational symmetry of the spin-1 antiferromagnet can be broken by an infinitesimal field t. Including the symmetry breaking field, the Hamiltonian is

$$H = J\mathbf{S} \cdot \mathbf{S} - t(\hat{\mathbf{m}} \cdot \mathbf{A}^\dagger)(\hat{\mathbf{m}} \cdot \mathbf{A}) \tag{3.14}$$

where $\hat{\mathbf{m}}$ is a unit vector which explicitly breaks rotational symmetry. In the laboratory, the term proportional to t will be produced by unavoidable magnetic field gradients [7], and can also be engineered using atomic techniques. Without loss of generality, I take $\hat{\mathbf{m}}$ to point in the $\hat{\mathbf{z}}$ direction. In terms of the operators a_i,

$$\begin{aligned} H &= -ta_0^\dagger a_0 + J\big[a_1^\dagger a_1^\dagger a_1 a_1 + a_{-1}^\dagger a_{-1}^\dagger a_{-1} a_{-1} \\ &\quad -2a_1^\dagger a_{-1} a_1 a_{-1} + 2a_1^\dagger a_{-1}^\dagger a_0 a_0 + 2a_0^\dagger a_0^\dagger a_1 a_{-1} \\ &\quad +2a_0^\dagger a_0(a_1^\dagger a_1 + a_{-1}^\dagger a_{-1})\big]. \end{aligned} \tag{3.15}$$

For large enough t, the state with $m = 0$ will be macroscopically occupied. Following Bogoliubov [66] I replace a_0 and $a_0^\dagger$ with the c-number $\sqrt{n_0}$, and expand the Hamiltonian to quadratic order in the fluctuations,

$$\begin{aligned} H &= -tN + (t + 2JN)(a_1^\dagger a_1 + a_{-1}^\dagger a_{-1}) \\ &\quad +2JN(a_1^\dagger a_{-1}^\dagger + a_1 a_{-1}) + \cdots, \end{aligned} \tag{3.16}$$

51

where the neglected terms are of higher order in the depletion. A Bogoliubov transformation diagonalizes the Hamiltonian, and, in the limit of larger N, the number of excited particles is

$$N_{ex}/N = (J/Nt)^{1/2}. \qquad (3.17)$$

Thus if $t \gg J/N$, the depletion is small, and the ground state is singly condensed. If $t \ll J/N$ the standard Bogoliubov theory breaks down. In this regime perturbation theory about the state $|S = 0\rangle$ converges, and the ground state is fragmented. A modified version of the Bogoliubov approach can be used in this latter regime [67].

There has been recent interest in distinguishing the mean field state $|\hat{\mathbf{n}}\rangle$ from the singlet state $|S = 0\rangle$ [68]. As only the latter of these is rotationally invariant, any experiment which is capable of measuring anisotropies (such as a series of Stern Gerlach experiments with different axes) would suffice to distinguish these states. As pointed out in Section 3.2.2, distinguishing the state $|S = 0\rangle$ from an ensemble of mean field states $|\hat{\mathbf{n}}\rangle$ with random $\hat{\mathbf{n}}$'s is impossible.

3.3.2 Rotating attractive cloud

There have been several recent papers investigating the eigenstate of a rotating harmonically trapped Bose gas with infinitesimal interactions (see [5, 69] and references therein). As a superfluid, the flow within a Bose condensate is strictly irrotational. A condensed gas can therefore only carry angular momentum if either it contains quantized vortices or it deforms its shape, breaking rotational invariance. The latter occurs for attractive interactions, and results in a fragmented ground state. For weak enough interactions, the most favorable deformation is a translation of the cloud from the rotation axis.

Consider a cloud of atoms in a harmonic trap with weak attractive interactions. The exact form of the interaction is unimportant and commonly either a point interaction or a harmonic interaction is used (for example Wilkin et al. [5] consider both of these, while Huang [69] gives general arguments about the equivalence of any rotationally invariant interaction). Although unphysical, the harmonic interactions are easier to handle, and I will consider them here.

This model consists of N bosons with positions r_i and momenta p_i, trapped in a harmonic well with frequency ω. These particles interact harmonically with a frequency $\sqrt{\kappa}$, resulting in a Hamiltonian

$$H = \sum_i \left(\frac{p_i^2}{2m} + \frac{m\omega^2 r_i^2}{2} \right) + \frac{m\kappa}{4} \sum_{i,j} (r_i - r_j)^2. \qquad (3.18)$$

I take attractive interactions $\kappa > 0$. Since the Hamiltonian (3.18) is harmonic, it can be diagonalized exactly. The center of mass mode is unaffected by the interactions and remains at frequency ω. All other modes are shifted to a higher frequency $\Omega = \sqrt{\omega^2 + \kappa N}$. This result is seen by explicitly constructing the canonical transformation that diagonalizes (3.18).

This transformation is described by a change from coordinates $r_1, r_2, ...r_N$, to $\tilde{r}_1, \tilde{r}_2, ...\tilde{r}_N$, via a mapping $\tilde{r}_i = X_{ij}r_j$, with $X_{ij}X_{kj} = \delta_{ik}$. The only restriction placed on X is that $X_{Nj} = 1/\sqrt{N}$, which forces $\tilde{r}_N = \sum_i r_i/\sqrt{N}$ to be proportional to the position of the center of mass. One applies the same transformation to the momenta of the particles, producing new momenta π_i. The commutation relationships are clearly maintained by this canonical transformation, and the transformed Hamiltonian is

$$H = \left(\frac{\pi_N^2}{2m} + \frac{m\omega^2 \tilde{r}_N^2}{2} \right) + \sum_i^{N-1} \left(\frac{\pi_i^2}{2m} + \frac{m\Omega^2 \tilde{r}_i^2}{2} \right), \tag{3.19}$$

yielding, as expected, one mode with frequency ω (the center of mass mode) and $N-1$ modes with frequency $\Omega = \hbar\sqrt{\omega^2 + \kappa N}$, which is greater than the energy of the center of mass mode. The transformation X is not unique, one (arbitrary) choice is,

$$X = \begin{pmatrix} \frac{1}{\sqrt{2}} & \frac{-1}{\sqrt{2}} & 0 & \cdots & & 0 \\ \frac{1}{\sqrt{6}} & \frac{1}{\sqrt{6}} & \frac{-2}{\sqrt{6}} & 0 & \cdots & 0 \\ \frac{1}{\sqrt{12}} & \frac{1}{\sqrt{12}} & \frac{1}{\sqrt{12}} & \frac{-3}{\sqrt{12}} & 0 & \cdots & 0 \\ \vdots & & & & & \\ \frac{1}{\sqrt{N}} & \frac{1}{\sqrt{N}} & \frac{1}{\sqrt{N}} & \frac{1}{\sqrt{N}} & \cdots & \frac{1}{\sqrt{N}} & \frac{1}{\sqrt{N}} \end{pmatrix}. \tag{3.20}$$

The lowest energy state with $L\hbar$ units of angular momentum has all of the angular momentum carried by the center of mass co-ordinate, and in dimensionless units is

$$\Psi = \sqrt{\frac{N}{\pi^N L!}} (\tilde{z}_N)^L \exp\left(-\sum_i r_i^2/2 \right). \tag{3.21a}$$

$$= \frac{1}{\sqrt{\pi^N L!}} \left(\sum_{i=1}^N z_i \right)^L \exp\left(-\sum_i r_i^2/2 \right), \tag{3.21b}$$

where the symbol $z_i = x_i + iy_i$ represents the position of the particle in the $x - y$ plane. For $L \sim N$, the single particle density matrix has $\sqrt{L/N}$ large eigenvalues of size $N\sqrt{N/L}$, and is therefore fragmented.

This fragmented state can be understood in terms of singly condensed states which break rotational invariance. A particularly simple demonstration of this connection

involves writing

$$\left(\sum_{i=1}^{N} z_i\right)^L \propto \frac{1}{2\pi} \int_0^{2\pi} d\phi \, e^{-iL\phi} \prod_i \exp(ae^{i\phi}z_i), \tag{3.22}$$

for any real number α. Using this decomposition, the lowest energy state with L units of angular momentum can be expressed as a sum of condensed states,

$$\Psi \propto \int d\phi \prod_i \exp(\alpha e^{i\phi}z_i)e^{-r_i^2/2}. \tag{3.23}$$

The integrand is a Gaussian shaped condensate displaced a distance α from the origin along a ray which makes an angle ϕ to the x axis. This state also has momentum α per particle in the direction perpendicular to its displacement, and therefore has angular momentum $N\alpha^2$. Setting $\alpha = \sqrt{L/N}$, yields a state with angular momentum L. A similar analysis was carried out by Pethick and Pitaevskii [70].

3.3.3 Toroidal clouds

Like the attractive condensate in a harmonic trap, an attractive condensate in a toroidal trap will spontaneously break rotational symmetry when given sufficient angular momentum. For sufficiently strong confinement an atomic cloud in a toroidal trap of radius R can be modeled by a one dimensional Hamiltonian,

$$H = \sum_\ell \frac{\hbar^2\ell^2}{2mR^2}a_\ell^\dagger a_\ell + \frac{g}{2}\sum_{\ell_1+\ell_2=\ell_3+\ell_4} a_{\ell_1}^\dagger a_{\ell_2}^\dagger a_{\ell_3} a_{\ell_4} \tag{3.24}$$

The annihilation operator a_ℓ acts on a particle in the state which has $\ell\hbar$ units of angular momentum. Once again g parameterizes the interactions. The characteristic length associated with the interactions is $L_g = m/\hbar^2 g$.

Before proceeding I should caution that one dimensional systems can act in peculiar ways. For instance, unlike three dimensions, where a gas with attractive interactions collapses to a point, the one dimensional gas forms a stable soliton. This behavior can be understood from energetic arguments. Consider an attractive condensate ($g < 0$) in d dimensions with a characteristic length L. The kinetic energy per particle associated with confining the cloud is of order $\hbar^2/mL^2$. The interactions provide a potential energy per particle of $-|g|(N/L^d)$. For $d > 2$, the energy is minimized by making L as small as possible, while for $d = 1$, the minimum energy is at finite L given by $L = L_s \approx L_g/N \sim 1/|g|N$. My analysis will start from the extremely dilute limit, where the soliton length scale L_s is larger than the system size. In such a situation the ground state of Eq. (3.24) is uniform.

One dimensional systems also have a density of states which is very large at low energies, making the system particularly susceptible to both thermal and quantum mechanical fluctuations. Consequently there is no long-range order in one dimension [71]. Such considerations are only important in the thermodynamic limit, and are not a concern here.

Under rotation at frequency Ω the Hamiltonian in Eq. (3.24) transforms as $H \rightarrow H - \Omega \sum_\ell (\hbar \ell) a_\ell^\dagger a_\ell$. In the absence of interactions the ground state is then $(a_\ell^\dagger)^N |\text{vac}\rangle$, where ℓ is the closest integer to Ω/Ω_0, with $\Omega_0 = \hbar^2/mR^2$. Weak interactions will principally mix the two lowest energy states. It is therefore reasonable to truncate Eq. (3.24) to two levels. Without any loss of generality I will limit the discussion to $0 < \Omega < \Omega_0$, where these two states have $\ell = 0$ and $\ell = 1$, so that

$$
\begin{aligned}
H_{\text{eff}} \quad = \quad & \hbar(\Omega_0/2 - \Omega) a_1^\dagger a_1 \\
& + \frac{g}{2}(a_0^\dagger a_0^\dagger a_0 a_0 + a_1^\dagger a_1^\dagger a_1 a_1 + 4 a_0^\dagger a_1^\dagger a_1 a_0).
\end{aligned}
\tag{3.25}
$$

Angular momentum is conserved, so within this truncated model both $n_0 = a_0^\dagger a_0$ and $n_1 = a_1^\dagger a_1$ are conserved, implying that the eigenstates are of the form $|n_0\rangle = (a_0^\dagger)^{n_0}(a_1^\dagger)^{n-n_0}|\text{vac}\rangle$, with energies

$$
E(n_0) = gn^2/2 + (gn_0 + \hbar\Omega_0 - \hbar\Omega)(n - n_0).
\tag{3.26}
$$

For repulsive interactions E is concave down, and the ground state is always $n_0 = 0$ or $n_0 = n$, depending on whether Ω is greater or less than $\Omega_0/2$. Note that for $|\Omega - \Omega_0/2| < 2g/\hbar$ there is an energy barrier separating $n_0 = 0$ and $n_0 = n$, leading to metastable persistent currents, the topic of Chapter 4.

For attractive interactions, E is concave up, and when $|\Omega - \Omega_0/2| < 2|g|/\hbar$ the ground state is fragmented. In terms of symmetry breaking, one can understand the fragmented state as the result of the formation of a large soliton at some particular place along the ring. Averaging over all possible locations of the soliton gives rise to the fragmented state. As I have reduced the system to a two well model, all of the previous discussion of two level systems is directly applicable.

A more sophisticated analysis of this model for weak interactions has been performed by Ueda and Leggett [72]. Additionally, for arbitrary interactions one can solve for the ground state of a one dimensional Bose gas with periodic boundary conditions using the Bethe ansatz [59], and one finds that this symmetry breaking picture remains accurate for strong interactions.

If the toroidally trapped Bosons have an internal degree of freedom, a spin texture can play the role of rotation, producing similar results [73].

3.3.4   Multiple wells

The obvious generalization of a two well Josephson junction is a Josephson array, featuring multiple wells with weak tunneling between neighbors. Such a system is realized in experiments involving atoms trapped in optical lattices [74], and is depicted in Fig. 3.3.
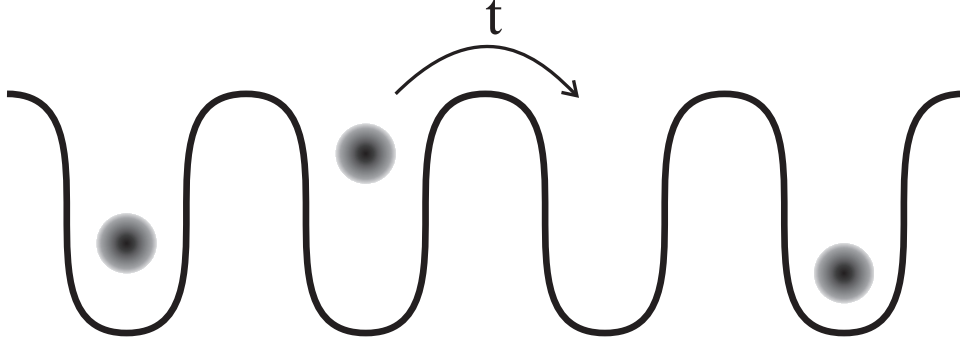
Figure 3.3: Schematic of an atomic Josephson junction array. The atoms are trapped in a standing-wave light field, and can hop from one minima to another. The hopping is controlled by a parameter t.

This system boasts a localization-delocalization transition, where for weak enough tunneling the atoms in each well are localized. In this regime the condensate is fragmented into M pieces, where M is the number of wells. For stronger tunneling the system is singly condensed and superfluid. The model used to describe this system is the boson Hubbard model,

$$H = -t \sum_{\langle ij \rangle} c_i^\dagger c_j + \frac{U}{2} \sum_i c_i^\dagger c_i^\dagger c_i c_i. \tag{3.27}$$

The operator c_i annihilates a particle in the ith well, and $\langle ij \rangle$ denotes a sum over nearest neighbors only. The parameter t controls the tunneling, while $U > 0$ controls the interaction strength. In the absence of tunneling the ground state simply consists of a separate condensate in each of the M wells, $(\prod_i c_i^\dagger)^{N/M}|\text{vac}\rangle$. This state has M condensates and is fragmented. Within standard mean field theory one breaks the phase symmetry between each pair of wells. In the absence of tunneling these phases ϕ_i are arbitrary, and all wavefunctions of the form

$$\psi = \frac{1}{\sqrt{N!}} \left(\frac{1}{\sqrt{M}} \sum_i c_i^\dagger e^{i\phi_i} \right)^N |\text{vac}\rangle, \tag{3.28}$$

are degenerate. The tunneling term locks these phases.

An ingenious method of finding the phase boundary between localized and delocalized regimes was introduced by Fisher et al. [75] and recently revisited by Oosten et al. [76]. This phase boundary also separates the fragmented and singly condensed regimes. Fisher's approach is based upon the observation is that in the localized regime the interactions dominate over tunneling, and one cannot used approximations where the interactions are treated as small. In this approach, one instead approximates the hopping term $c_i^\dagger c_j$, expanding the field operators in this term as $c_i = \psi + \delta c_i$, where $\psi = \langle c_i \rangle$ is the superfluid order parameter, which I take to be real. In the localized state $\psi = 0$, while in the superfluid state $|\psi|^2$ approximates the density of particles. To first order in the fluctuation the kinetic term is

$$c_i^\dagger c_j \approx \psi^2 + \psi(deltac_j + \delta c_i^\dagger) = \psi(c_j + c_i^\dagger) - \psi^2. \tag{3.29}$$

Introducing a chemical potential μ the effective mean-field Hamiltonian reads

$$H \;=\; \sum_i \left[-2td\psi(c_i + c_i^\dagger) - \mu c_i^\dagger c_i + (U/2)c_i^\dagger c_i^\dagger c_i c_i \right] \tag{3.30}$$
$$+2dt\psi^2 M$$

where d is the number of nearest neighbors, and M is the number of sites. Note that the different sites are decoupled. Self-consistency requires that $\psi = \langle c_i \rangle$.

This approximate Hamiltonian can be analyzed much like the asymmetric Josephson junction in Section 3.7.1. Each site i decouples, and the wavefunction of the $i'th$ site is $|f\rangle = \sum_j f_j(c_i^\dagger)^j|\text{vac}\rangle/\sqrt{j!}$. The coefficients f_i obey a difference equation with constraints,

$$(E + \mu j - Uj(j-1)/2)f_j \;+\; 2td\psi\sqrt{j+1}\,f_{j+1} \tag{3.31a}$$
$$+\; 2td\psi\sqrt{j}\,f_{j-1} = 0$$
$$\sum_j |f_j|^2 \;=\; 1 \tag{3.31b}$$
$$\sum_j j|f_j|^2 \;=\; N/M \tag{3.31c}$$
$$\sum_j (f_j^* f_{j+1}\sqrt{j+1}) \;=\; \psi. \tag{3.31d}$$

Within this approximation the single particle density matrix is

$$\langle c_i^\dagger c_j \rangle = \delta_{ij}(N/M) + (1 - \delta_{ij})|\psi|^2, \tag{3.32}$$

which has one eigenvalue of size $N/M + (M-1)|\psi|^2$, and $M-1$ eigenvalues of size $N/M - |\psi|^2$. As expected, the state is singly condensed when $|\psi|^2 \sim N/M$.

For $U \gg 4tdN/M$ the tunneling is exponentially suppressed and at most two f_j's are non-zero. Writing N/M as $n + y$ where n is integral and $0 \le y < 1$, the non-zero f_j's are $f_n = \sqrt{1-y}$ and $f_{n+1} = y$, yielding $|\psi|^2 = y(1-y)(n+1)$. Assuming $n \gg 1$ the largest eigenvalue of the single particle density matrix is $N[y(y-1) + \mathcal{O}(1/M)]$. Thus with even an infinitesimal tunneling, there will be a single condensate if the number of particles is incommensurate ($y \ne 0, 1$).

For $U \ll 4tdN/M$ the difference equation, Eq. (3.31a) can be replaced by a differential equation, and the ground state is always singly condensed. One advantage of a multiple well system over a single Josephson junction is that the symmetry breaking is readily detected here. This point is illustrated by considering bosons in an optical lattice. An experimentalist can look for the symmetry breaking by turning off the lattice and observing the density pattern formed when the clouds overlap. In the singly condensed regime all of the wells have the same phase, so the density pattern will be characteristic of multi-slit diffraction. That is it will be a periodic array of very narrow spikes, the width of the spikes scaling as $1/M$. The fragmented state will also yield a periodic density pattern, but within each period there will be no definite structure. Such behavior was seen by Anderson and Kasevich [74].

3.4 Further examples

In addition to the examples given in Section 3.3, there are a large number of Bose systems which, within mean field theory, are found to break a symmetry. Although the exact ground states are not known for these systems, from our general arguments I expect that the ground states are fragmented. Here I give two such examples.

3.4.1 Phase separation

Depending upon the interaction parameters, mixtures of bosons in a trap can be miscible or immiscible. The various particles could be different hyperfine states of a single atom [77], different isotopes, or even different chemical species. Immiscible species will phase separate, generically breaking some spatial symmetry. The ground state here will be fragmented, and the symmetry broken states will be singly condensed.

A particular simple example of this phenomenon was discussed by Esry [78], who considered a cigar-shaped trap containing ^{85}Rb and ^{87}Rb. Atomic ^{85}Rb has an extremely large negative scattering length, implying an attractive interaction. Conversely the interaction between ^{87}Rb atoms is repulsive, as is the interspecies scatter-

ing. Thus it is energetically favorable for the two atoms to phase separate, maximizing the scattering between ^{85}Rb atoms, and minimizing the interspecies scattering.

By solving the Gross-Pitaevskii equation, Esry was able to show that for sufficiently large number of ^{87}Rb atoms, the mean field ground state broke parity symmetry, with all of the ^{87}Rb atoms at one end of the cigar and all of the ^{85}Rb atoms at the other. The true ground state involves a linear superposition of both symmetry breaking states. More detailed discussion of this phenomena can be found in [79] and references within.

3.4.2 Vortex structures

As observed experimentally, a rotating Bose condensate may contain vortices [10, 80]. Except in the case of a single straight vortex line, rotational invariance is broken by the presence of these vortices, and the true ground state will be fragmented. The fragmentation of finite temperature vortex arrays is discussed in Section 3.5

3.5 Finite temperature

Fragmentation is more prevalent at finite temperature than at zero temperature. The basic reason is that when the temperature is larger than the tunneling energy, the phases between different condensates are randomized by thermal fluctuations. This notion is easily demonstrated by a non-interacting Josephson junction, governed by the Hamiltonian

$$H = -t(a^\dagger b + b^\dagger a). \tag{3.33}$$

This Hamiltonian is diagonal in the basis of symmetric and asymmetric states, for which the creation operators are $(a^\dagger + b^\dagger)/\sqrt{2}$, and $(a^\dagger - b^\dagger)/\sqrt{2}$, so the single particle density matrix will be diagonal in this basis. At zero temperature only the symmetric state is occupied, and there is a single condensate. At very large temperature each of these states will be equally occupied so the system will be fragmented. For intermediate temperatures, the occupation of each of these states is

$$n_a^s = \frac{\sum_{m=-N/2}^{N/2}(N/2 \pm m)e^{2t\beta m}}{\sum_{m=-N/2}^{N/2} e^{2t\beta m}} \tag{3.34}$$

$$= \frac{N}{2} \mp \left(\frac{N+1}{2} \coth(\beta t(N+1)) - \frac{1}{2} \coth(\beta t) \right). \tag{3.35}$$

The upper and lower signs are used for the symmetric and antisymmetric states. There is a smooth crossover between a singly condensed state at $T = 0$, and a

59
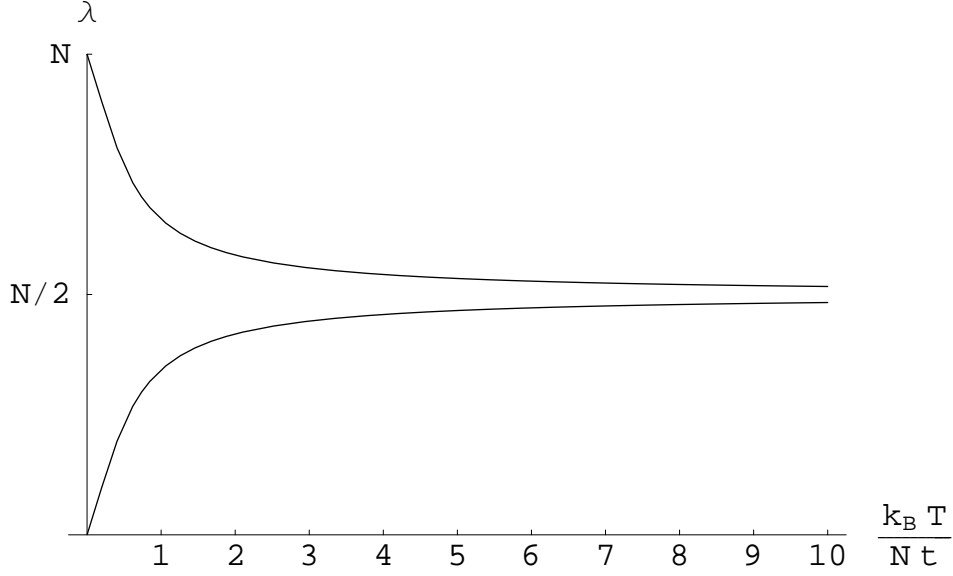
Figure 3.4: Eigenvalues of non-interacting Josephson junction at finite temperature. The temperature is scaled by the tunneling t. At zero temperature there is one large eigenvalue, while at high temperature both eigenvalues are of the same size.

fragmented state at $T \gg Nt/k_B$. These eigenvalues are plotted in Fig. 3.4.

A qualitatively different example of how finite temperature effects fragment a condensate is a vortex lattice. Imagine a bucket of ^{4}He rotating at frequency Ω. The ground state of the system will contain a triangular array of vortices with n_v vortices per unit area. At finite temperature the vortex lattice will be thermally excited, giving rise to a decay in the phase correlations across the sample. Let $\psi(r)$ be the superfluid order parameter coarse grained on a scale large compared to the vortex spacing. According to [81], for large separations $|r - r'|$, the correlation function $\langle \psi^*(r')\psi(r') \rangle$ decays as $|r - r'|^{-\eta}$, where $\eta = 1/(3\pi^2 \rho r_v \Lambda^2)$ is proportional to the ratio of the distance between particles to the distance between vortices. This expression is correct as $|r - r'|$ becomes large. Here the particle number density is ρ, the thermal wavelength is $\Lambda = \sqrt{2\pi/mk_b T}$ and the distance between vortices is r_v. This algebraic decay of correlations in real space corresponds to an algebraic decay in momentum space. For $\eta < 3$, the occupation of the $k = 0$ mode scale as $N_0 \sim L^{3-\eta}$, and as as $k \to 0$ the $k \neq 0$ modes scale as $N_k \sim k^{\eta-3}$. Thus the number of macroscopically occupied modes scale as L^η.

For a typical helium experiment, $\eta < 10^{-8}$, and the depletion caused by this effect is negligible. Experiments on alkali gases at MIT [82] create a vortex lattice with $r_v \sim 5\mu$m and a particle density $\rho \sim 10^{14}$cm^{-3}, giving a rough estimate of $\eta \sim 10^{-3}$, which is also a minor correction. Experiments with smaller vortex lattices in Paris

[10] have a similar vortex spacing $r_v \sim 2\mu$m, and density $\rho \sim 10^{14}$cm^{-3}, yielding a comparable value for η. Although vortex lattices in current experiments are not thermally fragmented, there does not appear to be any fundamental impediment to making η larger.

3.6 Summarizing remarks

Bose condensation is a very robust phenomenon. The fragmentation of a singly condensate into many condensates is therefore a surprising and unexpected phenomenon. In all cases that I have explored, the root cause of fragmentation is the presence of a symmetry which can be broken by an infinitesimal perturbation. Consequently, fragmentation is ubiquitous, but also very fragile and difficult to detect.

3.7 Mathematical details

3.7.1 Josephson junctions

In this Section I present an analysis of both symmetric and asymmetric Josephson junctions. Many of these results can be found elsewhere (for example, [16, 83, 84]), but it is useful to revisit them in a manner which is tied into the present discussion.

Symmetric junctions

Here I analyze the crossover of a symmetric Josephson Junction from a singly condensed to a fragmented ground state. The Hamiltonian of an ideal junction is

$$H = -t(a^\dagger b + b^\dagger a) - g a^\dagger b^\dagger b a, \qquad (3.36)$$

where a and b are annihilation operators for two spatially separated wells, t is a tunneling matrix element, and g parameterizes the interactions. I focus on repulsive interactions, $g > 0$.

As discussed by Leggett [16], the system described by Eq. (3.36), has three distinct behaviors. For $t \ll g/N$, the Fock regime, no tunneling occurs. For $g/N \ll t \ll Ng$, the Josephson regime, tunneling occurs at a rate governed by the Josephson plasma frequency $\omega_J^2 = 2tgN$. For $Ng \ll t$, the Rabi regime, the system behaves as a collection of non-interacting particles undergoing Rabi oscillations between the two wells.

I now derive this structure and investigate the single particle density matrix using two methods. First I explicitly calculate the ground state wavefunction in the form,

$$|f\rangle = \sum_m f_m |N/2 + m, N/2 - m\rangle, \tag{3.37}$$

where the state $|n_a, n_b\rangle$ contains n_a particles in well a and n_b particles in well b. The eigenvalue equation $H|f\rangle = E|f\rangle$ is a matrix equation

$$[g(N^2/4 - m^2) + E]f_m \quad + \quad t[(N/2 - m)(N/2 + m + 1)]^{1/2} f_{m+1} \tag{3.38}$$
$$+ \quad t[(N/2 + m)(N/2 - m + 1)]^{1/2} f_{m-1} = 0.$$

In both the Fock and Josephson regimes, f_m is sharply peaked at $m = 0$ with width $\delta m \ll N^{1/2}$, and this equation may be approximated as

$$[g(N^2/4 - m^2) + E]f_m + [tN/2]f_{m+1} + [tN/2]f_{m-1} = 0. \tag{3.39}$$

This assumption about the width of f_m is readily verified *a posteriori*. In the Fock regime, $t \ll g/N$, perturbation theory converges, and the ground state has $f_m = \delta_{m0} + \mathcal{O}(tN/g)$. The single particle density matrix is fragmented with two eigenvalues of size $(N/2)(1 + \mathcal{O}(tN/g))$. In the Josephson limit, a semiclassical approximation is valid and the discrete eigenvalue equation can be replaced by a differential equation $(E + gN^2/4)f(m) = -(tN/2)\partial_m^2 f(m) + gm^2 f(m)$, whose ground state is $f(m) \propto \exp(-m^2/2\xi^2)$, with $\xi^4 = tN/2g$. In the Josephson limit the off-diagonal matrix element is given by $\langle a^\dagger b \rangle = (N/2)\exp(-1/4\xi^2)$, implying that up to exponentially small corrections, the single particle density matrix has a single large eigenvalue of size N, and the state is singly condensed. Note that the number fluctuations $\langle (n_a - n_b)^2 \rangle - \langle (n_a - n_b) \rangle^2$ are sub-Poissonian, and this regime corresponds to a squeezed state in number-phase space. Finally, in the Rabi regime, perturbation theory about the state $(a^\dagger + b^\dagger)^N |\text{vac}\rangle/N! 2^{N/2}$ converges, and once again the state is singly condensed.

This same structure can be understood from within Bogoliubov theory, where the field operators a and b are expressed as a mean field plus fluctuations, $a = \sqrt{N/2} + \tilde{a}$, $b = \sqrt{N/2} + \tilde{b}$. Adding a chemical potential μ to the Hamiltonian, and expanding to second order in the fluctuations,

$$H = \left(g(N/2)^2 - (\mu + t)N\right) + \sqrt{N/2}(N/2 - (\mu + t))(\tilde{a} + \tilde{a}^\dagger + \tilde{b} + \tilde{b}^\dagger) \tag{3.40}$$
$$+ (gN - \mu)(\tilde{a}^\dagger \tilde{a} + \tilde{b}^\dagger \tilde{b}) + (gN/4)(\tilde{a}\tilde{a} + \tilde{a}^\dagger \tilde{a}^\dagger + \tilde{b}\tilde{b} + \tilde{b}^\dagger \tilde{b}^\dagger) - t(\tilde{a}\tilde{b}^\dagger + \tilde{b}^\dagger \tilde{a}).$$

Setting $\mu = N/2 - t$ eliminates the linear terms, and the quadratic terms are diagonalized via a Bogoliubov transformation. The resulting depletion is $N_d = (\epsilon - E)/2E$,

where $\epsilon = 2t + gN/2$, and $E^2 = \epsilon^2 - (gN/2)^2$. For $t \gg Ng$ the depletion is negligible, $N_d \ll 1$. This vanishing depletion characterizes the Rabi regime. For $Ng \gg t \gg g/N$ the depletion is $N_d = \sqrt{gN/32t} + \mathcal{O}((t/gN)^0)$, which is much greater than 1 but much less than N, as one expects in the Josephson regime. For $g/N \gg t$ the depletion is of order 1, signalling a breakdown of the Bogoliubov theory, and the system enters the Fock regime.

Asymmetric junctions

In Section 3.7.1 I briefly describe how fragmentation appears in a double well system. A crucial point in that example is that the two levels are degenerate. Here I extend the model to that of an asymmetric double well, finding that as long as the energy difference between the two states is less than the interaction energy gN, then the asymmetry plays a minor role, and the system possesses the same three regimes: Rabi, Josephson, and Fock. When the energy difference between the two states is greater than gN, the system is always singly condensed. The Fock regime of the asymmetric well shows additional structures as one changes the bias.

The asymmetric double-well system is described by a Hamiltonian

$$
\begin{aligned}
H &= -t(a^\dagger b + b^\dagger a) + \epsilon(a^\dagger a - b^\dagger b) \\
&\quad + (g/2)(a^\dagger a^\dagger aa + b^\dagger b^\dagger bb).
\end{aligned}
\tag{3.41}
$$

The wells are split by an energy 2ϵ and there is a tunneling of strength t between them. I will assume repulsive interactions $g > 0$, and with no loss of generality take $\epsilon \geq 0$.

For small asymmetries, $\epsilon \ll g/N$, the analysis performed for the symmetric system works without modification, and one has three regimes: Rabi, Josephson, and Fock, their boundaries unaffected by ϵ. Larger asymmetries are more complicated; one has the same three regimes, but their boundaries are shifted, and the Fock regime contains extra structure. I will first address this extra structure, and then consider the boundaries of these regimes.

Writing the wavefunction as Eq. (3.37), the f's obey the discrete eigenvalue equation

$$
\begin{aligned}
[g(N/2 - N^2/4 - m^2) - 2\epsilon m + E]f_m &+ t[(N/2 - m)(N/2 + m + 1)]^{1/2} f_{m+1} \\
&+ t[(N/2 + m)(N/2 - m + 1)]^{1/2} f_{m-1} = 0.
\end{aligned}
\tag{3.42}
$$

The extreme limit of the Fock regime is when $t = 0$. In this limit, the eigenstates are of the form $f_m = \delta_{m\bar{m}}$, for any integer $\bar{m}$, corresponding to the state $(a^\dagger)^{N/2+\bar{m}}(b^\dagger)^{N/2-\bar{n}}|\text{vac}\rangle$. When $\epsilon < gN/2$, the ground state has $\bar{m}$ equal to the closest integer to $-\epsilon/g$. This state is degenerate when $-\epsilon/g$ is half integral.

Adding a sufficiently small t will only change this structure near the degeneracy points. To find the implications of $t \neq 0$, I take $\epsilon = (n+1/2+\delta)g$, where $n < N/2$ is an integer, and δ is a small number with $|\delta| < 0.5$. In this case the only non-zero f's will be f_{-n} and f_{-n-1}, and in this restricted space the eigenvalue equation becomes

$$\begin{pmatrix} \bar{E} - g\delta & \Delta \\ \Delta & \bar{E} + g\delta \end{pmatrix} \begin{pmatrix} f_{-n} \\ f_{-n-1} \end{pmatrix} = 0, \tag{3.43a}$$

$$\Delta = t\sqrt{(N/2-n)(N/2+n+1)}, \tag{3.43b}$$

where $\bar{E} = E + gn + gn^2 + gN/2 - gN^2/4 + g\delta + 2gn\delta$. The ground state energy is given by $\bar{E}^2 = (g\delta)^2 + t^2(N/2-n)(N/2+n+1)$. This state has the form $\psi = \alpha|N/2+n, N/2-n\rangle + \beta|N/2+n+1, N/2-n-1\rangle$, with single-particle density matrix elements

$$\langle a^\dagger a \rangle = N/2 + n + |\beta|^2 \tag{3.44a}$$
$$\langle a^\dagger b \rangle = \beta\alpha\sqrt{(N/2-n)(N/2+n+1)} \tag{3.44b}$$
$$\langle b^\dagger a \rangle = \beta\alpha\sqrt{(N/2-n)(N/2+n+1)} \tag{3.44c}$$
$$\langle b^\dagger b \rangle = N/2 - n - |\beta|^2. \tag{3.44d}$$

The system has its greatest level of coherence when $\delta = 0$, where the coefficients α and β are equal and the two eigenvalues are

$$EV = N/2 \pm (1/4)\sqrt{N^2 + 2N + 12n^2 + 12n + 4}. \tag{3.45}$$

For large N and small n this leads to an eigenvalue of size $3N/4$ and another of $N/4$. It is startling that the tunneling of a single particle leads to such a large increase in the coherence of the single particle density matrix.

The system has its lowest level of coherence when $\delta = -1/2$, where the coefficient β vanishes, and the two eigenvalues are

$$EV = N/2 \pm n. \tag{3.46}$$

The structure discussed here is clearly seen in Fig. 3.5 where I plot the size of the largest eigenvalue of the single particle density matrix as a function of t and ϵ. In this plot, $N = 10$ particles are used, and the energy scale is set by taking $g = 1$.

Darker colors correspond to a smaller eigenvalue. This figure was constructed by numerically diagonalizing the Hamiltonian in the 11×11 dimensional space of all 10 particle wavefunctions.

The boundary of the Fock regime corresponds to the breakdown of perturbation theory in powers of t. To zeroth order in t, the ground state is $f_m = \delta_{m\bar{m}}$, with $m = -\epsilon/g$ (the discreteness of the variables is irrelevant for an order of magnitude estimate). To first order in t, $f_{\bar{m}\pm 1}$ are non-zero; for example

$$f_{\bar{m}+1} = (t/g)\sqrt{(N/2 + \bar{m} + 1)(N/2 - \bar{m})}. \qquad (3.47)$$

As long as $f_{\bar{m}+1} \ll 1$ the original calculation is consistent. Thus in order to be in the Fock regime one needs $t \ll g/\sqrt{N^2/4 - \epsilon^2/g^2}$.

Similarly, the boundary of the Rabi regime is characterized by the breakdown of perturbation theory in powers of g. An order of magnitude estimate of this boundary is found by comparing the interaction energy gN with a typical excitation energy, $E = (t^2 + \epsilon^2)^{1/2}$. When these energies are comparable, one is at the boundary between the Rabi and Josephson regime.

3.7.2 Proof of indistinguishability of an ensemble of singly condensed states and a fragmented state

I conclude this Chapter by showing that up to terms of order $n/(N-n)$, the n-particle reduced density matrix of an N particle system is identical for an ensemble of singly condensed states and for a fragmented state. The required assumption is that the fragmented state can be expressed as a sum over the symmetry-broken condensed states which make up the ensemble. The consequence of this result is that it is very difficult to distinguish condensed and fragmented states.

To emphasize these consequences, consider a particularly simple fragmented state consisting of a coherent superposition of N particles in state a, and N particles in state b;

$$|\psi\rangle = \frac{1}{\sqrt{2N!}} \left((a^\dagger)^N + (b^\dagger)^N \right) |\text{vac}\rangle. \qquad (3.48)$$

This state is a "Schrödinger Cat" state, consisting of a quantum superposition of two macroscopically distinct wavefunctions, and the single particle density matrix has two large eigenvalues. If one takes $n < N$ particles out of this state, they will either all be a atoms, or all be b atoms. So as far as any n particle measurements are concerned, one can imagine that instead of having a highly correlated state, one has an ensemble of singly condensed states, half of the states consist of N particles in state a, and
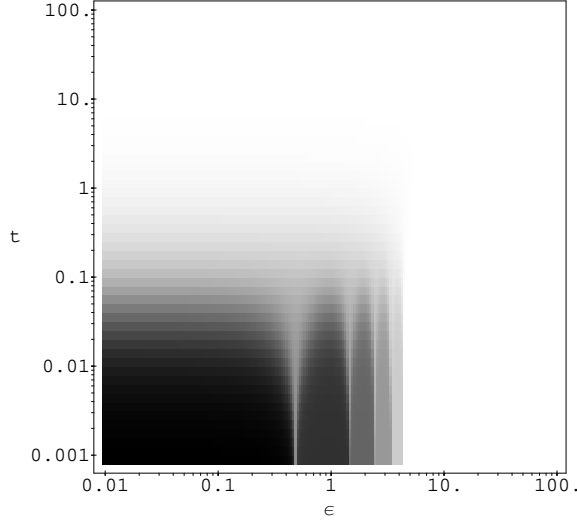
Figure 3.5: Density plot of the largest eigenvalue λ_{max} of the single particle density matrix of a system of $N = 10$ particles in an asymmetric double well where the interactions are characterized by $g = 1$, the tunneling by t and the asymmetry by ϵ [see Eq. (3.41)]. Black corresponds to the minimum value $\lambda_{\mathrm{max}} = 5$, while white corresponds to the maximum value $\lambda_{\mathrm{max}} = 10$. There are three distinct regimes, the Fock regime (darker area) where t is perturbative, the Rabi regime where g is perturbative, and an intermediate Josephson regime. The boundary between the Josephson and Rabi regime lies within the white area of the plot. The plateaus in the Fock regime are understood by setting $t = 0$, in which case there are a fixed integral number of particles in each well. As one tilts the wells it becomes favorable to increase the number of particles in the lower well. At the boundaries between the plateaus there is a marked increase in the size of the largest eigenvalue coincident with an avoided crossing of energy levels.

the other half of N particles in state b. One must perform a huge conceptual leap to replace Eq. (3.48) with a classical ensemble of condensed states. Such a replacement means that as far as any individual run of our experiment is concerned, the state is condensed into either $(a^\dagger)^N|\text{vac}\rangle$ or $(b^\dagger)^N|\text{vac}\rangle$.

In a more generic situation one begins with a fragmented state of the form

$$|f\rangle \propto \sum_{g \in G} |g\rangle. \tag{3.49}$$

The states $|g\rangle$ are singly condensed, and are labeled by elements of the symmetry group G. For example, Eq. (3.6) is a fragmented state of this form. The normalization of $|f\rangle$ is not important. The (many particle) density matrix corresponding to this state is

$$\rho_f = |f\rangle\langle f| \propto \sum_{g,g'} |g\rangle\langle g'|. \tag{3.50}$$

The n-particle reduced density matrices $\rho_f^{(n)}$ are formed when all but n of the particles are traced over. All n particle properties of the system are encoded in $\rho^{(n)}$. These reduced density matrices are most familiar in a position basis, where they are given by

$$\rho_f^{(n)}(r_1, \ldots r_n, r_1' \ldots r_n') \tag{3.51}$$
$$\propto \sum_{g,g'} \langle g|\psi^\dagger(r_n) \cdots \psi^\dagger(r_1)\psi(r_1) \cdots \psi(r_n)|g'\rangle.$$

In this equation, $\psi(r)$ is the field operator, which annihilates a particle at position r. I have neglected the normalization of this density matrix, as it can be simply restored by equating the trace of $\rho^{(n)}$ to $n!$.

I now compare this fragmented state to an ensemble of condensed states, with a density matrix

$$\rho_i \propto \sum_{g \in G} |g\rangle\langle g|. \tag{3.52}$$

The index i is chosen to indicate that this is an incoherent (classical) sum of condensed states. Analogous to Eq. (3.51), the reduced density matrices are

$$\rho_i^{(n)}(r_1, \ldots r_n, r_1' \ldots r_n') \propto \tag{3.53}$$
$$\sum_g \langle g|\psi^\dagger(r_n) \cdots \psi^\dagger(r_1)\psi(r_1) \cdots \psi(r_n)|g\rangle.$$

Depletion plays no role in my argument, so for simplicity I take

$$|g\rangle \;=\; (N!)^{-1/2} \left(\int d^3r \, \psi^\dagger(r)\phi_g(r) \right)^N |\text{vac}\rangle \tag{3.54a}$$
$$=\; (N!)^{-1/2}(\psi_g^\dagger)^N|\text{vac}\rangle, \tag{3.54b}$$

67

where $\phi_g(r)$ is the wavefunction for the single particle state which is macroscopically occupied, and $\psi_g^\dagger$ is the operator which creates a particle in this state. Using this ansatz,

$$\rho_f^{(n)} \propto \sum_{g,g'} \langle \mathrm{vac}|(\psi_g)^N \psi^\dagger(r_n)\cdots\psi^\dagger(r_1) \tag{3.55a}$$
$$\times \psi(r_1)\cdots\psi(r_n)(\psi_{g'}^\dagger)^N|\mathrm{vac}\rangle$$

$$\propto \sum_{g,g'} \left(\phi_g^*(r_n)\cdots\phi_g^*(r_1) \right. \tag{3.55b}$$
$$\left. \times \phi_{g'}(r_1)\cdots\phi_{g'}(r_n)\right) \left[D_{gg'}\right]^{N-n} .$$

Generically the overlap $D_{gg'} = [\int d^3r\,\phi_g^*(r)\phi_{g'}(r)]$ is peaked about $g = g'$, and for $N \gg n$, the factor $(D_{gg'})^{N-n}$ can be replaced by a Gaussian of width $\mathcal{O}(1/\sqrt{N-n})$. Consequently, I can expand the rest of the sum, $[\phi_g^*(r_n)\cdots\phi_g^*(r_1)\phi_{g'}(r_1)\cdots\phi_{g'}(r_n)]$, to quadratic order about $g = g'$. This quadratic term is at most of order n, yielding

$$\rho_f^{(n)} \propto \sum_g (\phi_g^*(r_n)\cdots\phi_g^*(r_1)\phi_{g'}(r_1)\cdots\phi_{g'}(r_n) \tag{3.56}$$
$$+\mathcal{O}\left(n/(N-n)\right),$$

which to leading order equals $\rho_i^{(n)}$.

Chapter 4

Persistent Currents

The ability to support metastable current carrying states in multiply connected settings is one of the prime signatures of superfluidity. In this Chapter I calculate the stability of these currents against decay via thermal fluctuations, finding that the lifetimes of metastable currents can be tuned from much longer to much shorter than experimental time scales. The research presented in this Chapter was performed in collaboration with Paul Goldbart and Yuli Lyanda-Geller, and is published in Physical Review A [85].

4.1   Introduction

Multiply connected superfluid and superconducting systems can support states in which a persistent macroscopic particle current flows. While not truly eternal, these states can have extraordinarily long life times, their decay requiring the occurrence of certain relatively infrequent but nevertheless topologically accessible (quantum or thermal) collective fluctuations [86, 87, 88, 89]. The purpose of this Chapter is to address, theoretically, the ability of BEC alkali gas systems in multiply connected settings to support metastable current carrying states, and to address the stability and decay of such states via thermal fluctuations.

From a theoretical perspective, superfluidity is naturally addressed in a multiply connected setting, particularly that of a thin torus where the fluid can be treated in a quasi one dimensional manner. Thus there are a fairly large number of theoretical works looking at Bose gases in a toroidal trap [72, 73, 90, 91]. Several proposals for experimental multiply connected structures have been suggested. Figure 4.1 illustrates the toroidal geometry which I study here. A similar geometry has been realized at JILA, in a disk magnetic trapped filled with two hyperfine states of ru-
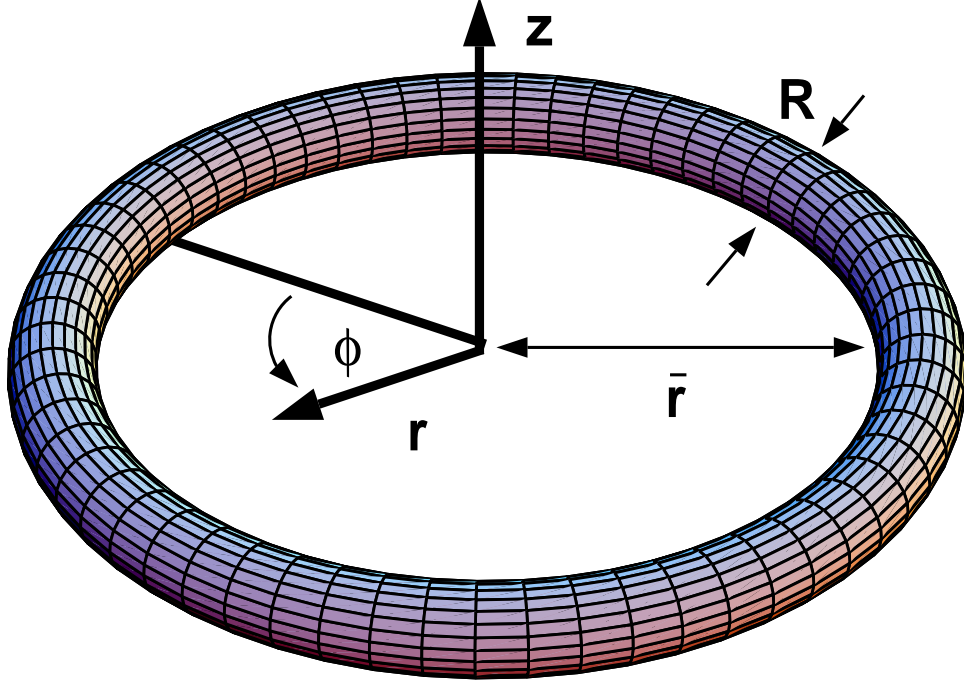
Figure 4.1: Envisaged geometry of a trap supporting metastable current carrying BEC states. The condensate healing length ξ_{MF} is regarded as being small, compared with the circumference of the torus $L \ (= 2\pi\bar{r})$, but larger than its thickness R.

bidium [92]. One of the species migrates to the center of the trap, leaving a toroidal volume for the other species, as depicted in Fig. 4.2. Another mechanism for creating a toroidal trap is to take a conventional simply connected trap, and shine a narrow laser beam through its center. When blue detuned from an atomic transition, such a laser beam presents a repulsive dipole force which restricts the atoms to a toroidal region. Microfabricated toroidal traps [94] and all optical toroidal traps [93] have also been suggested.

4.2 Gross Pitaevskii functional

I adopt a phenomenological description in which the state of the BEC system is characterized by a macroscopic wavefunction $\Psi(\mathbf{r}, t)$, in terms of which the condensate density n and current density $\mathbf{j}$ are given by

$$n(\mathbf{r}) \;=\; |\Psi(\mathbf{r})|^2, \tag{4.1a}$$

$$\mathbf{j}(\mathbf{r}) \;=\; \frac{\hbar}{2im}\left(\Psi^*\nabla\Psi - \Psi\nabla\Psi^*\right). \tag{4.1b}$$

a

b
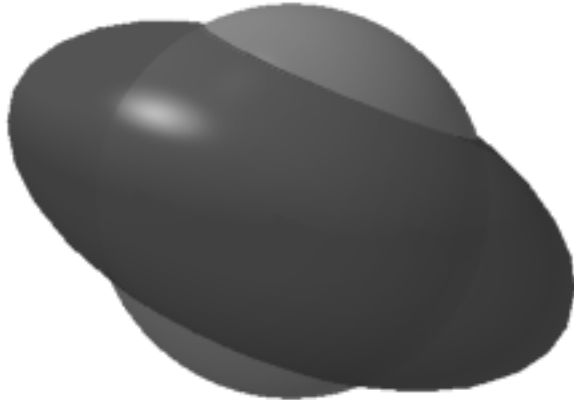
Figure 4.2: A multiply connected trap realized at JILA [92]. In a) a standard disk shaped harmonic trap is shown. In b) one sees the trap filled with two atomic hyperfine states. Due to their relative buoyancies, one state migrates to the center leaving a toroidal volume for the second species.

The energy $\mathcal{F}$ of the state is given by the Gross Pitaevskii form

$$\mathcal{F} = \int d^3r \left\{ \frac{\hbar^2}{2m} |\nabla\Psi|^2 + (V(\mathbf{r}) - \mu) |\Psi|^2 + \frac{g}{2} |\Psi|^4 \right\}, \qquad (4.2)$$

where m is the mass of an individual atom, $V(\mathbf{r})$ is an effective external potential describing the magnetic and optical confinement of the atoms, μ is the chemical potential, and g ($\equiv 4\pi\hbar^2 a/m$) represents the interatomic interaction, with a being an effective scattering length. Equation (4.2) can be derived from the microscopic equations of motion by making the variational ansatz that all of the condensed particles are in a state with wavefunction $\Psi(\mathbf{r}, t)$ (see Appendix C.4.1). This equation ignores the presence of noncondensed particles, which play the important role of a bath of energy and angular momentum that will enable the persistent currents to decay. The techniques of Chapter 6 provide kinetic equations to describe these noncondensed particles, but the problem at hand is dominated by energetics and not kinetics, so these detailed equations are not needed.

I consider trap potentials $V(\mathbf{r})$ that confine the gas to a cylindrically symmetric toroidal region (Fig. 4.1). Hence, V depends only on r and z, where $\{r, \phi, z\}$ are the usual cylindrical polar coordinates. Moreover, I restrict my attention to systems in which the circumference of the torus L ($= 2\pi\bar{r}$) is considerably greater than the condensate healing length ξ_{MF} [$\approx (\hbar^2/mg\bar{n})^{1/2}$, where $\bar{n}$ is related to the maximum particle-density], and the thickness of the torus R is comparable to or smaller than ξ_{MF}. This corresponds to a regime of low condensate-density. There are two main reasons for considering this setting: (i) there would be no locally-stable current-carrying states if L were comparable to or smaller than ξ_{MF}; (ii) for thicker samples (i.e. $R > \xi_{\mathrm{MF}}$), the relevant dissipative processes by which the persistent current decays become significantly more complicated (ultimately involving the nucleation of vortex rings) [95].

4.3   Thermally activated processes

This Chapter is concerned with events in which the system decays from some metastable current-carrying state Ψ_{m} (which is a local minimum of $\mathcal{F}$) to a lower-energy (and typically more stable) state via a thermal fluctuation.[1] The current decays through a dissipative process during which the condensate density shrinks in magnitude over a

---

[1] In the temperature regime considered here (i.e. $T \sim T_{\mathrm{c}}$), quantum fluctuations contribute less significantly than thermal fluctuations, and will therefore be disregarded.

region whose length is comparable to ξ_{MF}. Dynamically, one can envisage this process as occurring via the passage of a vortex across the sample (Fig. 4.3): a free-energy barrier must be overcome for this event to occur. The height of this barrier δF is given by the difference between the free energy of (the metastable state) Ψ_{m} and that of the transition state Ψ_{t}, i.e. the lowest possible free-energy high point en-route through configuration space between the initial and final metastable states. A schematic drawing of the free energy landscape is shown in Fig. 4.4. This thermally activated process should occur at a rate $\omega_0 e^{-\delta \mathcal{F}/kT}$, where, as shall be discussed later, the attempt frequency ω_0 does not contribute significantly to the temperature-dependence of the rate.

4.3.1 Metastable states

In order to calculate the barrier heights, I first identify the collection of metastable current carrying states $\{\Psi_{\mathrm{m}}\}$ and the intervening saddle point states $\{\Psi_{\mathrm{t}}\}$. Both families of states are stationary points of $\mathcal{F}$, and therefore satisfy the time independent Gross Pitaevskii equation

$$\frac{\delta \mathcal{F}}{\delta \Psi^*} = -\frac{\hbar^2}{2m} \nabla^2 \Psi + (V(\mathbf{r}) - \mu)\,\Psi + g|\Psi|^2 \Psi = 0, \tag{4.3}$$

subject to periodic boundary conditions in the coordinate ϕ.

Near T_c, where the thermal fluctuations are most important, the number of condensed particles is small, and it is reasonable to assume that the interaction energy is small compared to the transverse level spacing. This is the quasi 1D limit where the wavefunction may be written as

$$\Psi(r, \phi, z) = F(\phi)\,\mathcal{R}(r, z). \tag{4.4}$$

The transverse wavefunction $\mathcal{R}$ is the lowest energy solution of the eigenproblem,

$$-\frac{\hbar^2}{2m}\left(r^{-1}\partial_r r\,\partial_r + \partial_z^2\right)\mathcal{R} + V(r, z)\,\mathcal{R}_\nu = \lambda \mathcal{R}. \tag{4.5}$$

Inserting the ansatz (4.4) into (4.3) gives a one dimensional Gross Pitaevskii equation for the wavefunction $F(\phi)$,

$$F'' + \alpha F - \beta \Gamma |F|^2 F = 0, \tag{4.6}$$

where primes denote derivatives with respect to ϕ, and the coefficients are

$$\alpha \equiv 2m\bar{r}^2\,(\mu - \lambda)\,/\hbar^2, \tag{4.7a}$$

$$\beta \equiv 2m\bar{r}^2 g/\hbar^2, \tag{4.7b}$$

$$\Gamma \equiv \int dz \int r\,dr\,\,|\mathcal{R}|^4. \tag{4.7c}$$

a)

b)
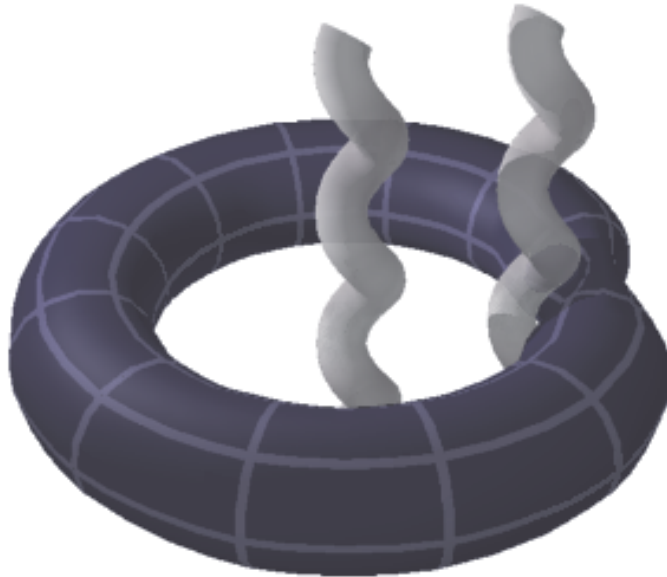
Figure 4.3: The phase slip event can be thought of as occurring when a "virtual" vortex crosses through the toroidal condensate. In a) one sees a toroidal cloud with two units of circulation per particle. This circulation can be thought of as due to the presence of two vortices in the center of the ring. In b) one of the vortices attempts to cross the condensate. This phase slip event reduces the angular momentum of each particle by $\hbar$. There is a barrier to this process because the density has to vanish at the point where the vortex crosses, requiring a larger density elsewhere. This density buildup costs energy.
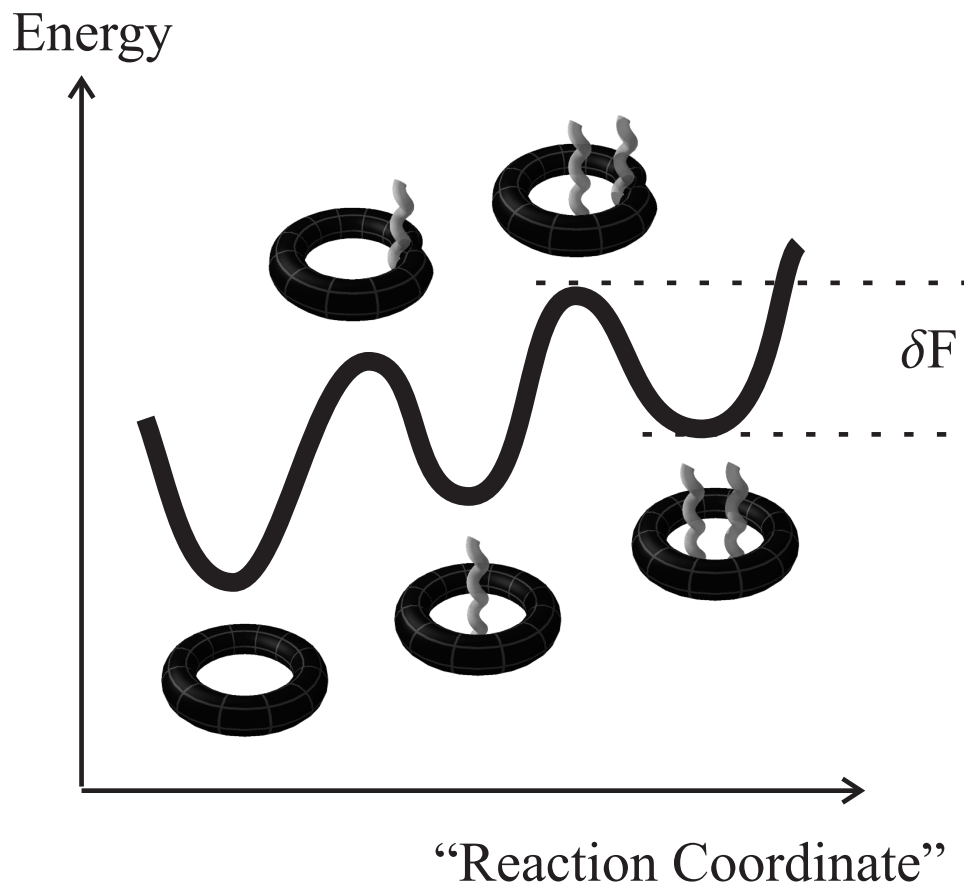
Figure 4.4: Schematic drawing of free energy landscape. The vertical axis shows the energy of a state. The horizontal axis is a relevant reaction coordinate (for example, the mean angular momentum per particle). Phase slip events take the system from one minima to another. The extrema are labeled by pictures which depict the positions of the "virtual vortices." The number of such vortices gives the circulation each particle in the toroidal trap carries. In the transition states, a vortex is escaping.

Corrections to this simple approximation are discussed in [85].

The uniform current carrying states are described by (4.4) with $F(\phi) = f_m e^{iS_M}$, with f_m constant, and S_M winding uniformly,

$$f_m^2 = N_m/2\pi = (\alpha - n_m^2)/\beta\Gamma, \tag{4.8a}$$

$$S_m = n_m\phi, \tag{4.8b}$$

with integral n_m. In these expressions, N_m is the number of condensed particles. Physically, Γ^{-1} is R^2L, the volume occupied by the condensate. By considering the second variation of $\mathcal{F}$ it can be readily shown that these states are local minima (and hence metastable) provided $n\zeta_m \leq 1$, where $\zeta_m \equiv (4\pi/\beta\Gamma N_m)^{1/2} \approx 2\pi\xi_{MF}/L$ is the dimensionless coherence length. (This limit on the maximum stable value of n_m is the same as one would find using Landau's criterion for the critical velocity.)

4.3.2 Transition states

As is readily verified [85], the transition states $\Psi_t = f_t\, e^{iS_t}\mathcal{R}$ are given by

$$f_t^2 = (N_t/2\pi)\left(1 - \Delta^2\mathrm{sech}^2(\Delta\phi/\zeta_t)\right), \tag{4.9a}$$

$$f_t^2\, \partial_\phi S_t = (N_t/2\pi)\, n_t. \tag{4.9b}$$

Far from a region of length ξ_{MF}, the amplitude f_t is constant ($f_t^2 \sim N_t/2\pi$) and the phase S_t winds uniformly ($S_t \sim n_t\phi$). The coefficients in Eq. (4.9) appear simplest when expressed in terms of the dimensionless coherence length $\zeta_t \equiv (4\pi/\beta\Gamma N_t)^{1/2}$:

$$N_t/2\pi = (\alpha - n_t^2)/\beta\Gamma, \tag{4.10a}$$

$$n_t = n - \pi^{-1}\cos^{-1}(n_t\, \zeta_t), \tag{4.10b}$$

$$\Delta^2 = 1 - (n_t\, \zeta_t)^2. \tag{4.10c}$$

As N_m and N_t differ only by quantities of order ξ_{MF}/L, either of them may be used to characterize the number of condensed particles. A typical transition state is depicted in Fig. 4.5. The transition states must have the property that they are saddle points of $\mathcal{F}$ with only one direction of negative curvature. (This unstable direction is the relevant reaction coordinate.) Within the quasi 1D approximation this condition is always true. In [85] I consider corrections to this approximation and show that this condition remains true as long as $\xi_{MF} > R$.

Having found the relevant states, I now calculate the free energy barrier for dissipative fluctuations. Straightforward substitution shows that states, $\Psi = f\, e^{iS}\mathcal{R}$,
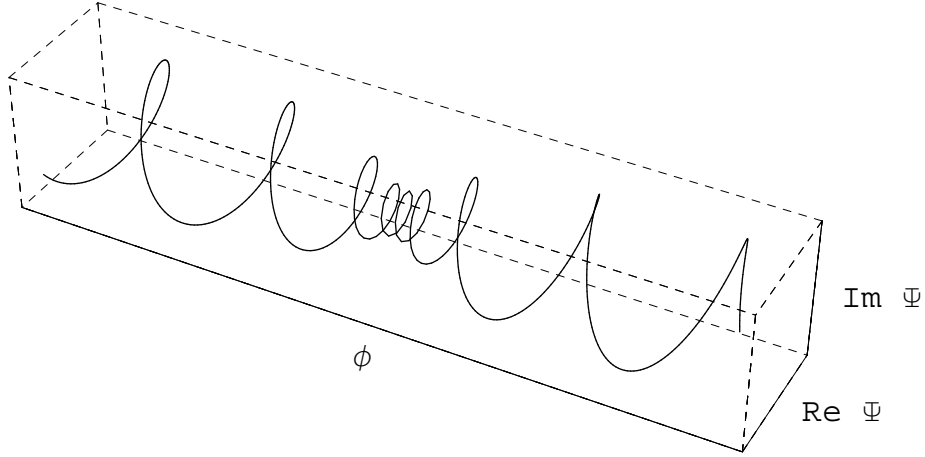
Figure 4.5: The real and imaginary parts of Ψ_T, plotted versus the angle ϕ. The length of the dip in the density is roughly the coherence length ξ_{MF}, which is exaggerated to bring out the structure of the phase slip. In reality, this length is always shorter than the distance over which the phase changes by 2π.

satisfying Eq. (4.3) have a free energy

$$\mathcal{F} = -\frac{g\Gamma}{2} \int d\phi \, |f(r)|^4. \tag{4.11}$$

Using this expression, along with Eq. (4.8) and Eq. (4.9), one finds that

$$\delta\mathcal{F} = \frac{1}{2}\delta\mathcal{F}_0 \left[\Delta \left(2 + (n_{\mathrm{t}} \, \zeta_{\mathrm{t}})^2 \right) - 3 n_{\mathrm{t}} \, \zeta_{\mathrm{t}} \cos^{-1}(n_{\mathrm{t}} \, \zeta_{\mathrm{t}}) \right], \tag{4.12}$$

where $\delta\mathcal{F}_0$ is the long wavelength (i.e. $n_{\mathrm{t}} \to 0$) value of $\delta\mathcal{F}$, i.e.,

$$\delta\mathcal{F}_0 = \frac{\hbar^2}{m} \left(\frac{32 N_{\mathrm{t}}^3 a}{9 R^2 L^3} \right)^{1/2}. \tag{4.13}$$

4.4   Decay rates

I now develop order of magnitude estimates for the decay rates of metastable states via thermal fluctuations in realistic atomic traps. Consider ^{87}Rb, for which the scattering length a_s is 5.8nm. I take a harmonic trapping potential $V(\mathbf{r}) = (1/2)m\omega^2[(r - \bar{r})^2 + z^2]$, whose ground state width $\sqrt{\hbar/m\omega}$ can be identified with the width of the condensate R. To estimate T_c I consider N noninteracting atoms in the potential $V(\mathbf{r})$. By virtue of the geometry (i.e. $R \ll L$) one can ignore the curvature of the torus, giving a density of states $\rho(E) = (4/3)(1/\hbar\omega)^2(mL^2/2\pi^2\hbar^2)^{1/2}E^{3/2}$. Integrating this with the Bose occupation factor reveals that $T_c \approx 1.28(\hbar^2/m)(N/R^4L)^{2/5}$. For

77

example, if one assumes that $N \approx 10^6$, $N_t \approx 2.5 \times 10^4$, $R \approx 1\mu$m, and $L \approx 100\mu$m then $\delta\mathcal{F}_0/k_B = 3.2\mu$K, and $T_c = 0.28\mu$K. The barrier height is sensitive to changes in N_t, and can therefore be manipulated by heating or cooling the sample.

The Arrhenius formula for the decay rate in terms of the barrier height is $\Gamma \approx \omega_0 e^{-\delta\mathcal{F}/kT}$. The attempt frequency ω_0 can be estimated by using the value of the microscopic relaxation time τ, together with the assumption that each coherence volume in the sample fluctuates independently [86]. A realistic estimate for τ is the classical collision time for a dilute gas [i.e. $\tau^{-1} \sim \sigma n v \sim a^2(N/V)(k_B T/m)^{1/2} \sim 5 \times 10^4$ Hz], giving lifetimes for the metastable states on the order of seconds. Even beyond the limits of validity of this calculation, one expects $\delta\mathcal{F}$ to be a monotonically increasing function of the density. Hence, the barriers can be extremely large at low temperatures, allowing a continuous tuning of the metastable state lifetime from microseconds to times longer than the lifetime of the condensate.

4.5   Detection and creation

I now discuss two of the issues necessary for the experimental testing of the predictions presented in this Chapter. First, how does one create a current carrying state? The most promising techniques for creating persistent currents are those that have been used to create vortices [10, 80, 82]. The simplest approach is to stir the condensate by deforming and rotating the trap that contains the atoms. The other method is to use a phase imprinting technique. Since the superfluid velocity is proportional to the gradient of the phase, by changing the phase one can give angular momentum to the condensate. The phase is shifted by illuminating the condensate with off resonant light through an appropriate mask. Detailed numerical simulations of creating persistent currents with this technique are found in [96].

The second important experimental matter is how to detect a current carrying state. Perhaps the least difficult scheme would make use of present phonon imaging techniques [97]. The experimental configuration could be as follows: A pulse of laser light generates a local rarefaction of the condensate, which then travels as two waves, one moving clockwise, the other counterclockwise. By nondestructive imaging techniques one might then observe where the two waves meet, which gives the velocity of the metastable supercurrent. This is only feasible if the speed of sound c is comparable to the velocity v with which the condensate moves around the annulus. Linearizing Eq. (4.6) gives $c = (g\Gamma N_m/2\pi m)^{1/2} \approx 1.2$mm/s, which is only 30 times greater than $v = \hbar/m\bar{r} \approx 46\mu$m/s.

As an alternative scheme, one can perform an interference experiment where a nonrotating condensate is overlapped with the toroidal cloud [92]. If the toroidal cloud is rotating, the spatially varying phase will be visible in the resulting interference pattern.

4.6 Coherent vs. incoherent pathways

Throughout this calculation I have assumed that a single condensate always exists. More generally, the transition state could have a fragmented condensate (see Chapter 3) or even a more complicated structure with no condensation at all. Based upon the intuition that I have gained from the study in Chapter 3, I expect that the energy of the transition state would change much if one broadens the allowable class of states. It should also be noted that any single measurement that tried to catch the phase slip on film would undoubtedly see a single condensate at all times (see Section 3.2.2).

Chapter 5

Finite Temperature Collapse of a Gas with Attractive Interactions

In this Chapter I present a study of the mechanical stability of the weakly interacting Bose gas with attractive interactions. My major concern here is the role of finite temperature, and I show that the non-condensed particles play a crucial role in determining the region of stability, including providing a mechanism for collapse in the non-condensed cloud. Furthermore, I demonstrate that the mechanical instability prevents BCS-type "pairing" in the attractive Bose gas. I extend these results to describe domain formation in spinor condensates. The research in this chapter was performed with Gordon Baym, and has been published in Physical Review A [98].

5.1 Introduction

5.1.1 The system of interest

At high densities, attractive interactions drive a mechanical instability in atomic clouds. At low densities these clouds are stabilized by quantum mechanical and entropic effects. The presence of both these stabilizing mechanisms makes attractive Bose gases unique. For comparison, interstellar hydrogen has a similar instability, the Jeans instability, in which gravity competes with thermal pressure [8]; however quantum mechanics plays no role in the stability of hydrogen clouds, and the collapse is therefore much less rich.

Experimentally, stability and collapse has been observed in clouds of degenerate ^{7}Li [24] and ^{85}Rb [25], both of which have attractive interactions. Previous theoretical studies of the attractive Bose gas, typically numerical, have been limited to zero [99] or very low [100] temperature. Here I give a simple analytic description of the region of

stability and threshold for collapse valid from zero temperature to well above the Bose condensation transition, and thus provide a consistent global picture of the instability. Contrary to previous predictions, at finite temperature the non-condensed particles can play a significant role in the collapse.(A very recent variational calculation by Tempere et al. [101] is capable of describing the collapse over a range of temperatures comparable to the approach presented here.)

5.1.2   Results

My results are summarized in the phase diagram in Fig. 5.1 which shows three regions: normal, Bose condensed, and collapsed. This third region is not readily accessible experimentally; the system becomes unstable at the boundary (the solid line in the figure). The gross features of the phase diagram can be understood qualitatively with dimensional arguments similar to those in section 1.2.5. At low temperatures the only stabilizing force is the zero-point motion of the atoms. This "quantum pressure" (which should not be confused with the Fermi pressure which stabilizes neutron stars) has a characteristic energy per particle, $E_Q \sim \hbar^2 V^{-2/3}/m$, where $\hbar$ is Planck's constant, V is the volume in which the cloud is confined, and m is the mass of an atom. The attractive interactions which drive the collapse are associated with an energy $U = \hbar^2 a_s n/m$, where n is the density, and a_s $(= -1.45\,\text{nm}$ for ^7Li and $-20\,\text{nm}$ for $^{85}\text{Rb})$ is the s-wave scattering length. Comparison of U with E_Q indicates that for low temperatures the density n at collapse should be $n \sim (V^{2/3}a_s)^{-1}$, independent of temperature. At high temperatures, the stabilizing force is thermal pressure, $P = -T\partial S/\partial V$, which is characterized by the thermal energy $E_T \sim k_B T$. Here comparison of U with E_T indicates that at high temperatures the density of collapse should be $n \sim mk_B T/\hbar^2 a_s$, linear in temperature. The crossover between the quantum and classical behaviors ($n \propto T^0$ and $n \propto T$) occurs near T_c. The collapse, as described here, is a phenomena in which the cloud as a whole participates, not just the condensate.

In this Chapter, I calculate the last point of metastability against collapse. As one approaches this point, the system will generally undergo an earlier dynamical collapse, driven by thermally activated processes [102], as in a first order Van der Waals transition, or quantum tunneling [103], both of which destabilize the cloud. The actual dynamics of collapse are, however, beyond the scope of this Chapter. The dynamics can be described by the tools of Chapter 6.

a) Density [cm⁻³]

Collapsed

Condensed

Normal

Temperature [µK]

b) Density [cm⁻³]

Collapsed

Condensed

Normal
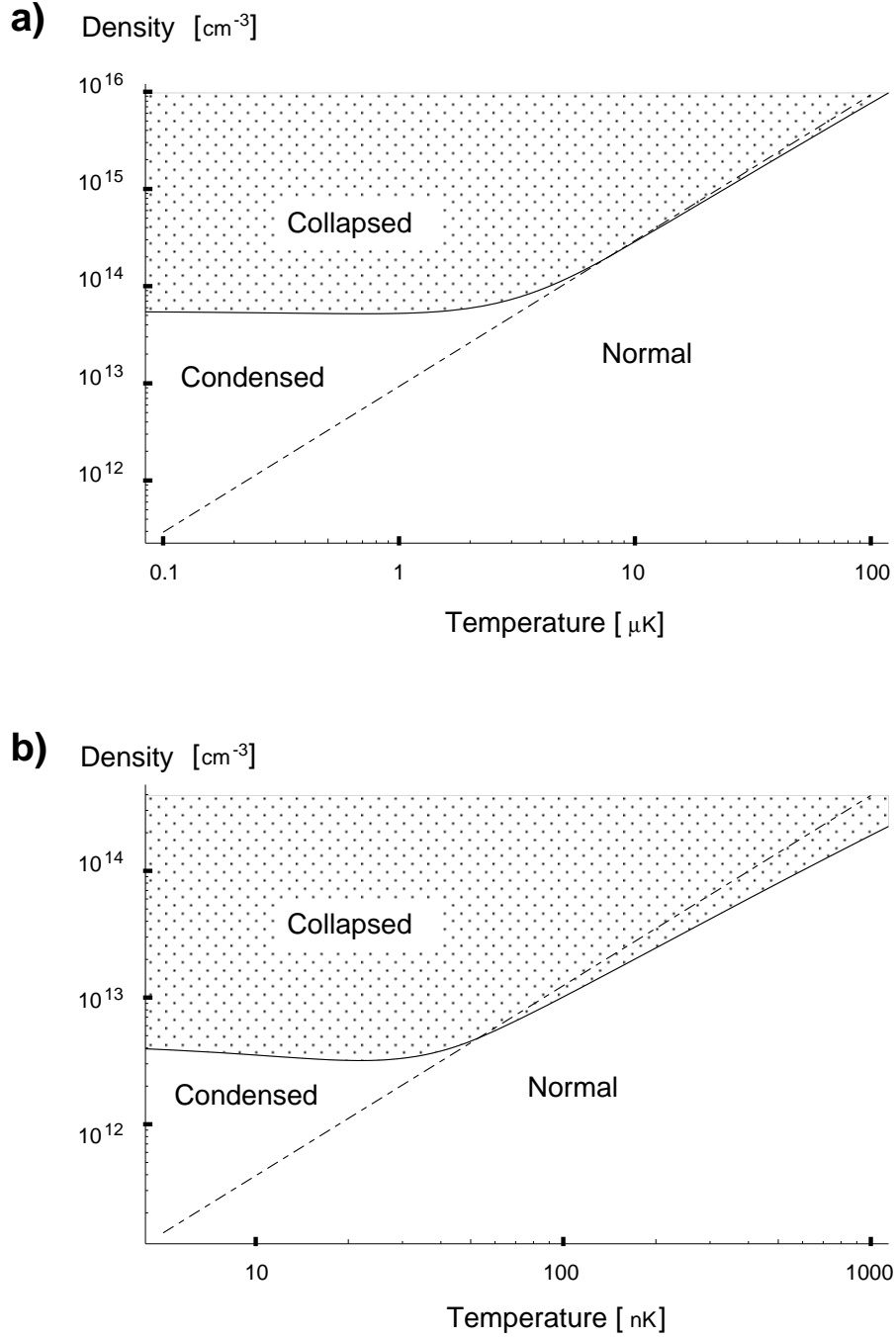
Temperature [nK]

Figure 5.1: Phase diagram, density n [cm^{-3}] versus temperature T, for a cloud of attractive bosons. a) For a cloud of ^{7}Li with spatial extent $L = 3.15\mu$m and scattering length $a_s = -1.45$nm, corresponding to the experiments in Ref. [1], performed at T near 300 nK. b) For a cloud of ^{85}Rb with scattering length $a_s = -20$nm and spatial extent $L = 3\mu$m, corresponding to the recent experiments in Ref. [2], performed at T near 15 nK. Note the logarithmic scales. The solid line separates the unstable (shaded) region from the stable region. The dashed line, representing the Bose condensation transition has been continued into the collapsed region to illustrate that the two lines intersect. This diagram is drawn for a uniform but finite cloud, but can be applied to harmonically trapped gases by taking n to be the central density in the trap.

5.1.3 Method

My basic approach is to identify the collapse with an instability in the lowest energy mode of the system (the breathing mode in a spherically symmetric cloud). As the system goes from stable to unstable, the frequency of this mode goes from real to complex, passing through zero when the instability sets in. The density response function, $\chi(k, \omega)$, which measures the response of the cloud to a probe at wavevector k and frequency ω, diverges at the resonant frequencies of the cloud. Therefore, by virtue of the vanishing frequency of the lowest energy mode, the collapse is characterized by

$$\chi(k = 2\pi/L, \omega = 0)^{-1} = 0. \tag{5.1}$$

Here $k = 2\pi/L$ is the wavevector of the unstable mode, whose wavelength L should be of order the size of the system. Equation (5.1) implicitly determines the line of collapse in the temperature-density plane.

To evaluate the response function analytically, I use a local-density approximation, replacing the response function $\chi(k, \omega)$ of the inhomogeneous cloud by that of a gas with uniform density n. The response of the uniform gas is evaluated at the same frequency and wavevector as for the inhomogeneous system, and n is given by the central density of the atomic cloud. The local-density approximation should be valid for temperatures large enough that the thermal wavelength, $\Lambda_T = (2\pi\hbar^2/mk_BT)^{1/2}$, is much smaller than the size of the trap, in particular that $k\Lambda_T/4\sqrt{\pi}$ be small (see the expansion in Appendix E.4.3 on page 164). In all experiments to date, this condition is satisfied, and I treat $k\Lambda_T/4\sqrt{\pi}$ as a small parameter in this calculation.[1] With this approximation, I calculate the line of collapse using the theory of $\chi(k, \omega)$ of a uniform gas (reviewed in appendix E).

In the experiments on ^{7}Li, the atoms are held in a magnetic trap[2] with a harmonic confining potential $V(r) = \frac{1}{2}m\omega^2r^2$, with $\omega \approx 2\pi \times 145s^{-1}$.This potential gives the cloud a roughly Gaussian density profile (see Section 5.4). The temperature T is typically 50 times the trap energy $\hbar\omega \approx 7nK$, so the parameter $k\Lambda_T/4\sqrt{\pi}, \approx \sqrt{\hbar\omega/2k_BT} \approx 0.10$, is small. The experiments on ^{85}Rb use softer traps, $\hbar\omega \approx 0.6nK$, and colder temperatures $T \approx 15nk$, so that $k\Lambda_T/4\sqrt{\pi} \approx 0.14$.

The local density approximation used here provides a framework for investigating

---

[1] My derivation of the condensate's response is valid at arbitrarily low temperatures, as it does not rely upon an expansion in powers of $k\Lambda_T/4\sqrt{\pi}$. In regimes where the noncondensate fraction is small, my analysis of the system's stability can likewise be continued to $T = 0$.

[2] The traps used are slightly asymmetric, and the frequencies quoted here are the geometric mean of the three frequencies along each principal axis; see [24, 25].

the interplay of condensation and collapse. Although the results are not as accurate as can be obtained through numerical simulations (comparing with previous numerical work [100], I find that my results are always well within a factor of two of those calculated using more sophisticated models), the conceptual and computational advantages of working with a uniform geometry far outway any loss in accuracy. Due to their simplicity, the arguments used here provide an essential tool in choosing which parameter ranges to investigate in future experiments and computations.

The tools introduced to discuss the collapse of an attractive gas can also be used to describe other instabilities in trapped Bose gases. In Section 5.5 and 5.6, I apply these methods to the problem of BCS type pairing between bosons, and towards domain formation in spinor condensates.

5.2 Simple limits

5.2.1 Zero temperature

To illustrate my approach, I first consider the stability of a zero temperature Bose condensate. The excitation spectrum of a uniform gas is [105]:

$$\hbar^2 \omega_k^2 = \varepsilon_k^2 + 2gn\varepsilon_k \equiv E_k^2, \tag{5.2}$$

where $\varepsilon_k = \hbar^2 k^2/2m$ and $g = 4\pi\hbar^2 a_s/m$. In the attractive case, $g < 0$, all long wavelength modes with $\varepsilon_k < 2|g|n$ have imaginary frequencies and are unstable. A system of finite size L only has modes with $k > 2\pi/L$, and for larger k has an excitation spectrum similar to Eq. (5.2). If $|g|n < \hbar^2\pi^2/mL^2$, the unstable modes are inaccessible and the attractive Bose gas is stable.

This information is included in the density response function $\chi(k,\omega)$ of the dilute zero-temperature gas [104], which gives the change in density n induced by an external potential U, of wavevector k and frequency ω, coupled to the density:

$$\chi(k,\omega) = \frac{\delta n}{\delta U} = \frac{nk^2}{m(\omega^2 - E_k^2/\hbar^2)} \tag{5.3}$$

The poles of χ are at the excitation energies, $\pm E_k$. In particular, $\chi(k = 2\pi/L, \omega = 0)$ diverges when $|g|n = \hbar^2\pi^2/mL^2$.

5.2.2 High temperature $(T \gg T_c)$

To illustrate the procedure further I calculate the stability of an attractive Bose gas at temperatures much larger than T_c, where thermal pressure is the predominant

stabilizing force. Quantum effects are negligible in this limit, and the line of collapse is simply the spinodal line of the classical liquid-gas phase transition,[3] as characterized by Mermin [106]. One can neglect finite size effects, and look for an instability in the uniform gas at zero wavevector, $k = 0$, corresponding to finding where $\chi(k = 0, \omega = 0)$ diverges. The susceptibility $\chi(0,0) = -\partial n/\partial \mu$ (where μ is the chemical potential), is proportional to the compressibility of the system, which diverges when the gas becomes unstable.

At high temperature one can work in the Hartree Fock approximation, where the density is given by the self consistent solution of

$$n = \int \frac{d^3 p}{(2\pi\hbar)^3} \frac{1}{e^{\beta(\epsilon_p - \mu)} - 1}, \tag{5.4}$$

with Hartree Fock quasiparticle energies $\epsilon_p = \varepsilon_p + 2gn$; here $\beta = 1/k_B T$. In the classical limit ($\beta\mu \ll -1$), $n = e^{\beta(\mu - 2gn)}/\Lambda_T^3$. The response $\chi(0,0)$ has the structure of the random phase approximation (RPA),

$$\chi(k,\omega) = \frac{\chi_0(k,\omega)}{1 - 2g\chi_0(k,\omega)}, \tag{5.5}$$

where $\chi_0(0,0) = -\left(\partial n/\partial \mu\right)_\epsilon$ (where the ϵ are held fixed) is the "bare" response. In the classical limit $\chi_0(0,0) = -\beta n$. Since $\chi_0(0,0)$ is negative, the repulsive system ($g > 0$) is stable. For attractive interactions however ($g < 0$), the denominator of Eq. (5.5) vanishes when $2g\chi_0 = 1$, which in the classical limit occurs when $2|g|n = k_B T$.

The above calculation is only valid well above T_c. When $|\mu| \lesssim \hbar^2/mL^2$, finite size effects start to become important, and a more sophisticated approach is needed. If one blindly used the above result near T_c one would erroneously find that the instability towards collapse prevents Bose condensation from occurring. This difficulty can be avoided by working with the finite wavevector response $\chi(k = 2\pi/L, \omega = 0)$, to which we now turn.

5.3   Density response function

I calculate the response χ in the RPA, with the approximation that the bare responses of the condensate and non-condensed particles are taken to be those of a non-interacting system (see appendix E). This approach, employed by Szépfalusy

---

[3] In the theory of liquid-gas phase transitions, the spinodal line is the curve on the phase diagram where $\partial P/\partial V = 0$, which represents the edge of the co-existence region, beyond which supercooled vapor cannot exist.

and Kondor [107] in studying the critical behavior of collective modes of a Bose gas, and later modified by Minguzzi and Tosi [108] to include exchange, is simple to evaluate analytically, and is valid both above and below T_c. It generates an excitation spectrum which is conserving [109] and gapless [104]. At zero temperature it yields the Bogoliubov spectrum, Eq. (5.2), and above T_c it becomes the standard RPA with exchange.

The susceptibility in this approximation has the form,

$$\chi(k, \omega) = \frac{\chi_0^c + \chi_0^n + g\chi_0^c\chi_0^n}{(1 - g\chi_0^c)(1 - 2g\chi_0^n) - 4g^2\chi_0^c\chi_0^n}, \tag{5.6}$$

where χ_0^c and χ_0^n are the condensate and non-condensed particle contributions to the response of the non-interacting cloud,

$$\chi_0^n(k, \omega) = \int \frac{d^3q}{(2\pi)^3} \frac{f(q - k/2) - f(q + k/2)}{\hbar\omega - (\varepsilon_{q+k/2} - \varepsilon_{q-k/2})}, \tag{5.7a}$$

$$\chi_0^c(k, \omega) = \frac{n_0}{\hbar\omega - \varepsilon_k} - \frac{n_0}{\hbar\omega + \varepsilon_k}. \tag{5.7b}$$

Here n_0 is the condensate density, the $\varepsilon_k = k^2/2m$ are the free particle kinetic energies, and the Bose factors $f(k)$ are given by $(e^{-\beta(\varepsilon_k - \mu)} - 1)^{-1}$. In appendix E I derive this response function. A general discussion of quantum mechanical response functions appears in appendix C. At zero temperature $\chi_0^n = 0$ and the susceptibility reduces to that in Eq. (5.3), while above T_c, $\chi_0^c = 0$, and χ reduces to Eq. (5.5). Figure E.2, on page 161, shows the class of diagrams summed in this approximation.

Expanding χ_0^n in the small parameter $k\Lambda_T$ (see details in appendix E.4.3), one finds for $T > T_c$,

$$g\chi_0^n(k, 0) = -2\frac{a_s}{\Lambda_T}\left[\frac{4\pi}{k\Lambda_T}\arctan|\varepsilon_k/4\mu|^{1/2} + g_{1/2}(e^{\beta\mu}) - |\pi/\beta\mu|^{1/2} + \mathcal{O}(k\Lambda_T)\right], \tag{5.8}$$

where $g_\nu(z) \equiv \sum_j z^j/j^\nu$ is the polylogarithm function. For chemical potential μ much larger in magnitude than k_BT, the system is classical, and Eq. (5.8) reduces to $g\chi_0^n = -\beta gn$, as in the Hartree-Fock approach, Section 5.2.2. Below T_c the chemical potential of the non-interacting system vanishes and the response functions are:

$$g\chi_0^n(k, 0) = -\frac{4\pi^2 a_s}{k\Lambda_T^2} + \mathcal{O}((k\Lambda_T)^0), \tag{5.9a}$$

$$g\chi_0^c(k, 0) = -16\pi\frac{a_s n_0}{k^2}. \tag{5.9b}$$

Using these expressions one calculates the spinodal line separating the stable and unstable regions of Fig. 5.1 by setting $k = 2\pi/L$ and solving the equation

$$\chi^{-1} \propto 1 - g(\chi_0^c + 2\chi_0^n) - 2g^2\chi_0^c\chi_0^n = 0, \tag{5.10}$$

which gives the line of collapse as a function of μ and T (for $T > T_c$), or as a function of n_0 and T (for $T < T_c$). I use the following relations to plot the instability on the $n - T$ phase diagram,

$$n = \begin{cases} \Lambda_T^{-3} g_{3/2}(e^{\beta\mu}), & T > T_c \\ n_0 + \Lambda_T^{-3}\zeta(3/2), & T < T_c, \end{cases} \qquad (5.11)$$

with the Riemann Zeta function $\zeta(3/2) = g_{3/2}(1) \approx 2.6$. The line of condensation $n = \Lambda_T^{-3}\zeta(3/2)$ separates the condensed and non-condensed regions.

Equations (5.9a) and (5.9b) indicate that below T_c the noncondensate response χ_0^n scales as $k^{-1} \sim L$, while the condensate response χ_0^c scales as $k^{-2} \sim L^2$. For realistic parameters, L is the largest length in the problem, so that the condensate dominates the instability except when n_0 is much smaller than n. Since the condensate is very localized, even a few particles in the lowest mode make n_0 locally much greater than the density of noncondensed particles. In Fig. 5.2 I show how the line of instability depends on the size of the system, L.

Substituting Eq. (5.9) into Eq. (5.10) one calculates the maximum stable value of the condensate density n_0,

$$(n_0)_{\max} = \frac{\pi}{4L^3}\left(\frac{L}{|a_s|}\right)\left(\frac{T^* - T}{T^* + T}\right), \quad T < T^*, \qquad (5.12)$$

where $T^* = \hbar^2/2mk_B L|a_s|$ is the temperature at which the line of collapse crosses the line of condensation. For all greater temperatures, $(n_0)_{\max} = 0$, and there is no condensation.

From Eq. (5.12) one sees that $(n_0)_{\max}$ decreases monotonically with temperature, from its maximum value $(n_0)_{\max}^{T=0} = \pi/4L^2|a_s|$, to zero at $T = T^*$. Using parameters from experiments [24, 25], one finds for the lithium trap at Rice, $(N_0)_{\max}^{T=0} = L^3(n_0)_{\max}^{T=0} = 1700$, and $T^* = 7.5~\mu\text{K}$, and for the JILA rubidium-85 trap, $(N_0)_{\max}^{T=0} = 120$, and $T^* = 46$ nK .

One can verify the accuracy of the expansion in $k\Lambda_T$ by including the next order term of Eq. (5.9a) in the calculation of $(n_0)_{\max}$. While this next term has a negligible effect for lithium, there is a small change in the shape of $(n_0)_{\max}$ for rubidium. Most notably, the curve is rounded near $T = 0$, and T^* is increased to 53nK. The maximum number of condensed particles vs. temperature for the two experiments are plotted in Fig. 5.3; these results are consistent with the experiments, and agree quite well with numerical mean-field calculations [100]. In particular, my curve $(N_0)_{\max}(T)$ for lithium has a slope of $-1/2.2$ nK at $T = 0$, which lies between the calculated slopes of Davis et al. and Houbiers et al. [100]. Although $(n_0)_{\max}$ decreases with temperature,
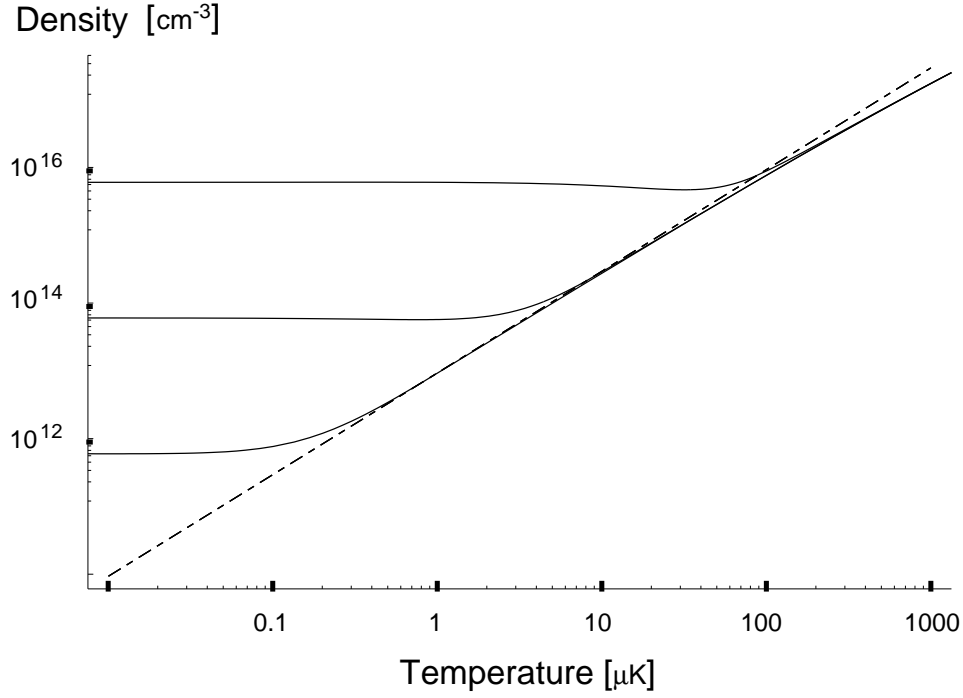
Figure 5.2: Scaling of the instability threshold with system size. Solid lines show the maximum stable density n_{max} for a given temperature. From the top, the system size is $L = 0.3, 3, 30\ \mu$m. The other parameters are the same as in Fig. 5.1. The dashed line indicates the Bose-Einstein condensation transition. Note the three scaling regimes; at low temperature, $n_{\mathrm{max}} \sim L^{-2}$, near the critical temperature $n_{\mathrm{max}} \sim L^{-3/2}$, and at high temperatures n_{max} is independent of L

the non-condensed density n' increases ($n' = \Lambda^{-3}\zeta(3/2)$). Thus the total density at collapse need not be monotonic with temperature (cf. the low temperature region of Fig. 5.1b).

Future condensate experiments at higher temperatures and densities should be able to study the structure in Eq. (5.12), and map out the phase diagram in Fig. 5.1. The rubidium experiments are performed at temperatures near T^*, where the spinodal line intersects T_c, and in principle should be able to explore the crossover between the quantum mechanical and classical behavior of the instability. The lithium experiments are much further away from exploring this regime, and in the current geometry, inelastic processes make such an investigation impractical.[4] Since T^* is proportional to $1/L$, a softer trap could be used to bring this crossover down to lower temperatures where these difficulties are less severe (see Fig. 5.2). More precise numerical studies at higher temperatures are needed to guide these experiments.

5.4   Modeling the harmonic trap

Most experimental and theoretical results are reported in terms of numbers of particles instead of density. By appropriately modeling the density distribution of a harmonically trapped gas, one can present my conclusions in such a form. Once the interactions are strong enough to modify the density distribution significantly, the system undergoes collapse; thus one can take the density distribution to be that of non-interacting particles. For $k_B T \gg \hbar\omega$, the density profile is well-approximated by

$$n(r) = \int \frac{d^3p}{(2\pi)^3} \frac{1}{e^{\beta(\varepsilon_p + V(r) - \mu)} - 1} + n_0 e^{-r^2/d^2}, \tag{5.13}$$

where $V(r) = m\omega^2 r^2/2$ is the confining potential, with characteristic length $d = (\hbar/m\omega)^{1/2}$. The density of condensed particles at the center of the trap is n_0. Above T_c $n_0 = 0$, and below T_c, $\mu = 0$. Integrating over space,

$$N = \begin{cases} (k_B T/\hbar\omega)^3 \, g_3(e^{\beta\mu}), & T > T_c \\ (k_B T/\hbar\omega)^3 \, \zeta(3) + (\pi\hbar/m\omega)^{3/2} \, n_0, & T < T_c. \end{cases} \tag{5.14}$$

The instability occurs in the lowest energy mode of the system, the breathing mode, whose wavevector is proportional to $1/d$. In a zero temperature non-interacting

---

[4] At a temperature of 5μK, a 3.15μm cloud of ^{7}Li collapses at a density of $n = 1.39 \times 10^{14}$cm^{-3}. At such a high density the dominant decay mechanism is three-body collisions, giving a lifetime $\tau = (G_3 \, n^2)^{-1}$, where G_3 is a constant determined from three-body scattering. Using the theoretical estimate [110], $G_3 = 2.6 \times 10^{-28}$, I find that $\tau = 200ms$. At $T = 10\mu K$ the lifetime is only $\tau = 40ms$.
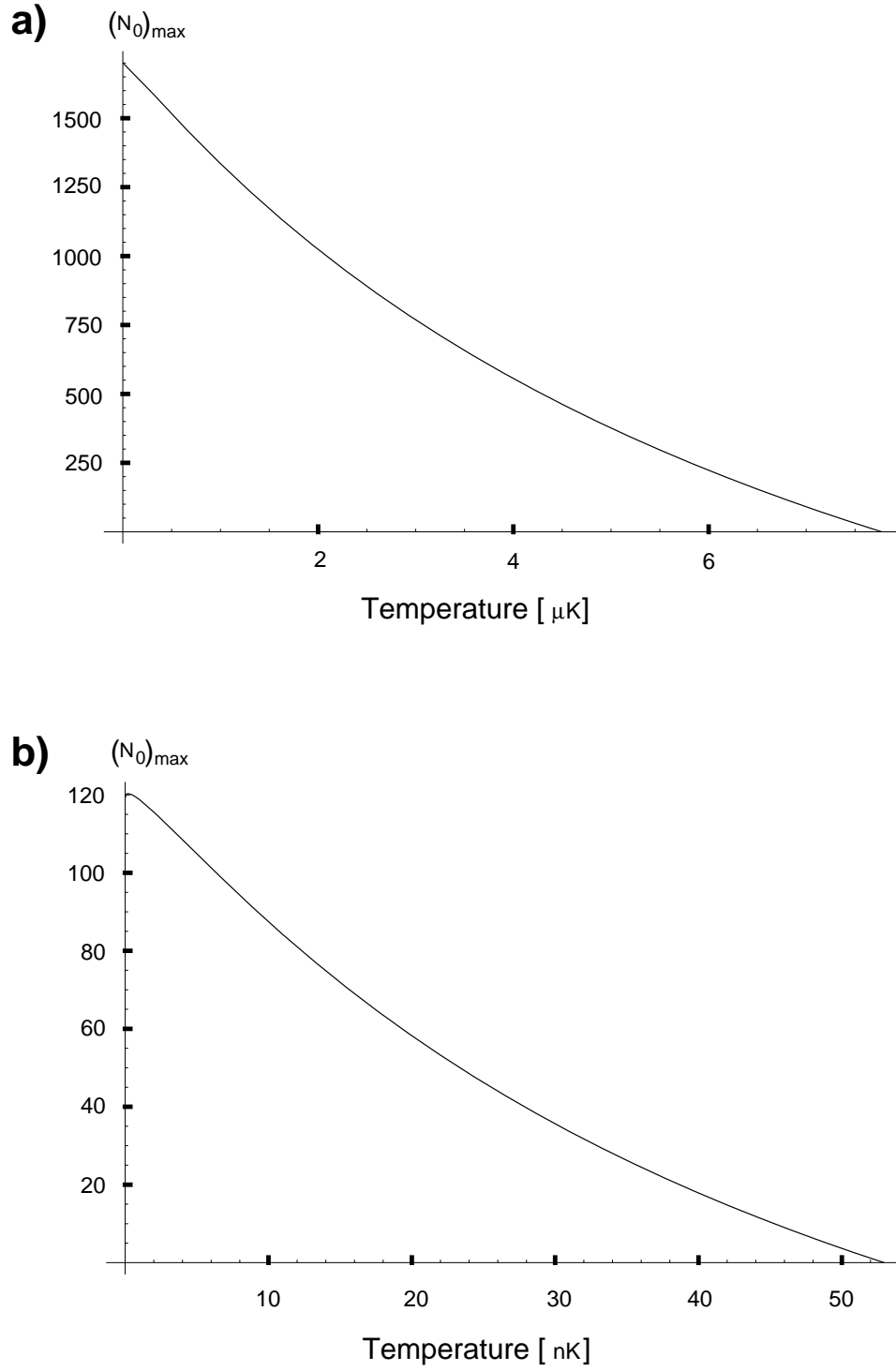
Figure 5.3: Maximum number of condensed particles as a function of temperature, for the a) ^{7}Li and b) ^{85}Rb experiments. The $(k\Lambda_T)^0$ terms in Eq. 5.9a have been included in producing these plots, giving a slightly different shape than that quoted in Eq. (5.12).

gas the breathing mode has a density profile $\delta\rho \propto (2r^2/d^2 - 3) \exp(-r^2/d^2)$, where r is the radial coordinate. In momentum space this distribution is peaked at wavevector $k = 2/d$. At finite temperature thermal pressure increases the radius of the cloud and the wavevector of the breathing mode becomes smaller. Since the response of the non-condensed cloud is relatively insensitive to the wavevector, I look for an instability at $k = 2/d$.

The resulting phase diagram, Fig. 5.4, is similar to that in Fig. 5.1. The most significant difference is that the line of collapse follows the condensation line (on the scale of the figure they appear to coincide over a significant temperature range). This behavior can be understood by noting that for trapped particles, condensation results in a huge increase in the central density of the cloud (a standard diagnostic of BEC).

5.5 Pairing

With minor changes the formalism presented here can be used to investigate the instability towards forming loosely bound dimers, or "pairs," the Evans-Rashid transition. Such an instability occurs in an electron gas at the superconducting BCS transition [111], and has been predicted by Houbiers and Stoof [100, 112] to occur in the trapped alkalis. The pairing is signalled by an instability in the T-matrix of the normal phase [113], which plays the role that the density response function plays in the collapse. Again, I simulate the finite size of the cloud by looking for an instability at $k = 2\pi/L$, compared with $k = 0$ in a bulk sample. In analogy to Eq. (5.5), the T-matrix can be written as a ladder sum,

$$T(k, \omega) = \frac{g}{1 - g\Xi(k, \omega)}. \tag{5.15}$$

In this equation, k is the relative momentum of the pair. The instability towards pairing is signalled by $T \to \infty$, when $g\Xi = 1$. To the same level of approximation as Eq. (5.7a), the medium-dependent part of the "pair bubble" Ξ is

$$\Xi(k, \omega) = \int \frac{d^3q}{(2\pi)^3} \frac{f(q - k/2) + f(q + k/2)}{\hbar\omega - (\varepsilon_{q+k/2} + \varepsilon_{q-k/2})}. \tag{5.16}$$

Setting $\omega = 0$, and expanding in small $k\lambda_T$ (see appendix E.4.3), one finds

$$g\Xi(k, \omega = 0) = -4\frac{a_s}{\Lambda_T} \left[\frac{4\pi}{k\Lambda_T} \arctan\left(\frac{|\epsilon_k/4\mu|^{1/2}}{1 + |\epsilon_k/4\mu|^{1/2}} \right) \right. \tag{5.17}$$

$$\left. + g_{1/2}(e^{\beta\mu}) - |\pi/\beta\mu|^{1/2} + \mathcal{O}(k\Lambda_T) \right].$$
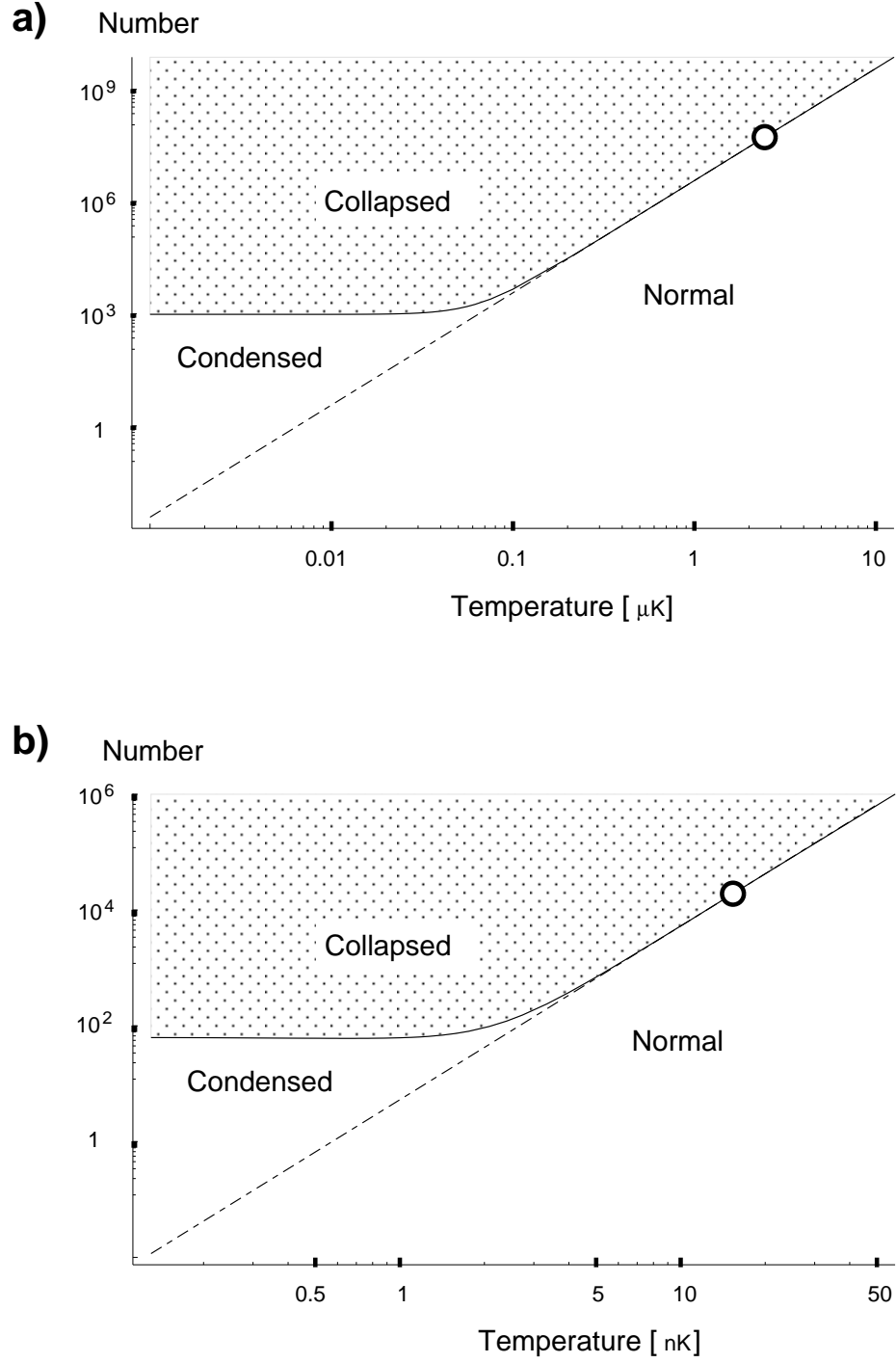
Figure 5.4: Phase diagram, number N versus temperature T, for harmonically trapped bosons with attractive interactions; a) ^{7}Li, b) ^{85}Rb. The parameters used correspond to Fig. 1. The open circle marks where the spinodal line meets with the BEC phase transition.

Except for the argument of the arctangent, this expression is identical to twice $g\chi_0^n$ as given in Eq. (5.8). Since arctangent is a monotonic function, and its argument here is smaller than in Eq. (5.8), one sees that $g\Xi < 2g\chi_0^n$, which implies that the instability towards collapse occurs at a lower density than the pairing instability. Thus I conclude that the pairing transition does not occur in an attractive Bose gas. Interestingly, in the classical limit, the instabilities towards pairing and collapse coincide.

5.6 Domain formation in spinor condensates

The approach used here to discuss the collapse of a gas with attractive interactions also describes domain formation in spinor condensates, and gives a qualitative understanding of experiments at MIT [9] in which optically trapped ^{23}Na is placed in a superposition of two spin states. Although all interactions in this system are repulsive, the two different spin states repel each other more strongly than they repel themselves, resulting in an effective attractive interaction. The collapse discussed earlier becomes, in this case, an instability towards phase separation and domain formation. The equilibrium domain structure is described in [114]. Here I focus on the formation of metastable domains [115].

The ground state of sodium has hyperfine spin $F = 1$. In the experiments the system is prepared so that only the states $|1\rangle = |F = 1, m_F = 1\rangle$ and $|0\rangle = |F = 1, m_F = 0\rangle$ enter the dynamics. The effective Hamiltonian is then

$$H = \int d^3r \, \frac{\nabla \psi_i^\dagger \cdot \nabla \psi_i}{2m} + V(r)\psi_i^\dagger \psi_i + \frac{g_{ij}}{2}\psi_i^\dagger \psi_j^\dagger \psi_j \psi_i. \qquad (5.18)$$

where ψ_i ($i = 0, 1$) is the particle destruction operator for the state $|i\rangle$; summation over repeated indices is assumed. The effective interactions, $g_{ij} = 4\pi\hbar^2 a_{ij}/m$, are related to the scattering amplitudes $a_{F=0}$ and $a_{F=2}$, corresponding to scattering in the singlet ($F_1 + F_2 = 0$) and quintuplet ($F_1 + F_2 = 2$) channel, by [9, 114, 116]:

$$\tilde{a} \equiv a_{11} = a_{01} = a_{10} = a_{F=2}, \qquad (5.19a)$$

$$\delta a \equiv a_{11} - a_{00} = (a_{F=2} - a_{F=0})/3. \qquad (5.19b)$$

Note that the $|1\rangle + |0\rangle$ channel is purely $F = 2$ for identical bosons, since the $F = 1$ state is anti-symmetric and the scattering is purely s-wave. Numerically, $\tilde{a} = 2.75$nm and $\delta a = 0.19$nm. In the equations of motion, these lengths appear as $\tilde{g} = 4\pi\hbar^2 \tilde{a}/m$ and $\delta g = 4\pi\hbar^2 \delta a/m$. Initially the condensate is static with density $n = 10^{14}$cm^{-3}, and all particles in state $|1\rangle$. A radio-frequency pulse places half the atoms in the

$|0\rangle$ state without changing the density profile. Subsequently the two states phase separate and form $40 \pm 15 \ \mu$m thick domains. The trap plays no role here, so I neglect $V(r)$ in Eq. (5.18) and consider a uniform cloud.

Within a mean field approximation, one writes $\psi_i = \sqrt{n_{m=i}}e^{i\phi_i}$, and the equations of motion for ϕ_i and $n_{m=i}$ are derived by making stationary the action $\mathcal{S} = \int dt \left[\int d^3r \, (1/2i)(\partial_t\psi^*\psi - \psi^*\partial_t\psi) - H\right]$, leading to a set of "hydrodynamic equations",

$$\partial_t n_{m=i} + \nabla \cdot (n_{m=i}\nabla\phi_i) = 0 \tag{5.20a}$$

$$\partial_t\phi_i - (\nabla^2\sqrt{n_{m=i}})/2m\sqrt{n_{m=i}} + g_{ij}n_{m=j} = 0, \tag{5.20b}$$

the first of which is a continuity equation, and the second is analogous to Euler's equation for an ideal fluid. The initial stages of domain formation can be understood by linearizing these equations about $n_{m=0} = n_{m=1} = n/2$. After eliminating the phase variables, and Fourier transforming with respect to space and time,

$$\begin{pmatrix} \omega^2 - \varepsilon_k(\varepsilon_k + \tilde{g}n + \delta g\, n) & -\tilde{g}n\varepsilon_k \\ -\tilde{g}n\varepsilon_k & \omega^2 - \varepsilon_k(\varepsilon_k + \tilde{g}n) \end{pmatrix} \begin{pmatrix} \delta n_{m=0} \\ \delta n_{m=1} \end{pmatrix} = 0. \tag{5.21}$$

Here $\delta n_{m=i} = n_{m=i} - n/2$ is the fluctuation of the density of each species, and as before $\varepsilon_k = k^2/2m$. When δg is set to zero, the two solutions of these equations represent a pure spin wave, where $\delta n_{m=0} + \delta n_{m=1} = 0$, or a pure density wave where $\delta n_{m=0} = \delta n_{m=1}$. For arbitrary δg, the spectrum of these modes become $\omega^2 = \varepsilon\left(\varepsilon + \tilde{g}n - \delta g\, n/2 \pm [(\tilde{g}n)^2 + (\delta g\, n/2)^2]^{1/2}\right)$, which for small δg is

$$\hbar^2\omega_{ph}^2 = \left(\frac{\hbar^2 k^2}{2m}\right)^2 + \tilde{g}n\frac{\hbar^2 k^2}{m} + \mathcal{O}(\delta g), \tag{5.22a}$$

$$\hbar^2\omega_{sp}^2 = \left(\frac{\hbar^2 k^2}{2m}\right)^2 - \delta g\, n\frac{\hbar^2 k^2}{4m} + \mathcal{O}((\delta g)^2). \tag{5.22b}$$

Similar excitation spectra were found in [117]. The subscripts ph or sp refer to the phonon or spin-wave character of the excitations. Since $\delta g > 0$, the long-wavelength spin excitations have imaginary frequencies. The mode with the largest imaginary frequency grows most rapidly, and the width of the domains formed should be comparable to the wavelength λ of this mode. By minimizing Eq. (5.22b) one finds $\lambda = \sqrt{2\pi/n\,\delta a} \sim 20\mu$m, in rough agreement with the observed domain size.

To connect these unstable modes to our previous discussion of the collapse more explicitly, I note that in the mean field approximation, the interaction in Eq. (5.18) is only a function of $n_{m=0}$ and n, the density of particles in the state $|0\rangle$ and the total

density, respectively:

$$\langle H_{int} \rangle = \int d^3 r \left(\frac{\tilde{g}}{2} n^2 - \frac{\delta g}{2} n_{m=0}^2 \right), \tag{5.23}$$

which shows explicitly the effective attractive interaction.

Chapter 6

Kinetic Theory

This Chapter develops the kinetic theory needed to describe a finite temperature gas of Bose condensed atoms. The approach used here was developed in the 1960's by a series of authors, most notably Kadanoff and Baym [113] and Kadanoff and Kane [118]. Recently several authors have applied these, or similar, ideas to trapped atomic gases [119, 120, 121, 122, 123]. The underlying theory is complex, and the main goal of most of these studies is to produce approximations that allow a real problem to be solved.

In writing this Chapter I have three goals. First, and foremost, I want to develop a formalism which can be applied to understanding a series of experimentally relevant problems where both the coherent motion of the condensate and the incoherent motion of the non-condensed particles play equal roles. These problems include the dynamics of vortex decay, and the dynamics of domain formation in a spinor condensate. Second, with the aid of a small toy model, I would like to clarify how a Bogoliubov quasiparticle differs from the collective condensate excitations with the same dispersion. Finally, I would like to present a very compact derivation of the kinetic equations which is of general interest.

The kinetic theory developed here is highly nontrivial. Readers may wish to familiarize themselves with the material in Appendix E where a simpler linearized theory is presented, and the material in Appendix C where response functions are discussed.

6.1   Overview

In classical mechanics one describes the kinetics of a gas/liquid via a phase-space distribution function $f(R, p, T)$, which measures the probability of having a particle of

momentum p at position R and time T. This distribution function obeys a Boltzmann equation, typically of the form

$$(\partial_T + (\mathbf{p}/m) \cdot \nabla_R - (\nabla U) \cdot \nabla_p)f = I[f]. \tag{6.1}$$

The left hand side of the Boltzmann equation describes the motion of the gas particles if they were non-interacting; U is an arbitrary external field, m is the particle mass, and ∇_R and ∇_p are gradients with respect to position and momentum variables. The right hand side, the collision integral, describes the interactions between the particles, and is a nonlinear function of f. The collision integral drives the system towards equilibrium, and has the structure,

$$I[f](R, p, T) = \sum_q (\mathcal{R}_{q \to p} - \mathcal{R}_{p \to q}), \tag{6.2}$$

where $\mathcal{R}_{p \to q}$ is the total rate of particles scattering from momentum p to momentum q. Classically, $\mathcal{R}_{p \to q}$ is proportional to the number of particles in the state p, and so one usually writes $\mathcal{R}_{p \to q} = \Gamma_{p \to q} f(q)$.

In a quantum theory one can derive a similar equation. The key is to recognize that the single particle Green's function $G^< = \langle \psi^\dagger(r_{1'}, t_{1'})\psi(r_1, t_1)\rangle$ behaves like a phase space distribution. After writing $G^<(r_1, t_1, r_{1'}, t_{1'})$ in terms of the center of mass coordinates $R = (r_1 + r_{1'})/2$ and $T = (t_1 + t_{1'})/2$, and the relative coordinates $r = (r_1 - r_{1'})$ and $r = (t_1 - t_{1'})$, one can Fourier transform with respect to the relative coordinates,

$$G^<(p, \omega, R, T) = \int d^3r \, dt \, e^{i\omega t - ip \cdot r} G^<(r, t; R, T). \tag{6.3}$$

If one integrates the resulting function over p, one gets the density of occupied states in real space. Integrating over r, gives the density of occupied states in momentum space. Thus $G^<(p, \omega, R, T)$ holds all of the physics that is contained in the classical $f(R, p, T)$. In quantum mechanics, the energy of a particle ω is not independent of its momentum p, requiring one to carry around an extra variable. When there is a well-defined dispersion relationship, one can produce a quantum mechanical phase space distribution function that is only a function of R, p, T.

Although I am interested in $G^<$, it is a instructive to first understand the time ordered Green's function $G = \langle T(\psi^\dagger \psi)\rangle$. In a nonequilibrium (Schwinger-Keldysh) formalism, the time ordering operator T, orders operators along a contour in the complex time plane. This contour, illustrated in Fig. 6.1 begins at time $t = -\infty$, follows the real axis to $t = +\infty$, returning to $t = -\infty - i\beta$. Periodic boundary conditions on this path ensure that the system is in thermal equilibrium at time
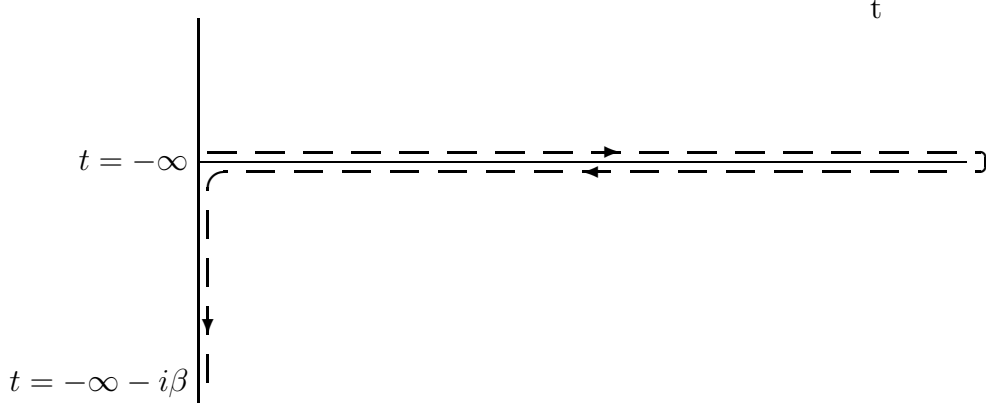
Figure 6.1: Contour in complex time used in the Schwinger-Keldysh formalism.

$t = -\infty$. In all subsequent integrals, time integrals will implicitly follow this contour, and space integrals will be over three dimensions. The equations for G take the form of a convolution,

$$\int d\bar{2}\, G^{-1}(1, \bar{2}) G(\bar{2}, 1') = \delta(1 - 1'). \tag{6.4}$$

Here I have introduced the notational shorthand of using numbers to represent coordinates, such as 1 represents $\{r_1, t_1\}$. In a normal system, after converting to relative and center of mass (COM) coordinates, G^{-1} obeys the equation

$$G^{-1}(p, \omega, R, T) = \omega - p^2/2m - V(R, T) - \Sigma(R, T; p, \omega), \tag{6.5}$$

which defines the self-energy Σ. Unfortunately the convolution in Eq. (6.4) is not simple in term of the variables R, p, T, ω that describe the distribution function.

The Boltzmann equation only describes the evolution of the system close to equilibrium in the presence of slowly varying disturbances. One can use this assumption of slow variation to derive a "semi-classical" scheme for approximating the convolution. For pedagogical purposes I first show how this semiclassical method works in an abstract setting. Let F be the convolution of two arbitrary functions A and B,

$$F(X, x) = A * B = \int d\bar{x}\, A(x_1, \bar{x}) B(\bar{x}, x_{1'}), \tag{6.6}$$

where $x_1 = X - x/2$ and $x_{1'} = X + x/2$. By replacing $\bar{x}$ with the relative coordinate r, one finds,

$$F(X, x) = \int dr\, A(R_A = X + r/2, r_A = x - r) B(R_B = X + (r - x)/2, r_B = r). \tag{6.7}$$

In analogy to the expected behavior of the Green's functions, suppose A and B are peaked near $r_A = 0$, and $r_B = 0$, each falling off on a length scale ξ. Suppose

98

further that A and B vary only slowly as a function of their COM coordinates, with a length scale L. Up to corrections of relative order ξ/L, the functions A and B can be expanded to give

$$F(X,x) \;=\; \int dr\, A(X, x-r)B(X,r) + \partial_X A(X, x-r)\frac{r}{2}B(X,r) \qquad (6.8)$$
$$-\frac{(x-r)}{2}A(X, x-r)\partial_X B(X,r) + \cdots$$

This expresses F as a series of terms, each of which is a convolution in the variable x. The Fourier transform of F with respect to the relative coordinate is then

$$F(X,p) = \int dx\, e^{-ixp}F(X,x) = A(X,p)B(X,p) + \frac{i}{2}\partial_X A\partial_p B - \frac{i}{2}\partial_p A\partial_x B. \qquad (6.9)$$

This convolution identity is the key to my derivation of the quantum Boltzmann equation.

Turning back to the Green's functions, the length scale over which the center of mass of G changes is set by the external potential. This length is L. The rate of change of the relative coordinate is set by the temperature and interactions. This length scale, denoted ξ, is the coherence length. One builds Σ from G's, and the same length scales govern its behavior. Thus, as long as $\xi \ll L$ one can expand the convolution for the equations of motion of G. (Similar arguments follow for the convolution in the time domain.)

At this point it is convenient to introduce further notation. I define the Poisson brackets $\{A, B\}$ by

$$\{A, B\} = (\nabla_R A \cdot \nabla_P B - \nabla_P A \cdot \nabla_R B) - (\partial_T A\partial_\omega B - \partial_\omega A\partial_T B). \qquad (6.10)$$

Then the convolution identity (6.9) is compactly written

$$A * B = AB + (i/2)\{A, B\}. \qquad (6.11)$$

Stepping back for a moment, the classical Boltzmann equation, Eq. (6.1), is described by

$$\{\omega - p^2/2m - V(R,T), f(R,p,T)\} = I[f]. \qquad (6.12)$$

Applying the convolution identity (6.11) to the equation for G,

$$(G^{-1} * G)(p, \omega, R, T) = 1 = (G_0^{-1} - \Sigma)G + \frac{i}{2}\{(G_0^{-1} - \Sigma, G\}. \qquad (6.13)$$

Looking at a frequency $\omega \to \omega \pm i\eta$, for small η, one can write this equation in terms of its real and imaginary parts

$$G(\omega \pm i\eta) \;=\; Re[G(\omega)] \mp iA/2 \qquad (6.14a)$$
$$\Sigma(\omega \pm i\eta) \;=\; Re[\Sigma(\omega)] \mp i\Gamma/2. \qquad (6.14b)$$

99

This leaves four equations

$$(G_0^{-1} - Re[\Sigma])(Re[G]) \quad + \quad (\Gamma/2)(A/2) \tag{6.15a}$$

$$\pm \quad (\{\Gamma/4, Re[G]\} - \{(G_0^{-1} - Re[\Sigma]), A/4\}) = 1$$

$$(G_0^{-1} - Re[\Sigma])(A/2) \quad - \quad (\Gamma/2)(Re[G]) \tag{6.15b}$$

$$\pm \quad (\{\Gamma/4, Re[G]\} - \{(G_0^{-1} - Re[\Sigma]), A/4\}) = 0.$$

These are most transparent in the following form

$$\begin{pmatrix} G_0^{-1} - Re[\Sigma] & \Gamma/2 \\ -\Gamma/2 & G_0^{-1} - Re[\Sigma] \end{pmatrix} \begin{pmatrix} Re[G] \\ A/2 \end{pmatrix} = \begin{pmatrix} 1 \\ 0 \end{pmatrix} \tag{6.16a}$$

$$\{\Gamma, Re[G]\} - \{(G_0^{-1} - Re[\Sigma]), A\} = 0. \tag{6.16b}$$

The matrix is easily inverted to give the well-known results [113]

$$Re[G] = (G_0^{-1} - Re[\Sigma])/((G_0^{-1} - Re[\Sigma])^2 + (\Gamma/2)^2) \tag{6.17a}$$

$$A = \Gamma/((G_0^{-1} - Re[\Sigma])^2 + (\Gamma/2)^2). \tag{6.17b}$$

When Γ vanishes one must interpret the Lorentzian as a Dirac delta function.

We now have enough tools to investigate $G^<$. The equations of motion for $G^<$ can be derived from the equations for G, taking $t_1 < t_{1'}$, in which case

$$\int d\bar{2} \quad (G_0^{-1}(1,\bar{2}) - \Sigma(1,\bar{2}))G(\bar{2}, 1')$$

$$= \int d\bar{2}\, G_0^{-1}(1,\bar{2})G^<(\bar{2}, 1') - \int^{t_1} d\bar{2}\, \frac{1}{i}\Sigma^>(1,\bar{2})G^<(\bar{2}, 1')$$

$$- \int_{t_1}^{t_{1'}} d\bar{2}\, \frac{1}{i}\Sigma^<(1,\bar{2})G^<(\bar{2}, 1') - \int_{t_{1'}} d\bar{2}\, \frac{1}{i}\Sigma^<(1,\bar{2})G^>(\bar{2}, 1') \tag{6.18a}$$

$$= \int d\bar{2} \left[G_0^{-1}(1,\bar{2})G^<(\bar{2}, 1') - \left(\frac{1}{i}\Theta(1 - \bar{2})[\Sigma^>(1,\bar{2}) - \Sigma^<(1,\bar{2})] \right) G^<(\bar{2}, 1') \right.$$

$$\left. + \Sigma^<(1,\bar{2}) \left(\frac{1}{i}\Theta(1' - \bar{2})[G^>(\bar{2}, 1') - G^<(\bar{2}, 1')] \right) \right], \tag{6.18b}$$

where $\Theta(x)$, the Heaviside step function, is zero for negative arguments and otherwise equals 1. Since G_0^{-1} is strictly local in time one does not have to worry about breaking the G_0^{-1} integrals up. Eq. (6.18b) is simple expressed in terms of retarded/advanced response functions,

$$G^A(12) = \frac{-1}{i}\Theta(2 - 1)[G^>(1, 2) - G^<(1, 2)] \tag{6.19a}$$

$$\Sigma^R(12) = \frac{1}{i}\Theta(1 - 2)[\Sigma^>(1, 2) - \Sigma^<(1, 2)], \tag{6.19b}$$

100

in terms of which the equations of motion read,

$$(G_0^{-1} - \Sigma^R) * G^< - \Sigma^< * G^A = 0. \tag{6.20}$$

Following the same procedure for $t_1 > t_{1'}$, one finds

$$(G_0^{-1} - \Sigma^R) * G^> - \Sigma^> * G^A = 0. \tag{6.21}$$

I now switch to center-of mass and relative coordinates, assuming $L \gg \xi$,

$$(G_0^{-1} - \Sigma^R)G^< - \Sigma^< G^A + \frac{i}{2}(\{(G_0^{-1} - \Sigma^R), G^<\} - \{\Sigma^<, G^A\}) = 0 \tag{6.22}$$

As with the equations of motion for G, one can break this equation up into a real and imaginary parts. Using the relations

$$G^A(\omega) = G(\omega + i\eta) = ReG(\omega) + iA(\omega)/2 \tag{6.23a}$$
$$\Sigma^R(\omega) = \Sigma(\omega + i\eta) = Re\Sigma(\omega) - i\Gamma(\omega)/2; \tag{6.23b}$$

one finds

$$\{\Gamma/4, G^<\} - \{\Sigma^<, A/4\} = (G_0^{-1} - Re\Sigma)G^< - \Sigma^< ReG \tag{6.24a}$$
$$\{(G_0^{-1} - Re\Sigma), G^<\} - \{\Sigma^<, ReG\} = -(\Gamma G^< - \Sigma^< A) \tag{6.24b}$$
$$= -(\Sigma^> G^< - \Sigma^< G^>). \tag{6.24c}$$

The last relationship appears as Eq. (9-30) in Kadanoff and Baym [113], and has the structure of a Boltzmann equation [cf. (6.12)]; the left hand side contains streaming terms, while the right is a collision integral. The functions $\Sigma^>$ and $\Sigma^<$ are the rates of scattering out of and into a given chunk of phase space. The functions $G^<$ and $G^>$ are the number of particles and the number of holes available in that chunk of phase space.

When A is strongly peaked about a few discrete points, one can label those points by a quantum number ν, and write $A = \sum_\nu A^\nu$. One then splits $G^<$ into a product $f_\nu A^\nu$. The Poisson bracket obeys the Leibniz "product" rule, which for scalars reads $\{A, BC\} = \{A, B\}C + \{A, C\}B$, and along with Eq. (6.16b), gives us,

$$\{(G_0^{-1} - Re\Sigma), f_\nu\} A^\nu + \{\Gamma^\nu f^\nu - \Sigma^<, ReG\} + \{ReG, f^\nu\}\Gamma^\nu = -(\Gamma^\nu f_\nu - \Sigma^<)A^\nu, \tag{6.25}$$

where Γ^ν is defined analogously to A^ν. In equilibrium, $\Sigma^< = \Gamma^\nu f^\nu$. Equation (6.24a) forces A to be strongly peaked. See [113] for concrete examples that clarify this structure.

6.2 Condensed system

6.2.1 Basic problems

In the condensed system, the Green's function $G^<$ is a two-by-two matrix (cf. appendix C.4.1). However, for the weakly interacting system, the elementary excitations are still quasiparticles, for which one should be able to find a Boltzmann equation. There does not exist a one to one correspondence between particles and quasiparticles, so the constraints imposed by number conservation have a different form in a condensed and noncondensed system. Matrix Green's functions also appear in systems of particles with internal degrees of freedom. The matrix structure arising from internal degrees of freedom is simpler to deal with than the one arising from the presence of a condensate.

In the last Section, all formulae which did not explicitly refer to real and imaginary parts of functions are correct for more general matrix propegators (I was careful with operator ordering). However one needs to take Hermitian and anti-Hermitian parts of equations instead of real and imaginary. This is complicated by the fact that the Hermitian and anti-Hermitian parts of the various matrices do not commute.

Since the different components do not commute, it is very hard to solve the resulting equations. One might hope that one could formally manipulate the matrix equations in the same manner as one does the scalar equations. Unfortunately the basic assumptions underlying these manipulations only hold for scalar Green's functions. For example, the decomposition of $G^<$ into the product fA relies upon the relationship $\{A, f(A)\} = 0$. This relationship is an obvious corollary of the chain rule $\{A, f(B)\} = \{A, B\} f'(B)$, along with $\{A, A\} = 0$. Unfortunately, neither the chain rule, nor the latter identity are true for matrices. For example, consider the two by two matrix $A = \omega \tau_1 + t \tau_2$, for which the Poisson bracket reads $\{A, A\} = 2i\tau_3 \neq 0$.

The most promising scheme to deal with these difficulties is to project the equations of motion onto Pauli matrices. This approach seems manageable, at least at the mean field level. Instead of the two equations one has for the scalar case (one real, one imaginary), one ends up with eight equations (four Pauli matrices, both real and imaginary). In the next Section I investigate Bogoliubov theory in the context of this formalism.

Alternatively one can make approximations which simplify the structure of the matrix equations of motion. For example the Hartree-Fock approximation of Stoof et al. [123], and the Popov approximation of Griffin et al. [120], each omit off-diagonal terms in G_0^{-1}. For many problems such an approximation is appropriate.

6.3 Bogoliubov theory

In simple mean-field theories of the Bose gas (see appendix C.4.1), the inverse Green's function is of the form

$$G_{MF}^{-1} = G_0^{-1} - \Sigma_{MF} = \omega\tau_3 - \epsilon - \Delta\tau_1, \tag{6.26}$$

where τ_ν is a Pauli matrix, and the coefficients are generically calculated in some self-consistent manner. In the simplest of these theories, the Bogoliubov approximation, $\epsilon(R, P, T) = p^2/2m + gn_0(R, T)$, and $\Delta(R, P, T) = gn_0(R, T)$. For the remainder of this Section I neglect the subscripts MF. In a uniform, time independent system, the spectral density is

$$\begin{aligned} A &= 2\pi\delta(G^{-1}) = 2\pi\left[\delta(\omega - E) - \delta(\omega + E)\right]\left[\frac{\omega}{2E}\tau_3 + \frac{\epsilon}{2E} - \frac{\Delta}{2E}\tau_1\right], &(6.27)\\ &= 2\pi\delta(\omega^2 - E^2)\left[\omega\tau_3 + \epsilon - \Delta\tau_1\right] &(6.28) \end{aligned}$$

which can also be thought of as

$$A = 2\pi\delta(\omega - E)\begin{pmatrix} u \\ v \end{pmatrix}\begin{pmatrix} u^* & v^* \end{pmatrix} - 2\pi\delta(\omega + E)\begin{pmatrix} v^* \\ u^* \end{pmatrix}\begin{pmatrix} v & u \end{pmatrix}, \tag{6.29}$$

where the Bogoliubov factors are

$$u = \sqrt{\frac{\epsilon + E}{2E}}, \tag{6.30a}$$

$$v = -\sqrt{\frac{\epsilon - E}{2E}}. \tag{6.30b}$$

This representation of A is useful, along with the representation

$$G^{-1} = (\omega - E)\begin{pmatrix} u \\ -v \end{pmatrix}\begin{pmatrix} u^* & -v^* \end{pmatrix} - (\omega + E)\begin{pmatrix} v^* \\ -u^* \end{pmatrix}\begin{pmatrix} v & -u \end{pmatrix}. \tag{6.31}$$

For our purposes the representation in terms of Pauli matrices, Eq. (6.27) is easiest to work with.

Now consider a slowly varying $n_0(R, T)$. By construction $G^{-1}A = 0$, but the Poisson bracket is

$$\begin{aligned} \{G^{-1}, A\} &= \{\omega^2 - \epsilon^2 + \Delta^2, f/2\} + \tau_1(\{\epsilon, \Delta f\} - \{\Delta, \epsilon f\}) &(6.32)\\ &\quad + i\tau_2(\{\Delta, \omega f\} - \{\omega, \Delta f\}) + \tau_3(\{\omega, \epsilon f\} - \{\epsilon, \omega f\}), \end{aligned}$$

with $f = 2\pi\delta(\omega^2 - E^2)$. The first term, proportional to the identity, is zero, but the others are generically finite. Thus this spectral density does not obey the semiclassical equations of motion.

The physical reason why this spectral density does not work is that it violates number conservation. This violation occurs because as the spectrum changes, the relationship between the number of quasiparticles and the number of real particles changes. The collisionless Boltzmann equation conserves the number of quasiparticles, so the spectral density has to be modified to take into account fluctuations in the number of condensed particles.

To find the correct spectral density, I consider an arbitrary matrix of the form $A = a_0 + \sum_\nu a_n \tau_\nu$. The equation

$$\{G^{-1}, A\} = 2iG^{-1}A, \tag{6.33}$$

can then be broken up into eight components,

$$\{\omega, a_3\} - \{\epsilon, a_0\} - \{\Delta, a_1\} = 0 \tag{6.34a}$$

$$\{\epsilon, a_1\} + \{\Delta, a_0\} = -2\omega a_2 \tag{6.34b}$$

$$\{\epsilon, a_2\} = 2\omega a_1 + 2\Delta a_3 \tag{6.34c}$$

$$\{\epsilon, a_3\} - \{\omega, a_0\} = -2\Delta a_2 \tag{6.34d}$$

$$0 = \omega a_3 - \epsilon a_0 - \Delta a_1 \tag{6.34e}$$

$$\{\omega, a_2\} = 2\Delta a_0 + 2\epsilon a_1 \tag{6.34f}$$

$$\{\Delta, a_3\} + \{\omega, a_1\} = -2\epsilon a_2 \tag{6.34g}$$

$$\{\Delta, a_2\} = 2\epsilon a_3 - 2\omega a_0.. \tag{6.34h}$$

Solving so many simultaneous partial differential equations is difficult. By combining Eqs. (6.34f,6.34c,6.34h), one finds that a_2 satisfies

$$\{\omega^2 - \epsilon^2 + \Delta^2, a_2\} = 0. \tag{6.35}$$

Thus a_2 is a function of $\omega^2 - E^2$. The matrix element a_2 is closely related to the change in the number of quasiparticles. In equilibrium it vanishes.

These equations are amenable to a perturbative analysis where one formally treats the Poisson brackets in (6.33) as small, which amounts to an expansion in powers of ξ/L. Writing $A = \sum_\nu A^{(\nu)}$, this analysis yields a hierarchy,

$$G^{-1}A^{(0)} = 0 \tag{6.36}$$

$$G^{-1}A^{(1)} = -i/2\{G^{-1}, A^{(0)}\} \tag{6.37}$$

$$G^{-1}A^{(2)} = -i/2\{G^{-1}, A^{(1)}\}, \tag{6.38}$$

and so on. As previously discussed, $A^{(0)} = 2\pi\delta(\omega^2 - E^2)[\omega\tau_3 + \epsilon - \Delta\tau_1]$. Iterating these equations, and using the identity $x\delta'(x) = -\delta(x)$, one finds $A^{(1)} = -2\pi\delta'(\omega^2 -$

$E^2)\tau_2(\epsilon\{\Delta,\omega\} + \omega\{\epsilon,\Delta\} + \Delta\{\omega,\epsilon\})$. These first order corrections have little effect except to enforces particle conservation.

6.4 Response to a sudden change of interaction strength

As a simple example to illustrate some of the issues raised by the kinetic approach presented in this Chapter, I explore a uniform gas subjected to a sudden change of interaction strength. In principle this situation could be experimentally realized through the use of Feshbach resonances which allow the tuning of atomic interactions [124]. I first study this problem using elementary means. I then use the machinery developed in the preceding Sections to rederive these results.

6.4.1 The scenario

Before time $t = 0$ a uniform cloud of non-interacting bosons is in equilibrium. At $t = 0$ interactions are suddenly turned on. The system is no longer in equilibrium, and various excitations are generated. These excitations are generated on a timescale of order the inverse mean field energy $\tau_{\mathrm{MF}} \approx \hbar/gn$, where $g = 4\pi\hbar^2 a_s/m$. These excitations equilibrate on the collision time $\tau_c \approx 1/(n\sigma v)$. The times scale as different powers of the scattering length; $\tau_{\mathrm{MF}} \sim 1/a_s$, while $\tau_c \sim 1/a_s^2$. Thus one expects a clear separation of timescales with $\tau_{\mathrm{MF}} \ll \tau_c$. Introducing typical parameters of Bose gas experiments, $\tau_{\mathrm{MF}} \approx 0.6$ms, and $\tau_c \approx 17$ms.

Due to this separation of timescales one can look at the two processes separately, the generation of excitations and their equilibration. The former is described by a collisionless (mean field) kinetic theory. There is a very interesting technical issue here, in that within a collisionless kinetic theory, entropy is conserved and there is no generation of quasiparticles. Thus these excitations are collective in nature and represent an unusual oscillation of the condensate. Due to the presence of the condensate, the spectrum of these collective oscillations is the same as the spectrum of quasiparticle excitations.

6.4.2 Elementary approach

The mean field theory describing this situation can be derived from the Heisenberg equations for the field operator Ψ,

$$\left(i\partial_t + \frac{\nabla^2}{2m}\right)\Psi = g\Psi^\dagger\Psi\Psi. \tag{6.39}$$

One writes $\Psi = \psi + \tilde\psi$ where $\psi = \langle\Psi\rangle$ is a c-number which represents the condensate, and $\tilde\psi$ is the operator that annihilates a non-condensed atom. Taking the expectation value of Eq. (6.39) and keeping terms to quadratic order in the excitations, one arrives at a non-linear Schrödinger equation

$$\left(i\partial_t + \frac{\nabla^2}{2m}\right)\psi = g\psi^*\psi\psi + 2g\langle\tilde\psi^\dagger\tilde\psi\rangle\psi + g\langle\tilde\psi\tilde\psi\rangle\psi^*. \tag{6.40}$$

Varying ψ in Eq. (6.40) gives

$$\left(i\partial_t + \frac{\nabla^2}{2m}\right)\tilde\psi = 2g\psi^*\psi\tilde\psi + g\psi\psi\tilde\psi^\dagger. \tag{6.41}$$

where higher order terms have been ignored.

This approximation, a variant on the Bogoliubov approximation, obeys all of the standard conservation laws (energy, mass, and current). These laws are easily verified by noting that we could have derived the equations from functional differentiation of a functional Φ (see Appendix D). In particular, multiplying Eq. (6.40) and (6.41) by ψ^* and $\tilde\psi^\dagger$, and subtracting the complex conjugate, gives $\partial_t n_0 = -\partial_t\langle\tilde\psi^\dagger\tilde\psi\rangle = 2g\text{Im}(\psi^*)^2\langle\tilde\psi\tilde\psi\rangle$, and verifies number conservation. Note that the standard Bogoliubov theory, where the term $g\langle\tilde\psi\tilde\psi\rangle\psi^*$ is ignored, does not conserve particle number.

In this formalism, a time and space dependent chemical potential is introduced as the derivative of the condensates phase. One writes $\psi = \sqrt{n_0}\exp(i\phi)$, and defines

$$v_s \equiv (\nabla\phi)/m \tag{6.42}$$

$$\mu \equiv -\partial_t\phi - mv_s^2/2. \tag{6.43}$$

Using these definitions, one rewrites Eq. (6.40) as a set of equations,

$$\partial_t n_0 + \nabla\cdot(n_0 v_s) = 2gn_0\text{Im}(\langle\tilde\psi\tilde\psi\rangle e^{-2i\phi}) \tag{6.44}$$

$$\mu = \frac{\nabla^2\sqrt{n_0}}{2m\sqrt{n_o}} + g(n - n_0) + g\text{Re}(\langle\tilde\psi\tilde\psi\rangle e^{-2i\phi}). \tag{6.45}$$

Equation (6.44) has the structure of a continuity equation. The right hand side represents the transfer of particles between the condensate and normal cloud. The second

line (6.45) is analogous to Euler's equation for an ideal fluid. The term proportional to $\nabla^2\sqrt{n_o}$ is the "quantum pressure" term which played such an important role in Chapter 5.

The equation for the non-condensed atoms is simplified by performing a Bogoliubov transformation,

$$\tilde{\psi} = e^{i\phi} \sum_k \left[e^{ik\cdot r} u_k(t)\hat{b}_k + e^{-ik\cdot r} v_k^*(t)\hat{b}_{-k}^\dagger \right], \tag{6.46}$$

with c-number functions u and v and time independent boson operators $\hat{b}_k$ and $\hat{b}_{-k}^\dagger$. Since Eq. (6.41) is linear in $\tilde{\psi}$, this ansatz involves no further approximation. To ensure the proper commutation relationships, one must enforce $|u_k|^2 - |v_k|^2 = 1$. The resulting equation for u_k and v_k is

$$\begin{pmatrix} i\partial_t - \epsilon_k & -gn_0 \\ -gn_0 & -i\partial_t - \epsilon_k \end{pmatrix} \begin{pmatrix} u_k \\ v_k \end{pmatrix} = 0. \tag{6.47}$$

To the extent that one can ignore terms proportional to the depletion, the chemical potential is $\mu = g(2n - n_0)$, and $\epsilon = k^2/2m + gn_0$. In an inhomogeneous condensate one would also need a term corresponding to spatial gradients, and also allow for the presence of the superfluid velocity v_s.

The stationary solutions to Eq. (6.47) correspond to $(u_k, v_k) \sim e^{\pm iE_k t}$, where $E_k^2 = \epsilon_k^2 - (gn_0)^2$. The physical, positive frequency solutions, are best characterized by the bilinears (cf. 6.30),

$$|u_k|^2 = \frac{\epsilon + E}{2E} \tag{6.48}$$

$$|v_k|^2 = \frac{\epsilon - E}{2E} \tag{6.49}$$

$$u_k^* v_k = \frac{-gn_0}{2E}. \tag{6.50}$$

More generically, Eq. (6.47) can be formally integrated,

$$\begin{pmatrix} u_k(t) \\ v_k(t) \end{pmatrix} = \exp\left[it \begin{pmatrix} -\epsilon_k & -gn_0 \\ gn_0 & \epsilon_k \end{pmatrix} \right] \begin{pmatrix} u_k(t=0) \\ v_k(t=0) \end{pmatrix}. \tag{6.51}$$

In this expression I have ignored the time dependence of n_0 and v_s, both assumed to be slow and small. The exponential is simplified by noting that the square of its argument is proportional to the identity, yielding,

$$\begin{pmatrix} u_k(t) \\ v_k(t) \end{pmatrix} = \left[\cos(E_k t) + \frac{i\sin(E_k t)}{E_k} \begin{pmatrix} -\epsilon_k & -gn_0 \\ gn_0 & \epsilon_k \end{pmatrix} \right] \begin{pmatrix} u_k(t=0) \\ v_k(t=0) \end{pmatrix}. \tag{6.52}$$
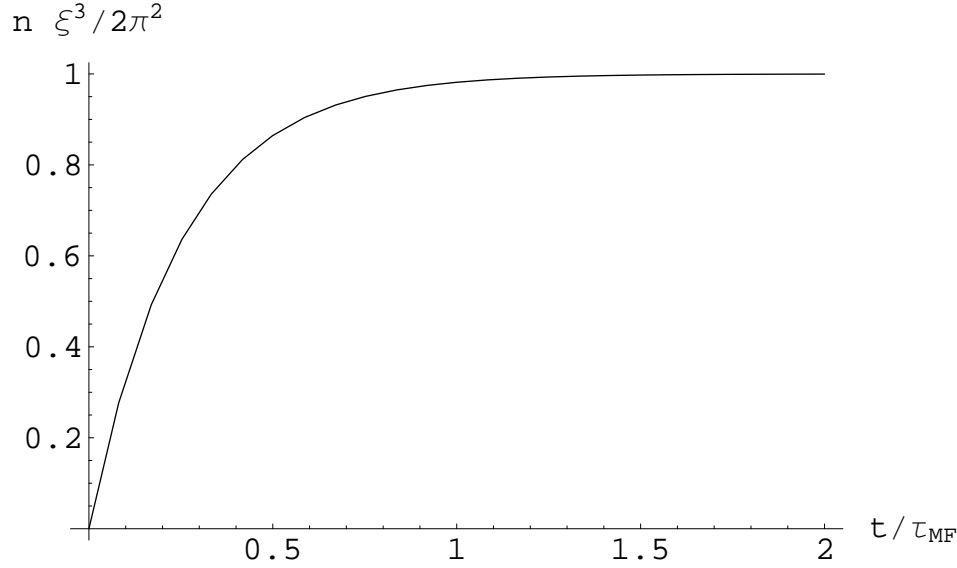
Figure 6.2: Non-condensed density as a function of time after interactions are suddenly turned on. The density is measured relative to its long-time value, and time is measured in terms of the mean field time.

It is readily verified that the constraint $|u_k|^2 - |v_k|^2 = 1$ is maintained by these dynamics.

Focusing on the case at hand, at $t \leq 0$, the system is in equilibrium with all of the particles in the condensate. This implies that $n_0 = n$ and that $\langle \tilde{\psi}^\dagger \tilde{\psi} \rangle = 0$. Using the ansatz in Eq. (6.46), $\langle \tilde{\psi}^\dagger \tilde{\psi} \rangle = \sum_k (v_k^2 + (u_k^2 + v_k^2)\langle b_k^\dagger b_k \rangle)$, which implies that $b_k|\Psi\rangle = 0$ and that $v_k = 0$. The normalization condition $u_k^2 - v_k^2 = 1$ then gives $u_k = 1$.

From Eq. (6.52) the factor v_k evolves as $v_k(t) = i(gn_0/E_k)\sin(E_k t)$. Thus the number of excited particles $\tilde{n} = \langle \tilde{\psi}^\dagger \tilde{\psi} \rangle = V^{-1} \sum_k |v_k|^2 = V^{-1}(gn_0/E_k)^2 \sin^2(E_k t)$. At long times, the phase of the sine wave is essentially random, and one can replace $\sin^2(E_k t)$ with $1/2$, giving $\tilde{n} = V^{-1} \sum_k (gn_0)^2/2E_k^2 = 2\pi^2/\xi_{\mathrm{MF}}^3$, where $\xi_{\mathrm{MF}}^2 = \hbar/gnm$ is the condensate healing length. The time required to reach this asymptotic value is of order $\tau_{\mathrm{MF}} = \hbar/(gn_0)$. The general integral analytically evaluates to

$$\tilde{n}(t) = 2\pi^2/\xi_{\mathrm{MF}}^3 \big(1 - \cosh(4t/\tau_{\mathrm{MF}}) + \sinh(4t/\tau_{\mathrm{MF}})\big). \tag{6.53}$$

This curve is shown in Fig. 6.2.

6.4.3 Further analysis

This model calculation seems quite simple, but the physics is actually quite strange. For example, as anticipated, the number of quasiparticles, $\langle b_k^\dagger b_k \rangle$, is conserved. Thus

these oscillations of particles into and out of the condensate are somehow just a more complicated oscillation of the condensate.

One gets further clues about this system by looking at the Green's function,

$$G(1,2) = \frac{1}{i} \left\langle T\left[\begin{pmatrix} \psi_1 \\ \psi_1^\dagger \end{pmatrix} (\psi_2^\dagger \ \ \psi_2) \right] \right\rangle, \tag{6.54}$$

and the functions $G^<$ and $G^>$, corresponding to the specific time orderings $t_1 < t_2$ and $t_1 > t_2$. To make contact to the material in the early part of this Chapter, I write these functions in terms of the central coordinate $T = (t_1 + t_2)/2$ and the relative coordinate $t = t_1 - t_2$.

In the example at hand, $\langle b^\dagger b \rangle = 0$, thus

$$G^>(1,2) = \begin{pmatrix} u(1) \\ v(1) \end{pmatrix} (u^*(2) \ \ v^*(2)) \tag{6.55a}$$

$$G^<(1,2) = \begin{pmatrix} v^*(1) \\ u^*(1) \end{pmatrix} (v(2) \ \ u(2)). \tag{6.55b}$$

Using the expressions for u and v in Eq. (6.52),

$$
\begin{aligned}
G^>(T,\omega,k) &= 2\pi\delta(\omega)\frac{gn}{2E^2} \begin{pmatrix} -gn\cos(2E_kT) & \epsilon\cos(2E_kT)-iE_k\sin(2E_kT) \\ \epsilon\cos(2E_kT)-iE_k\sin(2E_kT) & -gn\cos(2E_kT) \end{pmatrix} \tag{6.56a} \\
&\quad + 2\pi\delta(\omega-E_k)\frac{\epsilon+E}{2E} \begin{pmatrix} \frac{\epsilon+E}{2E} & -\frac{gn}{2E} \\ -\frac{gn}{2E} & \frac{\epsilon-E}{2E} \end{pmatrix} + 2\pi\delta(\omega+E_k)\frac{\epsilon-E}{2E} \begin{pmatrix} \frac{\epsilon-E}{2E} & -\frac{gn}{2E} \\ -\frac{gn}{2E} & \frac{\epsilon+E}{2E} \end{pmatrix}
\end{aligned}
$$

$$
\begin{aligned}
G^<(T,\omega,k) &= 2\pi\delta(\omega)\frac{gn}{2E^2} \begin{pmatrix} -gn\cos(2E_kT) & \epsilon\cos(2E_kT)-iE_k\sin(2E_kT) \\ \epsilon\cos(2E_kT)-iE_k\sin(2E_kT) & -gn\cos(2E_kT) \end{pmatrix} \tag{6.56b} \\
&\quad + 2\pi\delta(\omega-E_k)\frac{\epsilon-E}{2E} \begin{pmatrix} \frac{\epsilon+E}{2E} & -\frac{gn}{2E} \\ -\frac{gn}{2E} & \frac{\epsilon-E}{2E} \end{pmatrix} + 2\pi\delta(\omega+E_k)\frac{\epsilon+E}{2E} \begin{pmatrix} \frac{\epsilon-E}{2E} & -\frac{gn}{2E} \\ -\frac{gn}{2E} & \frac{\epsilon+E}{2E} \end{pmatrix}.
\end{aligned}
$$

All of the dynamics occurs in the $\omega = 0$ sector. This is a sign that these excitations are actually deformations of the condensate. Subtracting the Green's functions gives

$$A = G^> - G^< = 2\pi\delta(\omega-E) \begin{pmatrix} \frac{\epsilon+E}{2E} & -\frac{gn}{2E} \\ -\frac{gn}{2E} & -\frac{\epsilon-E}{2E} \end{pmatrix} - 2\pi\delta(\omega+E) \begin{pmatrix} \frac{\epsilon-E}{2E} & -\frac{gn}{2E} \\ -\frac{gn}{2E} & -\frac{\epsilon-E}{2E} \end{pmatrix}, \tag{6.57}$$

just as one finds in equilibrium. The spectral density A determines the dispersion and wavefunctions of the quasiparticles. Since A is independent of time, the quasiparticles are also unchanged in time. Because of the $\omega = 0$ structure, $G^<$ and $G^>$ are not simply proportional to A.

6.4.4 Kinetic approach

I now look at this problem in the language of the kinetic theory presented earlier in this Chapter. In the absence of collisions, the fundamental equation is

$$\{G_0^{-1} - \Sigma, G^<\} = \frac{-2}{i}(G_0^{-1} - \Sigma)G^<, \tag{6.58}$$

where $\{A, B\} = (\partial_\omega A \partial_T B - \partial_T A \partial_\omega B) - (\nabla_p A \nabla_R B - \nabla_R A \nabla_P B)$.

Within this approximation,

$$(G_0^{-1} - \Sigma)(k, T, \omega) = \tau_3 \omega - \epsilon_k - gn_0 \tau_1, \tag{6.59}$$

where $\epsilon_k = k^2/2m + gn_0$, and n_0 is taken to be independent of time. Since $G^<$ is Hermitian, it can be decomposed in terms of Pauli matrices,

$$G^< = g_0 + \sum_\nu g_\nu \tau_\nu, \tag{6.60}$$

where all of the g's are real. Blindly substituting this decomposition into Eq. (6.58), and using the relationship $\tau_\mu \tau_\nu = \delta_{\mu\ni} + i\epsilon_{\mu\nu\lambda}\tau_\lambda$, one finds the following six equations:

$$\partial_T g_3 = 0 \tag{6.61a}$$
$$\partial_T g_2 = 2(\epsilon)g_1 + 2(gn_0)g_0 \tag{6.61b}$$
$$\partial_T g_1 = -2\epsilon g_2 \tag{6.61c}$$
$$\partial_T g_0 = 2(gn_0)g_2 \tag{6.61d}$$
$$0 = \omega g_3 - \epsilon g_0 - (gn_0)g_1 \tag{6.61e}$$
$$0 = \omega g_2 \tag{6.61f}$$
$$0 = \omega g_1 + (gn_0)g_3 \tag{6.61g}$$
$$0 = \omega g_0 - \epsilon g_3, \tag{6.61h}$$

which correspond to (6.34) specialized to the present case. The algebraic equations can only be solved if the determinant vanishes,

$$\begin{vmatrix} \omega & & -gn_0 & -\epsilon \\ & \omega & & \\ gn_0 & & \omega & \\ -\epsilon & & & \omega \end{vmatrix} = \omega^2(\omega^2 - \epsilon^2 + (gn_0)^2) = 0, \tag{6.62}$$

requiring $\omega = 0, \pm E$. The distribution function will therefore have terms proportional to $\delta(\omega), \delta(\omega - E)$, and $\delta(\omega + E)$. Considering each of these cases in turn, the Green's

functions must have the general form,

$$G^< = A\delta(\omega - E) \begin{pmatrix} \epsilon - E & -gn_0 \\ -gn_0 & \epsilon + E \end{pmatrix} + B\delta(\omega + E) \begin{pmatrix} \epsilon + E & -gn_0 \\ -gn_0 & \epsilon + E \end{pmatrix} \qquad (6.63)$$

$$+ \delta(\omega) \begin{pmatrix} -gn_0 f_1(t) & \epsilon f_1(t) + i f_2(t) \\ \epsilon f_1(t) - i f_2(t) & -gn_0 f_1(t) \end{pmatrix},$$

where A and B are constants, and f_1 and f_2 are functions of time. One also has initial conditions

$$\int \frac{d\omega}{2\pi} G^<(T = 0) = (1 - \tau_3)/2, \qquad (6.64)$$

which tells us that $A - B = 2\pi/2E$, $f_2(0) = 0$, and $f_1(0) = (A + B)gn_0/\epsilon = (A + B)\epsilon/gn_0 - 2\pi/gn_0$. Thus $f_1(0) = 2\pi(gn_0/E^2)$, $A = 2\pi(\epsilon + E)/2E^2$, and $B = 2\pi(\epsilon - E)/2E^2$.

The differential equations in Eq. (6.61) reduce to two equations,

$$\partial_T f_2 = 2E^2 f_1 \qquad (6.65)$$

$$\partial_T f_1 = -2f_2, \qquad (6.66)$$

which are trivially integrated. As expected one recovers Eq. (6.56b).

Chapter 7

Electromagnetically Induced Transparency.

In this Chapter I describe the theory of electromagnetically induced transparency in a gaseous medium, and show how this effect is used to stop light. Two formalisms are discussed at length, a mean field theory, and an equilibrium Green's function calculation. I also say a few words about performing a non-equilibrium Green's function calculation, though a full analysis of such a theory goes beyond the scope of this thesis.

7.1 Introduction: the basic picture

The New York Times writes "Scientists bring light to full stop" [125]. A light beam is frozen in space. Is this the ultimate in delay lines? Will it be used for quantum computing? Most importantly, how does it work?

The premise is simple. Light, which is a harmonic vibration of the electromagnetic field, couples to polarons, harmonic vibrations of the polarization of a media – the coupled excitation is referred to as a polariton. If one finds a scheme where one can control the strength of the coupling, then one can adiabatically transform light into a polarization wave. Polarons have very little dispersion, so the excitation is then effectively stopped. At some later time one can transform the polaron back into a photon, and light continues on its way.

It is useful to ask what is the simplest system in which one can perform this trick. A first guess would be that one could use a cloud of two-level atoms. Unfortunately, such a system is too simple, since there is no way to control the strength with which light couples to the transition. Without being able to control the coupling strength,

one cannot adiabatically transfer the photon into a polaron. An even bigger problem with two-level atoms is that since one has no control of the coupling to the electromagnetic field, one has to contend with spontaneous emission, and the polaron will consequently have a very short lifetime.

The next level of sophistication is to use three-level atoms. Typically one considers a Λ configuration, as portrayed in Fig. 7.1. The levels 1 and 2 represent different hyperfine states of an atom, and there are no allowed transitions between them. The state 3 is an excited electronic state, which couples to both 1 and 2, through different polarizations of light, denoted α and β. There are three distinct polarization waves in this system, depending upon which of the two states are coupled. The various cases will be labeled by the symbols, P_{13}, P_{12}, P_{23}. The goal will be to convert α photons into P_{12} polarization waves. The switch which will turn on the coupling between the photon and the polarization wave is a laser of β photons.
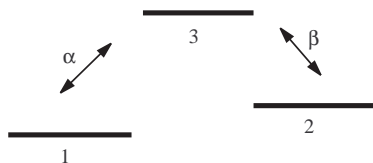
Figure 7.1: Electronic structure of a 3-level atom in the Λ configuration. Levels 1 and 3 are coupled by photons of polarization α, while levels 2 and 3 are coupled by photons of polarization β

Suppose one has an intense laser of β photons. An atom in the 1 state, could then absorb an α photon, jumping into the 3 state. Then the atom can be stimulated to emit a β photon, dropping into the 2 state. Thus, when the laser is on, P_{12} is coupled to the α photons. When the laser is off there is no coupling. This system can therefore be used to stop light. This process is schematically shown in Fig. 7.2.
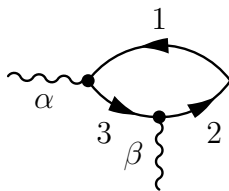
Figure 7.2: Schematic view of the transfer of a α photon into a P_{12} polarization wave. An α photon comes along and excites an atom from the 1 state to the 3 state, generating a P_{13} polaron. The excited atom emits a β photon, and changes the polaron into a P_{12} polarization wave.

One caveat is needed. At no point in the procedure can the atom ever have a

probability of occupying the 3 state. The 3 state is highly excited and couples strongly both α and β photons, consequently it has a relatively short lifetime. Any occupation of this state will result in an absorption of photons. It is the lack of absorption which gives this effect the name "electromagnetically induced transparency."

It is also useful to say a few words about momentum conservation. If the initial light beam has momentum k, and the coupling laser has momentum q, then the polaron will have momentum $k - q$. An interesting twist on the experiment is to convert the polaron back into a photon using a coupling beam of momentum $q' \neq q$. In this case the outcoming light will have momentum $k - q + q'$. This system could then be used as a very efficient router, where light can be stored and the out-coupled in an arbitrary direction.

7.2 A mathematical description of the system

The low energy physics of the light-atom system is given by the Hamiltonian,

$$
\begin{aligned}
H = & \sum_k \left[ck(\alpha_k^\dagger \alpha_k + \beta_k^\dagger \beta_k) + \sum_{\nu=1,2,3} (\epsilon_k + E_\nu)\psi_{\nu k}^\dagger \psi_{\nu k} \right] \\
& + \lambda \sum_{kq} \left[\alpha_q \psi_{3k+q}^\dagger \psi_{1k} + \alpha_q^\dagger \psi_{1k}^\dagger \psi_{3k+q} + \beta_q \psi_{3k+q}^\dagger \psi_{2k} + \beta_q^\dagger \psi_{2k}^\dagger \psi_{3k+q} \right] \\
& + \frac{2\pi \hbar^2 a_s}{m} \sum_{kqp} \sum_{\mu\nu} \psi_{\nu k}^\dagger \psi_{\mu p}^\dagger \psi_{\mu p - q} \psi_{\nu k + q}.
\end{aligned}
\tag{7.1}
$$

The first line gives the energies of the uncoupled modes. The photons of the two polarizations are annihilated by the operators α_k and β_k. Atoms in the electronic state ν with momentum k are annihilated by the operator $\psi_{\nu k}$. The atomic energy is written as $\epsilon_k + E_\nu$, where $\epsilon_k = k^2/2m$, and E_ν is the energy of the electronic state ν.

The second line of this Hamiltonian gives the coupling between the photon modes and the atomic transitions. The coupling constant λ is proportional to the dipole matrix element for the electronic transition, explicitly

$$
\lambda = -e\langle 1|x|3\rangle \sqrt{\frac{E_3 - E_1}{2\epsilon_0 V}},
\tag{7.2}
$$

Where $\langle 1|x|3\rangle$ is the dipole matrix element, e is the electron charge, ϵ_0 is the permitivity of space, and V is the volume of space. I assume that the same λ can be used for coupling states 3 and 2, as are used for 3 and 1. This approximation works well for the current experiments, but generically two such constants are needed. One sees

in the Hamiltonian that the photons couple to polarization operators

$$P_{ij}(q) = \sum_k \psi^\dagger_{ik+q}\psi_{jk}.$$ (7.3)

Finally, the last line of the Hamiltonian gives the interaction between the atoms. This interaction will only be important in that it will lead to some collisional broadening/decoherence. The collision cross-section is $\sigma = 4\pi a_s^2$. Some typical experimental parameters are given in table 7.1.

Table 7.1: Experimental Parameters: temperature T, density n, collision rate $1/\tau_c$, natural width of state 3 Γ_3, coupling constant λ, recoil energy $E_{\text{recoil}} = k^2/2m$, and a rate Γ_d associated with Doppler broadening (see Section 7.4)

	^{87}Rb (Phillips et al. [12])	^{23}Na (Liu et al. [11])
$(E_3 - E_1)/2\pi\hbar$	$3.8 \cdot 10^{14}$ Hz	$5.1 \cdot 10^{14}$Hz
$(E_2 - E_1)/2\pi\hbar$	$\sim 10^5$ Hz	$1.8 \cdot 10^9$ Hz
$k_B T/2\pi\hbar$	360K=$7.5 \cdot 10^{12}$ Hz	10^{-6} K=$2 \cdot 10^4$ Hz
n	10^{11}cm^{-3}	10^{13} cm^{-3}
a_s	5.8nm	4.9nm
$1/\tau_c$	$8.8 \cdot 10^4$ s^{-1}	$1.2 \cdot 10^4$s^{-1}
Γ_3	$3.4 \cdot 10^7$s^{-1}	$6.1 \cdot 10^7$s^{-1}
$\lambda^2 V/\hbar^2$	256 m^3/s^2	253 m^3/s^2
$E_{\text{recoil}}/2\pi\hbar$	$3.6 \cdot 10^4$Hz	$2 \cdot 10^4$ Hz
$\Gamma_d = \sqrt{E_{\text{recoil}}k_B T}/\hbar$	$5 \cdot 10^8$ Hz	$2 \cdot 10^4$Hz
$\sqrt{N}\lambda/\hbar$	$5.1 \cdot 10^9$ s^{-1}	$5.1 \cdot 10^{10}$s^{-1}

7.3 Mean field theory

There are two experiments which use an atomic gas to stop light. The group at the Rowland Institute [11] uses a cloud of ^{23}Na just above the BEC transition temperature. The group at Harvard [12] uses a hot (360K) cloud of ^{87}Rb. The former experiment is almost in the regime where all components of the experiment are coherent. The atoms are almost condensed, and all photon fields are generated by lasers. The system can therefore be adequately described by a zero-temperature mean field theory. Finite temperature effects are discussed in the following section.

First I restrict my attention to a single mode in each field, and ignore all incoherent processes such as spontaneous emission and atomic collisions (these can be put back

in phenomenologically). Second, as the experiments are performed in very dilute gases, I ignore the interactions between the atoms. Third, I ignore the dynamics of the β field – this is assumed to be controlled by the experimenter by turning a dial. With these assumptions, I write down the Heisenberg equations of motion for the field operators, treating the operators as c-numbers,

$$i\partial_t \psi_1 = E_1 \psi_1 + \lambda \alpha^* \psi_3 \tag{7.4a}$$

$$i\partial_t \psi_2 = E_2 \psi_2 + \lambda \beta^* \psi_3 \tag{7.4b}$$

$$i\partial_t \psi_3 = E_3 \psi_3 + \lambda \alpha \psi_1 + \lambda \beta \psi_2 \tag{7.4c}$$

$$i\partial_t \alpha = ck\alpha + \lambda \psi_1^* \psi_3. \tag{7.4d}$$

The recoil energies have been absorbed into E_ν. Two constants of motion are readily verified,

$$n = \sum_\nu |\psi_\nu|^2 \tag{7.5a}$$

$$n_* = |\alpha|^2 + |\psi_3|^2 + |\psi_2|^2, \tag{7.5b}$$

which are respectively the total density of atoms and the total density of "excitations."

I now look for equilibrium solutions to these equations. I take β to be on resonance, $\beta(t) = \beta e^{-i(E_3 - E_2)t}$, and rescale the frequencies of all the fields

$$\psi_i \rightarrow e^{-iE_i t} \psi_i \tag{7.6a}$$

$$\alpha \rightarrow e^{-i\omega_0 t}\alpha = e^{-i(E_3 - E_1)t}\alpha. \tag{7.6b}$$

The resonant frequency is $\omega_0 = E_3 - E_1$. After rescaling, the resulting equations are

$$i\partial_t \psi_1 = \lambda \alpha^* \psi_3 \tag{7.7a}$$

$$i\partial_t \psi_2 = \lambda \beta^* \psi_3 \tag{7.7b}$$

$$i\partial_t \psi_3 = \lambda \alpha \psi_1 + \lambda \beta \psi_2 \tag{7.7c}$$

$$i\partial_t \alpha = (ck - \omega_0)\alpha + \lambda \psi_1^* \psi_3. \tag{7.7d}$$

On resonance, $ck = \omega_0$; these equations are solved by $\alpha\psi_1 + \beta\psi_2 = 0 = \psi_3$, which can be conveniently written as $|\alpha|^2 = |\beta|^2 |\psi_2|^2 / |\psi_1|^2$. This state is known as a dark polariton, since it does not undergo spontaneous emission. Utilizing the conservation laws, one can relate $|\alpha|^2$ and $|\beta|^2$ in this dark state via the equation,

$$|\alpha|^2 = \frac{|\beta|^2 (n_* - |\alpha|^2)}{n - n_* + |\alpha|^2}, \tag{7.8}$$
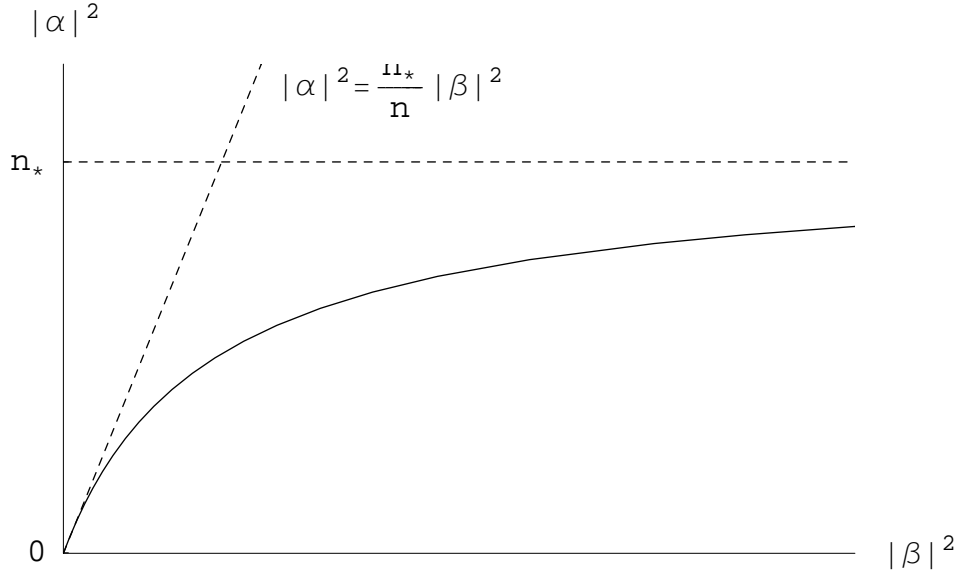
Figure 7.3: Relationship between probe and coupling beam intensity. The density of probe photons $|\alpha|^2$ vs. the density of coupling photons $|\beta|^2$, under the constraint that the total number of excitations is held constant. As $|\beta|^2 \to \infty$ the density of probe photons equals the total density of excitations n_*. If the coupling beam is adiabatically reduced, the probe photons are converted into polarons. When $|\beta|^2 \to 0$ no probe photons remain. Asymptotically, $|\alpha|^2 = (n_*/n)|\beta|^2$ as $|\beta|^2 \to 0$.

which is easily solved for $|\alpha|^2$,

$$|\alpha|^2 = \frac{1}{2}\sqrt{(n - n_* + |\beta|)^2 + 4|\beta|^2 n_*} - (n - n_* + |\beta|^2). \qquad (7.9)$$

In particular, $\beta \to \infty$, implies $|\alpha|^2 \to n_*$, and the excitation is a photon. When $\beta \to 0$, the magnitude $|\alpha|^2 \to 0$, and the excitation is a P_{12} polaron. At no point is state 3 ever occupied. By adiabatically changing β one can tune from the photon to the polaron. If $n_* \ll n$, one has a much more convenient expression

$$|\alpha|^2 = \frac{n_*|\beta|^2}{n + |\beta|^2}. \qquad (7.10)$$

The full expression (7.9) is plotted in Fig. 7.3.

Experimentally, light is stopped by adiabatically ramping the strength of the coupling laser. The experimentalist starts with a very strong β field. A laser of α photons is incident on the atomic cloud. While the light is inside the cloud, the β laser is slowly turned off, transforming the photons to polarons.

To understand the group velocity of the excitation one must look at the dispersion $\omega(k)$. Technically, this starts to become tricky, since one has to solve Eq. (7.7) for $ck \neq \omega_0$. To produce analytic results one has to expand in small parameters. For

example, the speed of light is calculated by expanding (7.7) in small $(ck - \omega_0)$. This procedure results in a velocity of $v = c/(1 + n\beta^2/(\alpha^2 + \beta^2)^2)$, which as $\alpha \to 0$ becomes $v = c/(1 + n/\beta^2)$.

A more straightforward approach is to expand in small α. Physically this expansion corresponds to assuming that the probe beam is weak (which is the experimentally relevant regime). To this end, I change from the particle operators ψ_i to the polarization operators $P_{ij} = \psi_i^\dagger \psi_j$,

$$
\begin{pmatrix}
i\partial_t - ck & -\lambda & & \\
-\lambda(n_1 - n_3) & i\partial_t - \omega_0 & -\lambda\beta & \\
& -\lambda\beta^* & i\partial_t - (E2 - E1) & \lambda\alpha \\
& & \lambda\alpha^* & i\partial_t - (E2 - E3)
\end{pmatrix}
\begin{pmatrix}
\alpha \\
P_{13} \\
P_{12} \\
P_{32}
\end{pmatrix}
=
\begin{pmatrix}
0 \\
0 \\
0 \\
\lambda\beta^*(n_3 - n_2)
\end{pmatrix},
\tag{7.11}
$$

where $n_i - \psi_i^\dagger \psi_i$. If one assumes α is small, one can ignore the coupling to P_{32}, finding a linear theory,

$$
\begin{pmatrix}
i\partial_t - ck & -\lambda & \\
-\lambda n & i\partial_t - \omega_0 & -\lambda\beta \\
& -\lambda\beta^* & i\partial_t - (E2 - E1)
\end{pmatrix}
\begin{pmatrix}
\alpha \\
P_{13} \\
P_{12}
\end{pmatrix}
=
\begin{pmatrix}
0 \\
0 \\
0
\end{pmatrix}.
\tag{7.12}
$$

I have approximated $n_1 - n_3$ by the total density of particles, n. One can phenomenologically introduce the spontaneous decay of state 3, by transforming $\omega_0 \to \omega_0 - i\Gamma$ in Eq. (7.12). Taking β to be on resonance, the eigenfrequencies solve

$$
(\omega - ck)[(\omega - \omega_0)^2 - \lambda^2\beta^2 - i\Gamma(\omega - \omega_0)] - \lambda^2 n(\omega - \omega_0) = 0.
\tag{7.13}
$$

The general solution to this cubic is not particularly enlightening. One can write this equation in a way which is conducive to solving iteratively for ω near ck,

$$
\omega - ck = \lambda^2 n \frac{\omega - \omega_0}{(\omega - \omega_0)^2 - \lambda^2\beta^2 - i\Gamma(\omega - \omega_0)}.
\tag{7.14}
$$

In particular, to first order one finds $v = c(1 - n/\beta^2)$. In Fig. 7.4, I plot the roots of Eq. (7.13) as a function of k.

On resonance, (i.e. when $\omega_0 = ck$) the eigenfrequencies are

$$
\omega = 0 \tag{7.15}
$$

$$
\omega = \mp\lambda\sqrt{n + \beta^2}. \tag{7.16}
$$
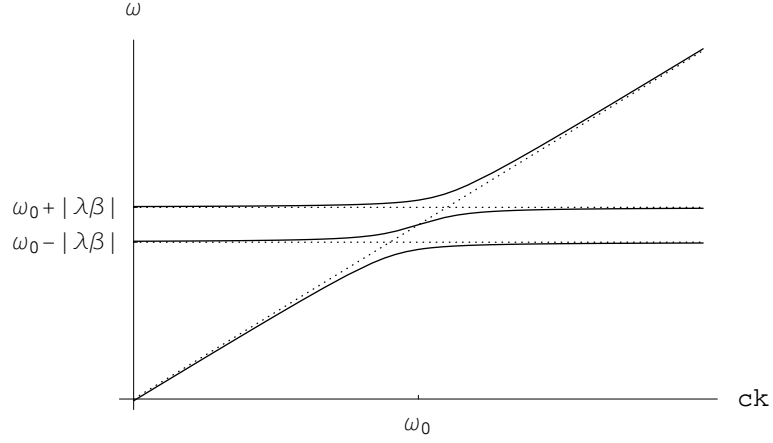
Figure 7.4: Resonant frequencies of the mean-field equations. The dashed line shows the frequencies when the coupling between the photons and the polarons are turned off.

On dimensional grounds, the adabaticity condition is that the rate of change of the laser intensity is much less than the minimum energy spacing between the modes, i.e.

$$\frac{\partial_t \beta}{\beta} \ll \frac{\lambda \sqrt{N}}{\hbar}. \tag{7.17}$$

For alkali atoms, this ratio is of order $10^8 - 10^{10} Hz$.

Transparency

An important point here is that even in the presence of spontaneous emission from state 3, the frequencies (7.15) and (7.16) are real, implying that there is no absorption. In contrast, in the absence of the coupling beam, the α photons would be quickly absorbed by the gas. This absorption results from generation of P_{13} excitations, which have a very short lifetime.
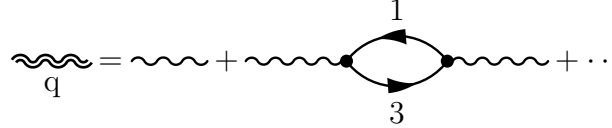
7.4 Equilibrium Green's functions

I now go beyond the mean field treatment by including various incoherent processes. I use the standard finite temperature equilibrium Green's functions as discussed in Appendix C. The formalism can be conveniently built up starting from the equations of motions for the field operators shown in Eq. (7.11). (This equation was presented as a mean-field equation, but as long as one keeps the operators normal ordered it is also true for the fields themselves.) I will however take a more intuitive, but equivalent, approach of diagrammatically building up the self-energies for the photon

and polaron Green's functions.

7.4.1 Two level atoms

A useful exercise to get used to this approach is to first consider a gas of two-level atoms interacting with light. This is equivalent to setting $\beta = 0$ and looking at the Green's function for α. The photon couples to the polarization by exciting atoms from state 1 to state 3,

$$\widetilde{}_{q} = \widetilde{} + \widetilde{}\!\!\bigcirc^{1}_{3}\!\!\widetilde{} + \cdots \tag{7.18}$$

In this case the self-energy is

$$\Sigma_\alpha(k,\omega) \;=\; \lambda^2 \Pi_{13}^{(0)}(k,\omega) = \overset{1}{\underset{3}{\bigcirc}} \tag{7.19}$$

$$= \frac{\lambda^2}{2\pi} \int \frac{dz}{\omega - z} \int \frac{d^3q}{(2\pi)^3} \int \frac{d\nu}{2\pi} \tag{7.20}$$

$$\left[G_3^>(k-q, z-\nu) G_1^<(q,\nu) - G_3^<(k-q, z-\nu) G_1^>(q,\nu) \right].$$

There is a gap of order $10000K$ between the 1-states and the 3-states, so in equilibrium there should be no occupation of the 3-states. Therefore the Green's functions have the simple form, $G_3^< = 0$ and $G_3^> = A_3 = 2\mathrm{Im}G_3$, where A_3 is the spectral density (see Appendix C.4). In the absence of any α photons, G_1 will be the free Green's function,

$$G_1(k) = \frac{1}{\omega - E_1 - k^2/2m}. \tag{7.21}$$

One is then lead to the simple result

$$\Sigma_\alpha(k,\omega) = \lambda^2 \int \frac{d^3q}{(2\pi)^3} f(\epsilon_q) G_3(k-q, \omega + E_1 + q^2/2m), \tag{7.22}$$

where $f(\epsilon_q)$ is the equilibrium occupation of a mode with energy ϵ_q. Taking into account spontaneous emission processes, one can approximate the propegator G_3 as

$$G_3(k,\omega) = \frac{1}{\omega - (E_2 + k^2/2m - i\Gamma_3/2)}, \tag{7.23}$$

which yields a self-energy,

$$\Sigma_\alpha(k,\omega) = \lambda^2 \int \frac{d^3q}{(2\pi)^3} \frac{f(\epsilon_q)}{\omega - \omega_0 + k \cdot q/m + i\Gamma/2}. \tag{7.24}$$

120

The resonant frequency is $\omega_0 = E_3 - E_1 + E_{\text{recoil}}$, where $E_{\text{recoil}} = k^2/2m$.

There are two cases in which the integral is trivial to perform. First, at zero temperature only the mode $q = 0$ is occupied, and

$$\Sigma_\alpha(k, \omega) = \frac{\lambda^2 n}{\omega - \omega_0 + i\Gamma/2}, \tag{7.25}$$

where n is the atomic density. The other simple case is when thermal broadening dominates over the natural width Γ. Thermal broadening only dominates at quite high temperatures, in which case one can take f to be a Boltzmann distribution, and neglect Γ in Eq. (7.24). Using the identity $(x - a)^{-1} = P(x - a)^{-1} \pm i\pi\delta(x - a)$, one can read off the imaginary part of Σ,

$$\text{Im}\Sigma_\alpha(k, \omega) = -\frac{\lambda^2 n}{2}\left(\frac{m}{2\pi k^2 T}\right)^{1/2} \exp\left(-\frac{m}{2k^2 T}(\omega - \omega_0)^2\right). \tag{7.26}$$

The resonance clearly has a width $\Gamma_d = \sqrt{4k_B T \epsilon_k}$. The crossover between the zero temperature behavior and the high temperature behavior occurs when $\Gamma_d = \Gamma$, which is equivalent to $k_B T = \Gamma^2/E_{\text{recoil}}$.

For a Gaussian distribution one can perform the integral for all temperatures without taking $\Gamma \to 0$. The resulting line shape extrapolates between a Lorentzian and a Gaussian (these two shapes are compared in Fig. 7.5). The basic trick involves first integrating out the momenta perpendicular to k, the resulting one-dimensional integral is of the form

$$I(x) = \frac{1}{\sqrt{\pi}}\int dt \frac{e^{-t^2}}{t - x}. \tag{7.27}$$

Not surprisingly, this same integral plays an important role in the random phase approximation to the density excitations of a gas of atoms discussed in Appendix E. To evaluate the integral, one expresses $(t - x)^{-1}$ as a Fourier integral

$$\begin{aligned} I(x) &= \frac{i}{\pi}\int_0^\infty ds \int_{-\infty}^\infty dt \exp\left(-t^2 - is(t - x)\right) \tag{7.28} \\ &= ie^{-x^2}(1 + \text{erf} ix), \tag{7.29} \end{aligned}$$

where $\text{erf}(x)$ is the error function. The end result is

$$\Sigma_\alpha(k, \omega) = \frac{\lambda^2 n}{2}\left(\frac{2}{\pi\Gamma_d^2}\right)^{1/2} \exp\left(-\frac{(\omega - \omega_0 - i\Gamma/2)^2}{\Gamma_d^2}\right)\left[i\text{erf}(i(\omega - \omega_0 - i\Gamma/2)/\Gamma_d) - i\right]. \tag{7.30}$$

For further discussion of polaritons in gases of two level atoms, see [126].
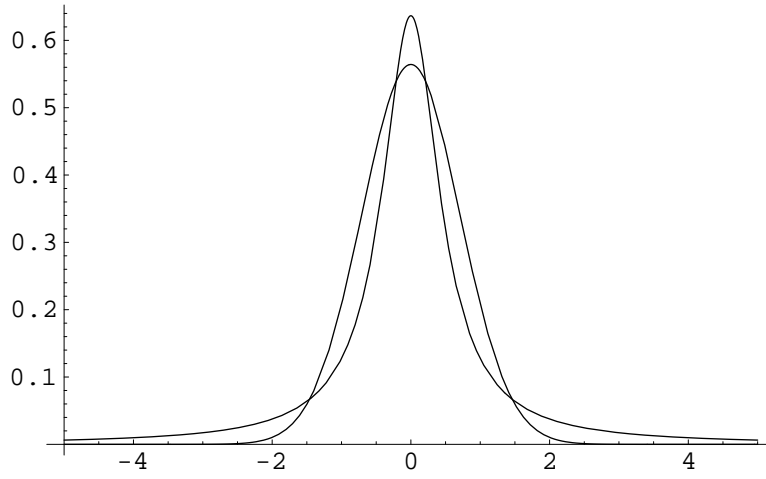
Figure 7.5: Comparison of a Lorentzian and a Gaussian

7.4.2 Three level atoms

With the simple polariton problem under our belts, it is quite straightforward to understand electromagnetically induced transparency. Adding the β photons mixes G_3 and G_2,

$$G_3(k,\omega) \quad = \quad \text{(diagram)} = \text{(diagram)} + \text{(diagram)} + \cdots \tag{7.31}$$

$$= \quad \frac{1}{\omega - (\epsilon_k + E_3 - i\Gamma/2) - \dfrac{\lambda^2|\beta|^2}{\omega - (\epsilon_{k-q_c} + E_2 + cq_c)}}, \tag{7.32}$$

where q_c is the momentum of the coupling laser. The self-energy of the α photons is found by substituting (7.32) into (7.22). Thus one needs to evaluate $G_3(k - q, \omega + \epsilon_q + E_1)$ where k is the momentum of the α photon, and q is a momentum which is integrated over. In the experiments, Doppler broadening is minimized by taking the probe beam of α photons to be colinear with the control beam of β photons. In this case $\mathbf{k}$ and $\mathbf{q_c}$ point in the same direction. For all practical purposes, these momenta are equal, $|k| = |q_c|$, and G_3 is

$$G_3(k - q, \omega + \epsilon_q + E_1) = \frac{\omega - \omega_1}{(\omega - \omega_1)(\omega - \omega_0 + k \cdot q/m + i\Gamma/2) - \lambda^2|\beta|^2}, \tag{7.33}$$

where $\omega_1 = (E_2 - E_1) + cq_c$. I will consider only the resonant case, $\omega_1 = \omega_0$. Even with k parallel to q_c, The expression (7.33) has some q dependence, which leads to Doppler broadening. Physically, this broadening arises from the coupling to state 3.

The integral in Eq. (7.22) again has two simple limits. At low temperature

$(T \ll \Gamma^2/E_{\text{recoil}})$,

$$\Sigma_\alpha(q,\omega) = \frac{\lambda^2 n(\omega - \omega_0)}{(\omega - \omega_0)^2 - \lambda^2\beta^2 + (\omega - \omega_0)i\Gamma/2}, \tag{7.34}$$

while at high temperature

$$\text{Im}\Sigma_\alpha(k,\omega) = -\lambda^2 n\frac{m\Lambda_T}{2k}\exp\left(-\frac{m}{2k^2T}\frac{[(\omega - \omega_0)^2 - \lambda^2\beta^2]^2}{(\omega - \omega_0)^2}\right). \tag{7.35}$$

For arbitrary temperatures (treating f using Boltzmann statistics),

$$\Sigma_\alpha(k,\omega) = -\lambda^2 n\left(\frac{m\Lambda_T}{2k}\right)\exp(-x^2)(i\text{erf}(ix) - i) \tag{7.36}$$

$$x = \left(\frac{\beta m}{2k^2}\right)^{1/2}\frac{(\omega - \omega_0)^2 - \lambda^2\beta^2 - i\Gamma(\omega - \omega_0)/2}{\omega - \omega_0}. \tag{7.37}$$

The statement of transparency is that $\text{Im}(\Sigma_\alpha) = 0$, which is true when $ck = \omega_0$.

I focus on zero temperature for a moment, where the photon propegator is

$$G_\alpha = \frac{(\omega - \omega_0)^2 - \lambda^2\beta^2 - i\Gamma(\omega - \omega_0)/2}{(\omega - ck)[(\omega - \omega_0)^2 - \lambda^2\beta^2 - i\Gamma(\omega - \omega_0)/2] - \lambda^2 n(\omega - \omega_0)}, \tag{7.38}$$

The denominator is familiar from the mean field theory in Section 7.3. The residues at each of the poles tell how much of the excitation is a photon. The residue at $\omega = ck = \omega_0$ is

$$R = \beta^2/(n + \beta^2). \tag{7.39}$$

In the language of Section 7.3 this residue is the ratio $|\alpha|^2/n_*$ discussed in Eq. (7.10). At finite temperature, the residue is

$$R = \lim_{\omega \to \omega_0}\left(1 - \Sigma/(\omega - \omega_0)\right)^{-1}, \tag{7.40}$$

where Σ is given in Eq. (7.36). As $z \to \infty$, the error function asymptotically behaves as

$$\text{erf}(iz) \sim \exp(z^2)/\sqrt{\pi}z, \tag{7.41}$$

which yields the same residue. One could have guessed that the residue is temperature independent. The only way that temperature could affect this state is through the Doppler shift of the atomic transitions. These shifts exactly cancel on resonance, resulting in a temperature independent residue.

7.5 Non-equilibrium Green's functions

For completeness, here I make a few notes about going beyond the equilibrium theory discussed in Section 7.4. This non-equilibrium theory is a topic I would like to address in the future.

The full kinetic theory can be discussed in terms of the matrix Green's function,

$$G = \frac{1}{i} \begin{pmatrix} \lambda \alpha^\dagger \alpha & \lambda P_{13}^\dagger \alpha & \lambda P_{12}^\dagger \alpha \\ \lambda \alpha^\dagger P_{13} & \lambda P_{13}^\dagger P_{13} & \lambda P_{12}^\dagger P_{13} \\ \lambda \alpha^\dagger P_{12} & \lambda P_{13}^\dagger P_{12} & \lambda P_{12}^\dagger P_{12} \end{pmatrix}. \tag{7.42}$$

The equations of motion for the Green's function is formally written as $G^{-1}G = 1$. At zero temperature, where ψ_1 is a c-number,

$$G^{-1} = \begin{pmatrix} i\partial_t - ck & -\lambda & 0 \\ -\lambda & (i\partial_t - \omega_0 + i\Gamma/2)/n & -\lambda\beta/n \\ 0 & -\lambda\beta^*/n & (i\partial_t - \omega_0)/n \end{pmatrix} \tag{7.43}$$

I have explicitly taken β to be on resonance, and have neglected the dispersion of the polarons. This expression is nothing but the equations of motion in Eq. (7.12). For time independent β, these equations are easily integrated to reproduce the results of the equilibrium theory. To describe a non-equilibrium theory, one can perform the Wigner transform outlined in Chapter 6. In general, the resulting equations need to be solved numerically, and its analysis is a topic of further research.

Chapter 8

Summary

Experiments on cold atomic clouds have demonstrated a diverse and extremely interesting set of phenomena. In this thesis I provided a theoretical description of a subset of these phenomena. I derived the effect of interactions on the phase transition temperature of a Bose gas. I calculated the lifetime of persistent currents in toroidal traps. I produced a phase diagram which describes the stability of a cloud of bosons with attractive interactions. I presented a kinetic theory for describing finite temperature clouds of degenerate particles. I explored the interaction of light with atomic clouds, providing a theoretical basis for experiments in which light is brought to a halt.

Appendix A

Mathematical Functions

A.1 The polylogarithm functions

This appendix is intended as a reference for the properties of the polylogarithm functions. Further details can be found in [127, 128, 129, 130].

The polylogarithm functions are defined by the series

$$g_\nu(z) = \sum_{j=1}^{\infty} \frac{z^j}{j^\nu}. \tag{A.1}$$

Analytically, they possess a singularity at $z = 1$, typically a logarithmic branch point. For $\nu > 1$ the limit $z \to 1$ of $g_\nu(z)$ is well defined and is equal to $\zeta(\nu)$.

The polylogarithm functions obey the relationship

$$z\frac{d}{dz}g_\nu(z) = \frac{d}{d\log z}g_\nu(z) = g_{\nu-1}(z). \tag{A.2}$$

This relationship, plus the closed form

$$g_o(z) = \frac{z}{1-z}, \tag{A.3}$$

allows one to calculate many of the properties of the polylogarithm functions for integral ν. In particular one can use this relationship to calculate an asymptotic expansion of $g_\nu(e^{-x})$ for small x. For this expansion I introduce the Bernoulli numbers B_n, defined by the generating function

$$\sum_n \frac{B_n x^n}{n!} = \frac{x}{e^x - 1} = x\, g_o(e^{-x}). \tag{A.4}$$

These numbers are tabulated in table A.1, and can be related to the Riemann zeta function via

$$B_n = (-1)^n n\, \zeta(1-n) \qquad n = 1, 2, \ldots \tag{A.5}$$

Integrating (A.4) one finds

$$g_\nu(e^{-x}) = \frac{(-x)^{\nu-1}}{(\nu-1)!}\left[-\log x + \sum_{m=1}^{\nu-1}\frac{1}{m}\right] + \sum_{\substack{k=0 \\ k\neq\nu-1}}^{\infty}\zeta(\nu-k)\frac{(-x)^k}{k!}. \qquad \nu = 1,2,3,\dots$$
(A.6)

The equivalent expression for non-integral ν is

$$g_\nu(e^{-x}) = \Gamma(1-\nu)x^{\nu-1} + \sum_{k=0}^{\infty}\zeta(\nu-k)\frac{(-x)^k}{k!}, \qquad \nu \neq 1,2,3,\dots \qquad \text{(A.7)}$$

One derives this latter expression by taking the Mellin-Barnes transform of $g_\nu(e^{-x})$ [131]. A form of Laplace transform, the Mellin transform of a function $f(x)$ is a function $F(s)$, related to the original by

$$F(s) = \int dx\, x^{s-1} f(x) \qquad \text{(A.8a)}$$

$$f(x) = \frac{1}{2\pi i}\int_{c-i\infty}^{c+i\infty} ds\, x^{s-1} F(s), \qquad \text{(A.8b)}$$

where the contour in the inverse transform must be taken to the right of all the singularities of $F(s)$. In practice the latter integral is performed via the residue theorem.

The Mellin transform of g_ν is

$$G_\nu(s) = \int_0^\infty g_\nu(e^{-x})x^{s-1}dx = \zeta(\nu+s)\Gamma(s). \qquad \text{(A.9)}$$

$G_\nu(s)$ is well defined for large enough s. One inverts the transform via a contour integral

$$g_\nu(e^{-x}) = \frac{1}{2\pi i}\int_{c-i\infty}^{c+i\infty} G_\nu(s)x^{-s}ds, \qquad \text{(A.10)}$$

where the contour is to the right of all singularities of $G_\nu(s)$. This integral is then evaluated using the residue theorem along with the following facts. 1) The function

Table A.1: Bernoulli numbers B_n, as defined by the generating function $\dfrac{t}{e^t - 1} = \sum_n B_n\dfrac{t^n}{n!}$.

B_0	B_1	B_2	B_3	B_4	B_5	B_6	B_7	B_8
1	$-\frac{1}{2}$	$\frac{1}{6}$	0	$-\frac{1}{30}$	0	$\frac{1}{42}$	0	$-\frac{1}{30}$

127

$\zeta(s)$ is regular, except at $s = 1$ where it has a pole with residue 1. 2) The function $\Gamma(s)$ is regular except when s is a non-positive integer. The residue of $\Gamma(s)$ at $s = -n$ is $(-1)^n/n!$. Summing over the residues gives equation (A.7).

Appendix B

The $\mu \to 0$ asymptotics of $\mathcal{F}$ for a noninteracting Bose gas.

Here I calculate the $\mu \to 0$ behavior of the grand canonical free energy of a non-interacting Bose gas. This result is used extensively in Chapter 2.

B.0.1 Mathematical structure of the expansion

I begin by developing some mathematical machinery. As in Section 2.1, I consider a generic system of non-interacting bosons with energy levels ε_i. Measuring the chemical potential μ from the ground state energy ε_o, The grand free energy is (cf. Eq. (2.6))

$$\mathcal{F} = -T \sum_j \sum_n \frac{e^{-\beta j(\varepsilon_n - \varepsilon_o - \mu)}}{j} \tag{B.1a}$$

$$= -T \sum_n g_1(e^{-\beta(\varepsilon_n - \varepsilon_o - \mu)}) \tag{B.1b}$$

$$= -T g_1(e^{\beta \mu}) + \mathcal{F}_{ex}, \tag{B.1c}$$

where $g_1(z) = -\log(1 - z)$. The contribution of the excited particles, $\mathcal{F}_{ex}$ is regular at $\mu = 0$, so this function can be expanded in a series in $\beta \mu$. Using the properties of the polylogarithm functions (see Appendix A.1),

$$\mathcal{F}_{ex} = -T \sum_n{}' \sum_{k=0}^{\infty} \frac{(\beta \mu)^k}{k!} g_{1-k}(e^{-\beta(\varepsilon_n - \varepsilon_o)}). \tag{B.2}$$

The prime indicates that the ground state is omitted from the sum. Equation (B.2) is the starting point for this analysis. The radius of convergence of (B.2) is limited

by the pole at $\mu = \varepsilon_1 - \varepsilon_o$. The coefficients of $\beta\mu$ in Eq. (B.2),

$$f_k = \sum_n{}' g_{1-k}(e^{-\beta(\varepsilon_n - \varepsilon_o)}), \tag{B.3}$$

are thermodynamic derivatives of the free energy with respect to the chemical potential, evaluated at $\mu = 0$. Hence they give the moments (in fact the cumulants) of the number of excited particles at temperatures below T_c. In particular:

$$< N_{ex} > = f_1 \tag{B.4a}$$

$$< \delta N_{ex}^2 > = \langle N_{ex}^2 \rangle - \langle N_{ex} \rangle^2 = f_2. \tag{B.4b}$$

I proceed by expanding f_k in powers of the inverse temperature β. The structure of the expansion is understood by writing

$$f_k = \int dE\, \rho_{ex}(E)\, g_{1-k}(e^{\beta E}) \tag{B.5a}$$

$$\approx \int dE\, \frac{\rho_{ex}(E)}{(\beta E)^k} + \mathcal{O}(\beta^{k-1}). \tag{B.5b}$$

where $\rho_{ex}(E)$ is the density of excited states. For low enough energies the density of states has the form $\rho(E) \sim E^\alpha / \gamma^{\alpha+1}$, where γ has the dimension of energy. If $k < \alpha + 1$ the integral converges and $f_k \sim (k_B T/\gamma)^{\alpha+1}$. Otherwise, the sum is infrared divergent, and will be dominated by the first term. On dimensional grounds the lowest energy state has energy $\varepsilon_1 \sim \gamma$, so in this latter case $f_k \sim (k_B T/\gamma)^k$.

To make these results more concrete, briefly consider point particles in a three dimensional box, where $\alpha = 1/2$ and $\gamma \sim \hbar^2/mL^2$. According to this argument, the number of excited particles is extensive, $N_{ex} = f_1 \sim L^3$, while the fluctuations are anomalously large $\langle \delta N_{ex}^2 \rangle = f_2 \sim L^4$. These large fluctuations in the number of non-condensed particles are related to the large fluctuations in the number of condensed particles (2.25).

B.0.2 The Mellin-Barnes Transform

To go beyond these order-of-magnitude estimates of f_k, one performs a Mellin-Barnes transform defined in equation (A.9). This transform allows one to express f_k as a sum of power-laws.

To produce an expansion of f_k in powers of β, one should take the Mellin transform of (B.3) with respect to β. This approach is inconvenient, since β is a dimensional quantity. Instead I introduce a dummy variable x multiplying β, then in the end one

can set $x = 1$. Thus I define

$$F_k(s) = \int dx\, x^{s-1} \sum_n{}' g_{1-k}\left(e^{-x\beta(\varepsilon_n - \varepsilon_o)}\right) \tag{B.6a}$$

$$= \sum_n{}' \sum_j \frac{1}{j^{1-k}} \int dx\, x^{s-1} e^{-x\beta j(\varepsilon_n - \varepsilon_o)} \tag{B.6b}$$

$$= \zeta(s+1-k)\Gamma(s)\sum_n{}' \left(\frac{1}{\beta(\varepsilon_n - \varepsilon_o)}\right)^s. \tag{B.6c}$$

The rightmost pole of $F_k(s)$ gives the leading order behavior of f_k as $\beta \to 0$. The zeta-function has a pole at pole at $s = k$ with residue 1. the Gamma function has poles at $s = -m$ (m=0,1,2,...) with residue $(-1)^m/m!$. The remainder, designated the spectral zeta function

$$Z(s) = \sum_n{}' \left(\frac{1}{\beta(\varepsilon_n - \varepsilon_o)}\right)^s, \tag{B.7}$$

contains all the information about the details of the system.

We now have a simple algorithm for finding the expansion of $\mathcal{F}$. First one finds the poles of Z(s), giving all of the singularities of $F_k(s)$. Assuming one only have to deal with isolated singularities (as is the case), it is a simple matter to directly write down f_k, since f_k is identically equal to the sum of the residues of $F_k(s)$,

$$f_k = \sum_{\text{poles } s_i} Res\{F_k(s), s_i\}. \tag{B.8}$$

In the following two Sections I specialize first to particles in a d-dimensional box, then to particles in a harmonic well.

B.0.3 Particles in a Box

The spectral zeta function for particles in a box, with dispersion

$$\varepsilon = (\hbar^2/2m\ell^2)(n_x^2 + n_y^2 + \cdots), \tag{B.9}$$

is discussed by Ziff et al. [127]. Following those authors, I introduce sums $C_d(s)$ given by

$$C_d(s) = \frac{\Gamma(s)}{\pi^s} \sum_{n_x, n_y, \ldots}{}' \frac{1}{(n_x^2 + n_y^2 + \cdots)^s}, \tag{B.10}$$

in terms of which the spectral zeta function is

$$\Gamma(s)Z(s) = \left(\frac{L}{\lambda}\right)^{2s} C_d(s). \tag{B.11}$$

131

Some sample values of the sums $C_d(s)$ are given in Table B.1. The function $C_d(s)$ is regular except for poles at $s = d/2$ and $s = 0$, where the residues are respectively 1 and -1. These singularities can be removed to produce an analytic function

$$\tilde{C}_d(s) = C_d(s) + \frac{1}{s} - \frac{1}{s - d/2} - \frac{1}{d/2}. \tag{B.12}$$

It will only be necessary to evaluate this function at $s = 0$ or $s = d/2$, where it is equal to the regular part of $C_d(s)$. The function $\tilde{C}_d(s)$ is tabulated in Table B.2.

Putting together the poles from $Z(s)$ and from the zeta function in (B.6c), one finds that for $k \neq 0, d/2$,

$$f_k = \left(\frac{\ell}{\Lambda}\right)^d \zeta(1 - d/2 - k) + \left(\frac{\ell}{\Lambda}\right)^{2k} C_d(k) - \zeta(1 - k), \tag{B.13a}$$

while for even d,

$$f_{d/2} = \left(\frac{\ell}{\Lambda}\right)^d \left(2\log\frac{\ell}{\Lambda} + \gamma + \tilde{C}_d(d/2)\right), \tag{B.13b}$$

and for $k = 0$,

$$f_0 = -2\log\frac{\ell}{\Lambda} - \gamma + \tilde{C}_d(0). \tag{B.13c}$$

In the latter two equations $\gamma \approx 0.577216$ is Euler's gamma, which appears here because $\zeta(s) = \frac{1}{s-1} + \gamma + \mathcal{O}(s - 1)$.

B.0.4 Harmonic Well

The harmonic well, with $\varepsilon = \hbar\Omega(n_1 + \cdots + n_d + d/2)$ is slightly easier to analyze than the uniform gas since the energy levels are evenly spaced. The spectral zeta function for a harmonically trapped gas is

$$Z(s) = (\beta\hbar\omega)^{-s} \sum_{n_x, n_y, \dots} \left(\frac{1}{n_x + n_y + \cdots}\right)^s, \tag{B.14a}$$

$$= (\beta\hbar\omega)^{-s} Q_d(s), \tag{B.14b}$$

where the sum is taken over all non-negative n, where not all of the n's are zero. The sum $Q_d(s)$ can be written as

$$Q_d(s) = \sum_n \frac{g_n^{(d)}}{n^s}, \tag{B.15}$$

Table B.1: Values for the lattice sum $C_d(s) = \dfrac{\Gamma(s)}{\pi^s} \displaystyle\sum_{n_x,n_y,\ldots}' \dfrac{1}{(n_x^2 + n_y^2 + \cdots)^s}$

	d=1	d=2	d=3
s=1	1.047197	∞	-2.8374
2	0.219324	0.610644	1.6752
3	0.131243	0.300514	0.5419
4	0.123694	0.263718	0.4278
5	0.157008	0.324039	0.5039
6	0.249700	0.507268	0.7741

Table B.2: Values for the lattice sum $\tilde{C}_d(s) = C_d(s) + \dfrac{1}{s} - \dfrac{1}{s - d/2} - \dfrac{2}{d}$.

	d=1	d=2	d=3
s=0	-1.95381	-0.89912	-0.4996
s=d/2	-1.95381	-0.89912	-0.4996

where $g_n^{(d)}$ is the number of ways of adding d non-negative numbers together to form the number n. Calculating $g_n^{(d)}$ is a famous boson counting problem,[1] and $g_n^{(d)}$ can be written in terms of a binomial coefficient,

$$g_n^{(d)} = \binom{n+d-1}{d-1}. \tag{B.16}$$

The binomial coefficients $\binom{n}{m}$, read "n choose m," give the number of ways of taking m objects out of a set of n, disregarding order. I now expand this in powers of n as

$$g_n^{(d)} = \frac{1}{\Gamma(d)} \sum_k \left[\begin{matrix} d \\ k \end{matrix} \right] n^{k-1}. \tag{B.17}$$

The Stirling numbers of the second kind $\left[\begin{smallmatrix} n \\ m \end{smallmatrix} \right]$, read "$n$ cycle m", give the number of ways of making m cycles of n objects. Table B.3 lists some of Stirling numbers. Note that $\left[\begin{smallmatrix} n \\ n \end{smallmatrix} \right] = 1$.

$Q_d(s)$ can now be written as

$$
\begin{aligned}
Q_d(s) &= \sum_{n=1}^{\infty} g_n^{(d)} \frac{1}{n^s} &\text{(B.18a)} \\
&= \sum_j \frac{1}{\Gamma(d)} \left[\begin{matrix} d \\ d-j \end{matrix} \right] \zeta(s+1-d+j), &\text{(B.18b)}
\end{aligned}
$$

with poles at $s = d, d-1, \ldots, 1$. I tabulate $Q_d(s)$ in Table B.4. Since there are so many poles, the full expression for f_k is rather daunting. The leading order behavior is

$$
f_k = \begin{cases}
(\beta\hbar\omega)^{-d} \zeta(d+1-k), & k < d \\
(\beta\hbar\omega)^{-d} \left(\sum_{l \neq 0} \left[\begin{smallmatrix} d \\ d-l \end{smallmatrix} \right] \zeta(1+l) + \Gamma(d) \left(-\log(\beta\hbar\omega) - \gamma + H_{d-1} \right) \right), & k = d \\
(\beta\hbar\omega)^{-k} \Gamma(k) Q_d(k), & k > d,
\end{cases} \tag{B.19}
$$

where $H_n = \sum_{m=1}^{n} \frac{1}{m}$ is the partial sum of reciprocals. Including higher order terms

---

[1] The standard counting argument goes as follows. The number of ways of writing n as a sum of d non-negative numbers is the same as the number of ways of writing $n + d$ as a sum on d positive numbers. The latter is calculated by writing down n tick marks, and asking how many ways are there to put $d - 1$ barriers in the $n + d - 1$ spaces between the tick marks. This gives

$$g_n^{(d)} = \binom{n+d-1}{d-1}.$$

Table B.3: Stirling numbers of the second kind $\left[{n \atop m}\right]$

	m=0	1	2	3	4	5
n=0	1					
1	0	1				
2	0	1	1			
3	0	2	3	1		
4	0	6	11	6	1	
5	0	24	50	35	10	1
6	0	120	274	225	85	15

Table B.4: Values for the lattice sum $Q_d(s) = \sum\limits_{n_x, n_y, \ldots} \left(\dfrac{1}{n_x + n_y + \cdots} \right)^s$.

	d=1	d=2	d=3	d=4	d=5
s=1	∞	∞	∞	∞	∞
2	1.64493	∞	∞	∞	∞
3	1.20206	2.84699	∞	∞	∞
4	1.08232	2.28438	3.70788	∞	∞
5	1.03693	2.11925	3.26144	4.4974	∞
6	1.01734	2.05427	3.1139	4.20104	5.32539

gives

$$f_k = \sum_{\substack{j=0 \\ j \neq d-k}}^{d-1} (\beta\hbar\omega)^{j-d} \frac{\Gamma(d-j)}{\Gamma(d)} \begin{bmatrix} d \\ d-j \end{bmatrix} \zeta(d+1-k-j) \tag{B.20}$$

$$+ (\beta\hbar\omega)^{-k}\Upsilon_k + \sum_n (\beta\hbar\omega)^n \zeta(-n-k+1) \frac{(-1)^n}{n!} Q_d(-n).$$

Where the contribution Υ_k is given by

$$\Upsilon_k = \begin{cases} Q'_d(0) - Q_d(0) \log \beta\hbar\omega \,, & k = 0 \\[2mm] (\Gamma(k)/\Gamma(d)) \sum_{l \neq d-k} \begin{bmatrix} d \\ d-l \end{bmatrix} \zeta(k+1-d+l) & \\ \quad + \Gamma(k)\left(-\log(\beta\hbar\omega) - \gamma + H_{k-1}\right) & 0 < k \leq d \\[2mm] \Gamma(k)Q_d(k) \,, & k > d \end{cases} \tag{B.21}$$

I tabulate $Q'_d(0)$, the derivative of $Q_d(s)$, in Table B.5.

Table B.5: Derivative of (the analytic continuation of) the lattice sum $Q'_d(0)$.

$Q'_1(0)$	$Q'_2(0)$	$Q'_3(0)$	$Q'_4(0)$	$Q'_5(0)$
-0.918939	-1.08436	-1.18229	-1.25176	-1.3054

Appendix C

Review of response functions

C.1   Introduction

Green's functions, and more general response functions, play an important role in this thesis. In this Appendix I review the concepts and techniques which are used in the rest of the thesis. In general my notation follows Kadanoff and Baym [113].

C.2   Linear response theory

Linear response theory is the general study of the response of a system to a weak probe. Because the probe is weak, it does not perturb the system. As a concrete example, let us consider the response of a resistor to an applied current. The response is quantified by measuring the voltage across the resistor. For weak enough currents, the voltage is proportional to the current. The impedance, $Z = \partial V / \partial I$, is the coefficient of proportionality.

The general framework in which one introduces linear response theory is to write the perturbation in the form

$$H_{\text{pert}}(t) = \alpha(t) A, \tag{C.1}$$

where A is the operator that the perturbation couples to (in our example A would be the voltage across the sample, since the energy is IV), and $\alpha(t)$ is a c-number describing the time dependence of the perturbation. One then looks at the time dependence of some other operator, B, which within the interaction picture is

$$B(t) = \langle T \left(e^{i \int_{-\infty}^{t} d\tau \, V(\tau)} \right) B \, T \left(e^{-i \int_{-\infty}^{t} d\tau \, V(\tau)} \right) \rangle. \tag{C.2}$$

In the interaction picture, the perturbation $H_{\text{pert}}(t)$ appears in the form

$$V(t) = e^{iH_0(t)} H_{\text{pert}}(t) e^{-iH_0(t)}. \tag{C.3}$$

To find the linear response, one expands the exponentials to first order in α,

$$\delta B(t) \;=\; \int_{-\infty}^{t} d\tau\, \alpha(\tau)\frac{1}{i}\langle[B(t), A(\tau)]\rangle, \tag{C.4}$$

$$\;=\; \int_{-\infty}^{\infty} d\tau\, \alpha(\tau)\chi_{BA}^{r}(t-\tau), \tag{C.5}$$

which defines the retarded response function

$$\chi_{BA}^{r}(t) = \theta(t)\frac{1}{i}\langle[B(t), A(0)]\rangle. \tag{C.6}$$

In the frequency domain, the response is particularly simple

$$\delta B(\omega) = \alpha(\omega)\chi_{BA}^{r}(\omega). \tag{C.7}$$

Thus our whole task is to calculate $\chi_{BA}^{r}(\omega)$.

The easiest route to calculating χ_{BA}^{r} leads one through the complex frequency plane. This detour is not surprising, since one often uses complex analysis to calculate Fourier transforms. One needs two expressions to continue. First, one needs the well known convolution identity

$$\int dt\, e^{i\omega t} f(t)g(t) \;=\; \int dt\, e^{i\omega t} \int \frac{d\nu}{2\pi} e^{-i\nu t} \int \frac{d\nu'}{2\pi} e^{-i\nu' t} f(\nu)g(\nu') \tag{C.8}$$

$$\;=\; \int \frac{d\nu}{2\pi} f(\nu)g(\omega - \nu). \tag{C.9}$$

The second expression one needs is the Fourier transform of a theta function

$$\int dt\, e^{i\omega t}\theta(t)e^{-\eta t} \;=\; \frac{-1}{i\omega - \eta} = \frac{i}{\omega + i\eta} \tag{C.10}$$

$$\int dt\, e^{i\omega t}\theta(-t)e^{\eta t} \;=\; \frac{1}{i\omega + \eta} = \frac{-i}{\omega - i\eta}. \tag{C.11}$$

To ensure convergence of the integrals, I have introduced an exponential that decays on a timescale $1/\eta$. At the end of the calculation I will take η to zero.

Using these simple expressions one finds

$$\chi_{BA}^{r}(\omega) = \int \frac{d\omega'}{2\pi} \frac{\chi_{[B,A]}(\omega)}{\omega - \omega' + i\eta}, \tag{C.12}$$

where

$$\chi_{[B,A]}(\omega) \;=\; \int dt\, e^{i\omega t}\langle[B(t), A(0)]\rangle \tag{C.13}$$

$$\;=\; -2\,\mathrm{Im}\chi_{BA}^{r}(\omega). \tag{C.14}$$

The last equality is seen by using the identity

$$\frac{1}{\omega - \omega' + i\eta} = P\frac{1}{\omega - \omega'} - i\pi\delta(\omega - \omega') \tag{C.15}$$

which is easily proven by contour integration. Equation (C.14) only holds when ω is real.

There are very efficient techniques to calculate $\chi_{[B,A]}(\omega)$. These make use of the time ordered response function

$$\chi_{BA}(t) = \frac{1}{i}\langle T\left(A(0)B(t)\right)\rangle, \tag{C.16}$$

which is closely associated with

$$\chi_{BA}^{>}(t) = \langle B(t)A(0)\rangle, \tag{C.17}$$
$$\chi_{BA}^{<}(t) = \langle A(0)B(t)\rangle. \tag{C.18}$$

In the frequency plane, the time ordered response function is

$$\chi_{BA}(\omega) = \int dt\, e^{i\omega t}\frac{1}{i}\left(\theta(t)\chi_{BA}^{>}(t) + \theta(-t)\chi_{AB}^{<}(t)\right) \tag{C.19}$$
$$= \int\frac{d\omega'}{2\pi}\frac{\chi_{[B,A]}(\omega')}{\omega - \omega'}. \tag{C.20}$$

The retarded and time-ordered response functions are simply related,

$$\chi_{BA}^{r}(\omega) = \chi_{BA}(\omega + i\eta). \tag{C.21}$$

Most manipulations of the time-ordered functions take advantage of the fact that they are periodic in imaginary time. The basic argument is that this periodicity follows from the cyclical invariance of the trace,

$$\langle B(t)A(0)\rangle = \text{Tr}\left\{e^{-\beta(H-\mu N)}\left[e^{iHt}B(0)e^{-iHt}\right]A(0)\right\} \tag{C.22}$$
$$= \text{Tr}\left\{e^{-\beta(H-\mu N)}\left[e^{\beta(H-\mu N)}e^{-iHt}A(0)e^{iHt}e^{-\beta(H-\mu N)}\right]B(0)\right\} \tag{C.23}$$
$$= \langle A(-(t+i\beta))B(0)\rangle \tag{C.24}$$
$$= \langle A(0)B(t+i\beta)\rangle. \tag{C.25}$$

The end expression will look slightly different if A does not commute with N. Further complications arise when one is dealing with Fermi operators, but for our purposes these can be ignored. By convention one defines time ordering so that $t = -i\beta$ is later than $t = 0$. Thus

$$\chi_{BA}(t = 0) = \chi_{BA}(t = -i\beta). \tag{C.26}$$

Hence χ_{BA} can be expanded as a Fourier series,

$$\chi_{BA}(t) = \frac{1}{-i\beta} \sum_{\nu} e^{-i\omega_\nu t} \chi_{BA}(\omega_\nu). \tag{C.27}$$

The Matsubara frequencies ω_ν are restricted to multiples of $(2\pi/-i\beta)$,

$$\omega_\nu = \frac{2\pi\nu}{-i\beta}, \qquad \nu = 0, \pm 1, \pm 2, \dots. \tag{C.28}$$

The periodicity also leads to the equality,

$$\chi_{BA}^{>}(\omega) = e^{\beta\omega} \chi_{BA}^{<}(\omega), \tag{C.29}$$

which combined with

$$\chi_{[B,A]} = \chi_{BA}^{>} - \chi_{BA}^{<}, \tag{C.30}$$

gives

$$\chi_{BA}^{>} = \chi_{[B,A]} \left(1 + \frac{1}{e^{\beta\omega}-1} \right) \tag{C.31}$$

$$\chi_{BA}^{<} = \chi_{[B,A]} \left(\frac{1}{e^{\beta\omega}-1} \right). \tag{C.32}$$

One recognizes the thermal occupation of a boson mode in the last expression. Physically $\chi_{[B,A]}(k,\omega)$ represents the *spectral density*, which counts the number of modes at wave number k and energy ω. The functions $\chi_{BA}^{<}$ and $\chi_{BA}^{>}$ represent the density of occupied and unoccupied states. The relations (C.31) and (C.32) are only true in an equilibrium ensemble, though (C.30) holds generically.

I now invert the Fourier series in (C.27),

$$\int_0^{-i\beta} dt\, e^{i\omega_\nu t} \chi_{BA}(t) = \chi_{BA}(\omega_\nu) \left(\frac{1}{-i\beta} \right) \int_0^{-i\beta} dt \tag{C.33}$$

$$= \chi_{BA}(\omega_\nu). \tag{C.34}$$

Equation (C.33) may be written as an integral over all ω,

$$\int_0^{-i\beta} dt\, e^{i\omega_\nu t} \chi_{BA}(t) = \int_0^{-i\beta} dt\, e^{i\omega_\nu t} \frac{1}{i} \chi_{BA}^{>}(t) \tag{C.35}$$

$$= \int \frac{d\omega}{2\pi} \int_0^{-i\beta} dt\, e^{i(\omega_\nu - \omega)t} \left(\frac{1}{i} \chi_{BA}^{>}(\omega) \right) \tag{C.36}$$

$$= \int \frac{d\omega}{2\pi} \frac{1 - e^{-\beta\omega}}{\omega_\nu - \omega} \chi_{BA}^{>}(\omega). \tag{C.37}$$

Using (C.31) one sees that

$$\chi_{BA}(\omega_\nu) = \int \frac{d\omega}{2\pi} \frac{A(\omega)}{\omega_\nu - \omega}, \tag{C.38}$$

140

thus proving that the series coefficients $\chi_{BA}(\omega_\nu)$ are equal to the Fourier transform along the real axis $\chi_{BA}(\omega = \omega_\nu)$. Thus one can use the Matsubara Green's functions and the real-time Green functions interchangeably.

The real time Green's functions because have obvious physical meaning, however the imaginary time functions are easier to calculate. In the retarded real time functions, temperature information is carried by the state of the system at time $t = -\infty$. In the time-ordered imaginary-time functions, temperature information is carried by the cyclic boundary conditions. In both of these cases, it is only the unperturbed system that is in thermodynamic equilibrium and the perturbation will in general give a non-equilibrium state.

C.3 Sum rules

Often in working with this formalism that one has use for certain "sum rules." These involve taking various moments of $\chi_{[B,A]}(\omega)$. The first rule is a statement that the total spectral weight is given by the commutator of A and B,

$$\int \frac{d\omega}{2\pi} \chi_{[B,A]}(\omega) = \chi_{[B,A]}(t=0) = [B, A]. \tag{C.39}$$

The second rule, known as the *f-sum* rule is

$$\lim_{\omega \to \infty} \omega^2 \chi_{BA}(\omega) = \int \frac{d\omega}{2\pi} \omega \chi_{[B,A]}(\omega) = i \frac{\partial}{\partial_t} \chi_{[B,A]}(t) \Big|_{t=0} = [[B, H], A]. \tag{C.40}$$

The third rule is that

$$\int \frac{d\omega}{2\pi} \frac{\chi_{[B,A]}(\omega)}{\omega} = -\chi_{BA}(\omega = 0). \tag{C.41}$$

The function $\chi_{BA}(\omega = 0)$ is the static response of the system. It represents the response of the system to very slowly turning on the perturbation. By definition, this is the adiabatic, or isoentropic, response. One is also interested in the isothermal response of the system, where the temperature of the system is held fixed while the perturbation is turned on. Given specific quantities A and B one can use Maxwell relationships to connect the two responses. In the general case it is simpler to use the microscopics.

One defines the static isothermal response of B to a perturbation of the form $\delta H = \alpha A$, by writing

$$\chi_{(T)} = \frac{\delta B}{\delta \alpha} = \frac{Tr \, e^{-\beta H} B}{Tr \, e^{-\beta H}} \tag{C.42}$$

$$= -\beta \left[\langle AB \rangle - \langle A \rangle \langle B \rangle \right]. \tag{C.43}$$

By redefining A and B to be $\tilde{A} = A-<A>$ and $\tilde{B} = B-<B>$, one can always set $\langle A \rangle \langle B \rangle = 0$. Thus without loss of generality,

$$
\begin{align}
\chi_{(T)} &= -\beta \chi^<_{BA}(t=0) \tag{C.44} \\
&= -\beta \int \frac{d\omega}{2\pi} \chi^<_{BA}(\omega) \tag{C.45} \\
&= -\beta \int \frac{d\omega}{2\pi} f(\omega) \chi_{[B,A]}(\omega). \tag{C.46}
\end{align}
$$

Now if the spectral weight is concentrated at energies much less that T, then one can replace $f(\omega)$ with $(\beta\omega)^{-1}$, telling us $\chi_{(T)} \approx \chi_{BA}$.

C.4   Green's functions

This Appendix would not be complete without mentioning the most important response function, the single particle Green's function, which is the response of the system to adding or removing a particle. As with more general response functions, there is a whole zoo of Green's functions, defined by

$$
\begin{align}
G(12) &= \frac{1}{i} \langle T \left(\Psi(1)\Psi^\dagger(2) \right) \rangle \tag{C.47} \\
G^<(12) &= \langle \Psi(1)\Psi^\dagger(2) \rangle \tag{C.48} \\
G^>(12) &= \langle \Psi^\dagger(2)\Psi(1) \rangle \tag{C.49} \\
G^R(12) &= \frac{1}{i}\theta(1-2)(G^>(12) - G^<(12)) \tag{C.50} \\
G^A(12) &= \frac{-1}{i}\theta(2-1)(G^>(12) - G^<(12)) \tag{C.51} \\
A(12) &= G^>(12) - G^<(12). \tag{C.52}
\end{align}
$$

Here a short hand notation is used where a number, such as 1, represents the time and space coordinates t_1 and r_1. The Fourier transforms $G^<(\omega)$ and $G^>(\omega)$ are particularly important as they give the density of available single-particle states and the density of occupied single-particle states.

A convenient approach to calculating these Green's functions is to approximate and solve the partial differential equations that these functions obey. These equations are derived from the equations of motion for the field operators. For concreteness, considers a set of particles interacting through a point interaction of strength g, with Hamiltonian

$$
H = \int d^3r \frac{\nabla\Psi^\dagger\nabla\Psi}{2m} - \mu\Psi^\dagger\Psi + \frac{g}{2}\Psi^\dagger\Psi^\dagger\Psi\Psi. \tag{C.53}
$$

Including the chemical potential μ in the Hamiltonian has no effect on the dynamics, but makes thermodynamic relationships simpler. With this Hamiltonian, the field operators obey an equation of motion

$$i\partial_t \Psi(r,t) = [\Psi, H] = -\frac{\nabla_r^2}{2m}\Psi(r,t) - \mu\Psi(r,t) + g\Psi^\dagger(r,t)\Psi(r,t)\Psi(r,t). \qquad \text{(C.54)}$$

Multiplying on the right by $\Psi^\dagger(r',t')$, time ordering and taking the expectation value,

$$\left(i\partial_t + \frac{\nabla_r^2}{2m} + \mu\right)G(rt,r't') - g\langle T\Psi^\dagger(r,t)\Psi(r,t)\Psi(r,t)\Psi^\dagger(r',t')\rangle = \delta(t)\delta^3(r-r').$$
$$\text{(C.55)}$$

The delta function on the right results from the time derivative of the time ordering operator. Conventionally the interaction term is expressed in terms of a self-energy $\Sigma(rt, r't')$. The self-energy is most easily defined by expanding (C.55) in terms of the Matsubara frequencies, and Fourier transforming with respect to $r - r'$;

$$(\omega_\nu - k^2/2m + \mu - \Sigma(k,\omega_\nu))G(k,\omega_\nu) = 1. \qquad \text{(C.56)}$$

The self-energy is typically calculated perturbatively. Some manipulations of these equations are discussed in Chapter 6.

C.4.1 Anomalous Green's functions

In the presence of a condensate the Green's functions develop a matrix structure. Here I briefly discuss the origin of this structure.

Since there are a macroscopic number of particles in a condensate, removing a single particle from the condensed mode makes no difference to the system. This property is captured by stating that the field operator Ψ has a non-zero expectation value $\psi = \langle\Psi\rangle$. The function $\psi(r) = \sqrt{N_0}\phi(r)$ corresponds to the square root of the number of condensed particles times the wavefunction of the condensate. Thus the field operator can be decomposed into a mean field part and fluctuations, $\Psi = \psi + \tilde{\psi}$. Taking the expectation value of (C.54),

$$(i\partial_t + \nabla^2/2m + \mu - g|\psi|^2)\psi = 2g\psi\langle\tilde{\psi}^\dagger\tilde{\psi}\rangle + g\psi^*\langle\tilde{\psi}\tilde{\psi}\rangle + g\langle\tilde{\psi}^\dagger\tilde{\psi}\tilde{\psi}\rangle. \qquad \text{(C.57)}$$

When the right hand side is neglected this equation is the Gross Pitaevskii equation, which is accurate when the number of non-condensed particles is small. Many alkali gas experiments are very well described by this "nonlinear Schrödinger equation." For a uniform condensate this equation is readily satisfied by setting μ equal to the mean field energy, $\mu = gn_0$.

By considering the right hand side of (C.57) one sees that in addition to ordinary Green's functions of the form $\langle \tilde{\psi}^\dagger \tilde{\psi} \rangle$, one also has to consider *anomalous* Green's functions, $\langle \tilde{\psi}\tilde{\psi} \rangle$. The regular and anomalous functions are conveniently described by a matrix

$$\overleftrightarrow{G}(rt, r't') = \frac{1}{i} \begin{pmatrix} \langle T\left(\tilde{\psi}(r,t)\tilde{\psi}(r',t')\right)\rangle & \langle T\left(\tilde{\psi}(r,t)\tilde{\psi}(r',t')\right)\rangle \\ \langle T\left(\tilde{\psi}(r,t)\tilde{\psi}(r',t')\right)\rangle & \langle T\left(\tilde{\psi}(r,t)\tilde{\psi}(r',t')\right)\rangle \end{pmatrix}. \tag{C.58}$$

Analogous to (C.55), this matrix Green's function obeys an equation of motion

$$(\omega\overleftrightarrow{\tau}_3 - k^2/2m\overleftrightarrow{\tau}_0 - \overleftrightarrow{\Sigma}(k,\omega))\overleftrightarrow{G}(k,\omega) = \overleftrightarrow{\tau}_0. \tag{C.59}$$

The matrix $\overleftrightarrow{\tau}_3$ is a Pauli matrix and $\overleftrightarrow{\tau}_0$ is the identity. A large class of approximations for the self-energy are discussed in Appendix D. Where no confusion is likely to arise I omit the '$\leftrightarrow$' symbol on tensors and '$\rightarrow$' on vectors.

Appendix D

Conserving (Φ-derivable) approximations

In this Appendix I review the structure of Φ-derivable Green's function approximations, verifying that they obey the standard conservation laws (number, energy, and momentum) [109]. These conservation laws are critical for correctly describing the behavior of an atomic gas. A simple Φ-derivable approximation is used in Chapter 6.4. After a short discussion of conservation laws, I perturbatively develop Φ to second order in the interactions. This second order functional in conjunction with the kinetic theory of Chapter 6, provides a very accurate non-equilibrium theory of a degenerate Bose gas.

D.1 Basic structure

As discussed in Section C.4.1, a condensed system is described by breaking up the field operator Ψ into a mean field part $\psi = \langle \Psi \rangle$ and a fluctuation $\tilde{\psi}$. One is naturally lead to a matrix formulation of the equation of motion where,

$$\vec{\psi} \;=\; \begin{pmatrix} \psi \\ \psi^\dagger \end{pmatrix} \tag{D.1}$$

$$\overleftrightarrow{G} \;=\; \begin{pmatrix} G_{11} & G_{12} \\ G_{21} & G_{22} \end{pmatrix} = \frac{1}{i} \begin{pmatrix} \langle \tilde{\psi}\tilde{\psi}^\dagger \rangle & \langle \tilde{\psi}\tilde{\psi} \rangle \\ \langle \tilde{\psi}^\dagger\tilde{\psi}^\dagger \rangle & \langle \tilde{\psi}^\dagger\tilde{\psi} \rangle \end{pmatrix}. \tag{D.2}$$

The equations of motion for these functions are schematically written as

$$\overleftrightarrow{G}_0^{-1}\vec{\psi} \;=\; \vec{\eta} \tag{D.3}$$

$$(\overleftrightarrow{G}_0^{-1} - \overleftrightarrow{\Sigma})\overleftrightarrow{G} \;=\; \overleftrightarrow{\delta}. \tag{D.4}$$

In these equations $\overleftrightarrow{G}_0^{-1} = i\overleftrightarrow{\tau}_3\partial_t + \nabla^2/2m\overleftrightarrow{\tau}_0$, where $\overleftrightarrow{\tau}_3$ is a Pauli matrix, $\overleftrightarrow{\tau}_0$ is the two-by-two identity matrix, and adjacent operators are convoluted. The symbol $\overleftrightarrow{\delta} = \delta(t-t')\delta^3(r-r')\overleftrightarrow{\tau}_0$ is the identity. The source term, $\vec{\eta}$, and the self-energy, $\overleftrightarrow{\Sigma}$, are complicated functionals of $\vec{\psi}$ and $\overleftrightarrow{\Sigma}$.

D.2   Conservation laws

One can guarantee conservation laws are satisfied if $\overleftrightarrow{\Sigma}$ and $\vec{\eta}$ are related to a functional of ψ and G via the relations [109],

$$2\eta = \frac{\delta\Phi}{\delta\psi^*} \tag{D.5}$$

$$i\Sigma_{ij} = \frac{\delta\Phi}{\delta G_{ji}}, \tag{D.6}$$

where $\vec{\eta} = (\eta, \eta^*)$. The symmetries of Φ give rise to conservation laws. For example, conservation of particle number is related to the $U(1)$ gauge symmetry of Φ. This number conservation is easily demonstrated, starting with the identity

$$\delta\Phi = \int d1 \sum_j \frac{\delta\Phi}{\delta\Psi_j(1)}\delta\Psi_j(1) + \int d1\,d1' \left[\sum_{ij}\frac{\delta\Phi}{\delta G_{ij}(11')}\delta G_{ij}(11')\right] \tag{D.7}$$

$$= \int d1\, 2\left(\eta^*(1)\delta\psi(1) + \eta(1)\delta\psi^*(1)\right) + \int d1\,d1' \sum_{ij} i\Sigma_{ij}(11')\delta G_{ji}(1'1). \tag{D.8}$$

Here a notational short-hand is used where the symbol 1 is used in place of time and space co-ordinates t_1, t_1. I now consider a local gauge change of the form

$$\vec{\psi} \rightarrow e^{i\Lambda\overleftrightarrow{\tau}_3}\vec{\psi} \tag{D.9}$$

$$\overleftrightarrow{G} \rightarrow e^{i\Lambda\overleftrightarrow{\tau}_3}\overleftrightarrow{G}e^{-i\Lambda\overleftrightarrow{\tau}_3}, \tag{D.10}$$

which gives to lowest order

$$\delta\psi = i\Lambda\psi \tag{D.11}$$

$$\delta G = i(\Lambda\overleftrightarrow{\tau}_3\overleftrightarrow{G} - \overleftrightarrow{G}\overleftrightarrow{\tau}_3\Lambda). \tag{D.12}$$

Thus the variation in Φ is

$$\delta\Phi = \int d1\,\Lambda(1)\left(2i\eta^*(1)\psi(1) - 2i\eta(1)\psi^*(1)\right) \tag{D.13}$$

$$+ \int d1\,d1'\, i\Sigma(11')\left(i\Lambda(1')\tau_3 G(1'1) - i\Lambda(1)G(1'1)\tau_3\right)$$

$$= \int d1\,\Lambda(1)\left[2i(\eta^*(1)\psi(1) - \eta(1)\psi^*(1))\right. \tag{D.14}$$

$$\left. - \int d1'\,\mathrm{Tr}\tau_3\left(G(11')\Sigma(1'1) - \Sigma(11')G(1'1)\right)\right].$$

Since Φ is invariant under this gauge change, one must have $\delta\Phi = 0$, for an arbitrary choice of Λ, implying the expression in square brackets must vanish.

I now show that local number conservation is a consequence of this term vanishing. From Eq. (D.1), ψ obeys the equation of motion

$$\left(i\partial_t + \frac{\nabla^2}{2m}\right)\psi = \eta. \tag{D.15}$$

Multiplying by ψ^* and subtracting the complex conjugate yields

$$\partial_t(n_0) + \nabla \cdot (n_0 v_s) = -i(\psi^*\eta - \eta^*\psi). \tag{D.16}$$

Similarly, Eq. (D.2), reads

$$\left(i\tau_3\partial_t + \frac{\nabla^2}{2m}\right)G(11') = \delta(11') + \Sigma(1\bar{2})G(\bar{2}1'). \tag{D.17}$$

The adjoint equation to (D.17) reads

$$-i\partial_{t'}G(11')\tau_3 + \frac{\nabla'^2}{2m}G(11') = \delta(11') + G(1\bar{2})\Sigma(\bar{2}1'). \tag{D.18}$$

Multiplying by τ_3, subtracting the two equations, and setting $1' = 1$ yields

$$\partial_t iG(1,1) + \quad \nabla \cdot \left[\frac{1}{2im}(\nabla_1\tau_3 iG(1,1') - \nabla_{1'}iG(1,1')\tau_3)\right]_{1=1'} \tag{D.19}$$
$$= \int d\bar{2}\,\tau_3\Sigma(1\bar{2})G(\bar{2}1') - G(1\bar{2})\Sigma(\bar{2}1')\tau_3.$$

Thus

$$\partial_t(2n) \quad = \quad \partial_t(2n_0 + \mathrm{Tr}iG) \tag{D.20}$$
$$= \quad 2i(\eta^*\psi - \psi^*\eta) + \int d\bar{2}\,\mathrm{Tr}\,\tau_3(\Sigma(1\bar{2})G(\bar{2}1) - G(1\bar{2})\Sigma(\bar{2}1)) \tag{D.21}$$

which vanishes by virtue of Eq. (D.14).

D.2.1   Components

In some circumstances it is more convenient to work with the components G_{ij}, rather than the tensor $\overleftrightarrow{G}$. The components are not independent. For example, $G_{11}(1,1') = G_{22}(1',1)$. In computing the functional derivatives in (D.5), one needs to take the interdependencies into account. To ensure that one does not double-count any terms, it is convenient to take Φ, which is a functional of the matrix $G(1,1')$, and substitute

$$G_{11}(1,1') \quad \rightarrow \quad \frac{G_{11}(1,1') + G_{22}(1',1)}{2} \tag{D.22}$$
$$G_{22}(1',1) \quad \rightarrow \quad \frac{G_{11}(1,1') + G_{22}(1',1)}{2}. \tag{D.23}$$

147

Call this new functional Φ'. The derivatives of Φ' with respect to G_{12}, G_{21}, ψ, and $\psi^\dagger$, are all trivially equal to the derivatives of Φ. To show that $\delta\Phi'/\delta G_{11} = \delta\Phi/\delta G$, one writes

$$\frac{\delta\Phi'}{\delta G_{11}(1',1)} = \frac{1}{2}\frac{\delta\Phi'}{\delta G_{11}(1',1)} + \frac{1}{2}\frac{\delta\Phi'}{\delta G_{22}(1,1')} \tag{D.24}$$

$$= \frac{\Sigma_{11}(1,1') + \Sigma_{22}(1',1)}{2} \tag{D.25}$$

$$= \Sigma_{11}(1,1'). \tag{D.26}$$

In the rest of this Appendix, I make no distinction between Φ and Φ'. Equations written in matrix notation will refer to Φ, while equations written in components will refer to Φ'.

D.3   Self-energies

By definition, the self-energy is the sum of all irreducible diagrams which have one incoming line and one outgoing line. (A diagram is irreducible if it cannot be split into two by cutting a single propegator.) Figure D.1 shows all diagrams of Σ_{11} up to second order in the interaction. All of the diagrams on each row are equal. Figure D.2 shows the diagrams for Σ_{12} to the same order. Algebraically, the diagonal elements are

$$\begin{aligned}
-i\Sigma_{11}(11') = \ & \delta(1,1')2(-ig)(\psi^*\psi + iG_{11}) \\
& +2(-ig)^2 iG_{11}(1'1)(iG_{11}(11')iG_{11}(11') - \\
& \quad i(G_0)_{11}(11')i(G_0)_{11}(11')) \\
& +4(-ig)^2 iG_{11}(11')iG_{12}(11')iG_{21}(11') \\
& +4(-ig)^2\psi(1)\psi^*(1')iG_{12}(11')iG_{21}(11') \\
& +2(-ig)^2\psi^*(1)\psi(1')(iG_{11}(11')iG_{11}(11') - \\
& \quad i(G_0)_{11}(11')i(G_0)_{11}(11')) \\
& +4(-ig)^2\psi(1)\psi(1')iG_{11}(11')iG_{21}(11') \\
& +4(-ig)^2\psi^*(1)\psi^*(1')iG_{11}(11')iG_{12}(11') \\
& +4(-ig)^2\psi(1)\psi^*(1')iG_{11}(11')iG_{11}(1'1) \\
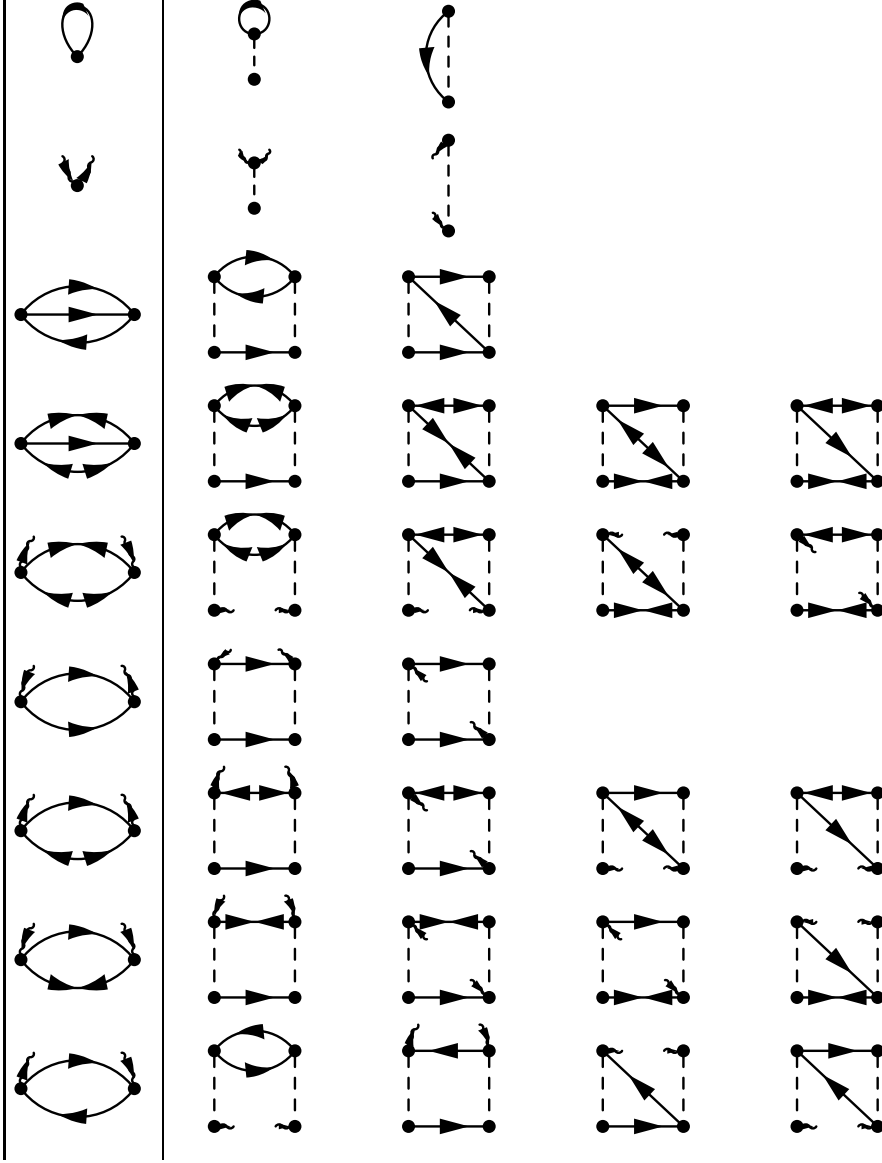& +\cdots,
\end{aligned} \tag{D.27}$$

Figure D.1: Terms in Σ_{11} up to second order in the interaction. Propegators, G_{11}, G_{12}, and G_{21} are respectively represented by diagrams ➤ , ►◄ , and ◄► . In the right hand columns the interaction is represented by a dashed line. For a point interaction, each of the diagrams on the right reduces to the diagram on the left in which the interaction is represented by a vertex with a dot. Short lines emanating from vertices represent condensate contributions $\langle\psi\rangle$ and $\langle\psi^\dagger\rangle$.
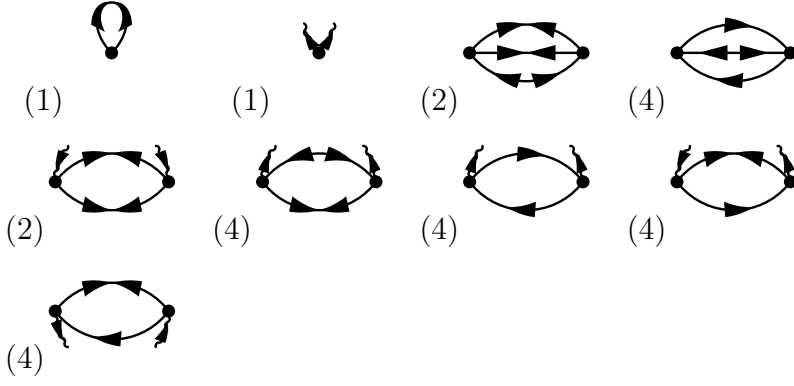
Figure D.2: Terms in Σ_{12} which are up to second order in the interaction. Unlike figure D.1, only the diagrams with point interactions are drawn, with the multiplicity listed in parenthesis.

while the off-diagonal ones are

$$
\begin{aligned}
-i\Sigma_{12}(11') = \; & \delta(1,1')(-ig)(\psi\psi + iG_{12}) \\
& +2(-ig)^2 iG_{12}(11')iG_{12}(11')iG_{21}(11') \\
& +4(-ig)^2 iG_{11}(11')iG_{11}(1'1)iG_{21}(11') \\
& +2(-ig)^2 \psi^*(1)\psi^*(1')iG_{12}(11')iG_{12}(11') \\
& +4(-ig)^2 \psi(1)\psi(1')iG_{12}(11')iG_{21}(11') \\
& +4(-ig)^2 \psi(1)\psi(1')iG_{11}(11')iG_{11}(1'1) \\
& +4(-ig)^2 \psi^*(1)\psi(1')iG_{11}(11')iG_{12}(11') \\
& +4(-ig)^2 \psi(1)\psi^*(1')iG_{11}(1'1)iG_{12}(11') \\
& + \cdots .
\end{aligned}
\tag{D.28}
$$

Here Σ is self-consistent; the expressions above use G and not G_0. The interaction $g = 4\pi\hbar^2 a_s/m$ is not the bare interaction, but rather comes from a repeated summing of binary interactions (the T-matrix), and to avoid double counting one must subtract the G_0's which appear in the above equations.
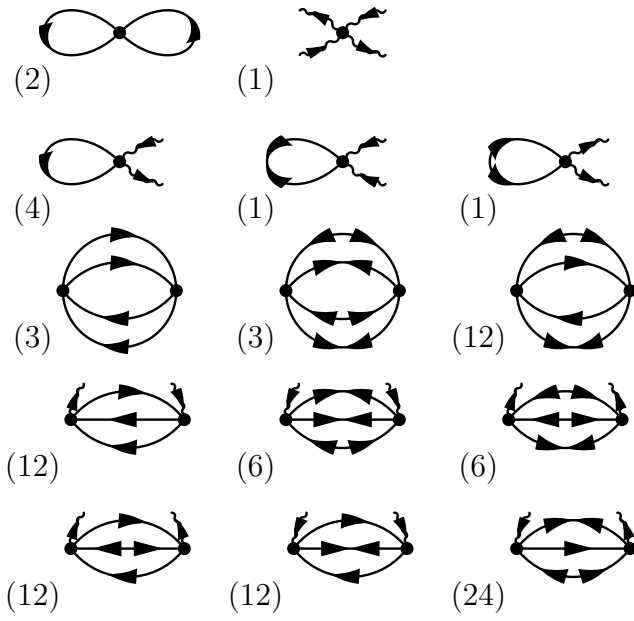
The source term in the condensate's equation of motion η is given by

$$
\begin{aligned}
\eta &= g\langle \Psi^\dagger \Psi \Psi \rangle \\
&= g\psi^*\psi\psi + 2g\psi iG_{11} + g\psi^* iG_{12} \\
&\quad -i\frac{g^2}{2}\int d^3r \int_0^{-i\beta} d\tau \; [4\psi^*(1')iG_{21}(11')iG_{11}(11')iG_{11}(11') \\
&\qquad\qquad +4\psi(1')iG_{11}(1'1)(\; iG_{11}(11')iG_{11}(11')- \\
&\qquad\qquad\qquad\qquad i(G_0)_{11}(11')i(G_0)_{11}(11')) \\
&\qquad\qquad +8\psi^*(1')iG_{11}(11')iG_{11}(1'1)iG_{12}(11') \\
&\qquad\qquad +8\psi(1')iG_{11}(1'1)iG_{12}(11')iG_{21}(11')] \\
&\quad +\cdots .
\end{aligned}
$$

(D.29)

These expressions are summed up by writing down Φ. To ease notation, we will use $G_\rightarrow$ as a short form of $(G_{11} + G_{22})/2$.

$$
\begin{aligned}
\Phi &= g\int d1 \left[|\psi|^4 + 4|\psi|^2 iG_\rightarrow + (\psi^*)^2 iG_{12} + (\psi)^2 iG_{21} + 2iG_\rightarrow iG_\rightarrow\right] \\
&\quad -i\frac{g^2}{3}\int d1\,d1' \Big[\; 3iG_\rightarrow(11')iG_\rightarrow(11')iG_\rightarrow(1'1)iG_\rightarrow(1'1) \\
&\qquad +3iG_{12}(11')iG_{21}(11')iG_{12}(1'1)iG_{21}(1'1) \\
&\qquad +12iG_\rightarrow(11')iG_{12}(11')iG_\rightarrow(1'1)iG_{21}(1'1) \\
&\qquad +12\psi(1)\psi^*(1')iG_\rightarrow(11')iG_\rightarrow(1'1)iG_\rightarrow(1'1) \\
&\qquad +6\psi(1)\psi(1')iG_{12}(11')iG_{12}(1'1)iG_{21}(1'1) \\
&\qquad +6\psi^*(1)\psi^*(1')iG_{21}(11')iG_{21}(1'1)iG_{12}(1'1) \\
&\qquad +12\psi^*(1)\psi^*(1')iG_\rightarrow(11')iG_{21}(1'1)iG_\rightarrow(1'1) \\
&\qquad +12\psi(1)\psi(1')iG_\rightarrow(11')iG_{12}(1'1)iG_\rightarrow(1'1) \\
&\qquad + 24\psi(1)\psi^*(1')iG_\rightarrow(11')iG_{12}(1'1)iG_{21}(1'1)\Big] .
\end{aligned}
$$

(D.30)

Φ differs from the free energy in that the second order terms have an extra factor of $1/3$. The relevant diagrams are shown in Fig. D.3.

Figure D.3: Second order expansion of Φ in powers of V. Only the diagrams with point interactions are drawn, but the multiplicity is listed in parenthesis.

Appendix E

Collisionless Excitations of a Spatially Uniform Weakly Interacting Gas

E.1   Introduction

In this Appendix I calculate the linear response of a gas of degenerate atoms in the collisionless regime. These results were used in Chapter 5 to calculate the stability of a gas of attractive atoms, and are the building blocks for the more sophisticated kinetic theory described in Chapter 6.

I begin by discussing a simple classical kinetic theory, the collisionless Boltzmann equation. I linearize this equation about equilibrium to find the elementary excitations of a classical gas. I show that a classical gas has a collisionless "zero-sound" mode that has the same dispersion relationship as the Bogoliubov spectrum of a zero temperature Bose gas. I then go through the equivalent procedure in a quantum mechanical system, producing the random phase approximation, and finding the excitation spectrum of a uniform Bose gas at arbitrary temperature. Those unfamiliar with the general theory of linear response functions may wish to glance at Appendix C, where I give a brief review of the subject.

E.2   The collisionless Boltzmann equation

I begin with a discussion of the collisionless Boltzmann equation, which describes a classical gas of particles with a mean-field treatment of their interactions. This equation is used in plasma physics, where its known as the Vlasov equation. Treating

the interactions via a mean-field, and introducing a weak perturbing field $U(x, t)$, the particles see a potential

$$V(x, t) = gn(x, t) + U(x, t), \tag{E.1}$$

where g parameterizes the interaction. In the absence of U, the density n is uniform.

Denoting the distribution of particles with momentum p, and position x, at time t, by $f(p, x, t)$, the collisionless Boltzmann equation reads

$$\partial_t f(p, x, t) + v \cdot \nabla_x f(p, x, t) + F \cdot \nabla_p f(p, x, t) = 0. \tag{E.2}$$

This equation simply states Newton's laws. The particles drift with velocity $v = p/m$, and accelerate according to the force $F = -\nabla_x V(x, t)$. Note that the density in (E.1) is

$$n(x, t) = \int \frac{dp}{(2\pi)^3} f(p, x, t). \tag{E.3}$$

In the absence of the perturbation $U(x, t)$, the Boltzmann equation is solved by the Maxwellian velocity distribution

$$f_0(p, x, t) = e^{-\beta(p^2/2m + gn - \mu)}. \tag{E.4}$$

The density n is uniform and solves the equation $n = e^{\beta\mu - gn}/\Lambda^3$, where $\Lambda^{-2} = mk_BT/2\pi\hbar^2$ is the thermal wavelength. Linearizing (E.2) about this solution gives

$$\partial_t \delta f + v \cdot \nabla_x \delta f + \beta f_0 v \cdot \nabla_x (U + g\delta n) = 0, \tag{E.5}$$

where δf and δn are respectively the variation of f and n.

It is convenient to Fourier transform (E.5) with respect to space and time, using the convention

$$g(k, w) = \int dx \int dt \, e^{-ik \cdot x + i\omega t} g(r, t). \tag{E.6}$$

Note, there are two momenta in the resulting equations; $p = mv$ is the physical momentum of the particles, and $\hbar k$ is the momentum associated with the Fourier transform of x. The transformed equation reads

$$-\omega \delta f + v \cdot k\delta f + \beta f_0 v \cdot k(U + g\delta n) = 0. \tag{E.7}$$

If $g = 0$, then $\delta f = \beta f_0(v \cdot k/(v \cdot k - \omega))$. Integrating over p, the response of the noninteracting gas is

$$\chi_0 = \left. \frac{\delta n}{\delta U} \right|_{g=0} = \int \frac{dp}{2\pi^3} \frac{\beta f_0 \, v \cdot k}{\omega - v \cdot k}. \tag{E.8}$$

154

In the complex frequency plane, this function contains a branch cut along the real frequency axis. In most circumstances one is interested in the retarded response, which is the analytic continuation from the upper half plane. One selects out this branch by taking $\omega \to \omega + i\eta$ in (E.8). Equation (E.7) is no more difficult to solve when $g \neq 0$. Solving for δf and integrating over p gives

$$\delta n = \chi_0(U + g\delta n). \tag{E.9}$$

This equation is interpreted as saying that the cloud responds not only to the external potential, but also to the mean field generated when its profile is distorted. The full response function is written as

$$\chi = \frac{\delta n}{\delta U} = \frac{\chi_0}{1 - g\chi_0}. \tag{E.10}$$

This expression involves all powers of the interaction.

To understand the response (E.10) one first needs to understand the structure of χ_0. In Eq. (E.8), the integral over the directions transverse to k is trivial, leaving

$$\chi_0(k, \omega) = -\beta n \frac{1}{\sqrt{\pi}} \int dt \frac{t e^{-t^2}}{t - \omega/\nu_k}. \tag{E.11}$$

All the k-dependence in this expression is buried in the characteristic energy scale

$$\nu_k = 2\sqrt{\epsilon_k T}. \tag{E.12}$$

For ease of reference, I denote the integral as

$$I(x) = \frac{1}{\sqrt{\pi}} \int dt \frac{t e^{-t^2}}{t - x}. \tag{E.13}$$

$I(x)$ can be written in terms of standard functions by expanding the ratio $t/(t-x)$ as a Fourier integral,

$$I(x) = 1 + \frac{2ix}{\sqrt{\pi}} \int_0^\infty ds \int dt\, e^{-t^2 - 2ist + 2ixs}. \tag{E.14}$$

The t integral is Gaussian, as is the subsequent s integral. In terms of the error function $\mathrm{erf}(z) = (2/\sqrt{\pi}) \int_0^z \exp(-z^2)$, the integral is

$$I(x) = 1 + i\sqrt{\pi}xe^{-x^2}(1 - \mathrm{erf}(-ix)). \tag{E.15}$$

The singularities of $I(x)$ all reside at $x = -i\infty$, signifying that any collective modes of the system are strongly overdamped. As I now show, in the interacting gas, these

singularities move towards the real axis, and for sufficiently strong interactions a collective "zero-sound" mode develops.

A useful trick for understanding the poles of the interacting system is to find the curves in the complex plane where $\text{Im}(\chi_0) = 0$, as shown in Fig. E.1. The poles of χ lie along these lines. The zeroes of χ_0 appear as the intersection of two of these lines. In the context of attractive interactions, the most important line of $\text{Im}(\chi_0) = 0$ lies on the imaginary axis, where as $\omega \to -i\infty$ the function $I(\omega)$ diverges to $+\infty$, but as $\omega \to i\infty$, the function $I(\omega) \to 0$. For attractive interactions $g < 0$, the pole on this line starts at $\omega = -i\infty$, but as interactions increase, the pole moves upwards. When $\beta g n = -1$, the pole reaches the real axis. For larger interactions, the pole crosses onto the physical sheet – signaling a breakdown of our approach. As described by Mermin [132], the pole crossing the real axis represents the spinodal line of a liquid-gas phase transition.

There is no instability for repulsive interactions. Instead there is a collective mode, whose frequency is given by the location of the pole on the line $\text{Im}(\chi_0) = 0$ which asymptotically approaches the real axis. One finds the dispersion of this excitation by looking at the large x expansion, $I(x) = -1/2x^2 + O(x^{-4})$. Using (E.10), the formula for χ, one arrives at

$$\chi = \frac{2n\epsilon_k}{\omega^2 - 2ng\epsilon_k}. \tag{E.16}$$

Thus there is a mode with linear dispersion $\omega = ck$, where the speed of sound is $c = \sqrt{ng/m}$. For consistency of the large x expansion, one must have $\omega^2 \gg \nu_k^2 = \epsilon_k T$, which translates into $ng \gg T$. In other words, this mode exists as long as the mean-field interactions dominate the temperature. It is no coincidence that this mode has the same dispersion as the zero-temperature Bogoliubov sound mode.

E.3   Random phase approximation

In this Section I perform the same calculation in the quantum regime. Much of the hard work has already been done in 1974 by Szépfalusy and Kondor [107], who were interested in how the modes below T_c match up with the modes above T_c. This investigation lead them to calculate the response of an interacting gas within the random phase approximation (RPA). They considered only the repulsive case, but it is not difficult to extend their work into the the more general setting.

The starting point, as before, is to calculate the density response function $\chi =$
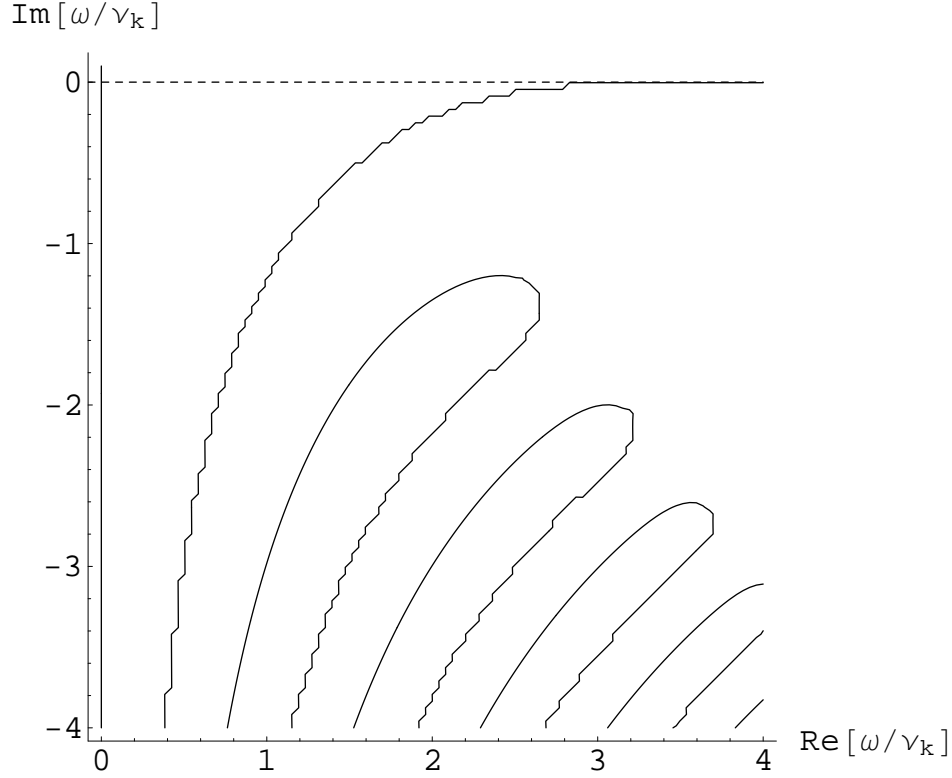
Figure E.1: Zeros of the imaginary part of the free response function $\chi_0(k,\omega)$ as a function of complex ω. The sign of χ_0 alternates on adjacent contours. In particular, the line on the imaginary axis has $\chi_0 < 0$, and the one to its right has $\chi_0 > 0$. Within a mean-field approximation, these lines represent the paths which the poles of χ follow as one increases the strength of the interactions. For attractive interactions, the singularities follow the $\chi_0 < 0$ lines, while for repulsive interactions, they follow the $\chi_0 > 0$ lines. In all cases the poles reside at $\omega = -i\infty$ when the interactions vanish. In the case of attractive interactions, a pole can cross the x axis, representing a mechanical instability. In the case of repulsive interactions, a pole can asymptotically approach the real axis, representing a collective "zero sound" mode.

$\delta n/\delta U$. The simplest approximation, the RPA, consists of a sum over bubbles,

$$\chi = \frac{\chi_0}{1 - g\chi_0}. \tag{E.17}$$

The physics here is the same as in the classical case. The density response is the direct response, plus the response to the mean field generated by the distorted density profile. The approximation comes in treating the direct response as χ_0, the susceptibility of the non-interacting system.

The most elementary approach to calculating χ_0 is to simply write down the response function in the time domain (cf. Appendix C)

$$\chi_0 = \frac{\delta \rho_q(0)}{\delta U_q(t)} = \frac{1}{i} \left[\langle T \left(\rho_q^\dagger(t) \rho_q(0) \right) \rangle_0 - \langle \rho_q^\dagger(t) \rangle_0 \langle \rho_q(0) \rangle_0 \right], \tag{E.18}$$

where ρ_q is the Fourier transform of the density operator,

$$\rho_q = \int d^3r \, e^{iq \cdot r} \, \langle \psi^\dagger(r) \psi(r) \rangle = \sum_k a_{k+q/2}^\dagger a_{k-q/2}. \tag{E.19}$$

The real-space operator $\psi(r)$ annihilates a particle at position r, while the momentum space operator a_k annihilates a particle with momentum k. Although I write n for the mean density, I use ρ_k, rather than n_k for the Fourier component of the density. The symbol n_k denotes the number of particles in a mode with momentum k; $n_k = a_k^\dagger a_k$. For the non-interacting system, the product of the two density operators in (E.18) factors, leaving a simple bubble,

$$\chi_0 = \frac{1}{i} \sum_k \langle T \left(a_{k-q/2}^\dagger(t) a_{k-q/2}(0) \right) \rangle_0 \langle T \left(a_{k+q/2}(t) a_{k+q/2}^\dagger(0) \right) \rangle_0. \tag{E.20}$$

Since the field operators evolve as

$$a_k(t) = e^{-i\epsilon_k t} a_k(0), \tag{E.21}$$

one can trivially perform the Fourier transform to arrive at

$$\chi_0(q, \omega) = \sum_k \frac{n_{k-q/2} - n_{k+q/2}}{\omega - \left(\epsilon_{k+q/2} - \epsilon_{k-q/2} \right)}. \tag{E.22}$$

A more sophisticated yet computationally simpler (and more instructive) way to arrive at the same formula is to write (cf. Eq. (C.12)

$$\langle T \left(\rho_q^\dagger \rho_q \right) \rangle(\omega) = \int \frac{d\omega'}{2\pi} \frac{\Pi(q, \omega')}{\omega - \omega'}, \tag{E.23}$$

where

$$\Pi(q, \omega) = -2Im\chi_0 = \langle [\rho_q^\dagger, \rho_q] \rangle(\omega). \tag{E.24}$$

As the imaginary part of χ, Π represents a decay rate – the rate at which particles scatter from momentum $k - q/2$ to momentum $k + q/2$.

Looking at the two terms in the commutator, one sees that there are two processes in Π. In the first process, a particle comes along with momentum $k-q/2$ and scatters into a state with momentum $k+q/2$, gaining an energy ω. The second process (which has a minus sign) has a particle with momentum $k + q/2$ scattering into a state with momentum $k - q/2$, losing energy ω. Thus the spectral density is

$$\Pi(q, \omega) = \sum_k \left[\left(n_{k-q/2}(1 + n_{k+q/2}) - n_{k+q/2}(1 + n_{k-q/2}) \right) \left(2\pi\delta(\epsilon_{k+q/2} - \epsilon_{k-q/2} - \omega) \right) \right],$$

(E.25)

which when substituted into (E.23) gives the same result as (E.22).

I now replace the sum over k with an integral. This is allowed as long as I treat the condensate separately (cf. the discussion in Chapter 2). Thus, following Szepfalusy and Kondor, I break the response function up into a regular part due to the non-condensed particles, and a singular part due to the condensate, $\chi_0 = \chi_0^n + \chi_0^c$. The regular part is

$$\chi_0^n(q, \omega) = \int \frac{d^3k}{(2\pi)^3} \frac{n_{k-q/2} - n_{k+q/2}}{\omega - (\epsilon_{k+q/2} - \epsilon_{k-q/2})},$$

(E.26)

and the singular part is

$$\chi_0^c(q, \omega) = \frac{n_0}{\omega - \epsilon_q} - \frac{n_0}{\omega + \epsilon_q}.$$

(E.27)

At zero temperature, only the singular part contributes, $\chi_0 = \chi_0^c$. Thus the response function of the interacting system is

$$\chi = \frac{\chi_0}{1 - g\chi_0} = \frac{2n_0\epsilon_q}{\omega^2 - \epsilon_q^2 - 2n_0 g\epsilon_q}.$$

(E.28)

Clearly, one has well defined excitations with energies given by the Bogoliubov expression

$$\omega = \sqrt{\epsilon_q^2 + 2gn_0\epsilon_q}.$$

(E.29)

As discussed in Section 5.2.2, for attractive interactions one finds an instability when the level spacing $\hbar^2/2mL^2$ is equal to $-2gn_0$. In the opposite limit of $T \gg T_c$, only the regular part contributes, $\chi_0 = \chi_0^n$, and the distribution functions n_q become classical $n_q = e^{-\beta(\epsilon_q - \mu)}$. Linearizing both the numerator and denominator of (E.26) in q allows us to recover the result of Section E.2,

$$(\chi_0)_{\text{classical}} = -\beta n I(\omega/\nu_q).$$

(E.30)

To discuss the intermediate regime (between zero T and classical) one has to study the analytic structure of χ_0^n. First, however, I introduce a more sophisticated version of the RPA, first used by Minguzzi and Tosi [108]. This improved approximation includes exchange forces, which are important for short range interactions.

E.3.1   The RPA with exchange

Equation (E.17) was based upon the assumption that the response to a perturbation δU is given by the classical result $\delta n = \chi_0(\delta U + g\delta n)$. This expression ignores exchange processes where the identical particles exchange momenta. By including this exchange term one produces Hartree-Fock approximation, $\delta n = \chi_0(\delta U + 2g\delta n)$. Unfortunately, this last expression cannot be applied to a condensed gas. The problem is that this factor of two only occurs if the coliding particles are in different states. Thus a scheme must be devised to account for the exchange interaction between non-condensed particles, but not between condensed ones.

Such a scheme was developed by Minguzzi and Tosi [108]. One looks separately at the change in the density of condensed and non-condensed atoms, δn_0 and $\delta\tilde{n}$. The factors of two are easily incorporated in a matrix expression,

$$\left(\begin{array}{c} \delta n_0 \\ \delta\tilde{n} \end{array} \right) = \left(\begin{array}{c} \chi_0^c \\ \chi_0^n \end{array} \right) \delta U + \left(\begin{array}{cc} \chi_0^c & 2\chi_0^c \\ 2\chi_0^n & 2\chi_0^n \end{array} \right) \left(\begin{array}{c} g\delta n_0 \\ g\delta\tilde{n} \end{array} \right), \qquad (E.31)$$

which gives the relationship

$$\chi = \frac{\delta n_0}{\delta U} + \frac{\delta\tilde{n}}{\delta U} = \frac{\chi_0^c + \chi_0^n + g\chi_0^c\chi_0^n}{(1 - g\chi_0^c)(1 - 2g\chi_0^n) - 4g^2\chi_0^c\chi_0^n}. \qquad (E.32)$$

An alternative view of this same approximation is to use Eq. E.17, but include the exchange interaction in χ_0. For example, for a non-condensed gas in the Hartree-Fock approximation, one would write

$$\chi_0^{HF} = \chi_0^n \left(1 + g\chi_0^n n + (g\chi_0^n n)^2 + \cdots \right), \qquad (E.33)$$

where successive exchange collisions are accounted for. Diagrammatic expressions for these different approximations are shown in Fig. E.2.

E.4   Analytic Structure of χ_0^n

In this Section I investigate the analytic structure of χ_0^n. Section E.4.1 will be devoted to deriving the following expression [107]

$$\chi_0^n(k,\omega) = -\frac{m}{\pi k\Lambda_T^2} \int_{(\omega-\epsilon_k)/\nu_k}^{(\omega+\epsilon_k)/\nu_k} dz \int dx \, \frac{x}{x-z} \frac{1}{e^{x^2-\beta\mu}-1}, \qquad (E.34)$$
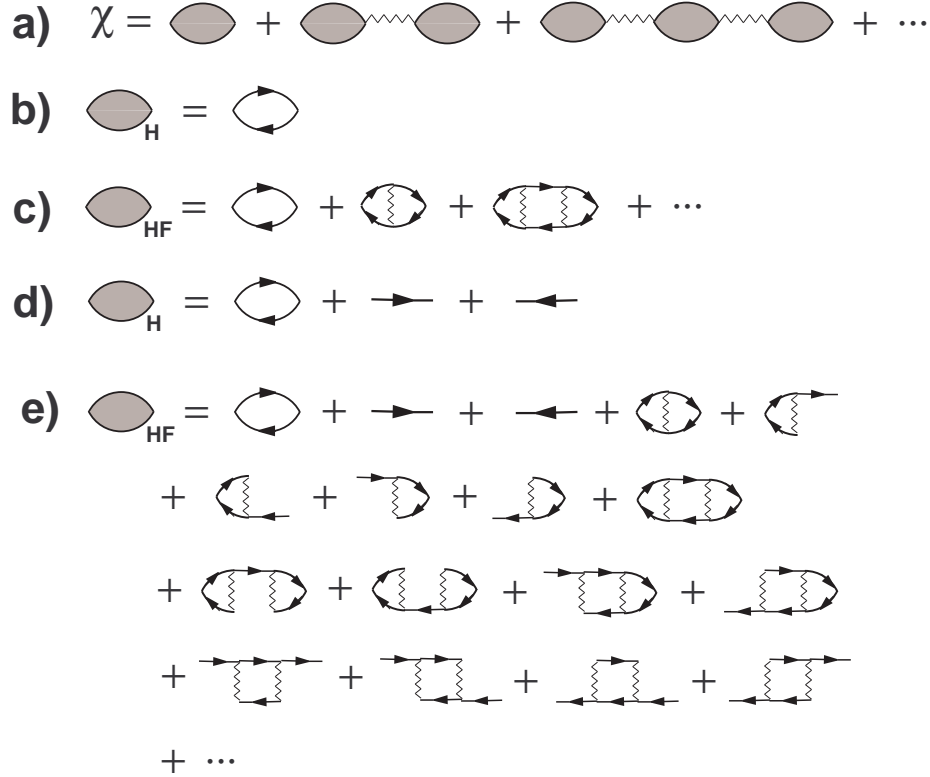
Figure E.2: Diagrammatic description of the approximation used for the response function. Lines with arrows represent propegators of the non-interacting system. Jagged lines represent the contact interaction between particles. a) Generically the response function can be expressed in terms of a polarization bubble (the bubble with shaded interior). b) In the Hartree approximation (RPA), the polarization bubble is taken to be the response of the non-interacting gas. c) In the Hartree-Fock approximation, the polarization bubble involves a sum over repeated exchange interactions. d) In a condensed system, the polarization bubble for the Hartree approximation must include terms where one of the particles is in the condensate. e) The Hartree-Fock approximation for the condensed gas requires writing all exchange graphs, noting that there is no exchange interaction between condensed atoms. The vertices in these figures with only a single solid line implicitly include an interaction with the condensate.

where once again $\nu_k = 2\sqrt{T\epsilon_k}$. Following this derivation I will give the asymptotic behavior of χ_0^n in various limits.

The x integral in (E.34) is the quantum mechanical version of the integral $I(t)$ introduced in Section E.2, and it shares many of the same analytic structures (for example it is a meromorphic function). The response function χ, is *not* meromorphic, as it contains logarithmic singularities in the complex frequency plane.

E.4.1 SK expression

In this section I derive Eq. (E.34). Starting with the general expression,

$$\chi_0^n(k,\omega) = \int \frac{d^3q}{(2\pi)^3} \frac{n_{q-k/2} - n_{q+k/2}}{\omega - (\epsilon_{q+k/2} - \epsilon_{q-k/2})}, \tag{E.35}$$

one splits the integrand into two terms, one containing $n_{q-k/2}$ and the other $n_{q+k/2}$. After shifting q by $\pm k/2$, one finds

$$\chi_0^n(k,\omega) = \int \frac{d^3q}{(2\pi)^3} n_q \left(\frac{1}{\omega - (\epsilon_{q+k} - \epsilon_q)} - \frac{1}{\omega - (\epsilon_q - \epsilon_{q-k})} \right). \tag{E.36}$$

The energies in the denominator can be expanded as $\epsilon_{q\pm k} = (q^2 + k^2 \pm 2kq\cos\theta)/2m$, where $\cos\theta$ is the angle between $\mathbf{q}$ and $\mathbf{k}$. The angular integrals are easily performed, leading to

$$\chi_0^n(k,\omega) = \frac{m}{(2\pi)^2 k} \int_0^\infty dq\, q^2\, n_q \log \left[\frac{(\bar{p} + k/2 - q)(\bar{p} - k/2 + q)}{(\bar{p} + k/2 + q)(\bar{p} - k/2 - q)} \right], \tag{E.37}$$

with $\bar{p} = m\omega/k$. One extracts the important structure by rewriting the logarithm as an integral of the form $\int dx/x$. Scaling all lengths by a multiple of the thermal wavelength gives

$$\chi_0^n(k,\omega) = \frac{-m}{\pi k \Lambda_T^2} \int_{z_-}^{z_+} dz\, I(z, \beta\mu) \tag{E.38}$$

$$I(z, \beta\mu) = \int_{-\infty}^\infty dx \frac{x}{x - z} \frac{1}{e^{x^2 - \beta\mu} - 1}, \tag{E.39}$$

where $z_\pm = \omega/2\sqrt{\varepsilon_k T} \pm k\Lambda_T/4\sqrt{\pi}$. In the limit $\beta\mu \to \infty$, $I(z, \beta\mu)$ agrees with the function I(z) defined on p. 155.

E.4.2 $\omega \to \infty$ structure of χ_0^n.

Here I investigate the high frequency response of the noninteracting system. This is a useful check on our analysis as the exact structure is a consequence of the f-sum

rule. As $\omega \to \infty$, the limits $z_\pm$ in the integral in (E.38) become very large, and one can expand (E.39) in powers of $1/z$,

$$I(z, \beta\mu) \;\to\; -\frac{1}{z^2}\int dx\, x^2 \frac{1}{e^{x^2-\beta\mu}-1} \tag{E.40}$$

$$= \; -\frac{1}{z^2}\sum_j e^{\beta j \mu}\int dx\, x^2 e^{-jx^2} \tag{E.41}$$

$$= \; -\frac{\Gamma(3/2)}{z^2}\sum_j \frac{e^{\beta j \mu}}{j^{3/2}} \tag{E.42}$$

$$= \; -\frac{\sqrt{\pi}}{2}\frac{g_{3/2}(e^{\beta\mu})}{z^2}. \tag{E.43}$$

Thus if $\omega \gg \epsilon_k$ the response function is

$$\chi_0^n(k,\omega) \;=\; -\frac{m}{\pi k \Lambda_T^2}\int_{(\omega-\epsilon_k)/\nu_k}^{(\omega+\epsilon_k)/\nu_k} dz \int dx\, \frac{x}{x-z}\frac{1}{e^{x^2-\beta\mu}-1} \tag{E.44}$$

$$\to \; -\frac{m}{\pi k \Lambda_T^2}\left(\frac{2\epsilon_k}{\nu_k}\right) I[\omega/\nu_k, \beta\mu] \tag{E.45}$$

$$= \; \frac{2\epsilon_k n}{\omega^2}, \tag{E.46}$$

where I've used that $n = g_{3/2}(e^\beta\mu)/\Lambda_T^3$. This is the result expected from the *f-sum* rule.

E.4.3 Long wavelength response

According to Eq. (E.38), at fixed ω, the $k \to 0$ limit of χ_0^n is equivalent to the $\omega \to \infty$ limit. Further analysis is needed to understand the $k \to 0$ structure as $\omega \to 0$.

Analytic structure of I.

The first step to understanding the low frequency, long wavelength response is to write I in terms of its poles in the complex z plane. This is accomplished by expanding the distribution function in terms of Matsubara frequencies,

$$\frac{1}{e^{x^2-\beta\mu}-1} = \sum_\nu \frac{1}{x^2-\beta\mu-2\pi i\nu}, \tag{E.47}$$

so that

$$I(z, \beta\mu) \;=\; \int dx\, \frac{1}{e^{x^2-\beta\mu}-1} + z^2\int dx\, \frac{1}{x^2-z^2}\left(\sum_\nu \frac{1}{x^2-\beta\mu-2\pi i\nu}\right). \tag{E.48}$$

The first integral is a Bose function $\sqrt{\pi}g_{1/2}(e^{\beta\mu})$. The second integral is evaluated with the residue theorem,

$$I(z,\beta\mu) = \sqrt{\pi}g_{1/2}(e^{\beta\mu}) - \frac{i\pi z}{2} + i\pi \sum_{\nu} \left(\frac{1}{z - \sqrt{\beta\mu + 2\pi i\nu}} + \frac{1}{\sqrt{\beta\mu + 2\pi i\nu}} \right). \quad \text{(E.49)}$$

The branches of the square roots are chosen so that they poses negative imaginary parts. This agrees with formula (A.3) of Szepfalusy and Kondor, even though their expression is much more complicated looking. At degeneracy, $\beta\mu \to 0$, and (E.49) becomes

$$I = \pi^{1/2}\zeta(1/2) - \frac{i\pi z}{2} + \frac{i\pi}{z} + i\pi \sum_{\nu \neq 0} \left(\frac{1}{z - \sqrt{2\pi i\nu}} + \frac{1}{\sqrt{2\pi i\nu}} \right). \quad \text{(E.50)}$$

The $k \to 0$ limit of $\chi(\omega = 0)$

Integration of the leading terms and setting $\omega = 0$ yields Eq. (5.8),

$$g\chi_0^n(k,0) = -2\frac{a_s}{\Lambda_T} \left[\frac{4\pi}{k\Lambda_T} \arctan|\varepsilon_k/4\mu|^{1/2} + g_{1/2}(e^{\beta\mu}) - |\pi/\beta\mu|^{1/2} + \mathcal{O}(k\Lambda_T) \right]. \quad \text{(E.51)}$$

The expansion parameter is $z_+ = k\Lambda_T/4\sqrt{\pi}$.

Asymptotics of the T-matrix

This is an appropriate place to discuss the asymptotics of the function Ξ, defined by (5.16). This function is analogous to χ_0^n, except it corresponds to a response in the particle-particle channel. Following the procedure of sec. E.4.1 to integrate out the angular variables, one writes Ξ as

$$\Xi(k,\omega) = \frac{-2m}{\pi k\Lambda_T^2} \int_{\bar{z}_-}^{\bar{z}_+} dz\, I(z), \quad \text{(E.52)}$$

with $\bar{z}_\pm = (k\Lambda/4\sqrt{\pi})[i\sqrt{1 + 2\omega/\varepsilon_k} \pm 1]$. Using the expansion in Eq. (E.49) gives Eq. (5.17),

$$g\Xi(k,\omega = 0) = -4\frac{a_s}{\Lambda_T} \left[\frac{4\pi}{k\Lambda_T} \arctan\left(\frac{|\epsilon_k/4\mu|^{1/2}}{1 + |\epsilon_k/4\mu|^{1/2}} \right) + g_{1/2}(e^{\beta\mu}) - |\pi/\beta\mu|^{1/2} + \mathcal{O}(k\Lambda_T) \right]. \quad \text{(E.53)}$$

E.4.4 The classical limit revisited

I now re-examine the classical limit discussed in Section E.2. My procedure there amounted to using a linearized dispersion, effectively confining the result to $\omega \gg \epsilon_k$. It is possible to calculate the exact result, in order to separate the quantum effects in (E.34) from the non-linear effects. I start with

$$\chi_0^n(k,\omega) = -\frac{m}{\pi k \Lambda_T^2} \int_{(\omega-\epsilon_k)/\nu_k}^{(\omega+\epsilon_k)/\nu_k} dz \int dx \, \frac{x}{x-z} \frac{1}{e^{x^2-\beta\mu}-1}, \tag{E.54}$$

then take the classical limit $1/(e^{x^2-\beta\mu}-1) \to e^{-(x^2-\beta\mu)}$, and use the identity $m/2\pi k = 1/\Lambda_T \nu_k \sqrt{\pi}$, in order to get

$$\chi_0^n(k,\omega)_c = -\beta n \frac{\nu_k}{2\epsilon_k} \frac{1}{\sqrt{\pi}} \int_{(\omega-\epsilon_k)/\nu_k}^{(\omega+\epsilon_k)/\nu_k} dz \int dx \, \frac{x e^{-x^2}}{x-z}, \tag{E.55}$$

where, as usual, $n = e^{\beta\mu}/\Lambda_T^3$. Turning back to Section E.4.1, one sees that the last integral is

$$\chi_0^n(k,\omega)_c = -\beta n \frac{\nu_k}{2\epsilon_k} \int_{(\omega-\epsilon_k)/\nu_k}^{(\omega+\epsilon_k)/\nu_k} dz \left[1 + i\sqrt{\pi} x e^{-x^2}(1 - \mathrm{erf}(-ix)) \right]. \tag{E.56}$$

Integrating by parts leaves us with the final expression

$$\chi_0^n(k,\omega)_c = \beta n \frac{\nu_k}{2\epsilon_k} \frac{i\sqrt{\pi}}{2} \left[e^{-t^2}(1 + \mathrm{erf}(it)) \right]_{t=(\omega-\epsilon_k)/\nu_k}^{t=(\omega+\epsilon_k)/\nu_k}. \tag{E.57}$$

Note that even when $\omega = 0$, this expression epends on ϵ_k,

$$\chi_0^n(k,\omega=0)_c = -\beta n \frac{\sqrt{\pi} e^{-(\epsilon_k/\nu_k)^2} \mathrm{erf}(i\epsilon_k/\nu_k)}{2(\epsilon_k/\nu_k)}. \tag{E.58}$$

For $\epsilon_k \ll T$ one can expand (E.58) in powers of ϵ_k/ν_k,

$$\chi_0^n(k,\omega=0)_c = -\beta n \left(1 - \frac{2}{3}\left(\frac{\epsilon_k}{\nu_k}\right)^2 + \frac{4}{15}\left(\frac{\epsilon_k}{\nu_k}\right)^4 + O(\epsilon_k) \right). \tag{E.59}$$

Appendix F

Low Energy Scattering

In this Appendix I review the theory of low energy scattering. This subject is particularly important for understanding Feshbach resonances, where the interactions between atoms are tuned by changing the magnetic field.

F.1 The Scattering amplitude

F.1.1 Definition

The basic picture of potential scattering is illustrated in Fig. F.1. One has an incoming wave e^{ikz} that is incident on a small impurity of size r_0 (positioned at the origin), and one asks what the far field wavefunction looks like. Generically

$$\psi(r) = e^{ikz} + f(k, \hat{r})\frac{e^{ikr}}{r}, \tag{F.1}$$

which has the form of the incoming wave plus a scattered wave. In the far field $r \gg r_0$, the scattering amplitude f can only be a function of the incident wave vector k, and on the direction $\hat{r}$. (In this equation f is also implicitly a function of the direction of the incoming wave, generically denoted $\hat{k}$ and here set to $\hat{z}$. For a spherically symmetric potential f is independent of $\hat{k}$.)

In the long wavelength limit $kr_0 \ll 1$ one expects that the scattering will become isotropic – the wave is too large to "see" the structure of the impurity. Thus one can drop the $\hat{r}$ dependences and only consider $f(k)$, referred to as the s-wave scattering amplitude. All of our discussions will be limited to this s-wave limit. The same argument implies that f does not have much momentum dependence. For the most part this statement is true and f can be replaced by $f(k = 0)$; however in the presence of a scattering resonance, f depends strongly on k. These resonances are of immense experimental importance.
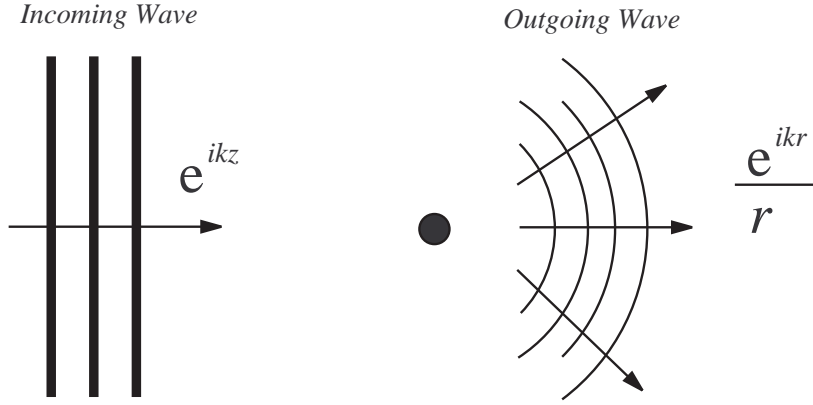
Figure F.1: Generic Scattering Geometry. An incoming plane wave e^{ikz} reflects off a small impurity.

It is worth mentioning that resonant scattering in higher momentum channels ("shape resonances"), can lead to angular dependence of f in the long wavelength limit. These resonances play no roles in current alkali gas experiments.

F.1.2 T-matrix

There are two problems in scattering theory. First, relating the scattering amplitude to the scattering potential, and second, relating the properties of the system to the scattering amplitude. The first problem amounts to solving the Schrödinger equation in the presence of the impurity, with the boundary condition that the incoming wave is e^{ikz}. Generically solving this equation requires the use of computers, but in principle is solvable to arbitrary precision.

As an alternative to computers, one can also use perturbation theory to solve the Schrödinger equation. For realistic atomic potentials perturbation theory is not going to work well. Nevertheless it is still useful to formally develop the scattering amplitude as a sum of terms, each one containing higher powers of V. One can then think of the scattered wavefunction as coming from multiple scattering from the impurity.

The standard approach to developing the perturbation series is to write the Schrödinger equation in integral form. Formally I write

$$\psi = \phi - \frac{1}{H_0 - E}V\psi, \tag{F.2}$$

where $\phi = e^{ikz}$ is the incident wave function, V is the scattering potential, $E = k^2/2m$ is the energy of the state, and $(H - E)^{-1}$ is the Green's function for the free

167

Schrödinger equation. Applying $H_0 - E$ to Eq. (F.2), one arrives at

$$(H_0 - E)\psi = -V\psi, \tag{F.3}$$

which is the conventional Schrödinger equation.

As can be verified directly, in momentum space and in real space, the Green's functions are given by

$$\langle q|\frac{1}{H-E}|q'\rangle = \frac{(2\pi)^3\delta^3(q-q')}{q^2/2m - E} \tag{F.4}$$

$$\langle r|\frac{1}{H-E}|r'\rangle = \frac{m}{2\pi}\frac{\exp(ik|r-r'|)}{|r-r'|}, \tag{F.5}$$

where $E = k^2/2m$. On physical grounds, I have chosen outgoing boundary conditions in Eq. (F.5). This latter result is only true in three dimensions. Getting away from my schematic notation, one writes Eq. (F.2) in one of two forms,

$$\psi(\mathbf{k}') = (2\pi)^3\delta^3(k\hat{\mathbf{z}} - \mathbf{k}') - 2m\int\frac{d^3q}{(2\pi)^2}\frac{V(k'-q)}{q^2 - (k')^2}\psi(\mathbf{q}), \tag{F.6}$$

$$\psi(\mathbf{r}) = e^{ikz} - \frac{m}{2\pi}\int d^3r'\frac{e^{ik|\mathbf{r}-\mathbf{r}'|}}{|\mathbf{r}-\mathbf{r}'|}V(r')\psi(r'), \tag{F.7}$$

The first equation is in momentum space, the second in real space. In this Section I only consider the real space equation (F.7), though later I will focus on (F.6). For simplicity I assume that $V(r)$ falls off over a lengthscale r_0. Longer range potentials can be treated, but such analysis is not particularly important for discussing neutral atoms.

In the far field, $r \gg r_0$, one can expand the difference $|\mathbf{r} - \mathbf{r}'|$ in the integral, to arrive at the equation

$$\psi(r) = e^{ikz} - \frac{m}{2\pi}\frac{e^{ikr}}{r}\int d^3r'\, e^{ik\hat{\mathbf{r}}\cdot\mathbf{r}'}V(r')\psi(r'). \tag{F.8}$$

Comparison with Eq. (F.1) gives an expression for the scattering amplitude,

$$f(k,\hat{r}) = -\frac{m}{2\pi}\int d^3r'\, e^{ik\hat{\mathbf{r}}\cdot\mathbf{r}'}V(r')\psi(r'). \tag{F.9}$$

One generates a perturbative solution to Eq. (F.7) by a simple iterative scheme. One starts by setting $\psi(r) = e^{ikz}$ on the right hand side of (F.7). This first order result is known as the Born approximation to scattering. This procedure is iterated by substituting the new value of ψ into the right hand side. In a schematic notation, one has

$$\psi = \left(1 - \frac{1}{H_0 - E}V + \frac{1}{H_0 - E}V\frac{1}{H_0 - E}V + \frac{1}{H_0 - E}V\frac{1}{H_0 - E}V\frac{1}{H_0 - E}V + \cdots\right)\phi. \tag{F.10}$$
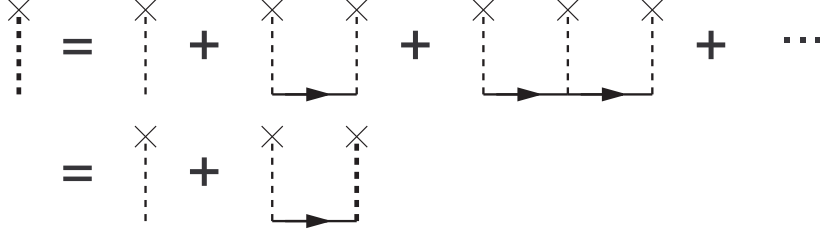
Figure F.2: Diagrammatic representation of the T-matrix equation. The T-matrix, designated by a dark dashed line connected to an "X", comes from multiple scattering off the potential. The soft dashed lines represent bare potential scattering.

This expression is compactly written as

$$\psi = \psi_0 - \frac{1}{H_0 - E}T\psi_0, \tag{F.11}$$

where the T-matrix is defined by

$$T = V + V\frac{1}{H_0 - E}V + V\frac{1}{H_0 - E}V\frac{1}{H_0 - E}V + \cdots \tag{F.12}$$

$$= V + V\frac{1}{H_0 - E}T. \tag{F.13}$$

A diagrammatic representation of Eq. (F.12) is shown in Fig. F.2. The scattering amplitude is then related to the on-shell T-matrix, by the expression

$$f(k) = \frac{-m}{2\pi\hbar^2}T(k). \tag{F.14}$$

For the many-body problem, or for the problem of scattering off many impurities, one in principle needs the off shell T-matrix.

To fully appreciate the structure of the T-matrix, one must go beyond s-wave scattering, and consider the generic scattering amplitude $f(\hat{k}, \hat{r}, k)$ defined by the asymptotic form

$$\psi(r) = e^{i\mathbf{k}\cdot\mathbf{r}} + f(k, \hat{k}, \hat{r})\frac{e^{ikr}}{r}. \tag{F.15}$$

The scattering amplitude is a function of the direction of the incoming wave $\hat{k}$, the direction of the outgoing wave $\hat{r}$, and the energy of the scattering particle, $k^2/2m$.

The T-matrix similarly is a function of three variables,

$$T(\mathbf{k}, \mathbf{k}', q) \equiv \langle k'|T(E = q^2/2m)|k\rangle \tag{F.16}$$

$$= \langle k'|V|k\rangle + \langle k'|V\frac{1}{H_0 - E}T|k\rangle. \tag{F.17}$$

The variables are the incoming momentum $\mathbf{k}$, the outgoing momentum $\mathbf{k}'$, and the energy $E = q^2/2m$. If one sets $|k| = |k'| = q$, one finds

$$f(k, \hat{k}, \hat{r}) = -\frac{m}{2\pi}T(k\hat{k}, k\hat{r}, k). \tag{F.18}$$

The off mass shell terms of T give information about the non-asymptotic behavior of the scattering. If one throws away all this information, such as one does in the pseudo-potential approximation, one finds that the T-matrix is independent of the momenta $\mathbf{k}$ and $\mathbf{k}'$, and is only a function of the energy q

$$T(\mathbf{k}, \mathbf{k}', q) = T(q) = \frac{-2\pi}{m} f(q). \tag{F.19}$$

This approximation will clearly break down when the momenta are of atomic dimensions.

F.1.3 Phase shifts

In the limit of s-wave scattering, the impurity only sees the part of the incoming wave that is spherically symmetric. One finds the spherically symmetric part of the incoming wave by integrating over the solid angle,

$$\int \frac{d\Omega}{4\pi} e^{ikz} = \frac{1}{2} \int_{-1}^{1} d\cos\theta \, e^{ikr\cos\theta} \tag{F.20}$$

$$= \frac{\sin(kr)}{kr}. \tag{F.21}$$

This wave has components which are propagating towards and away from the impurity, as is seen by representing the wavefunction as

$$\frac{\sin(kr)}{kr} = \frac{-1}{2i} \frac{e^{-ikr}}{kr} + \frac{1}{2i} \frac{e^{ikr}}{kr}. \tag{F.22}$$

The scattering can only affect the outgoing wave. Since particles are conserved, the only possible change it can make to the outgoing wave (in the asymptotic region) is to provide a phase shift, δ,

$$e^{ikr} \rightarrow e^{i(kr+2\delta)} = e^{ikr} + 2ie^{ikr}e^{i\delta}\sin\delta. \tag{F.23}$$

Thus, in complete generality, one can write the scattered wavefunction as

$$\psi(r) = e^{ikz} + \frac{e^{i\delta}\sin\delta}{k} \frac{e^{ikr}}{r}. \tag{F.24}$$

Comparing with Eq. (F.1) one arrives at an expression for the scattering amplitude in terms of the phase shift.

$$f(k) = e^{i\delta}\sin\delta/k. \tag{F.25}$$

F.1.4 Meaning of the scattering amplitude and the phase shift

On a microscopic level, δ has a clear meaning. It is the phase shift of the scattered wave, relative to what it would be without the impurity. In the following section I will show how this phase shift can be simply related to the density of states in the presence of the impurity. The scattering amplitude, f, is the amplitude that the particles are scattered. That is, $\sigma = 4\pi|f|^2$ is the number of scattered particles per unit flux of incoming particles. The cross section σ is the area that a classical target would have to have for the scattering probability to be the same.

An equivalent way to understand f is to look at the equation

$$\psi = e^{ikz} + f\frac{e^{ikr}}{r}. \tag{F.26}$$

The length f gives the distance from the impurity at which the flux of scattered particles equals the flux of incoming particles.

For small δ Eq. (F.25) can be expanded, and one finds that $f \approx \delta/k$.

F.2 Relationship of the scattering problem with the standing wave problem

In elementary quantum mechanics, the first problem one learns to solve is the "particle in a box." One takes the Hamiltonian $-\hbar^2\nabla^2/2m$, diagonalizes it via a Fourier series, and finds the complete spectrum. Later one learns how to do scattering problems, where one is not interested in the spectrum (which is continuous), but rather on transmission and reflection amplitudes. The relationship between these two problems is rarely completely clear.

One can connect the scattering problem and the standing wave problem by looking at scattering in a finite size box. The three dimensional case (when limited to the s-wave channel) is actually simpler than the one dimensional problem, so I will concentrate on it. I first "solve" the standing wave problem. Consider a small impurity with a potential $V(r)$ in the middle of a big spherical box of radius R. I wish to find the eigenvalues of the Schrödinger equation,

$$\left[\frac{-\nabla^2}{2m} + V(r)\right]\psi(\mathbf{r}) = E\psi(\mathbf{r}), \tag{F.27}$$

with the boundary condition that $\psi(R) = 0$. I take $\hbar = 1$, and restrict myself to spherically symmetric states. By substituting $\psi(r) = u(r)/r$, one can write s-wave

sector of the Schrödinger equation as

$$\left[\frac{-1}{2m}\frac{d^2}{dr^2} + V(r)\right]u(r) = Eu(r), \tag{F.28}$$

with the boundary condition $u(0) = u(R) = 0$. For r larger than the range of the potential, one can ignore $V(r)$, and this equation is just a free one dimensional Schrödinger equation. Thus in the asymptotic regime there is some δ such that the solution to (F.28) is $u(r) = \sin(kr + \delta)$. To satisfy the boundary conditions the momentum k must obey $kR + \delta = n\pi$, for some integer n.

Now imagine one performs a scattering experiment on the same potential. One sends in a wave $u(r) \sim e^{-ikr}$, and looks at what comes out. Thus one must solve Eq. (F.28) with the condition that the incoming part of u is $(-1/2i)e^{-ikr}$. Well, we know one solution of Eq. (F.28), which asymptotically is $u(r) = \sin(kr + \delta)$. Multiplying by $-2ie^{i\delta}$, one gets $u(r) = e^{-ikr} - e^{ikr}e^{2i\delta}$. Since solutions to the Schrödinger equation with a given boundary condition are unique, this u must be the scattered wavefunction. Comparing with Eq. (F.23), one sees that the δ which arises in solving the standing wave problem is the same as the δ which appears in the scattering problem. With this relationship one can solve the scattering problem by using the powerful computational techniques which have been developed for ground-state problems (see for example [134]).

F.2.1 Energy shifts

The relationship between scattered states and standing waves gives rise to a very nice graphical construction which allows one to relate the density of states to the phase shifts. Imagine one knows the phase shifts $\delta(k)$ (for example, see Fig. F.3). If one places the system in a box, the only states which obey the boundary conditions have $kR + \delta = n\pi$ for some integer n. Thus the allowed states have a wave vector given by the intersection of the lines $kR + \delta = n\pi$ and $\delta(k)$.

In the absence of an impurity the wave vectors allowed have $kR = n\pi$. Thus the shift in wave vector is $\delta k = -\delta/R$, and the change in the energy of a state is $\delta E = k\,\delta k/m = -\delta\,k/mR$, which is proportional to δ. As a historical note, this result was a point of confusion in the 1950's in the context of the many-body problem [133].

In the limit of large box, it is more convenient to talk about a density of states, rather than the energy of any particular state. Starting from the relation $kR + \delta = n\pi$, one finds that the density of s-wave states in k-space is

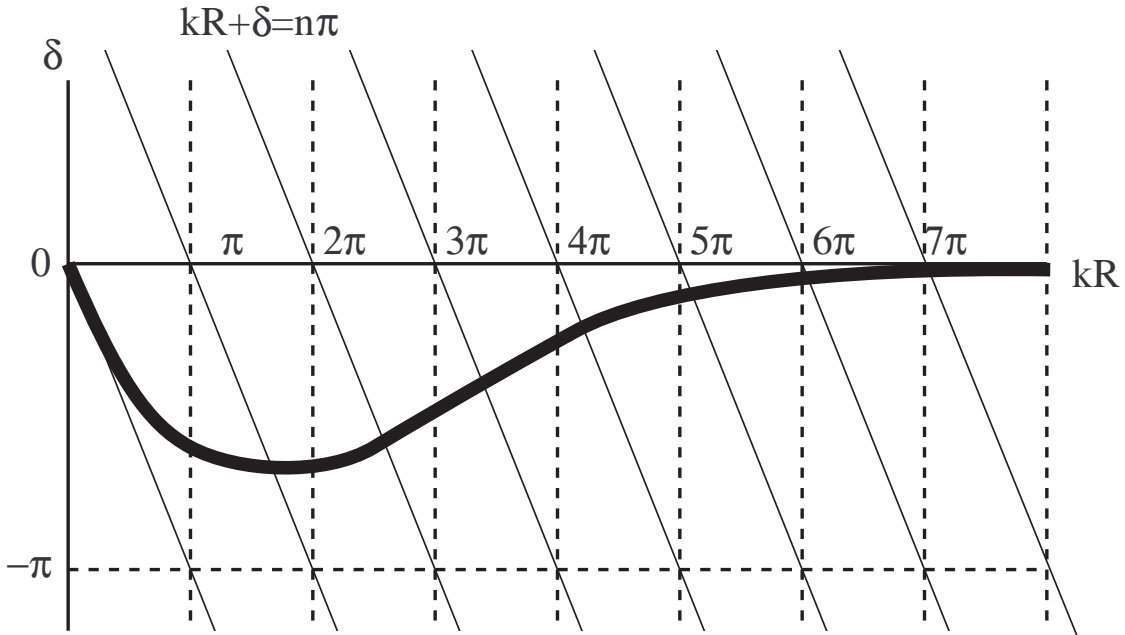$$\frac{\partial n}{\partial k} = \frac{R}{\pi} + \frac{\delta'(k)}{\pi}, \tag{F.29}$$

Figure F.3: Connecting phase shifts and energy shifts. The thick line represents the phase shift $\delta(k)$. In a box, $\sin(kR+\delta) = 0$, so the allowed states lie at the intersection of the thick line and the oblique lines $kR + \delta = 0$. As the box is made larger, the spacing between the oblique lines becomes smaller, and (on an absolute scale) they become more perpendicular to the k axis.

where $\delta'(k)$ is the derivative of δ with respect to k. The first term is the standard density of states in a 1-dimensional box, while the second term is the change in the density of states due to the impurity. Thus one interprets δ/π as the number of extra states with momentum less than k due to the impurity.

If one knows the density of states, then one can calculate For example, consider a spherical "bump" potential as depicted in Fig. F.4. The bump has radius r_0 and height $q^2/2m$. For $k \ll q$, the bump appears to be an infinite barrier, and the density of states should be $\partial n = (R - r_0)/\pi \, \partial k$, which is less than the density of states in the absence of the bump. The missing states have to go somewhere, and they are pushed to momenta near $k = q$. For $k \gg q$, the bump is irrelevant, and the density of states should be that of a free gas, $\partial n = R/\pi \, \partial k$. One should therefore see a density of states like the one in Fig. F.5. After integrating this curve, one arrives at a phase shift δ like the one depicted in Fig. F.6.

As a corollary to the theorem that $\delta(k)/\pi$ is the number of extra states, one has the general result that for a sufficiently well-behaved potential the $k = 0$ the phase shift is equal to π times the number of bound states. Generically $\delta(k \to \infty) = 0$, and the bound states are missing from the continuum.

173
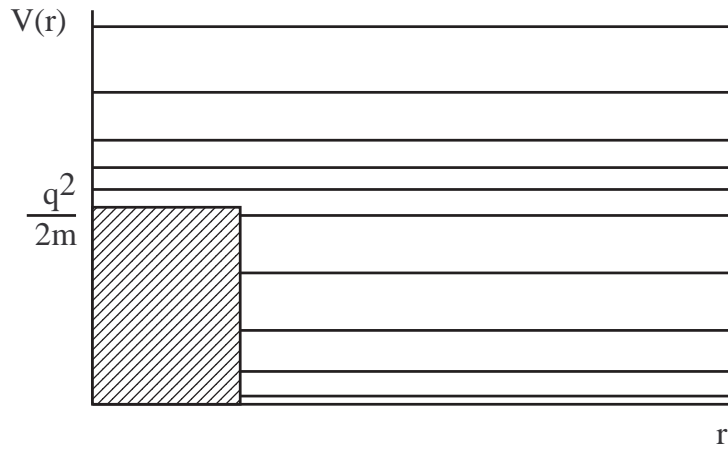
Figure F.4: Energy states for a spherical bump in a box. States are pushed up by the bump
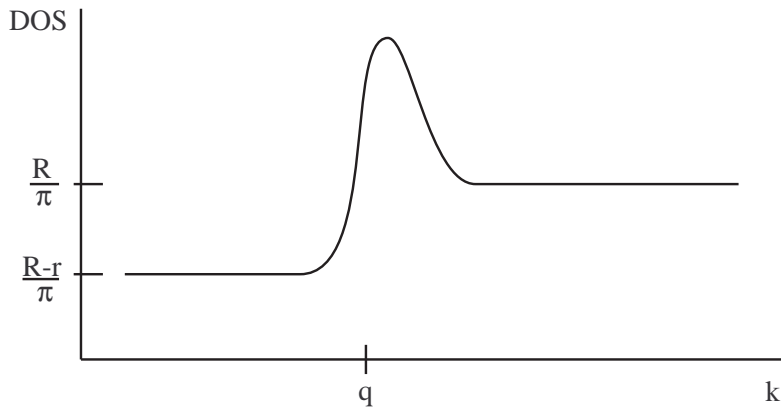
Figure F.5: Density of states for a spherical bump in a box (schematic). The potential has a height of $V_0 = q^2/2m$, and width r.
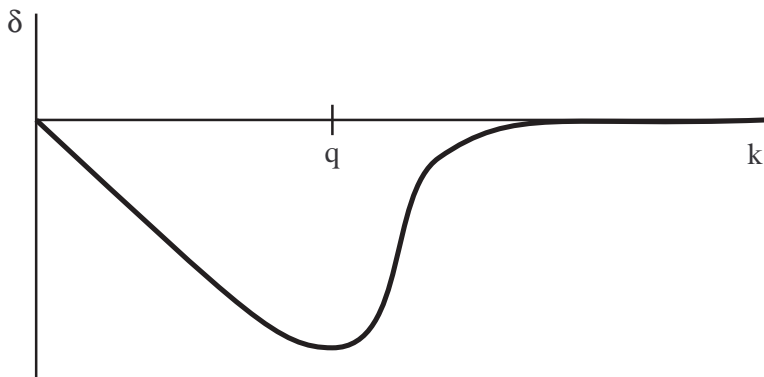

Figure F.6: Phase shift for a spherical bump in a box (schematic). The height of the potential is $q^2/2m$.

F.3   Sample phase shifts

In this section I plot a few illustrative phase shifts.

F.3.1   Hard wall

The simplest scattering potential is a hard wall:

$$V(r) = \begin{cases} \infty & r < r_0 \\ 0 & r > r_0. \end{cases} \tag{F.30}$$

The wavefunction must vanish at the edge of the wall, so $u(r) = \sin(k(r - r_0))$ and $\delta = -kr_0$. This example is pathological in that $\delta \to \infty$ as $k \to \infty$.

F.3.2   Attractive well

A slightly more complicated simple potential is the attractive spherical well,

$$V(r) = \begin{cases} -V_0 & r < r_0 \\ 0 & r > r_0. \end{cases} \tag{F.31}$$

This potential is not realistic but it possesses many of the features of more sophisticated atomic potentials. In particular there are low energy resonances whenever a new bound state enters the well. To find the phase shifts I write the wavefunction as

$$u(r) = \begin{cases} A \sin(k'r) & r < r_0 \\ B \sin(kr + \delta) & r > r_0, \end{cases} \tag{F.32}$$

where $(k')^2/2m - V_0 = k^2/2m$. Continuity of the wavefunction and its derivative are guaranteed by matching the logarithmic derivative at r_0, which gives

$$k' \cot(k'r_0) = k \cot(kr_0 + \delta). \tag{F.33}$$

Solving for δ gives

$$\tan \delta = \frac{k \sin k'r_0 \cos kr_0 - k' \sin kr_0 \cos k'r_0}{k' \cos k'r_0 \cos kr_0 + k \sin kr_0 \sin k'r_0}. \tag{F.34}$$

For different values of V_0 I plot $\delta(k)$ in Fig. F.7. For simplicity I introduce the momentum q, satisfying $V_0 = q^2/2m$, which marks the depth of the well. The most striking feature of these graphs is that when $\cos(qr_0) = 0$, the phase shift at $k = 0$ jumps. This happens because a new bound state enters the well at this point.
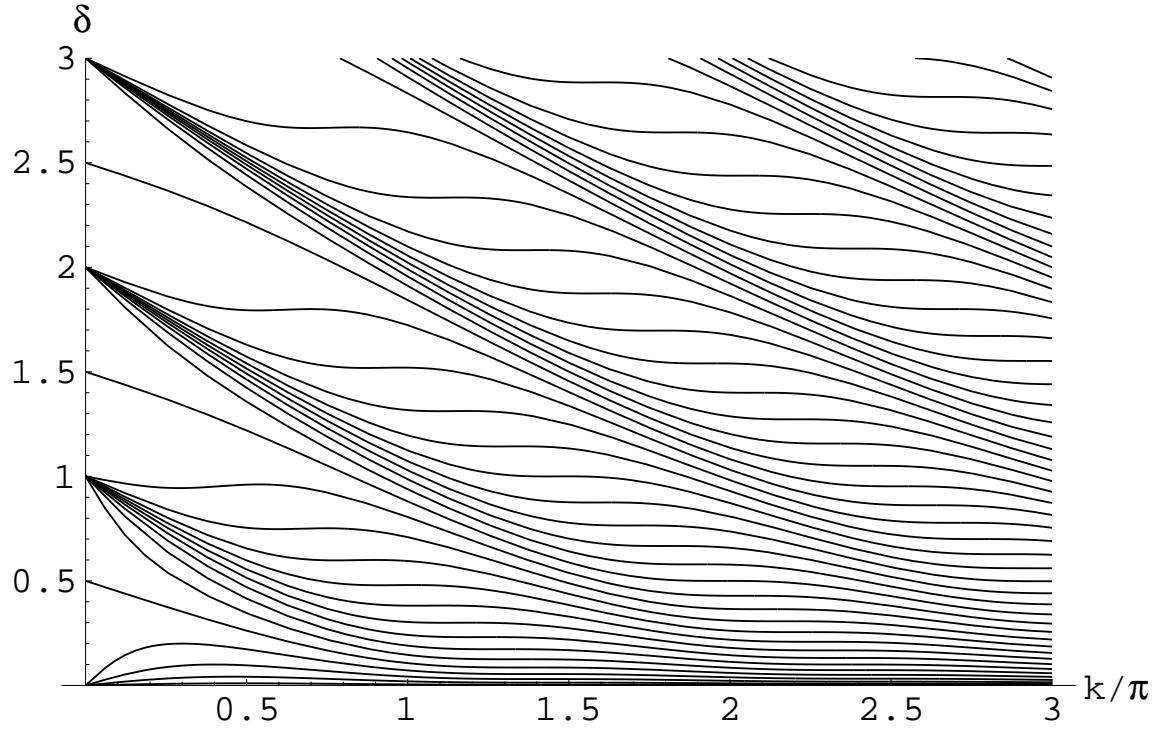
Figure F.7: Phase shifts for a spherical well potential. The depth of the well is $V_0 = q^2/2m$ and its radius is r_0. All momenta are measured in terms of r_0. The various lines show different values of q, each differing by $0.1\pi/r_0$. Resonances occur at $qr_0 = (n + 1/2)\pi$.
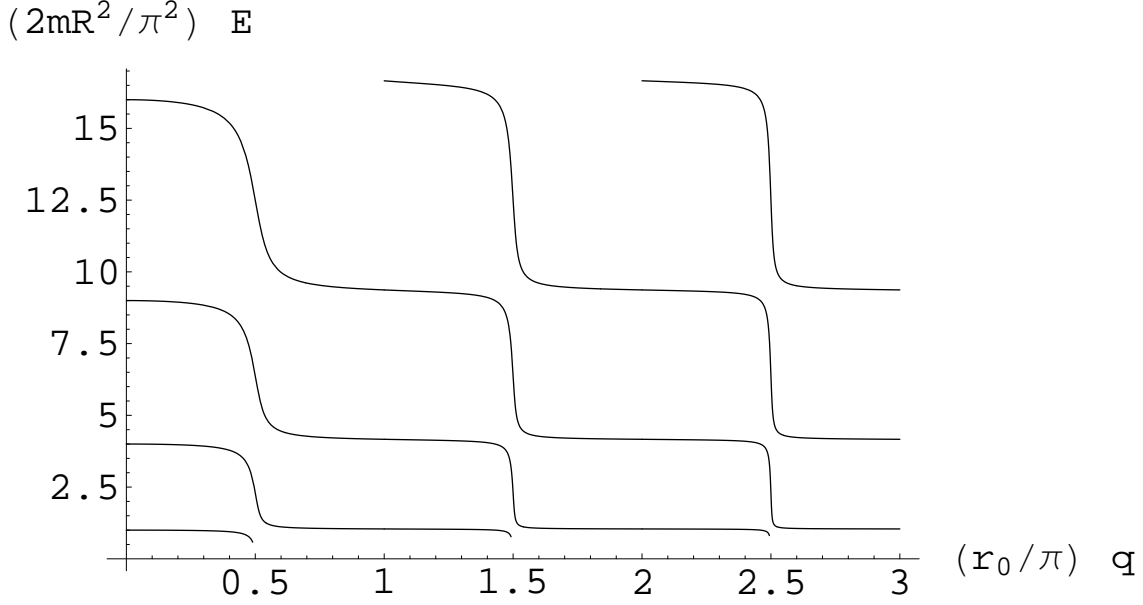
Figure F.8: Energy levels for an attractive well of radius r_0 and depth $V_0 = q^2/2m$ within a box of size R. The energy is measured in terms of the quantization energy of the large box, π^2/mR^2. The horizontal axis shows qr_0/π, a measure of the depth of the well. Resonances occur whenever $qr_0 = (n + 1/2)\pi$, and one of the continuum energy states drops into the well. For this plot $R = 50r_0$. Increasing R_0 makes the jumps sharper.

It is instructive to put this system in a box of size R, and calculate the energy of the first few levels as a function of q. As seen in Fig. F.8, whenever one passes through a resonance, the lowest energy state becomes bound, and the next level replaces it. What is happening is that each line has a fixed number of nodes, and at the resonance one of the nodes moves from outside the well to inside the well, drastically reducing the energy.

F.3.3 Resonant barrier

I next consider a resonant barrier potential, as shown in Fig. F.9,

$$V(r) = \begin{cases} 0 & r < r_0 \\ q^2/2m & r_0 < r < 2r_0 \\ 0 & r > 2r_0. \end{cases} \tag{F.35}$$

As opposed to the attractive well which possesses zero energy resonances, the resonant barrier has finite energy resonances resulting from the quasi-bound states which are
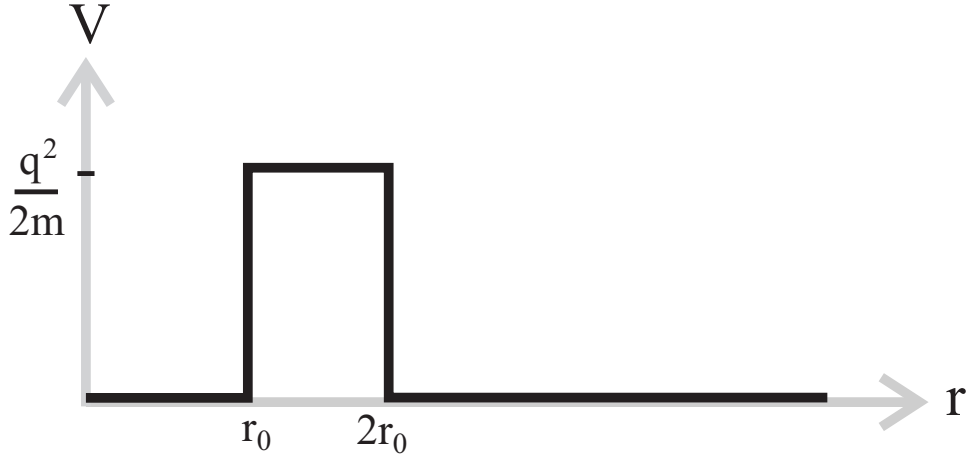
Figure F.9: Resonant barrier potential.

found at momenta where $\sin(kr_0) \approx 0$. At these resonances, one finds an extra state. From our understanding of δ'/π as the density of states, we should have a phase change of π near this momentum. As seen in Fig. F.10, this is indeed the case.

F.4   The pseudopotential

Here I discuss an expansion of the scattering amplitude in powers of kr_0, where r_0 is the length scale of the potential. This expansion takes the form

$$k \cot \delta = -\frac{1}{a_s} + \frac{1}{2}r_e k^2 + \mathcal{O}((r_0 k)^4). \tag{F.36}$$

The parameters a_s and r_e are known as the scattering length and the effective range. I emphasize that (F.36) is an expansion in $r_0 k$, and even when a_s is large, the remaining terms can be small. The pseudopotential approximation amounts to taking only the first term in this expansion.

One derives Eq. (F.36) via a matching argument. The Schrödinger equation obeyed by $u(r) = r\psi(r)$ is

$$\left(\frac{k^2 + \partial_r^2}{2m} - V(r)\right) u = 0. \tag{F.37}$$

For $r \ll r_0$, $V(r)$ dominates over k^2, and one writes

$$u(r) = \chi(r) + \mathcal{O}(k^2), \qquad r \ll r_0, \tag{F.38}$$

where $\chi(r)$ is independent of k. For $r \gg r_0$, the potential $V(r)$ vanishes and u takes on its asymptotic form

$$u(r) = A\sin(kr + \delta), \qquad r \gg r_0. \tag{F.39}$$

178
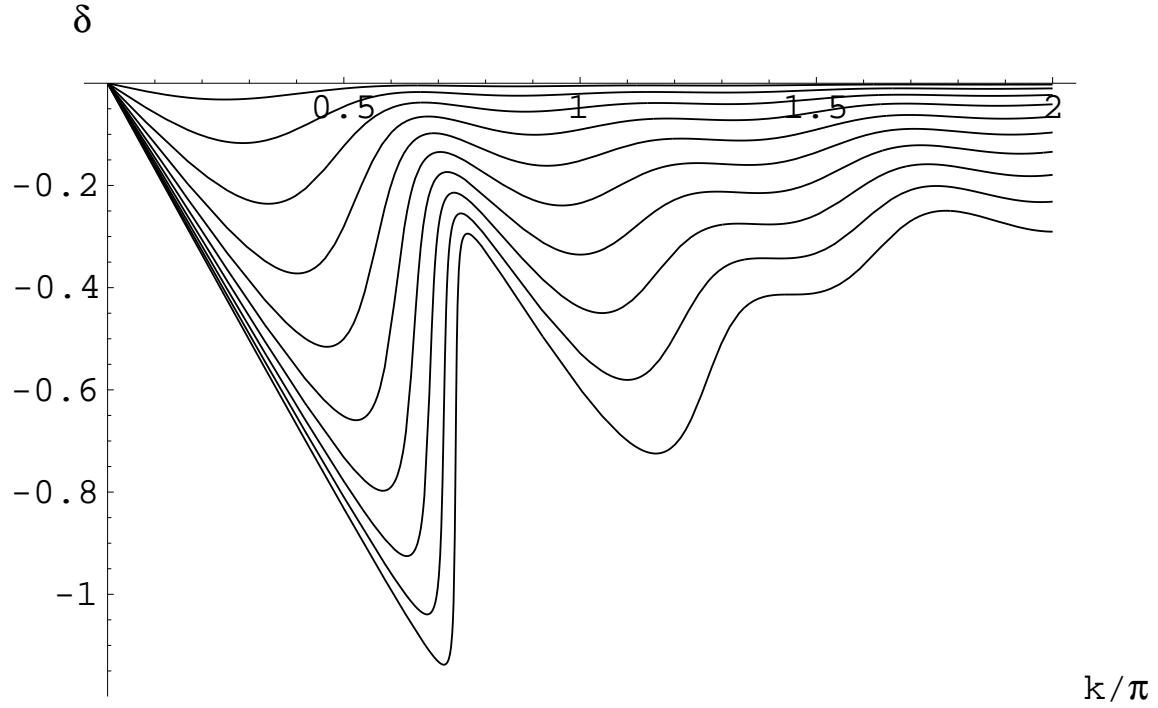
Figure F.10: Phase Shifts $\delta(k)/\pi$ for a resonant barrier potential. The momentum k is measured in units of π/r_0. Each line corresponds to a different barrier height.

I match the logarithmic derivatives at r_0, finding

$$k \cot(k r_0 + \delta) = \chi'/\chi + \mathcal{O}(k^2), \tag{F.40}$$

which gives the desired expansion of $k \cot \delta$ in powers of k^2.

In terms of $\cot \delta$ the scattering amplitude is

$$f = \frac{e^{i\delta} \sin \delta}{k} = \frac{1}{k \cot \delta + ik}. \tag{F.41}$$

So in the pseudo-potential approximation, the scattering amplitude is

$$f = \frac{-a}{1 + ika}. \tag{F.42}$$

For small ak, this looks like a point interaction. For large values of ak, this looks like a long-ranged $1/k$ potential.
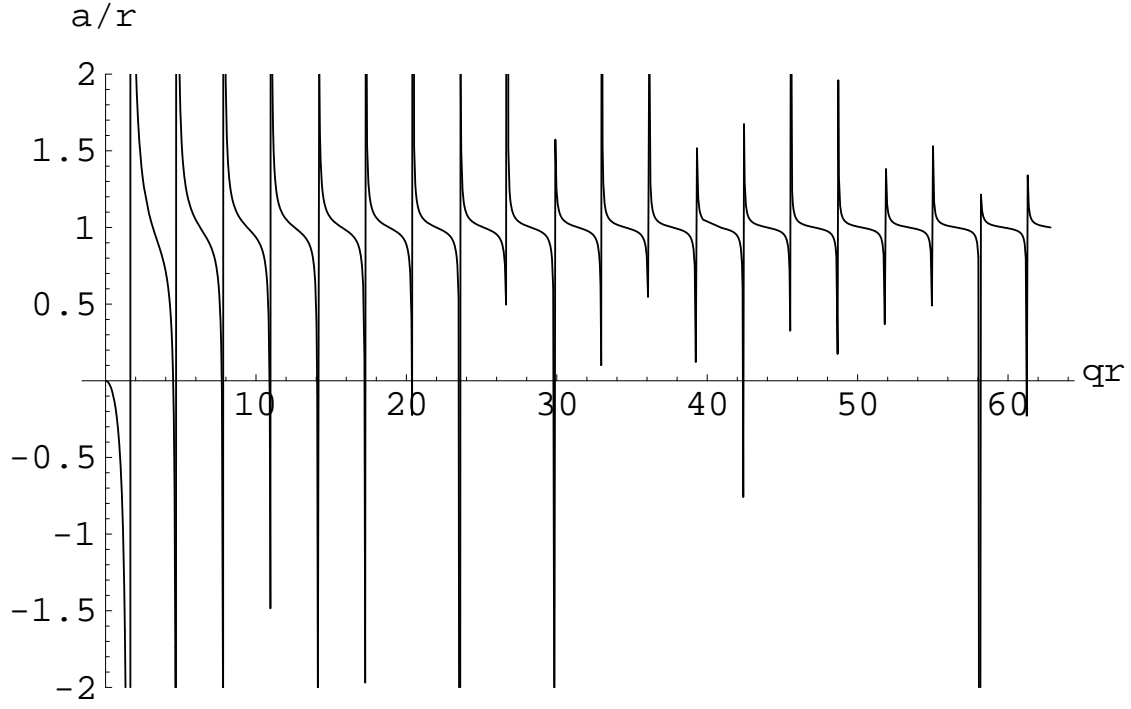
Figure F.11: Scattering length a for a spherical well of radius r and depth $V_0 = q^2/2m$.

F.4.1 The pseudo-potential for an attractive spherical well

As an example, one can expand Eq. (F.34) in powers of k, finding

$$k \cot \delta = \frac{-1}{a_s} + \frac{r_e k^2}{2} \tag{F.43}$$

$$a_s = r_0 - \frac{\tan q r_0}{q} \tag{F.44}$$

$$r_e = (\frac{1}{q} - r_0^2 q) \cos q r_o + r_0 \sin q r_0 + \frac{q^2 r_0^3 \cos^2 q r_0/3}{\sin q r_0 - q r_0 \cos q r_0}. \tag{F.45}$$

The effective range vanishes when a_s diverges. These quantities are plotted in Fig. F.11 and F.12.

F.5 Zero range potentials

For analytic calculations, the simplest potentials one can consider are zero-range potentials. These play an important role in many theoretical works, so it is worth considering them here. Zero range potentials are, by construction, singular. Thus, despite their analytic simplicity, these potentials require taking careful limits.
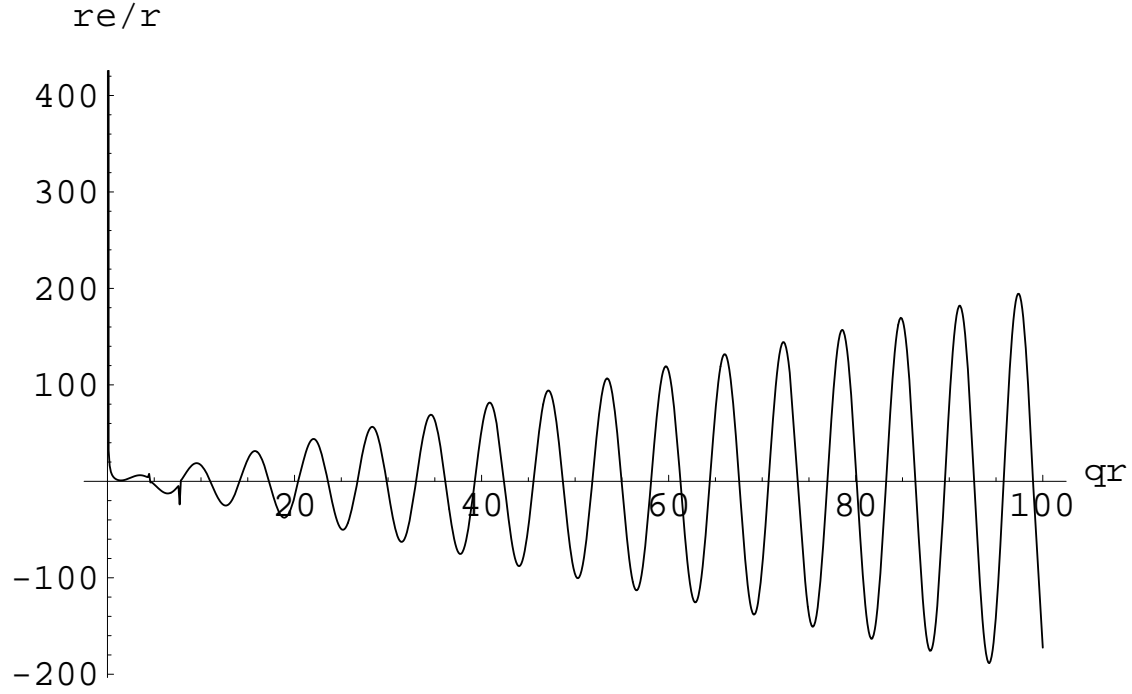
Figure F.12: Effective range re for a spherical well of radius r and depth $V_0 = q^2/2m$.

F.5.1   A structureless point scatterer

Consider a point scatterer with a potential $V(r) = V_0\delta(r - r')$. In momentum space, $V_k = V_0$. Scattering off this potential is described by the T-matrix equation (F.17),

$$T_{kk'}(\omega) = V_{kk'}(\omega + \sum_q V_{kq}G_0(q)T_{qk'}(\omega). \tag{F.46}$$

Since $V_{kk'}$ is independent of the momentum indices, T will also be independent of momentum. Using this result, the T-matrix is

$$T(\omega) = \frac{V_0}{1 - V_0\Theta}, \tag{F.47}$$

where Θ is given by

$$\Theta = \sum_k G_0(q, \omega) = \sum_q \frac{1}{\omega - q^2/2m}. \tag{F.48}$$

Replacing the sum with an integral,

$$\Theta = \frac{V}{(2\pi)^3} \int \frac{d^3q}{\omega - q^2/2m} \tag{F.49}$$

$$= \frac{V}{2\pi^2} \int \frac{dq\, q^2}{\omega - q^2/2m}, \tag{F.50}$$

181

one notices that the sum is ultraviolet divergent. This divergence is a consequence of the short range of the potential, and reflects the fact that a point interaction is unphysical. Any real potential will have a finite range, which will introduce a large q cutoff, Λ in this integral. The integral is readily evaluated to be

$$\Theta = \Theta_0 - \frac{imV\sqrt{2m\omega}}{2\pi} \tag{F.51}$$

$$\Theta_0 = -\frac{Vm\Lambda}{\pi^2}. \tag{F.52}$$

The T-matrix is then of the form

$$T = \frac{2\pi}{m}\frac{a_s}{1 + ia_s\sqrt{2m\omega}}, \tag{F.53}$$

where the scattering length is

$$a_s \equiv \frac{m}{2\pi}\frac{V_0}{1 - V_0\Theta_0}. \tag{F.54}$$

Note that if one takes the cutoff Λ to infinity at fixed V_0, then the scattering length vanishes. In this sense, there is no scattering off a delta-function potential in three dimensions. Only by scaling V_0 with Λ can a non-zero a_s be produced. This scaling of V_0 with Λ is the simplest example of *renormalization* which can be discussed. As previously discussed, a T-matrix of the form (F.53) gives a phase shift

$$\delta = \arg(T) = -\arctan(a_s k). \tag{F.55}$$

F.5.2   Scattering from a zero-range bound state

A simple generalization of the structureless point scatterer is to associate a bound state with the impurity. In such a case, the scattering is energy dependent, and

$$V_k = V_0 + \frac{|\alpha|^2}{\omega - \epsilon}, \tag{F.56}$$

where V_0 is a static potential at the origin, α is an amplitude for entering the bound state, and ϵ is the energy of the bound state. To illustrate the role of the bound state I set $V_0 = 0$, in which case

$$T = \frac{|\alpha|^2}{\omega - E + i(m/2\pi)|\alpha|^2\sqrt{2m\omega}}. \tag{F.57}$$

The energy E is

$$E = \epsilon + |\alpha|^2\Theta_0. \tag{F.58}$$

182

For E to be finite as $\Lambda \to \infty$ one must scale ϵ with Θ_0.

The T-matrix (F.57) leads to a phase shift of the form

$$\cot(\delta) = -\frac{1}{a_s k} + r_{\text{eff}} k^2 / 2, \tag{F.59}$$

where

$$a_s = \frac{-m|\alpha|^2}{2\pi E} \tag{F.60}$$

$$r_{\text{eff}} = \frac{-2\pi}{m^2 |\alpha|^2}. \tag{F.61}$$

A resonance occurs when $E = 0$.

The Green's function for the bound state is $T/|\alpha|^2$. Thus E *is* the energy of the bound. When $E > 0$, this state has a finite lifetime

$$\frac{1}{\tau} = \frac{m}{2\pi} |\alpha|^2 \sqrt{2mE}, \tag{F.62}$$

which is the result one would expect from Fermi's golden rule.

F.6 Feshbach resonances

As is clear from the above examples, tuning a resonance near zero energy has dramatic consequences for atomic scattering properties. Experimentally such tuning is carried out by applying magnetic fields. The field induced resonance is known as a Feshbach resonance.

The underlying principle is that due to the hyperfine interaction, two colliding atoms can form a bound state whose magnetic moment is not equal to the sum of the magnetic moments of the incoming atoms (total angular momentum is conserved, not total magnetic moment). Consequently, when a magnetic field is applied, the Zeeman shift of the bound state can be different from the shift of the scattering states. Thus the energy of the bound state is tunable. When its energy is set to zero one is at the resonance. The scattering properties near the resonance are described well by the model of Section F.5.2.

F.7 Multiple scattering

I now turn to the question of scattering off several small impurities which are much farther apart than the range of their potentials. As detailed in Section F.4, low energy

scattering off an individual impurity is described by the scattering length a_s. Letting n denote the density of scatterers, I am particularly interested in the limit where na_s^3 is of order 1. In this limit one encounters localization effects, and the scattering off of one impurity depends on the presence of all others.

F.7.1 Elementary approach

In this Section I frame the problem in terms of elementary quantum mechanics. Imagine that one has static impurities at positions $\mathbf{r_1}, \mathbf{r_2}, \ldots, \mathbf{r_n}$. The phase shifts for scattering off any of these impurities is $\delta_0(k)$. In a scattering experiment, the asymptotic wavefunction will be

$$\psi(r) = e^{ikz} + \sum_i f_i \frac{e^{ik|r-r_i|}}{|r - r_i|}, \tag{F.63}$$

where the f_i's will be independent of space. This wavefunction should be good, except on atomic distances close to individual impurities. Comparing with Eq. (F.1), the scattering amplitude for scattering from the collection of impurities is

$$f(k, \hat{r}) = \sum_i f_i e^{ik\mathbf{r_i} \cdot \hat{\mathbf{r}}}. \tag{F.64}$$

The s-wave component of this scattering amplitude is

$$f_s(k) = \int \frac{d\Omega}{4\pi} f(k) = \sum_i f_i \frac{\sin kr_i}{kr_i}. \tag{F.65}$$

In particular, when $kr_i \ll 1$ then

$$f_s(k) = \sum_i f_i. \tag{F.66}$$

My goal is to calculate the phase shift δ given by

$$f_s = \frac{e^{i\delta} \sin \delta}{k}. \tag{F.67}$$

I now determine the f_i's via the restriction that at each impurity, the phase shift is δ_0. Once we know f_i we know f. Near the ith impurity, the spherically symmetric part of ψ is defined by

$$\psi_i^{(s)}(|\mathbf{r} - \mathbf{r_i}|) = \int \frac{d\Omega'}{4\pi} \psi(\mathbf{r} = \mathbf{r'} + \mathbf{r_i}), \tag{F.68}$$

where $d\Omega'$ is a solid angle with respect to the variable r', which is centered at the impurity. The integration is straight forward and one finds

$$\psi_i^{(s)}(r - r_i) = \left(e^{ikz_i} + \sum_{j,j \neq i} f_j \frac{e^{ik|r_i - r_j|}}{|r_i - r_j|} \right) \frac{\sin k|r - r_i|}{k|r - r_i|} + f_i \frac{e^{ik|r - r_i|}}{|r - r_i|}. \tag{F.69}$$

I will use the symbol A_i for the term in large parentheses. We know that this term must have the form

$$\psi_i^{(s)}(r - r_i) = \frac{\sin(k|r - r_i| + \delta_0)}{k|r - r_i|}. \tag{F.70}$$

Equating these two expressions, one arrives at

$$f_i = A_i \frac{e^{i\delta_0} \sin \delta_0}{k}. \tag{F.71}$$

Using this expression in the definition of A_i one finds that A_i satisfies the following matrix equation,

$$\left(\delta_{ij} - e^{i\delta_0} \sin \delta_0 \frac{e^{ik|r_i - r_j|}}{k|r_i - r_j|} \right) A_j = e^{ikz_j}. \tag{F.72}$$

I denote the matrix on the left hand side of this equation by $1 - g$. Formally inverting this matrix gives

$$\begin{pmatrix} A_1 \\ \vdots \\ A_n \end{pmatrix} = \frac{1}{1 - g} \begin{pmatrix} e^{ikz_1} \\ \vdots \\ e^{ikz_n} \end{pmatrix}. \tag{F.73}$$

The total scattering amplitude f is then

$$f(k, \hat{k}, \hat{r}) = \frac{e^{i\delta_0} \sin \delta_0}{k} \begin{pmatrix} e^{-ik\hat{r} \cdot \mathbf{r_1}} & \cdots & e^{-ik\hat{r} \cdot \mathbf{r_n}} \end{pmatrix} \frac{1}{1 - g} \begin{pmatrix} e^{ik\hat{k} \cdot \mathbf{r_1}} \\ \vdots \\ e^{ik\hat{k} \cdot \mathbf{r_n}} \end{pmatrix} \tag{F.74}$$

$$= \frac{e^{i\delta_0} \sin \delta_0}{k} \sum_{ij} e^{ik(\hat{k} \cdot \mathbf{r_i} - \hat{r} \cdot \mathbf{r_j})} \left(\frac{1}{1 - g} \right)_{ij}. \tag{F.75}$$

Formally we are now done. If $kr_i \ll 1$ we neglect the e^{ikr_i}'s and get

$$e^{i\delta} \sin \delta = e^{i\delta_0} \sin \delta_0 \sum_{ij} \left(\frac{1}{1 - g} \right)_{ij}. \tag{F.76}$$

In this same approximation

$$g_{ij} = \begin{cases} \frac{e^{i\delta_0} \sin \delta_0}{k|r_i - r_j|} & i \neq j \\ 0 & i = j. \end{cases} \tag{F.77}$$

185

In the pseudo-potential approximation,

$$e^{i\delta_0} \sin \delta_0 = \frac{-a_s k}{1 + i a_s k}. \tag{F.78}$$

It is useful to study the structure of $(1-g)^{-1}$. The matrix g has the property that g_{ij} is a function only of the distance $|r_i - r_j|$, and is essentially a scattering amplitude times a propegator. One graphically thinks of g_{ij} as a directed line connecting impurity i to impurity j. Then $((1-g)^{-1})_{ij}$ is the sum over all paths connecting i to j.

F.7.2 T-matrix approach

With less work (but using more machinery) one can derive the results as the last Section by directly calculating the T-matrix, defined by

$$T = V + V \frac{1}{H_0 - E} T. \tag{F.79}$$

In the present case, $V = \sum_i V_i$ is the sum of the potentials for each scatterer. If one defines T_i as the sum of scattering off an individual impurity,

$$T_i = V_i + V_i \frac{1}{H_0 - E} T_i, \tag{F.80}$$

then T is given by a sum over all paths between scatters of T_i's with propegators between them,

$$T = \sum_i T_i + \sum_{i \neq j} T_i \frac{1}{H_0 - E} T_j + \cdots , \tag{F.81}$$

$$= \sum_i T_i + \sum_{ij} T_i (1 - \delta_{ij}) \frac{1}{H_0 - E} T_j + \cdots . \tag{F.82}$$

I introduce a matrix G_{ij} by

$$G_{ij} = (1 - \delta_{ij}) \frac{1}{H_0 - E} T_j, \tag{F.83}$$

so that the T-matrix is formally

$$T = \sum_{ij} T_i \left(\frac{1}{1 - G} \right)_{ij}. \tag{F.84}$$

To go any farther one needs to choose a basis. The most convenient basis for the current problem is in momentum space. If we treat the T_i's within the pseudo-potential approximation, then

$$T_i(k, k', q) = \langle k' | T_i(E = q^2/2m) | k \rangle = e^{i(k-k')r_i} \left(\frac{-2\pi}{mq} e^{i\delta_0} \sin \delta_0 \right). \tag{F.85}$$

For notational simplicity, I use the symbol x for the parentheses. The operator $T_i(H_0 - E)^{-1}T_j$ is evaluated by inserting a resolution of the identity

$$\langle k'|T_i(H_0 - E)^{-1}T_j|k\rangle = \int \frac{d^3\bar{k}}{(2\pi)^3} T(k, \bar{k}, q) \frac{2m}{\bar{k}^2 - q^2} T(\bar{k}, k', q) \qquad (F.86)$$

$$= x^2 e^{i(kr_j - k'r_i)} \frac{m}{2\pi} \frac{e^{iq|r_i - r_j|}}{q|r_i - r_j|}. \qquad (F.87)$$

In Eq. (F.81) all of the $e^{i\bar{k}r_i}$'s cancel, except for the one at the end and the one at the beginning. Thus T is given by

$$T(k, k', q) = x \sum_{ij} e^{i(kr_i - k'r_j)} M_{ij}(q), \qquad (F.88)$$

where $M_{ij}(q)$ is the sum of all paths going from i to j, each segment of the path going from impurity μ to impurity ν contributing $x(m/2\pi)e^{iq|r_\mu - r_\nu|}/(q|r_\mu - r_\nu|)$, which is readily seen to be identical to (F.75).

F.7.3 Two scatterers

Given the positions $r_1, r_2, \ldots, r_n$ of the scatterers we can now calculate δ in terms of δ_0. The simplest example of this procedure uses two scatterers. The matrix g_{ij} is given by

$$g = \begin{pmatrix} 0 & x \\ x & 0 \end{pmatrix} \qquad (F.89)$$

$$x = \frac{e^{ik|r_1 - r_2|}}{k|r_1 - r_2|} \sin \delta_0 e^{i\delta_0} \qquad (F.90)$$

$$\approx \frac{-a_s(1 + ikr)/r}{1 + ika_s}, \qquad (F.91)$$

where $r \equiv |r_1 - r_2|$ and a_s is the scattering length for scattering off a single impurity. Since g is proportional to a Pauli matrix, $g^2 = x^2$ is proportional to the identity. Thus $(1 - g)^{-1}$ is $(1 - x^2)^{-1}(1 + g)$. The scattering amplitude is then

$$f = \frac{e^{i\delta_0} \sin \delta_0}{k} \sum_{ij} \left(\frac{1}{1 - g} \right)_{ij} \qquad (F.92)$$

$$= \frac{e^{i\delta_0} \sin \delta_0}{k} \frac{1}{1 - x^2} (2 + 2x) \qquad (F.93)$$

$$= \frac{-\left(\frac{2a_s}{1 + a_s/r} \right)}{1 + i \left(\frac{2a_s}{1 + a_s/r} \right) k}. \qquad (F.94)$$

187

The last line follows from some simple algebraic rearrangements. The end result is that the scattering from two impurities looks like scattering from a single one with an effective scattering length

$$a_2 = \frac{2a_s}{1 + a_s/r}. \tag{F.95}$$

For $a_s \ll r$ the scattering is just additive. For $a_s \gg r$ the effective scattering length is cut off by the distance between the two impurities, and $a_2 \to 2r$.

It should be clear from this result that when particles are packed closer than their scattering lengths one cannot consider the scattering from each particle independently.

F.7.4 Low density limit

In the low density limit, $na_s^3 \ll 1$, the matrix elements g_{ij} are small, and the single scattering dominates. The phase shift for scattering off the collection of impurities is then additive, $\delta = N\delta_0$.

F.8 Scattering in the many body problem

This thesis is concerned with clouds of interacting atoms, described via a density n and scattering length a_s. In the dilute limit $na_s^3 \ll 1$, multiple scattering is suppressed, and the interaction can be treated perturbatively (see Chapter 2 and Appendix E). Most alkali gas experiments are in this regime. By using Feshbach resonances one should be able to tune the scattering length so that na_s^3 is no longer small. Understanding this strongly interacting regime is a major challenge facing the cold gas community.

References

[1] M. H. Anderson, J. R. Ensher, M. R. Matthews, C. E. Wieman, and E. A. Cornell, Science **269**, 198 (1995).

[2] K. B. Davis, M.-O. Mewes, M. R. Andrews, N. J. van Druten, D. S. Durfee, D. M. Kurn, and W. Ketterle, Phys. Rev. Lett. **75**, 3969 (1995).

[3] C. C. Bradley, C. A. Sackett, J. J. Tollett, and R. G. Hulet, Phys. Rev. Lett. **75**, 1687 (1995).

[4] M. Toda, R. Kubo, and N. Saito *Statistical physics*, Springer-Verlag, 1991.

[5] N. Wilkin, J. Gunn, and R. Smith, Phys. Rev. Lett. **80**, 2265 (1998).

[6] P. Nozières, in *Bose-Einstein Condensation*, edited by A. Griffin, D. W. Snoke, and S. Stringari (Cambridge University Press, 1995).

[7] T.-L. Ho and S. K. Yip, Phys. Rev. Lett. **84**, 4031 (2000).

[8] R. Bowers, and T. Deeming *Astrophysics II; Interstellar Matter and Galaxies* (Jones and Bartlett, Sudbury, MA, 1984).

[9] H.-J. Miesner, D. M. Stamper-Kurn, J. Stenger, S. Inouye, A. P. Chikkatur, and W. Ketterle, Phys. Rev. Lett. **82**, 2228 (1999).

[10] K. W. Madison, F. Chevy, W. Wohlleben, J. Dalibard, Phys. Rev. Lett. **84**, 806 (2000).

[11] C. Liu, Z. Dutton, C. H. Behroozi, L. V. Hau, Nature **409**, 490 (2001).

[12] D. F. Phillips, A. Fleischhauer, A. Mair, R. L. Walsworth, and M. D. Lukin, Phys. Rev. Lett. 86, 783 (2001).

[13] F. Dalfovo, S. Giorgini, L. P. Pitaevskii, and S. Stringari, Rev. Mod. Phys. **71**, 463 (1999).

[14] C. J. Pethick and H. Smith, *Bose-Einstein Condensation in Dilute Gases* (Cambridge University Press, to be published).

[15] A. S. Parkin and D. F. Walls, Phys. Rep. **303**, 1 (1998).

[16] A. J. Leggett, Rev. Mod. Phys. **73**, 307 (2001).

[17] E. Cornell, J. Res. Nat. Inst. Stand. Technol. **101**, 419 (1996).

[18] G. Baym and C. J. Pethick, Phys. Rev. Lett. **76**, 6 (1996).

[19] D. G. Fried, T. C. Killian, L. Willmann, D. Landhuis, S. C. Moss, D. Kleppner, and T. J. Greytak, Phys. Rev. Lett. **81**, 3811 (1998).

[20] F. P. Dos Santos, J. Lèonard, J. Wang, C. J. Barrelet, F. Perales, E. Rasel, C. S. Unnikrishnan, M. Leduc and C. Cohen-Tannoudji, Phys. Rev. Lett. **86**, 3459 (2001).

[21] A. Robert, O. Sirjean, A. Browaeys, J. Poupard, S. Nowak, D. Boiron, C. I. Westbrook, A. Aspect Science **292**, 461 (2001).

[22] A. G. Truscott, K. E. Strecker, W. I. McAlexander, G. Partridge, and R. G. Hulet, Science **291**, 2570 (2001); B. DeMarco and D. S. Jin, Science 285, 1703-1706 (1999); J. Cubizolles , F. Schreck , K. Corwin , L. Khaykovich, G. Ferrari, C. Salomon, *in preparation* (see http://www.lkb.ens.fr/recherche/atfroids/anglais/lithium.html)

[23] M. R. Andrews, C. G. Townsend, H.-J. Miesner, D. S. Durfee, D. M. Kurn, and W. Ketterle, Science **275**, 637 (1997).

[24] C.A. Sackett, H.T.C. Stoof, and R.G. Hulet, Phys. Rev. Lett. **80** 2031, (1998); C.A. Sackett, C.C. Bradley, M. Welling, and R.G. Hulet, Appl. Phys. B **65** 433, (1997); C.C. Bradley, C.A. Sackett, and R.G. Hulet, Phys. Rev. Lett. **78** 985, (1997); C.C. Bradley, C.A. Sackett, and R.G. Hulet, Phys. Rev. A **55** 3951, (1997).

[25] J. L. Roberts, N. R. Claussen, S. L. Cornish, E. A. Donley, E. A. Cornell, and C. E. Wieman, Phys. Rev. Lett. **86**, 4211 (2001); S. L. Cornish, N. R. Claussen, J. L. Roberts, E. A. Cornell, and C. E. Wieman, preprint, cond-mat/0004290.

[26] C.A. Sackett, H.T.C. Stoof, and R.G. Hulet, Phys. Rev. Lett. **80** 2031, (1998); Yu. Kagan, A.E. Muryshev, and G.V. Shlyapnikov, Phys. Rev. Lett. **81**, 933, (1998).

[27] P.A. Ruprecht, M.J. Holland, K. Burnett, and M. Edwards, Phys. Rev. A **51**, 4704 (1995).

[28] S. L. Cornish, N. R. Claussen, J. L. Roberts, E. A. Cornell, and C. E. Wieman, Phys. Rev. Lett. **85** 1795 (2000); J. L. Roberts, N. R. Claussen, J. P. Burke, Jr., C. H. Greene, E. A. Cornell, and C. E. Wieman, Phys. Rev. Lett. **81** 5109 (1998); S. Inouye, M. R. Andrews, J. Stenger, H.-J. Miesner, D. M. Stamper-Kurn, W. Ketterle, Nature **392** 151 (1998).

[29] A. Einstein Sitzungsber. Kgl. Preuss. Akad. Wiss. **1925**, 3 (1925).

[30] P. Grüter, D. Ceperley, and F. Laloë, Phys. Rev. Lett. **79**, 3549 (1997).

[31] T. Toyoda, Ann. Phys. (N.Y.) 141, 154 (1982); K. Huang, in Studies in Statistical Mechanics (North- Holland, Amsterdam, 1964), Vol. II; H. T. C. Stoof, Phys. Rev. A 45, 8398 (1992); M. Bijlsma and H. T. C. Stoof, Phys. Rev. A 54, 5085 (1996).

[32] G. Baym, J.-P. Blaizot, M. Holzmann, F. Laloë and D. Vautherin, Phys. Rev. Lett. **83** 1703 (1999).

[33] G. Baym, J.-P Blaizot, J. Zinn-Justin, Europhys. Lett. **49**, 150 (2000).

[34] J. R. Ensher, D. S. Jin, M. R. Matthews, C. E. Wieman, and E. A. Cornell, Phys. Rev. Lett. **77**, 4984 (1996).

[35] E. J. Mueller, G. Baym, and M. Holzmann, *accepted for publication* J. Phys. B; At. Mol. Opt. Phys (2001).

[36] N. Goldenfeld *Lectures on phase transitions and the renormalization group*, (Addison-Wesley, Reading, Massachusetts, 1992).

[37] M. Holzmann and W. Krauth, Phys. Rev. Lett. **83**, 2687 (1999).

[38] M. Wilkens, F. Illuminati, and M. Krämer, J. Phys. B: At. Mol. Opt. Phys. **33** (2000) L779 (2000).

[39] P. Arnold and G. Moore, cond-mat/0103228 (2001).

[40] V. Kashurnikov, N. Prokof'ev N, and B. Svistunov, cond-mat/0103149 (2001).

[41] G. Baym and C. Pethick *Landau Fermi liquid theory: concepts and applications*, (J. Wiley and Sons, New York, 1991).

[42] Illuminati F, Navez P, and Wilkens M 1999 *J. Phys. B: At. Mol. Opt. Phys.* **32**, L461.

[43] S. Giorgini, L. P. Pitaevskii, and S. Stringari, Phys. Rev. A **54**, 4633 (1996).

[44] P. Arnold and B. Tomasik, cond-mat/0105147.

[45] O. Penrose, Phil. Mag. **42**, 1373 (1951).

[46] O. Penrose and L. Onsager, Phys. Rev. **104**, 576 (1956).

[47] P. Nozières and D. Saint James, J. Physique **43**, 1133 (1982).

[48] M. Girardeau, Phys. Fluids **5**, 1468 (1962).

[49] F. Pollock, Phys. Fluids **10**, 473 (1967).

[50] E. J. Mueller, T.-L. Ho, G. Baym, and M. Ueda, *to be submitted to Physical Review A* (2001).

[51] H. G. Vaidya and C. A. Tracy, Phys. Rev. Lett. **42**, 3 (1979).

[52] P. C. Hohenberg and P. C. Martin, Ann. Phys. **34**, 291 (1965).

[53] Yu. Kagan, V. A. Kashurnikov, A. V. Krasavin, N. V. Prokof'ev, and B. V. Svistunov, Phys. Rev. A **61**, 043608 (2000); J. M. Kosterlitz and D. J. Thouless, J. Phys. C **6** 1181 (1973).

[54] D.S. Petrov, G.V. Shlyapnikov, and J.T.M. Walraven cond-mat/0104373.

[55] Yu. Kagan and B. V. Svistunov Phys. Rev. Lett. **79**, 3331 (1997).

[56] C. N. Yang, Rev. Mod. Phys. **34**, 694 (1963).

[57] W. Kohn and D. Sherrington, Rev. Mod. Phys. **42**, 1 (1970).

[58] I. Zapata, F. Sols, and A. J. Leggett, Phys. Rev. A. **57**, R28 (1998).

[59] Y. Castin and C. Herzog, "Bose-Einstein condensates in symmetry breaking states", Lecture Notes of the Cargèse School on Bose-Einstein condensates (July 2000); reprinted as cond-mat/0012040.

[60] J. Javanainen and S. M. Yoo, Phys. Rev. Lett. **76**, 161 (1996).

[61] Y. Castin and J. Dalibard, Phys. Rev. A **50**, 4330 (1997).

[62] D. M. Stamper-Kurn, M. R. Andrews, A. P. Chikkatur, S. Inouye, H. J. Miesner, J. Stenger, and W. Ketterle, Phys. Rev. Lett. **80**, 2027 (1998).

[63] C. K. Law, H. Pu, and N. P. Bigelow, Phys. Rev. Lett. **81**, 5257 (1998).

[64] M. Koashi and M. Ueda, Phys. Rev. Lett. **84**, 1066 (2000).

[65] T.-L. Ho, Phys. Rev. Lett. **81**, 742 (1998); T. Ohmi and K. Machida, J. Phys. Soc. Jpn. **67**, 1822 (1998).

[66] N. Bogoliubov, J. Phys. **11**, 23 (1947).

[67] M. Ueda, Phys. Rev. A **63**, 013601 (2001).

[68] J. Javanainen, J. Phys. B **33**, 5493 (2000).

[69] W.-J. Huang, Phys. Rev. A **63**, 015602 (2000).

[70] C.J. Pethick and L. Pitaevski, Phys. Rev. A **62**, 033609 (2000).

[71] N. Mermin and H. Wagner, Phys. Rev. Lett. **17**, 1133 (1966).

[72] M. Ueda and A. J. Leggett, Phys. Rev. Lett. **83**, 1489 (1999).

[73] Y. Lyanda-Geller and P. M. Goldbart, Phys. Rev. A **61**, 043609 (2000).

[74] B. P. Anderson and M. A. Kasevich in *Proceedings of the International School of Physics 'Enrico Fermi', Course CXL, Bose-Einstein Condensation in Atomic Gases,* (M. Inguscio, S. Stringari, and C. E. Wieman, Eds., IOS Press, Amsterdam, 1999), pp. 439-452.

[75] M. P. A. Fisher, P. B. Weichman, G. Grinstein, D. S. Fisher, Phys. Rev. B **40**, 546 (1988).

[76] D. Van Oosten, P. Van der Straten, and H. T. C. Stoof, Phys. Rev. A **63**, 053601 (2001).

[77] C.J. Myatt, E.A. Burt, R.W. Ghrist, E.A. Cornell and C.E. Wieman. Phys. Rev. Lett. 78, 586 (1997), H.-J. Miesner, D. M. Stamper-Kurn, J. Stenger, S. Inouye, A. P. Chikkatur, and W. Ketterle, Phys. Rev. Lett. **82**, 2228 (1999).

[78] B. D. Esry, Phys. Rev. A, **58**, 3399 (1998).

[79] B. D. Esry, and C. H. Greene, Phys. Rev. A, **59**, 1457 (1999).

[80] M. R. Matthews, B. P. Anderson, P. C. Haljan, D. S. Hall, C. E. Wieman, and E. A. Cornell, Phys. Rev. Lett. **83**, 2498 (1999).

[81] G. Baym, Phys. Rev. B **51**, 11697 (1995).

[82] J. R. Abo-Shaeer, C. Raman, J. M. Vogels, W. Ketterle, Science, **292**, 476 (2001).

[83] G. J. Milburn, J. Corney, E. M. Wright, and D. F. Walls, Phys. Rev. A **55**,4318 (1997).

[84] R. W. Spekkens and J. E. Sipe, Phys. Rev. A **59**, 3868 (1999).

[85] E. J. Mueller, P. Goldbart and Y. Lyanda-Geller, Phys. Rev. A **57**, 1505 (1998)

[86] W. A. Little, Phys. Rev. **156**, 396 (1967).

[87] J. Langer and V. Ambegaokar, Phys. Rev. **164**, 498 (1967).

[88] D. McCumber and B. Halperin, Phys. Rev. B **1**, 1054 (1970).

[89] See also M. Tinkham, *Introduction to Superconductivity* (McGraw-Hill, NY, 1975), Chap. 7.

[90] D. S. Rokhsar, Phys. Rev. Lett. **79**, 2164 (1997); D. S. Rokhsar, cond-mat/9709212.

[91] Y. Lyanda-Geller and P. M. Goldbart, Phys. Rev. A **61**, 3609 (2000); M. Nishida and S. Kurihara, J. Phys. Soc. Jpn. **68**, 3778 (1999); K. G. Petrosyan, and L. You, Phys. Rev. A **59**, 639 (1999); M. Benakli, S. Raghavan, A. Smerzi, S. Fantoni, and S. R. Shenoy, Europhys. Lett. **46**, 275 (1999); L. D. Carr, C. W. Clark, W. P. Reinhard, Phys. Rev. A **62**, 3610 (2000); L. Salasnich, A. Parola, L. Reatto, Physical Review A, vol. 59, 2990-2995 (1999).

[92] M.R. Matthews, B.P. Anderson, P.C. Haljan, D.S. Hall, C.E. Wieman, E.A. Cornell, Phys. Rev. Lett. **83**, 2498 (1999), B. P. Anderson, P. C. Haljan, C. E. Wieman, E. A. Cornell, Phys. Rev. Lett. **85**, 2845 (2000).

[93] E. M. Wright, J. Arlt, and K. Dholakia, Phys. Rev. A, **63**, 013608 (2001)

[94] G. Birkl, F. B. J. Buchkremer, R. Dumke, and W. Ertmer, Opt. Comm. **191**, 67 (2001); J. Reichel, W. Hänsel, P. Hommelhoff and T. W. Hänsch, Appl. Phys. B 72, 81-89, (2000).

[95] J. S. Langer and M. E. Fisher, Phys. Rev. Lett. **19**, 560 (1967); R. J. Donnelly, *Quantized Vortices in Helium II* (Cambridge University Press, 1991), Chap. 8.

[96] J. E. Williams, M. J. Holland Nature **401**, 568(1999).

[97] M. R. Andrew, K. M. Kurn, H.-J. Miesner, D. S. Durfee, C. G. Townsend, S. Inouye, and W. Ketterle, Phys. Rev. Lett. **79**, 553 (1997)

[98] E. J. Mueller and G. Baym, Phys. Rev. A **62**, 053605 (2000).

[99] P.A. Ruprecht, M.J. Holland, K. Burnett, and M. Edwards, Phys. Rev. A **51**, 4704 (1995).

[100] M. J. Davis, D. A. W. Hutchinson, and E. Zaremba, J. Phys. B **32**, 3993 (1999); T. Bergeman, Phys. Rev. A **55**, 3658 (1997); M. Houbiers and H. T. C. Stoof, Phys. Rev. A **54**, 5055 (1996); P.A. Ruprecht, M.J. Holland, K. Burnett, and M. Edwards, Phys. Rev. A **51**, 4704 (1995).

[101] J. Tempere, F. Brosens, L. F. Lemmens and J. T. Devreese, Phys. Rev. A, **61**, 043605 (2000).

[102] H. Saito and M. Ueda, preprint cond-mat/0006410; Yu. Kagan, A. E. Muryshev, and G. V. Shlyapnikov, Phys. Rev. Lett. **81**, 933 (1998); **79**, 2670 (1996); also see the experiments in Ref. [24, 25].

[103] C. Huepe, S. Métens, G. Dewel, P. Borckmans, and M. E. Brachet, Phys. Rev. Lett. **82**, 1616 (1999); M. Ueda and A. J. Leggett, Phys. Rev. Lett. **80**, 1576 (1998); Yu. Kagan, G. V. Shlyapnikov, and J. T. M. Walraven, Phys. Rev. Lett. **81**, 933 (1998); H. T. C. Stoof, J. Stat. Phys. **87**, 1353 (1997).

[104] A. Griffin, *Excitations in a Bose-Condensed Liquid* (Cambridge University Press, Cambridge, 1993).

[105] N.N. Bogoliubov, J. Phys. USSR, **11**, 23 (1947).

[106] N.D. Mermin, Ann. Phys. **18**, 421, 454 (1962); **21**, 99 (1963).

[107] P. Szépfalusy and I. Kondor, Ann. Phys. **82**, 1 (1974).

[108] A. Minguzzi and M. P. Tosi, J. Phys: Condens. Matter **9**, 10211 (1997).

[109] G. Baym, Phys. Rev. **127**, l39l (1962).

[110] A. J. Moerdijk, H. M. J. M. Boesten, and B. J. Verhaar, Phys. Rev. A **53**, 916 (1996); C. A. Sackett, J. M. Gerton, M. Welling, and R. G. Hulet, Phys. Rev. Lett. **82**, 876 (1999).

[111] J. Bardeen, L. N. Cooper, and J. R. Schrieffer, Phys. Rev. **108**, 1175 (1957).

[112] H. T. C. Stoof, Phys. Rev. A **49**, 3824 (1994).

[113] L.P. Kadanoff and G. Baym, *Quantum Statistical Mechanics* (W.A. Benjamin, New York, 1962).

[114] T. Isoshima, K. Machida, and T. Ohmi, Phys. Rev. A **60**, 4857 (1999).

[115] For a similar theoretical account, see P. Ao, and S. T. Chui, J. Phys. B **33**, 535 (2000).

[116] T.-L. Ho, Phys. Rev. Lett. **81**, 742 (1998).

[117] Similar excitation spectra are found in E.V. Goldstein and P. Meystre, Phys. Rev. A **55**, 2935 (1997).

[118] J. W. Kane and L. P. Kadanoff, J. Math. Phys. 6, 1902 (1965).

[119] A. Griffin in *Proceedings of the International School of Physics 'Enrico Fermi', Course CXL, Bose-Einstein Condensation in Atomic Gases,* (M. Inguscio, S. Stringari, and C. E. Wieman, Eds., IOS Press, Amsterdam, 1999), edited by M.Inguscio, S.Stringari and C. Wieman (Italian Physical Society,1999); cond-mat/9901172.

[120] M. Imamovic-Tomasovic and A. Griffin, Journ. of Low Temperature Physics, 122, 617 (2001); T. Nikuni and A. Griffin, Phys. Rev. A63, 033608-033628 (2001); M. Imamovic-Tomasovic and A. Griffin, in *Recent Progress in Non-Equilibrium Green's functions*, ed. by M. Bonitz (World Scientific, Singapore, 2000), p.404-417; A. Griffin, in *Bose-Einstein Condensation: From atomic physics to quantum liquids*, ed. by C.M. Savage and M. Das (World Scientific, Singapore, 2001); E. Zaremba, T. Nikuni and A. Griffin, Journ. Low Temp. Phys., 116, 277 (1999); Milena Imamovic-Tomasovic and Allan Griffin, Phys. Rev. A60, 494 (1999).

[121] R. Walser, J. Williams, J. Cooper, M. Holland Phys. Rev. A 59, 3878 (1999).

[122] C. W. Gardiner and P. Zoller, Phys. Rev. A, **55**, 2902 (1997); D. Jaksch, C. W. Gardiner, and P. Zoller, Phys. Rev. A. **55**, 575 (1997); C. W. Gardiner, Phys. Rev. A **56**, 1414 (1997); C. W. Gardiner, P. Zoller, R. Ballagh, and M. J. Davis, Phys. Rev. Lett. **79**, 1793 (1997); D. Jaksch, C. W. Gardiner and P. Zoller, Phys. Rev. A. **56**, 575 (1997); C. W. Gardiner, P. Zoller, Phys. Rev. A **58**, 536 (1998); D. Jaksch, C. W. Gardiner, K. M. Gheri and P. Zoller Phys. Rev. A **58**, 1450 (1998); C. W. Gardiner M. D. Lee, R. J. Ballagh, M. J. Davis and P. Zoller, Phys. Rev. Lett. **81**, 5266 (1998) ; C. W. Gardiner and P. Zoller, Phys. Rev. A **61**, 033601 (2000); M. D. Lee and C.W. Gardiner, Phys. Rev. A **62**, 033606 (2000); M. J. Davis, C. W. Gardiner and R. J. Ballagh, Phys. Rev. A **62**, 063608 (2000);

[123] U. Al Khawaja and H. T. C. Stoof Phys. Rev. A **62**, 53602 (2000).

[124] S. L. Cornish, N. R. Claussen, J. L. Roberts, E. A. Cornell, C. E. Wieman, Phys. Rev. Lett. **85**, 1795 (2000); S. L. Cornish, N. R. Claussen, J. L. Roberts, C. E. Wieman, Phys. Rev. Lett. **85**, 728 (2000). S. Inouye, M.R. Andrews, J. Stenger, H.-J. Miesner, D.M. Stamper-Kurn, and W. Ketterle, Nature **392**, 151 (1998).

[125] J. Glanz, New York Times (Jan. 18, 2001).

[126] B. V. Svistunov and G. V. Shlyapnikov, Sov. Phys. JETP **70**, 460 (1990); **71**, 71 (1990).

[127] R. M. Ziff, G. E. Uhlenbeck, and M. Kac, Phys. Rep. **32**, 169 (1977).

[128] Robinson, Phys. Rev. **83**, 678 (1951).

[129] Titchmarsh, *The theory of the Riemann Zeta-Function,* Oxford University Press, 1951.

[130] Whittaker and Watson, *Modern Analysis,* Cambridge University Press, 1947.

[131] Morse and Feshbach, *Methods of theoretical physics*, Technology Press, 1946.

[132] N.D. Mermin, Ann. Phys. **18**, 421 (1962); 454 (1962); **21**,99 (1963).

[133] G. Mahan, *Many-Particle Physics,* Plenum Press, New York, 1981.

[134] J. Shumway and D. M. Ceperley, cond-mat/9907309.

Index

asymmetric, 49, 63–65
experimental parameters, 45
regimes, 44
Josephson plasma frequency, 44

kinetics, 3, 72, 96–105

lithium, 12, 80–82, 87, 89, 90, 92
local density approximation, 83
localization, 45, 49, 56–58

Matsubara frequencies, 163
measurement
experiment, 9
fragmentation, 46–48
phase slips, 78
Mellin transform, 127, 130
metastability, 15, 69, 72, 73, 77, 81, 93
microchannel plate, 11
Monte-Carlo, 18

one dimensional gas, 54, 55
optical lattices, 56
optical molasses, 4

pairing, 2, 80, 91
partition function, 20
persistent currents, 2, 69–79
perturbation theory, 18, 31–35
phase diagram, 81, 82
phase shifts, 170–171
phase slip, 2, 69–79
phase transition
BEC, 1, 18–37
dimensionality, 21
liquid-gas, 85, 156
localization-delocalization, 56
photons, 16, 112–115
Poisson brackets, 99
polaritons, 16, 112–124
dark, 116
polarons, 16, 112, 117, 119, 124
polylogarithm, 22, 26, 86, 126–129
pseudo-potential, 178

quantum pressure, 81, 107
quasicondensate, 41

quasiparticle, 96, 102, 104

random phase approximation, 85, 156
rubidium, 12, 37, 77, 80–82, 87, 89, 90, 92, 115

scattering, 166–188
multiple, 183
resonances, 166
scattering amplitude, 166
Schrödinger Cat, 65
self-energy, 98, 120, 122, 146, 148
sodium, 4, 115
soliton, 55
spectral density, 103, 109
spin
fragmentation, 49–52
phase separation, 2, 16
textures, 55
Zeeman splitting, 6
spin:phase separation, 93
spinodal, 156
squeezed states, 48
Stern Gerlach experiment, 52
Stirling numbers, 134
sum rules, 141
superfluidity, 2, 69
symmetry breaking, 39–68
sympathetic cooling, 12

T-matrix, 164, 167–169, 170, 186–187
thermal activation, 72
thermal pressure, 81
trapping, 4, 83, 89
two level model, 42–45, 55

uncertainty principle, 4

vortex, 52, 59, 60, 78

zero sound, 157
zeta function, 22, 126
spectral, 131, 132

Vita

Erich Jon Mueller was born September 27, 1974, in Calgary, Canada. In 1996, he recieved an honours B.Sc. in mathematics and physics from the University of British Columbia in Vancouver, Canada; graduating top of his class. At UBC he studied both experimental and theoretical physics, first working with semiconductor quantum wells in the experimental laboratory of Jeff Young, then writing an undergraduate thesis on quantum measurement under the direction of Philip Stamp. Following his undergraduate studies, he spent five years studying quantum degenerate gases with Gordon Baym at the University of Illinois at Urbana-Champaign, earning his Ph.D. in theoretical physics in 2001. He is currently working with Tin-Lun Ho at the Ohio State University in Columbus, Ohio. His publications include:

E.J. Mueller, G. Baym, and M. Holtzmann, "Finite size scaling and the role of the thermodynamic ensemble in the transition temperature of a dilute Bose gas," cond-mat/0105359, *To be published in J. Phys. B,* (2001).

E.J. Mueller and G. Baym, "Finite Temperature Collapse of a Bose Gas with Attractive Interactions," Phys. Rev. A, **62**, 053605 (2000).

E.J. Mueller, P.M. Goldbart, Y. Lyanda-Geller, "Multiply-connected Bose-Einstein condensed alkali gases: Current-carrying states and their decay," Phys. Rev. A, **57**, R1505 (1998).

S.M. Sadeghi, S.R. Leffler, J. Meyer, and E. Mueller, "Optical-Field-Dependent Electron-Electron Scattering Effects and Gain Generation in the Intersubband Transitions of n-Doped Quantum Wells," J. Phys: Cond. Mat., **10**, 2489 (1998).